

Imperial College London
Department of Computing

AUTOMATED OPTIMIZATION OF
NUMERICAL METHODS FOR PARTIAL
DIFFERENTIAL EQUATIONS

FABIO LUPORINI

September 2016

Supervised by: Dr. David A. Ham, Prof. Paul H. J. Kelly

Submitted in part fulfilment of the requirements for the degree of
Doctor of Philosophy in Computing
of Imperial College London
and the Diploma of Imperial College London

Declaration

I herewith certify that the material in this thesis that is not my own work has been properly acknowledged and referenced.

Fabio Luporini

The copyright of this thesis rests with the author and is made available under a Creative Commons Attribution Non-Commercial No Derivatives licence. Researchers are free to copy, distribute or transmit the thesis on the condition that they attribute it, that they do not use it for commercial purposes and that they do not alter, transform or build upon it. For any reuse or redistribution, researchers must make clear to others the licence terms of this work.

Abstract

The time required to execute real-world scientific computations is a major issue. A single simulation may last hours, days, or even weeks to reach a certain level of accuracy, despite running on large-scale parallel architectures. Strict time limits may often be imposed too – 60 minutes in the case of the UK Met Office to produce a forecast.

In this thesis, it is demonstrated that by raising the level of abstraction, the performance of a class of numerical methods for solving partial differential equations is improvable with minimal user intervention or, in many circumstances, with no user intervention at all. The use of high level languages to express mathematical problems enables domain-specific optimization via compilers. These automated optimizations are proven to be effective in a variety of real-world applications and computational kernels.

The focus is on numerical methods based on unstructured meshes, such as the finite element method. The loop nests for unstructured mesh traversal are often irregular (i.e., they perform non-affine memory accesses, such as $A[B[i]]$), which makes reordering transformations for data locality essentially impossible for low level compilers. Further, the computational kernels are often characterized by complex mathematical expressions, and manual optimization is simply not conceivable. We discuss algorithmic solutions to these problems and present tools for their automation. These tools – the COFFEE compiler and the SLOPE library – are currently in use in frameworks for solving partial differential equations.

To Alice

Acknowledgements

In these two pages, I would like to express my gratitude to those who supported me during my studies at Imperial College.

My greatest thanks to my supervisors, Paul Kelly and David Ham, for the time they have spent with me. Your guidance and passion have been an incredible source of inspiration for my research. You probably do not even realize how much I have learnt from you, and for this I will be eternally grateful.

I have been extremely lucky to work next to Doru Bercea, Luigi Nardi, Florian Rathgeber, Francis Russell, Georgios Rokos, Lawrence Mitchell, Andrew McRae, Thomas Gibson, Miklós Homolya, Michael Lange. It has been a real pleasure to share the office with you. I think we have done some real science together, and all of you have contributed to my personal and professional growth. Thanks. Keep up the hard work, I am sure we will meet again!

I met Carlo Bertolli for the first time in 2008; he was a lab helper when I was a second year student in Computer Science at University of Pisa. He co-supervised my Bachelor thesis back in 2009. We kept in touch, and after a few years he suggested me to apply for a PhD position at Imperial. If I am writing these lines, it is also thanks to him and his guidance. So, thanks Carlo.

At the very beginning of my studies at Imperial, I met J. “Ram” Ramanujam. We have worked, shared many interesting stories (and trolls) about the Polyhedral model, and had many pizzas and coffees together. I consider you like my third, “unofficial” supervisor. Thanks!

With Emanuele Vespa I have shared my office for only one year, but our

friendship goes back to the good old days in Pisa (when we were young). I will miss you, but I am also sure we will always be in touch. I will really miss two things: 1) our (self-)trolling, especially for all those PhD students telling us that they had deadlines and were publishing stacks of papers everywhere, while we were spending most of our time chasing bugs and “understanding what to do next”; 2) playing Teeworlds.

I also thank my Italian friends, those in London (in particular, Francesca, Simone, Federico), those spread all over the world, and those who I talk with almost everyday. I am so glad that after all these years we still keep in touch.

Finally, my biggest thanks goes to those who have made this experience possible: Alice and our families. I like science, I love what I do, but without your love and support this PhD would have never been possible. My gratitude for these 4 years in London will be eternal.

Contents

1	Introduction	1
1.1	Thesis Statement	1
1.2	Overview	1
1.3	Thesis Outline and Contributions	2
1.4	Dissemination	5
2	Background	7
2.1	The Finite Element Method	7
2.1.1	Weak Formulation	8
2.1.2	Local and Global Function Spaces	9
2.1.3	The Reference Element	11
2.1.4	Assembly	12
2.1.5	Local Assembly Example: from Math to Code	13
2.2	Software Abstractions for Partial Differential Equation Solvers	18
2.2.1	Automating the Finite Element Method	19
2.2.2	The PyOP2 and OP2 Libraries	23
2.2.3	Stencil Languages	27
2.3	Compilers and Libraries for Loop Optimization	29
2.3.1	Loop Reordering Transformations	29
2.3.2	Composing Loop Tiling and Loop Fusion	31
2.3.3	Automation via Static Analysis	33
2.3.4	Automation via Dynamic Analysis	35
2.4	Domain-Specific Optimization	35
2.4.1	Tensor Contraction Engine	36
2.4.2	Halide	36

2.4.3	Spiral	37
2.4.4	Small-scale Linear Algebra	37
2.5	On the Terminology Adopted	38
3	Automated Sparse Tiling for Irregular Computations	43
3.1	Motivation	43
3.2	Context and Approach	45
3.3	Applying Loop Fusion and Loop Tiling is More Difficult than Commonly Assumed	47
3.4	Related Work	50
3.5	The Loop Chain Abstraction for Generalized Inspector/Ex- ecutor Schemes	52
3.5.1	Relationship between Loop Chain and Inspector . .	52
3.5.2	Definition of a Loop Chain	53
3.5.3	The Abstraction Revisited for Unstructured Mesh Ap- plications	54
3.6	Loop Chain, Inspection and Execution Examples	56
3.7	Data Dependency Analysis for Loop Chains	64
3.8	Formalization	66
3.8.1	The Generalized Sparse Tiling Inspector	66
3.8.2	The Generalized Sparse Tiling Executor	71
3.8.3	Computational Complexity of Inspection	73
3.9	Implementation	73
3.9.1	SLOPE: a Library for Sparse Tiling Irregular Com- putations	74
3.9.2	PyOP2: Lazy Evaluation and Interfaces	76
3.9.3	Firedrake/DMPlex: the S-depth Mechanism for Ex- tended Halo Regions	77
3.10	Performance Evaluation - Benchmarks	78
3.10.1	Sparse Jacobi	79
3.10.2	Airfoil	80
3.10.3	Outcome	82
3.11	Performance Evaluation - Seigen: an Elastic Wave Equation Solver for Seismological Problems	83
3.11.1	Computation	83
3.11.2	Setup and Reproducibility	87

3.11.3	Results and Analysis	92
3.12	Conclusions and Future Work	106
4	Minimizing Operations in Finite Element Integration Loops	109
4.1	Motivation and Related Work	109
4.2	Loop Nests, Expressions and Optimality	112
4.3	Transformation Space: Sharing Elimination	116
4.3.1	Identification and Exploitation of Structure	117
4.3.2	Global Analysis of the Expression	118
4.3.3	The Sharing Elimination Algorithm	120
4.3.4	Examples	122
4.4	Transformation Space: Pre-evaluation of Reductions	127
4.5	Transformation Space: Memory Constraints	129
4.6	Selection and Composition of Transformations	129
4.6.1	The Main Transformation Algorithm	129
4.6.2	The Cost Function θ	132
4.7	Formalization	133
4.8	Code Generation	136
4.8.1	Expressing Transformations with COFFEE	136
4.8.2	Independence from Form Compilers	137
4.8.3	Handling Block-sparse Tables	137
4.9	Performance Evaluation	138
4.9.1	Experimental Setup	138
4.9.2	Performance Results	140
4.10	Conclusions	146
4.11	Limitations and Future Work	146
5	Cross-loop Optimization of Arithmetic Intensity for Finite Element Integration	149
5.1	Recapitulation and Objectives	149
5.2	Low-level Optimization	152
5.2.1	Padding and Data Alignment	152
5.2.2	Expression Splitting	153
5.2.3	Model-driven Vector-register Tiling	156
5.3	Experiments	158
5.3.1	Setup	158

5.3.2	Test Environment	161
5.3.3	Rationale of the Experimentation	161
5.4	Experience with Traditional Compiler Optimizations	166
5.4.1	Loop Interchange	167
5.4.2	Loop Unrolling	167
5.4.3	Vector promotion	168
5.4.4	Loop Fusion	169
5.5	Related Work	170
5.6	Applicability to Other Domains	172
5.7	Conclusions	175
6	COFFEE: a Compiler for Fast Expression Evaluation	177
6.1	Overview	177
6.2	The Compilation Pipeline	178
6.3	Plugging COFFEE into Firedrake	180
6.3.1	Abstract Syntax Trees	180
6.3.2	Integration with Form Compilers	181
6.4	Rewrite Operators	182
6.5	Features of the Implementation	184
6.5.1	Tree Visitor Pattern	184
6.5.2	Flexible Code Motion	185
6.5.3	Tracking Data Dependency	186
6.5.4	Minimizing Temporaries	186
6.6	On the Compilation Time	187
6.7	Overview of Applications Exploiting COFFEE	187
7	Conclusions	189
7.1	Summary	189
7.2	Limitations	192
7.3	Future Research Directions	193

List of Tables

3.1	Summary of the notation used throughout the section. . . .	66
3.2	The tile data structure.	68
3.3	Worst-case computational costs of the main inspection phases.	73
3.4	Execution time reductions over the original implementation (in percentage) and speed-ups over the single-threaded tiled implementation for the sparse Jacobi solver with 15 threads.	79
3.5	Execution time (in seconds) and speed-ups over the slowest single-threaded implementation for the Airfoil benchmark. Respectively 16 and 24 threads/processes are used on the Sandy Bridge and Westmere machines.	80
3.6	Summary of the fusion schemes adopted in Seigen. The <i>S-depth</i> column represents the number of off-process cell layers.	87
3.7	Systems specification.	89
3.8	Summary of the meshes used for single-node experimentation in Seigen. d is the average number of degrees of freedom assigned to a process for a given variational form.	90
3.9	Comparing the Seigen completion time OT on Erebus (number of processes $n = 4$) and CX1-Ivy ($n = 20$).	94
3.10	Comparing the Seigen average compute time ACT on Erebus (number of processes $n = 4$) and CX1-Ivy ($n = 20$). . . .	95
3.11	Comparing the Seigen average compute and communication time ACCT on Erebus (number of processes $n = 4$) and CX1-Ivy ($n = 20$).	95

List of Figures

2.1	Affine mapping from the reference element \hat{K} to an element K	11
2.2	Distributed-memory parallelism in OP2 and PyOP2. Matching colors represent identical subsets of iterations. The image was inspired by an example in Rathgeber [2014].	26
3.1	Partitioning of the seed loop. The vertices are illustrated to make the connectivity of the mesh clear, although they do not belong to any partition yet.	57
3.2	A snapshot of the mesh after tiling L_0	58
3.3	The vertices are written by L_0 , so a projection must be computed before tiling L_1 . Here, the projection is represented by the colored vertices.	59
3.4	A snapshot of the mesh after tiling L_1	59
3.5	A snapshot of the mesh after tiling L_2	60
3.6	Tiling the program in Listing 7 for shared-memory parallelism can lead to conflicts. Here, the two green tiles eventually become adjacent, creating race conditions.	60

- 3.7 A snapshot of the two mesh partitions on Process 0 and Process 1 after inspecting the seed loop L_0 for distributed-memory parallelism. On each process, there are five tiles in total: two in the core region (green and violet), two in the boundary region (red and light blue), and T_{ne} . The boundary tiles can safely cross the owned and exec sub-regions (i.e., the private local iterations and the iterations to be redundantly computed, respectively). However, no tile can include iterations from both the core and the boundary regions. 62
- 3.8 A snapshot of the two mesh partitions on Process 0 and Process 1 at the end of the inspection for distributed-memory parallelism. T_{ne} expands over the boundary region, which minimizes the amount of redundant computation to be performed. At the end of the execution phase, the orange edges will contain “dirty values”, but correctness is not affected as the exec region only includes off-process data. The boundary tiles expand over the core region: this is essential for correctness since none of the red and blue entities from $[L_0, L_1, L_2]$ can be executed until the MPI communications have terminated. 63
- 3.9 Representation of an inverse map. The original map shows that the triangular cell 1 is adjacent to three vertices, namely 3, 7, and 9. The inverse map associates vertices to cells. Since the mesh is unstructured, different vertices can be incident to a different number of cells. The array `offset` determines the distance between two consecutive vertices in the inverse map. For instance, all entries in the inverse map between `offset[3]` and `offset[4]` are cells incident to vertex 3 (in the illustrated case, the first of these is cell 1). 70

3.10	Sparse tiling in the Firedrake-PyOP2-SLOPE framework. There are three ways of sparse tiling a loop chain: decorating a Firedrake program (1A), decorating a sequence of loops in a PyOP2 program (1B), writing both the loop chain and the inspector/executor codes explicitly in C through calls to SLOPE (1C). Both (1A) and (1B) use the <i>loop_chain</i> interface (details in Section 3.9.2). The kernels generated within a <i>loop_chain</i> are pre-processed in PyOP2 (2) and forwarded to SLOPE through its python interface (3). SLOPE now has access to the loop chain, so it can generate an inspector/executor scheme and return it to PyOP2 (4). The inspector is compiled and executed. The result, a schedule (i.e., the output of Algorithm 1), is cached and used as input to the executor. Each time the same <i>loop_chain</i> is encountered in a Firedrake/PyOP2 program, the corresponding schedule is reused.	75
3.11	The sub loop chains in the five fusion schemes. <i>Cells</i> , <i>int-facets</i> , and <i>ext-facets</i> represent respectively the cell, interior facet, and exterior facet assembly loops, while <i>mat-vec</i> represents a solver.	88
3.12	Search space exploration on Erebus with $n = 4$ MPI processes. Two meshes ($h \in \{1.0, 1.2\}$) and four polynomial orders ($q \in \{1, 2, 3, 4\}$) are shown. Each plot shows the average compute and communication time (ACCT, y-axis) of five fusion schemes and the original version. The seed tile size of a loop chain in an fs, in terms of seed loop iterations, is the product of the “tile size factor” (x-axis) and a pre-established multiplier (an integer in the range $[1, 4]$; full list at Jacobs and Luporini [2016]). With tiling, global maps, chunk partitioning, and the extended boundary region optimization are used.	98

3.14	Search space exploration on CX1-Ivy with $n = 20$ MPI processes. Two meshes ($h \in \{0.6, 0.8\}$) and four polynomial orders ($q \in \{1, 2, 3, 4\}$) are shown. Each plot shows the average compute and communication time (ACCT, y-axis) of five fusion schemes and the original version. The seed tile size of a loop chain in an fs, in terms of seed loop iterations, is the product of the “tile size factor” (x-axis) and a pre-established multiplier (an integer in the range $[1, 4]$; full list at Jacobs and Luporini [2016]). With tiling, global maps, chunk partitioning, and the extended boundary region optimization are used.	99
4.1	The loop nest implementing a generic bilinear form.	114
4.2	Reducing a simple multilinear loop nest to optimal form.	116
4.3	The temporary graph for an excerpt of code extracted from a hyperelastic model.	120
4.4	Applying sharing elimination to the bilinear form arising from a Poisson equation in 2D. The operation counts are $E(f(z_0, z_1, \dots) + IJK \cdot 18)$ (left) and $E(f(z_0, z_1, \dots) + I(J \cdot 6 + K \cdot 9 + JK \cdot 4))$ (right), with $f(z_0, z_1, \dots)$ representing the operation count for evaluating z_0, z_1, \dots , and common sub-expressions being counted once. The synthesis in Figure 4.4b is globally optimal apart from the pathological case $I, J, K = 1$	123
4.5	Using the ILP model to factorize the expression arising from the pressure equation.	124
4.6	Applying the <i>strategy selection analysis</i> to the bilinear form arising from a hyperelastic model in 2D.	126
4.7	Exposing (through factorization) and pre-evaluating a reduction.	127
4.8	The loop nest produced by the algorithm for an input as in Figure 4.1.	131
4.9	Simplified loop nest for a pre-multiplied mass matrix.	132
4.10	Performance evaluation for the <i>mass</i> matrix. The bars represent speed-up over the original (unoptimized) code produced by the FEniCS Form Compiler.	140

4.11	Performance evaluation for the bilinear form of a <i>Helmholtz</i> equation. The bars represent speed-up over the original (unoptimized) code produced by the FEniCS Form Compiler.	141
4.12	Performance evaluation for the bilinear form arising in an <i>elastic</i> model. The bars represent speed-up over the original (unoptimized) code produced by the FEniCS Form Compiler.	142
4.13	Performance evaluation for the bilinear form arising in a <i>hyperelastic</i> model. The bars represent speed-up over the original (unoptimized) code produced by the FEniCS Form Compiler.	143
5.1	The outer-product vectorization relies on permuting values directly within vector registers.	158
5.2	Restoring the storage layout is the last step of the outer-product vectorization. The figure shows how 4×4 elements in the top-left block of the element matrix A can be moved to their correct positions. Each rotation, represented by a group of three same-colored arrows, is implemented by a single shuffle intrinsic.	158
5.3	The Helmholtz bilinear form. The trial function u and the test function v belong to the space of continuous piecewise-defined polynomials of given degree (spanned by the usual Lagrange basis functions).	160
5.4	The Diffusion bilinear form. The trial function u and the test function v belong to the space of continuous piecewise-defined polynomials of given degree (spanned by the usual Lagrange basis functions).	160
5.5	The Burgers operator. The solution u and the test function v belong to the space of vector-valued continuous piecewise-defined polynomials of given degree (spanned by the usual Lagrange basis functions). ν is a constant scalar viscosity. A backward Euler time discretization is used.	160

5.6	Maximum performance improvement on a Sandy Bridge due to generalized loop-invariant code motion, padding and data alignment, outer-product vectorization, and expression splitting over the original code produced by Firedrake. The unroll and splitting factors – respectively for the outer-product vectorization and expression splitting – were determined empirically.	162
5.7	Maximum performance improvement on a Xeon Phi due to generalized loop-invariant code motion, padding and data alignment, outer-product vectorization, and expression splitting over the original code produced by Firedrake. The unroll and splitting factors – respectively for the outer-product vectorization and expression splitting – were determined empirically.	166
6.1	The COFFEE pipeline and its interaction with Firedrake. . .	178
6.2	AST representation of a C assignment in COFFEE.	181

Chapter 1

Introduction

1.1 Thesis Statement

Maximizing the performance of numerical methods for partial differential equations is a challenging task that can be facilitated by raising the level of abstraction, through which automated optimization becomes possible.

1.2 Overview

In many fields such as computational fluid dynamics, computational electromagnetics and structural mechanics, phenomena are modelled by partial differential equations. Numerical techniques, such as the finite volume method and the finite element method, are widely employed to approximate their solutions. Unstructured meshes are often used to discretize the computational domain, since they allow an accurate representation of complex geometries. The solution is sought by applying suitable numerical operations, or kernels, to the entities of a mesh, such as edges, vertices, or cells. On typical clusters of multi-core processors, usually, a kernel is executed sequentially by a process, while parallelism is achieved by assigning mesh partitions to different nodes or processes. This execution model is adopted by many real-world applications and frameworks.

The time required to apply the numerical kernels is a major issue, since the equation domain needs be discretized into an extremely large number of cells to obtain a satisfactory approximation of the solution, possibly of the order of trillions, as in Rossinelli et al. [2013]. For example, it has

been well established that mesh resolution is critical in the accuracy of numerical weather forecasts. However, operational forecast centers have a strict time limit in which to produce a forecast - 60 minutes in the case of the UK Met Office. Producing efficient kernels or improving the mesh iteration has a direct scientific payoff in higher resolution, and therefore more accurate, forecasts.

This thesis shows that the use of domain-specific languages for expressing a class of numerical methods based on unstructured meshes plays a crucial role in performance optimization. In the translation of the problem specification into low level code (e.g., C), a stack of compilers applies sophisticated transformations. Ideally, these transformations would manually be written, specialized, and tuned for each application and for each architecture. This is however unrealistic, as all fundamental rules of software engineering, including maintainability, extendibility, and modularity, would be violated.

As we shall demonstrate, optimizing applications via domain-specific compilers has significant advantages. First, simplicity: both the program structure and domain properties are captured by the high level syntax, which invaluablely simplifies the compiler's job. Second, portability: multiple applications use the same transformation pipeline, and execution on heterogeneous architectures may be supported. Third, separation of concerns. Application specialists focus on expressing simulations with a notation close to the mathematics of textbooks, whereas performance optimization is hidden in the lower abstraction layers.

1.3 Thesis Outline and Contributions

This thesis investigates two main topics: (i) the generalization of a compiler transformation known as *sparse tiling*, whose aim is to improve data locality in sequences of irregular loops; (ii) the optimization of so called *local assembly kernels* in finite element methods. In fact, the latter spans two research directions: (ii-a) the minimization of the operation count; (ii-b) the low level optimization of the code resulting from (ii-a), through novel and state-of-the-art loop transformations. For both (i) and (ii), *automation via domain-specific compilers* is a distinguishing feature. The order in which these topics are covered is detailed below.

The thesis comprises seven chapters, including the present introduction and the conclusions. Chapter 2 establishes the foundation for the contributions in the subsequent chapters. The basics of the finite element method, the state-of-the-art on automated code generation for unstructured mesh computations, and compiler optimization are reviewed. Chapters 3, 4, and 5, which respectively treat the aforementioned topics (i), (ii-a), and (ii-b), represent the core contributions of this thesis, as detailed next:

Chapter 3 Sparse tiling is a transformation that fuses and tiles loops performing indirect memory accesses (e.g., $A[B[i]]$). These loops are common when iterating over unstructured meshes. The research on sparse tiling was characterized by two phases:

1. The initial work was a joint international effort with people from several institutions: Michelle M. Strout, Christopher Krieger, and Catherine Olschanowsky (Colorado State University; fundamental contributions to the first version of the *generalized sparse tiling algorithm* for shared-memory architectures, performance evaluation of the Jacobi sparse matrix solver benchmark); Carlo Bertolli (IBM T. J. Watson; tiling algorithm, debugging); J. “Ram” Ramanujam (Louisiana State University; formalization); Gheorghe-Teodor Bercea and Paul H. J. Kelly (Imperial College; tiling algorithm, performance evaluation of the Airfoil benchmark). The design and the implementation of the first sparse tiling algorithm in the OP2 library were entirely performed by the author of this thesis.
2. The work has later been extended in four directions: a more efficient sparse tiling algorithm for shared-memory architectures; support for distributed-memory architectures, with contributions from Michael Lange (Imperial College); automation in the Firedrake framework through the SLOPE library; extensive performance evaluation with a real-world application (Seigen, an elastic wave equation solver for seismological problems). SLOPE implements sparse tiling and is a by-product of this thesis.

Chapter 4 An algorithm for minimizing the operation count in a class of

local assembly kernels is devised and evaluated. This algorithm, which exploits fundamental mathematical properties of finite element operators, is proven to achieve a locally optimal operation count. Rewrite operators, such as factorization and generalized loop-invariant code motion, as well as cost models are used to this purpose. The algorithm is implemented in COFFEE, a domain-specific compiler conceived and written by the author of this thesis. COFFEE is integrated with Firedrake, a system capable of solving partial differential equations expressed in mathematical syntax through the finite element method [Rathgeber et al., 2015]. As such, the technology developed in this chapter is in use in a number of projects built on top of Firedrake.

Chapter 5 The low level optimization of the code resulting from the minimization algorithm in Chapter 4 is studied. A number of transformations, both novel (inspired by the kernel structure and/or domain properties) and well-known (although specialized to take advantage of kernel properties), are introduced. SIMD vectorization and register locality on state-of-the-art CPUs are the primary target. The implementation is carried out in COFFEE, hence the technology developed is available to Firedrake users. Some transformations – the ones which are proven to provide systematic performance improvements across a range of problems – are automatically introduced during the default optimization process performed by COFFEE. Extensive performance evaluation provides compelling evidence about the effectiveness of the transformations. In particular, the Intel Xeon Phi experimentation was performed in collaboration with Ana Lucia Varbanescu (Delft University of Technology).

Finally, Chapter 6 describes the conception, architecture and interface of COFFEE. This is a technical chapter, in which implementation choices and optimization strategies are discussed.

Summarizing, this thesis advances the state-of-the-art by introducing new performance optimizations for a class of unstructured mesh computations (with emphasis on the finite element method) and by automating them through two new software components: SLOPE and COFFEE.

1.4 Dissemination

The tools developed in this thesis are released under open source licenses. The underlying theory has been exposed to the scientific community through various publications and presentations.

Publications From this thesis derive three main publications; a further publication is planned for the most recent achievements in sparse tiling. In chronological order:

- M.M. Strout, F. Luporini, C.D. Krieger, C. Bertolli, G.-T. Bercea, C. Olschanowsky, J. Ramanujam, and P.H.J. Kelly. *Generalizing run-time tiling with the loop chain abstraction*, in Parallel and Distributed Processing Symposium (IPDPS), 2014 (Strout et al. [2014]). This conference paper generalizes sparse tiling to arbitrary sequences of irregular loops (i.e., Chapter 3, first research phase on sparse tiling, as explained in Section 1.3).
- F. Luporini, A.L. Varbanescu, F. Rathgeber, G.-T. Bercea, J. Ramanujam, D.A. Ham, and P.H.J. Kelly. *Cross-loop optimization of arithmetic intensity for finite element local assembly*, in ACM Transactions on Architectures and Code Optimizations (TACO), 2015 (Luporini et al. [2015]). This journal paper describes the work on the low level optimization of local assembly kernels (i.e., Chapter 5).
- F. Luporini, D.A. Ham, P.H.J. Kelly. *An algorithm for the optimization of finite element integration loops*, submitted to ACM Transactions on Mathematical Software (TOMS), 2016 (Luporini et al. [2016a]). This journal article introduces the operation count minimization algorithm for local assembly kernels (i.e., Chapter 4).

Other publications – the result of collaborations with people at Imperial College – are not reported here since they do not contribute directly to the thesis.

Presentations A number of formal and informal presentations were given at various conferences, workshops, and meetings. The most relevant, in chronological order, are:

- *Generalised Sparse Tiling for Unstructured Mesh Computations in the OP2 Framework*. Compilers for Parallel Computing (CPC) workshop, 2013.
- *COFFEE: an Optimizing Compiler for Finite Element Local Assembly*. FEniCS workshop, 2014.
- *Optimization of Arithmetic Intensity for Finite Element Assembly*. GungHo! workshop, 2014.
- *Cross-loop Optimization of Arithmetic Intensity and Data Locality for Unstructured Mesh Applications*. Oxford Many-core seminars, 2014.
- *Cross-loop Optimization of Arithmetic Intensity for Finite Element Local Assembly*. High Performance and Embedded Architecture and Compilation (HiPEAC) conference, 2015.
- *Generating high performance finite element kernels using optimality criteria*. SIAM Parallel Processing for Scientific Computing (PP) conference, 2016.
- *An algorithm for the optimization of finite element integration loops*. Platform for Research In Simulation Methods (PRISM) workshop, 2016.

Software The research described in this thesis has led to the development of two software components.

- COFFEE, a compiler for optimising the arithmetic intensity of expressions embedded in loop nests [Luporini, 2014a].
- SLOPE, a library for fusing sequences of loops characterized by indirect memory accesses [Luporini, 2016b].

Chapter 2

Background

The foundations of the thesis are established in this chapter. A top-down approach is followed. The first topic treated is the mathematical theory of the finite element method. How this theory is translated into software is subsequently discussed; in particular, a revolutionary approach based upon automated code generation is explored. The core libraries that make this approach possible are surveyed. The state of the art in performance optimization is then reviewed, with emphasis on the fundamental class of loop reordering transformations. An overview of the successful domain-specific abstractions that have inspired some of the core contributions of this thesis concludes the chapter. Some of the relevant related work is introduced, although extended literature review is provided in the later chapters.

2.1 The Finite Element Method

Computational methods based upon finite elements are used to approximate the solution of partial differential equations (henceforth, PDEs) in a wide variety of domains. The mathematical abstraction used in the finite element method is extremely powerful: not only does it help reasoning about the problem, but also provides systematic ways of deriving effective computer implementations. This, however, has a price in terms of complexity. Here, we limit ourselves to reviewing the aspects that are essential for understanding the contributions in Chapters 4 and 5. The content and the notation used in this section are inspired by Rathgeber

[2014], Logg et al. [2012] and Ølgaard and Wells [2010]. For a complete treatment of the subject, the reader is invited to refer to Brenner and Scott [2007].

2.1.1 Weak Formulation

In a *boundary value problem*, the solution of a (partial) differential equation subject to a set of *boundary conditions* is sought. The boundary conditions specify the behaviour of the unknown at the domain boundary.

We introduce two spaces of functions, U and V , called respectively trial space and test space. These function spaces may have desirable properties, such as differentiability. We consider the *variational* or *weak* formulation of a linear boundary value problem¹

$$\text{Find } u \in U \text{ such that } a(u, v) = L(v) \quad \forall v \in V \quad (2.1)$$

where u is the sought problem solution. In this formulation, a is a bilinear form (a map $U \times V \rightarrow \mathbb{R}$, linear in each argument separately) and L is a linear form (a linear map $V \rightarrow \mathbb{R}$). The term “variational” stems from the fact that the test function v can vary arbitrarily. The reader unfamiliar with the theory of Hilbert spaces may find this formulation unusual. The underlying idea of the variational formulation consists of “transferring” certain requirements on the unknown (e.g., differentiability) to v .

In the finite element method, the variational problem is discretized by using *discrete* trial and test spaces, namely $U_h \subset U$ and $V_h \subset V$. This leads to restating (2.1) as

$$\text{Find } u_h \in U_h \subset U \text{ such that } a(u_h, v_h) = L(v_h) \quad \forall v_h \in V_h \subset V \quad (2.2)$$

Let $\{\psi_j\}_{j=1}^N$ be a set of basis functions spanning U_h and let $\{\phi_i\}_{i=1}^N$ be a set of basis functions spanning V_h . The unknown solution u can be approximated as a linear combination of the basis functions $\{\psi_j\}_{j=1}^N$,

$$u_h = \sum_{j=1}^N \hat{u}_j \psi_j. \quad (2.3)$$

¹Non-linear problems require refinements that are out of the scope of this review.

The equation in (2.2) can then be reformulated as:

$$\sum_{j=1}^N \hat{u}_j a(\psi_j, \phi_i) = L(\phi_i), \quad i = 1, 2, \dots, N \quad (2.4)$$

From the solution of the linear system

$$Au = b \quad (2.5)$$

where

$$\begin{aligned} A_{ij} &= a(\psi_j, \phi_i) \\ b_i &= L(\phi_i) \end{aligned} \quad (2.6)$$

we determine the set of *degrees of freedom* U to express u_h . The matrix A and the vector b can be seen as the discrete operators arising from the bilinear form a and from the linear form L for the given choice of basis functions.

The underlying assumption of this formulation is that the finite dimensional subspaces U_h and V_h can be constructed. As elaborated in Section 2.1.2, U_h and V_h are constructed by decomposing the PDE domain into a set of *finite elements* and by combining the local function spaces defined on these elements.

2.1.2 Local and Global Function Spaces

In the finite element method, the domain Ω of the PDE is partitioned into a finite set of disjoint cells $\{K\}$; that is, $\bigcup K = \Omega$ and $\bigcap K = \emptyset$. This forms a *mesh*.

Finite elements As originally formalized in Ciarlet [1976], a finite element is a triple $\langle K, \mathcal{P}_K, \mathcal{L}_K \rangle$, where:

- K is a cell in the mesh with non-empty interior and piecewise smooth boundary;
- \mathcal{P}_K is a finite dimensional “local” function space of dimension n_K ;

- the set of degrees of freedom (nodes) \mathcal{L}_K is a basis $\{l_1^K, l_2^K, \dots, l_{n_K}^K\}$ for \mathcal{P}'_K , the dual space of \mathcal{P}_K .

This definition allows imposing constraints on the set of basis functions $\{\phi_1^K, \phi_2^K, \dots, \phi_{n_K}^K\}$ spanning \mathcal{P}_K . For instance, to enforce a *nodal basis* for \mathcal{P}_K – a particularly useful property for expressing solutions in U_h – we can impose that the relationship

$$l_i^K(\phi_j^K) = \delta_{ij}, \quad i, j = 1, 2, \dots, n_K \quad (2.7)$$

where δ_{ij} is the Kronecker delta, must be satisfied. This allows the expression of any $v \in \mathcal{P}_K$ as

$$v = \sum_{i=1}^{n_K} l_i^K(v) \phi_i^K. \quad (2.8)$$

Each linear functional in \mathcal{L}_K is used to evaluate one degree of freedom of v in terms of the chosen nodal basis. In other words, we can refer to both the coefficients U introduced in the previous section and \mathcal{L}_K as the degrees of freedom.

Example: the triangular degree 1 Lagrange element The following example is extracted from Logg et al. [2012]. Consider a triangular cell K and let \mathcal{P}_K be the space of polynomials of order 1 on K . Let \mathcal{L}_K be the set of bounded linear functionals representing point evaluation at the vertices \mathbf{x}^i ($i = 1, 2, 3$) of K such that

$$\begin{aligned} l_i^K : \mathcal{P}_K &\rightarrow \mathbb{R} \\ l_i^K(v) &= v(\mathbf{x}^i) \end{aligned} \quad (2.9)$$

Since if v is zero at each vertex then v must be zero everywhere, \mathcal{L}_K really is a basis for \mathcal{P}'_K , so what we have defined is indeed a finite element. In particular, if we take $\mathbf{x}^1 = (0, 0)$, $\mathbf{x}^2 = (1, 0)$, $\mathbf{x}^3 = (0, 1)$, we have that the nodal basis is given by:

$$\phi_1(\mathbf{x}) = 1 - x_1 - x_2, \quad \phi_2(\mathbf{x}) = x_1, \quad \phi_3(\mathbf{x}) = x_2. \quad (2.10)$$

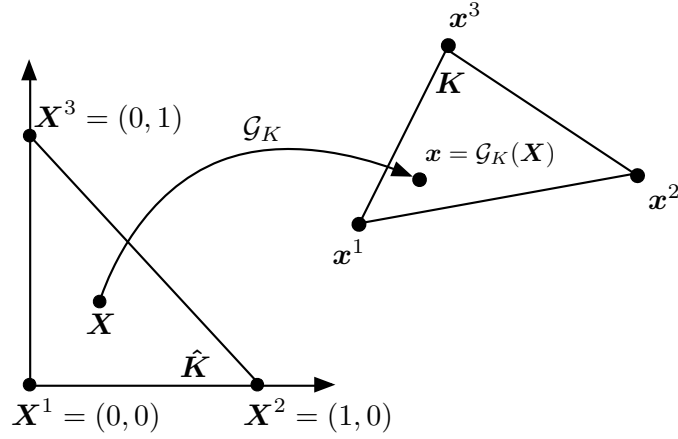


Figure 2.1: Affine mapping from the reference element \hat{K} to an element K .

Construction of the global function spaces A *local-to-global mapping* allows to patch together the finite elements to form a global function space, for instance the set of trial functions $U_h = \text{span}\{\psi_j\}_{j=1}^N$ introduced in Section 2.1.1. A local-to-global mapping is a function

$$\iota_K : [1, n_K] \rightarrow [1, N] \quad (2.11)$$

that maps the local degrees of freedom \mathcal{L}_K to global degrees of freedom \mathcal{L} . The mappings ι_K , together with the choice of \mathcal{L}_K , determine the continuity of a function space or, in simpler words, the continuity of a function throughout the domain Ω . The reader is invited to refer to Logg et al. [2012] for a comprehensive description of this step.

2.1.3 The Reference Element

One of the central aspects of the finite element method is that global function spaces are often defined in terms of a *reference finite element* $\langle \hat{K}, \hat{\mathcal{P}}, \hat{\mathcal{L}} \rangle$ and a set of invertible mappings $\{\mathcal{G}_K\}_K$ from \hat{K} to each cell in the mesh such that $K = \mathcal{G}_K(\hat{K})$. This situation is illustrated in Figure 2.1.

For each K , \mathcal{G}_K also allows to generate \mathcal{P}_K and \mathcal{L}_K . The complexity of this process depends on the mapping itself. In the simplest case, the mapping is affine; that is, expressible as $\mathcal{G}_K(\hat{x}) = M_K \hat{x} + w_K$, where M_K and w_K are, respectively, some matrix and vector.

2.1.4 Assembly

The *assembly* is the phase in which the matrix A and the vector b in (2.6) are constructed. This is accomplished by adding the contributions from each K to A and b . Let us consider the bilinear form a . Since the operator is linear, we can express a as

$$a = \sum_K a_K \quad (2.12)$$

where a_K is an element bilinear form. We can then define the local element matrix

$$A_i^K = a_K(\psi_{i_1}^K, \phi_{i_2}^K) \quad (2.13)$$

where $i \in \mathcal{I}_K$, the index set on A_i^K . That is, $\mathcal{I}_K = \{(1,1), \dots, (n_U, n_V)\}$, with n_U and n_V representing the number of degrees of freedom for the local trial functions $\psi^K \in U_h^K$ and the local test functions $\phi^K \in V_h^K$. The element matrix A^K is therefore a (typically dense) matrix of dimension $n_U \times n_V$.

Now let ι_K^U and ι_K^V be the local-to-global mappings for the local discrete function spaces U_h^K and V_h^K . We can define, for each K , the collective local-to-global mapping $\iota_K : \mathcal{I}_K \rightarrow \mathcal{I}$ such that

$$\iota_K(i) = (\iota_K^U(i_1), \iota_K^V(i_2)), \quad \forall i \in \mathcal{I}_K. \quad (2.14)$$

This simply maps a pair of local degrees of freedom to a pair of global degrees of freedom. Let \mathcal{T} be the subset of the cells in the mesh in which ψ_{i_1} and ϕ_{i_2} are both non-zero. Note that here we are considering the global functions whose restrictions to K gives $\psi_{i_1}^K$ and $\phi_{i_2}^K$. By construction, ι_K is invertible if $K \in \mathcal{T}$. At this point, we have all the ingredients to formulate the computation of A as the sum of local contributions from the elements in the mesh:

$$\begin{aligned} A_i &= \sum_{K \in \mathcal{T}} a_K(\psi_{i_1}, \phi_{i_2}) \\ &= \sum_{K \in \mathcal{T}} a_K(\psi_{(\iota_K^U)^{-1}(i_1)}^K, \phi_{(\iota_K^V)^{-1}(i_2)}^K) = \sum_{K \in \mathcal{T}} A_{\iota_K^{-1}(i)}^K \end{aligned} \quad (2.15)$$

Similar conclusions may be drawn for the linear form L . We observe that this computation can be implemented as a single iteration over all cells in the mesh. On each cell, A^K is computed and added to A using the corresponding inverse map. This approach is particularly efficient because it only evaluates the non-zero entries in the sparse matrix A . More trivial implementations are possible, although they are rarely used in practice because of the higher computational cost.

We conclude with a clarification concerning the terminology. The assembly process is often described as a two-step procedure: *local assembly* and *global assembly*. The former consists of computing the contributions of each element (i.e., the element matrices A^K); the latter represents the “coupling” of all A^K into A . As we shall see, one of the main subjects of this thesis is the computational optimization of the local assembly phase.

2.1.5 Local Assembly Example: from Math to Code

Because of its relevance in this thesis, we illustrate local assembly in a concrete example, the evaluation of the element matrix for a Laplacian operator.

2.1.5.1 Specification of the Laplacian operator

Consider the weighted Laplace equation

$$-\nabla \cdot (w \nabla u) = 0 \quad (2.16)$$

in which u is unknown, while w is prescribed. The bilinear form associated with the weak variational form of the equation is:

$$a(v, u) = \int_{\Omega} w \nabla v \cdot \nabla u \, dx \quad (2.17)$$

The domain Ω of the equation is partitioned into a set of cells (elements) T such that $\bigcup T = \Omega$ and $\bigcap T = \emptyset$. Assuming for simplicity that the sets of trial and test functions are the same and by defining $\{\phi_i^K\}$ as the set of local basis functions spanning U and V on the element K , we can express the local element matrix as

$$A_{ij}^K = \int_K w \nabla \phi_i^K \cdot \nabla \phi_j^K \, dx \quad (2.18)$$

The element vector L can be determined in an analogous way.

2.1.5.2 Monomials

In this example, the element tensor is expressed as a single integral over the cell domain. In general, it is expressed as a sum of integrals over K , each integral being the product of derivatives of functions from sets of discrete spaces and, possibly, functions of some spatially varying coefficients. We refer to such integrals as the *monomials* of the form.

2.1.5.3 Assembly with Quadrature

A_{ij}^K is numerically evaluated by means of a quadrature scheme. A quadrature scheme approximates an integral by evaluating the integrand at a set of *quadrature points*, each point multiplied with some suitable *quadrature weight*, and summing these values. By mapping the computation to a reference element as explained in Section 2.1.3 and by using the assembly procedure detailed in Section 2.1.4, a quadrature scheme for the Laplacian operator on K is as follows

$$\begin{aligned} A_{ij}^K &= \int_K w \nabla \phi_i^K \cdot \nabla \phi_j^K \\ &\approx w \sum_{k=1}^{N_q} W_k \nabla \phi_i^K(\mathbf{x}^k) \cdot \nabla \phi_j^K(\mathbf{x}^k) |\det \mathcal{G}'_K(\mathbf{x}^k)|, \end{aligned} \quad (2.19)$$

where $\{\mathbf{x}^1, \mathbf{x}^2, \dots, \mathbf{x}^{N_q}\}$ is the set of N_q quadrature points, and $\{W_1, W_2, \dots, W_{N_q}\}$ the corresponding set of quadrature weights scaled such that $\sum_{k=1}^{N_q} W_k = |\hat{K}|$.

To compute a local basis function ϕ_i^K from a reference element basis function Φ_i we exploit the inverse map \mathcal{G}_K^{-1} , which allows us to write ϕ_i^K as $\phi_i^K = \Phi_i \circ \mathcal{G}_K^{-1}$. To evaluate the gradient of a basis function ϕ_i^K at a quadrature point \mathbf{x}^k , with $\mathbf{x}^k = \mathcal{G}_K(\mathbf{X}^k)$ and $\mathbf{X}^k \in \hat{K}$, we therefore have to compute a matrix-vector product

$$\nabla_{\mathbf{x}} \phi_i^K(\mathbf{x}^k) = ((\mathcal{G}'_K)^{-1})^T(\mathbf{x}^k) \nabla_{\mathbf{X}} \Phi_i(\mathbf{X}^k). \quad (2.20)$$

The term $(\mathcal{G}'_K)^{-1}$ represents the inverse of the Jacobian matrix originat-

ing from the change of coordinates. The resulting scalar-valued expression for each entry A_{ij}^K , assuming Ω to be a domain of dimension d , reads as:

$$A_{ij}^K = \sum_{k=1}^{N_q} \sum_{\alpha_3=1}^n \phi_{\alpha_3}(\mathbf{X}^k) w_{\alpha_3} \sum_{\alpha_1=1}^d \sum_{\alpha_2=1}^d \sum_{\beta=1}^d \frac{\partial X_{\alpha_1}}{\partial x_{\beta}} \frac{\partial \phi_i^K(\mathbf{X}^k)}{\partial X_{\alpha_1}} \frac{\partial X_{\alpha_2}}{\partial x_{\beta}} \frac{\partial \phi_j^K(\mathbf{X}^k)}{\partial X_{\alpha_2}} \det \mathcal{G}'_K W^k. \quad (2.21)$$

2.1.5.4 Assembly with Tensor Contraction

Consider the case in which $\mathcal{G}_K : \hat{K} \rightarrow K$ is an affine mapping. Exploiting linearity, associativity and distributivity of the involved mathematical operators, we can rewrite (2.21) as

$$A_{ij}^K = \sum_{\alpha_1=1}^d \sum_{\alpha_2=1}^d \sum_{\alpha_3=1}^n \det \mathcal{G}'_K w_{\alpha_3} \sum_{\beta=1}^d \frac{\partial X_{\alpha_1}}{\partial x_{\beta}} \frac{\partial X_{\alpha_2}}{\partial x_{\beta}} \int_{K_0} \phi_{\alpha_3} \frac{\partial \phi_i}{\partial X_{\alpha_1}} \frac{\partial \phi_j}{\partial X_{\alpha_2}} dX. \quad (2.22)$$

A generalization of this transformation has been proposed in Kirby and Logg [2006]. By only involving reference element terms, the integral in the equation can be pre-evaluated and stored in temporary variables. The evaluation of the local tensor can then be abstracted as

$$A_{ij}^K = \sum_{\alpha} A_{ij\alpha}^0 G_K^{\alpha} \quad (2.23)$$

in which the pre-evaluated “reference tensor” $A_{ij\alpha}^0$ and the cell-dependent “geometry tensor” G_K^{α}

$$A_{ij\alpha}^0 = \int_{K_0} \phi_{\alpha_3} \frac{\partial \phi_i}{\partial X_{\alpha_1}} \frac{\partial \phi_j}{\partial X_{\alpha_2}} dX, \quad (2.24)$$

$$G_K^{\alpha} = \det \mathcal{G}'_K w_{\alpha_3} \sum_{\beta=1}^d \frac{\partial X_{\alpha_1}}{\partial x_{\beta}} \frac{\partial X_{\alpha_2}}{\partial x_{\beta}} \quad (2.25)$$

are exposed.

2.1.5.5 Qualitative Comparison of Quadrature and Tensor Contraction

Depending on form and discretization, the relative performance of the two approaches can vary quite dramatically. The presence of derivatives

or coefficient functions in the input form increases the rank of the geometry tensor, which makes the traditional quadrature mode preferable for “complex” forms, due to a lower operation count. On the other hand, the tensor contraction mode leads to significant speed-ups in a wide class of “simple” forms, in which the geometry tensor remains sufficiently small. The discretization, particularly the relative polynomial order of trial, test, and coefficient functions, also plays a key role in the resulting operation count.

2.1.5.6 Towards a new Algorithm for Local Assembly

The quadrature and tensor contraction modes have been implemented in the FEniCS Form Compiler [Kirby and Logg, 2006], which we review in later sections. In this compiler, a heuristic is used to choose the most suitable mode for a given form. It consists of analysing each monomial in the form, counting the number of derivatives and coefficient functions, and checking if this number is greater than a constant found empirically [Logg et al., 2012]. In Chapter 4, *a novel algorithm* that goes beyond the dichotomy between quadrature and tensor contraction modes will be introduced.

2.1.5.7 Code Examples

A possible C implementation of (2.21) is illustrated in Listing 1. We assume a domain of dimension $d = 2$ and polynomial order 1 Lagrange elements. The values at the quadrature points of the derivatives of the basis functions are pre-tabulated in the B and D arrays (representing, respectively, the derivatives with respect to the coordinates x and y). The values at the quadrature points of the basis functions spanning the field w are pre-tabulated in the array C. Pre-tabulation, which is made possible by mapping the computation to a reference element, is fundamental to speed up the local assembly phase. The summation over the $N_q = 6$ quadrature points is implemented by the `i` loop. The summation over α_3 for expressing w is implemented by the loop `r`. The summations over the spatial dimensions α_1, α_2 and β have been expanded in the “assembly expression” that evaluates the local element matrix A . The K array includes the four components of the inverse of the Jacobian matrix for the change

LISTING 1: A possible implementation of Equation 2.21 assuming a 2D triangular mesh and polynomial order 1 Lagrange basis functions.

```

1 void weighted_laplace(double A[3][3], double **coords, double w[3])
2 {
3     // Compute Jacobian
4     double J[4];
5     compute_jacobian_triangle_2d(J, coords);
6
7     // Compute Jacobian inverse and determinant
8     double K[4];
9     double detJ;
10    compute_jacobian_inverse_triangle_2d(K, detJ, J);
11    const double det = fabs(detJ);
12
13    // Quadrature weights
14    static const double W[6] = 0.5;
15
16    // Basis functions
17    static const double B[6][3] = {{...}} ;
18    static const double C[6][3] = {{...}} ;
19    static const double D[6][3] = {{...}} ;
20
21    for (int i = 0; i < 6; ++i) {
22        double f0 = 0.0;
23        for (int r = 0; r < 3; ++r) {
24            f0 += (w[r] * C[i][r]);
25        }
26        for (int j = 0; j < 3; ++j) {
27            for (int k = 0; k < 3; ++k) {
28                A[j][k] += (((((K[1]*B[i][k]) + (K[3]*D[i][k])) *
29                    ((K[1]*B[i][j]) + (K[3]*D[i][j])))) +
30                    (((K[0]*B[i][k]) + (K[2]*D[i][k])) *
31                    ((K[0]*B[i][j]) + (K[2]*D[i][j]))))) * det * W[i] * f0;
32            }
33        }
34    }
35 }

```

of coordinates.

The evaluation of integrals becomes more computationally expensive if the complexity of the variational form grows, in terms of number of coefficients and differential or algebraic operators involved. A scenario in which the computation of the local element tensor requires more than hundreds or even thousands of floating point operations is not pathological. An excerpt from one such example is shown in Listing 2: here, in the main assembly expression, 14 distinct arrays are accessed (with the same array referenced multiple times within the expression) along with several other constants. The loop trip counts are also larger due to the different choice of finite elements.

LISTING 2: Local assembly implementation for a Burgers problem on a 3D mesh using polynomial order $q = 1$ Lagrange basis functions.

```

1 void burgers(double A[12][12], double **coords, double **w)
2 {
3     // Compute Jacobian
4     double J[9];
5     compute_jacobian_triangle_3d(J, coords);
6
7     // Compute Jacobian inverse and determinant
8     double K[9];
9     double detJ;
10    compute_jacobian_inverse_triangle_3d(K, detJ, J);
11    const double det = fabs(detJ);
12
13    // Quadrature weights
14    static const double W[5] = {...}
15
16    // Basis functions
17    static const double B[5][12] = {...}
18    static const double C[5][12] = {...}
19    //11 other basis functions definitions
20    ...
21    for (int i = 0; i<5; i++) {
22        double f0 = 0.0;
23        //10 other declarations (f1, f2,...)
24        ...
25        for (int r = 0; r<12; r++) {
26            f0 += (w[r][0]*C[i][r]);
27            //10 analogous statements (f1, f2, ...)
28        }
29    }
30    for (int j = 0; j<12; j++) {
31        for (int k = 0; k<12; k++) {
32            A[j][k] += ...
33            + ((K[5]*F9) + (K[8]*F10))*Y1[i][j]) + ... +
34            + (((K[0]*C[i][k]) + (K[3]*D[i][k]) + (K[6]*E[i][k]))*Y2[i][j]))*f11) +
35            + (((K[2]*C[i][k]) + (K[5]*D[i][k]) + (K[8]*E[i][k]))*((K[2]*E[i][j]) + ...))) +
36            + <roughly a hundred sum/muls go here>...) *det*W[i];
37        }
38    }
39 }
40 }

```

2.2 Software Abstractions for Partial Differential Equation Solvers

The performance optimizations studied in this thesis target different layers of abstraction. In this section, we review these abstractions and established software.

2.2.1 Automating the Finite Element Method

The need for rapid implementation of high performance, robust, and portable finite element methods has led to approaches based on automated code generation. This has been proven extremely successful in the context of the FEniCS [Logg et al., 2012] and Firedrake [Rathgeber et al., 2015] projects. In these frameworks, the weak variational formulation of a problem is expressed at high level by means of a domain-specific language. The mathematical specification is manipulated by a form compiler that generates a representation of the assembly operators. Such representation may first be transformed for performance optimization and, subsequently, translated into C code, compiled and executed. This entire process occurs at run-time: both FEniCS and Firedrake were indeed written in Python to simplify the analysis of the top-level domain-specific language. When the operators are assembled, a linear system needs be solved. For this, the PETSc library [Balay et al., 2015] is employed. In the following, we expand on the components of this tool-chain that are relevant for the following chapters. We focus on Firedrake, rather than FEniCS, because all algorithms and techniques developed in this thesis have been integrated with this framework.

2.2.1.1 Problem Specification

Firedrake uses a mathematical language called UFL, the *Unified Form Language* [Alnæs et al., 2014], to symbolically express variational formulations of a problem. For this, it provides different kinds of operators, including differential and algebraic operators, as well as elementary functions. The language is unrelated to meshes, function spaces, and solvers. UFL starts analyzing the input form to collect some useful information; it then applies some preliminary transformations, such as automatic differentiation; eventually, it emits a representation suitable for the underlying compiler.

The UFL representation of the weighted Laplace operator shown in (2.17) is given in Listing 3. When constructing a finite element, three pieces of information are specified: *family*, *cell*, and *polynomial degree*. The *family* represents the element type. UFL supports several families, including the traditional *Continuous Galerkin* and *Discontinuous Galerkin* elements as well as mixed elements such as $H(\text{div})$ and $H(\text{curl})$. This makes it pos-

LISTING 3: UFL specification of the weighted Laplace operator defined in (2.17).
In orange the keywords of the language.

```

1 element = FiniteElement ('Lagrange', triangle, 1)
2
3 u = TrialFunction(element)
4 v = TestFunction(element)
5 w = Coefficient(element)
6
7 a = w*dot(grad(v), grad(u))*dx

```

sible to solve problems with different requirements on the continuity of the functions, as thoroughly described in Logg et al. [2012]. The *cell* represents the shape of the reference element: possible values include *triangle*, *quadrilateral* and *tetrahedron*. The *polynomial degree* drives the number of degrees of freedom in an element.

UFL will be used to generate kernels for experimentation; a deep understanding of the language, however, is not required for this thesis.

2.2.1.2 Form Compilers

The transformed UFL (e.g., after automatic differentiation has been applied) is passed to a form compiler, where a representation of the assembly operators is constructed. The *FEniCS Form Compiler*, or FFC, was originally used by Firedrake for this task. FFC, which supports the quadrature and tensor contraction modes illustrated in Section 2.1.5, was later modified to emit abstract syntax trees (ASTs) instead of C code. More recently, FFC has been supplanted by the *Two-Stage Form Compiler*, or TSFC. Just like FFC, TSFC emits abstract syntax trees (ASTs). The optimizations described in Chapters 4 and 5 are implemented by manipulating these ASTs in a lower-level compiler, COFFEE, whose structure will be outlined in Chapter 6.

TSFC has two main features:

- It is a *structure-preserving compiler* in that it keeps intact the structure of algebraic operations (e.g., index sums, inner products), rather than committing to a specific implementation. This lets the lower-level compiler to explore the space of all possible transformations.
- In contrast to FFC, it supports the compilation of complicated forms characterized by extensive use of tensor algebra. TSFC can effi-

ciently identify repeated sub-expressions and assign them to temporary variables, thus drastically reducing the code generation time.

Summarizing, in Firedrake the translation of the problem specification is characterized by a neat separation of concerns:

- UFL is the mathematical language to express weak formulations of problems.
- TSFC progressively lowers the finite element specification by producing a general AST. Some nodes in the ASTs are decorated to keep track of domain properties (e.g., linearity of an expression in test and trial functions), exploitable in later optimization stages.
- COFFEE applies code transformations for improving the performance of the operators returned by TSFC.

The conception and the design of the COFFEE layer, as well as its optimization algorithms, are amongst the main contributions of this thesis. These topics are treated in Chapters 4, 5 and 6.

2.2.1.3 Iteration over the Mesh

Finite element problems require the application of computational *kernels* over the discretized equation domain. In Firedrake, this is accomplished through *PyOP2*, a domain specific language embedded in Python relying on just-in-time compilation and execution [Markall et al., 2013].

Several kinds of kernels may need be executed in a Firedrake program. Computationally expensive kernels arise from the assembly operators presented in Section 2.1.4. Other kernels are required for the application of boundary conditions as well as for the interpolation and projection of fields. The fact that a kernel is a local operation – its application on an element of the mesh is independent of the application on any another element – suits parallel execution naturally. This does not mean, however, that parallelizing a finite element computation is straightforward. As clarified in Section 2.2.2, a kernel can update a field either directly or indirectly. In the latter case, a subset of values, for instance the degrees of freedom at the boundary between two elements, may receive contributions from two different processes/threads, which requires non-trivial coordination.

PyOP2 supports the parallel application of kernels over unstructured meshes, a key requirement for the finite element method. It also provides global data structures such as sparse matrices, which are essential when it comes to solve linear systems.

The PyOP2 abstraction implements another separation of concerns. The kernels, which encode the numerics of the finite elements formulation of a problem, are produced at higher layers through the Firedrake’s language and form compiler, while the parallel application of kernels over the mesh is entirely handled by PyOP2.

The PyOP2 layer, and its relationship with the OP2 library Giles et al. [2011], are documented in more detail in Section 2.2.2.

2.2.1.4 Unstructured Meshes

PyOP2 represents meshes by means of sets and fixed-arity maps. Possible sets are topological entities such as cells or degrees of freedom. A map is an object describing the adjacency relationship between the elements of two distinct sets (e.g., a map from cells to degrees of freedom). Sets and maps are constructed at a higher layer, in particular by Firedrake with the help of an additional software module, PETSc’s *DMplex* [Lange et al., 2015].

DMplex is a data management abstraction representing unstructured mesh data through direct acyclic graphs. It relieves PyOP2 of the duty of handling complex operations such as partitioning for parallel execution and reordering for efficient memory accesses. The abstraction used in DMplex is very flexible, so a number of optimizations are enabled. For instance, the fact that partition boundaries can be made arbitrarily deep facilitates communication-computation overlap, as well as the introduction of low level transformations such as loop fusion (a contribution of this thesis, Chapter 3).

2.2.1.5 Solving systems of equations

One of the key ideas behind the success of Firedrake is relying on available software to implement specific components of the finite element method. This philosophy is also applied to the solution of linear systems, for which

the *Portable, Extensible Toolkit for Scientific Computation* library [Balay et al., 2015], or PETSc, is employed.

PETSc is entirely implemented in C, although its Python interface *petsc4py* makes it accessible by a framework like Firedrake. It provides a wide range of parallel algorithms for solving linear and nonlinear systems, as well as a considerable number of options to drive the solvers. Similarly to Firedrake, PETSc never attempts to reinvent science: many functionalities are implemented on top of existing libraries (e.g., BLAS) or offered via third-party implementations through suitable wrappers.

2.2.2 The PyOP2 and OP2 Libraries

PyOP2 is inspired by and shares many ideas with OP2² [Giles et al., 2011], although it differs in a few yet significant ways. In this section, we first describe the common features and then focus on the aspects that are peculiar to PyOP2.

2.2.2.1 Programming Model

OP2 offers abstractions for modeling an unstructured mesh, in terms of *sets* (e.g. vertices, edges), *maps* between sets (e.g., a map from edges to vertices to express the mesh topology), and *datasets* associating data to each set element (e.g. 3D coordinates to each vertex).

OP2 programs are expressed as sequences of parallel loops, or `op_par_loop`. A simplistic example is provided in Listing 4. Each loop applies a computational *kernel* to every element in a mesh set. These kernels can access data associated to either the loop iteration set (direct access) or to other sets (indirect access) through maps. Maps are implemented as arrays of indices, so an indirect access requires, from a computational viewpoint, an additional memory access (e.g., `A[B[i]]`).

The running example includes three parallel loops. Let us focus on the first of them. This loop iterates over the `edges` set (whose declaration is omitted for brevity), as indicated by the first parameter of the `op_par_loop` function. The loop applies `kernel1` to every element in the indicated iteration space, i.e. to each edge. `kernel1` reads data associated to an

²The name OP2 indicates that this is the second software engineering iteration of the OPlus library, or Oxford Parallel Library.

LISTING 4: Section of a toy (Py)OP2 program. OP2 syntax is used.

```
1 void kernel1 (double * x, double * tmp1, double * tmp2) {  
2     *tmp1 += *x;  
3     *tmp2 += *x;  
4 }  
5  
6 // loop over edges  
7 op_par_loop (edges, kernel1,  
8             op_arg_dat (x, -1, OP_ID, OP_READ),  
9             op_arg_dat (temp, 0, edges2vertices, OP_INC),  
10            op_arg_dat (temp, 1, edges2vertices, OP_INC))  
11  
12 // loop over cells  
13 op_par_loop (cells, kernel2,  
14             op_arg_dat (temp, 0, cells2vertices, OP_INC),  
15             op_arg_dat (temp, 1, cells2vertices, OP_INC),  
16             op_arg_dat (temp, 2, cells2vertices, OP_INC),  
17             op_arg_dat (res, -1, OP_ID, OP_READ))  
18  
19 // loop over edges  
20 op_par_loop (edges, kernel3,  
21             op_arg_dat (temp, 0, edges2vertices, OP_INC),  
22             op_arg_dat (temp, 1, edges2vertices, OP_INC))
```

edge (direct access) and increments the two adjacent vertices with the read value (indirect access). This information, essential for parallelization and optimization, is indicated to OP2 through the *access descriptors*, or `op_arg_dat`. The first access descriptor uses the special keyword `OP_ID` for the data array `x`, which simply means that `x` is being accessed directly, i.e. with the identity function. In addition, it tells through `OP_READ` that such access is of type read. The second and third access descriptors express that `temp`, a dataset associated with vertices, will be incremented (`OP_INC`) by `kernel1`, and that this increment occurs indirectly through the map `edges2vertices`. The index array `edges2vertices` maps each edge index into the indices of its two incident vertices, with the integer values of 0 and 1 in the access descriptors indicating which of the two vertices should be considered.

2.2.2.2 Execution Model for Shared-Memory Parallelism

A fundamental property of parallel loops is that the execution order of iterations does not influence the result. The shared-memory parallelization of a loop in OP2 (and PyOP2) exploits this property. In essence, the iteration space is partitioned and different partitions are executed concurrently by distinct threads, with the restriction that indirect increments to

data values shared by two or more partitions must be serialized.

Consider again the first loop of the running example. The edges iteration set is partitioned. Partitions that share values associated with `temp` are considered adjacent (from a topological point of view, these are the partitions connected through one or more vertices). The accesses to `temp` are of type increment, so the adjacent partitions are considered conflicting and are assigned a different color. At run time, partitions with the same color can be executed in parallel, while partitions with different colors will be scheduled serially. The execution of elements inside a partition is serialized, since each partition is executed atomically by a single thread. This scheme prevents race conditions by construction.

This process is applied on a per-loop basis and is implemented exploiting the information provided through the access descriptors. Optionally, external libraries can be used to reorder the partitions so that data locality is improved.

2.2.2.3 Execution Model for Distributed-Memory Parallelism

Distributed-memory parallelism is conceptually simpler than shared-memory parallelism. During the OP2 initialization phase, sets, maps, and datasets are partitioned and then distributed to different processes. For executing a parallel loop, MPI messages may need be exchanged to update any out-of-date values along the partition boundaries. This phase is overlapped with the execution of a set of local, or “core”, iterations. Once both phases have finished, the remaining boundary iterations are computed.

To implement this parallelization scheme, the iterations of each locally stored OP2 set are divided into four contiguous regions:

Core Iterations owned that can be processed without reading halo data.

Owned Iterations owned that can be processed only by reading halo data.

Exec halo Off-process iterations that are redundant executed because they indirectly access owned iterations.

Non-exec halo Off-process iterations that only need be read to compute the exec halo iterations.

This situation is depicted in Figure 2.2. Clearly, a good partitioning maximizes the ratio between the sizes of the core and non-core regions.



Figure 2.2: Distributed-memory parallelism in OP2 and PyOP2. Matching colors represent identical subsets of iterations. The image was inspired by an example in Rathgeber [2014].

2.2.2.4 PyOP2 Features

PyOP2 distinguishes itself from OP2 in a number of ways.

- An OP2 program is analyzed statically. A source-to-source compiler produces a legal C program, which can subsequently be compiled and executed. PyOP2, on the other hand, is implemented in Python, so code generation occurs at run-time; the generated C code applies a computational kernel over a set of elements. One problem with OP2 is that its source-to-source compiler is quite limited in the analysis of input programs. PyOP2 does not have this problem, because objects like sets, maps and parallel loops are constructed and inspected during the interpretation of the source program itself. This makes PyOP2 easily composable with other layers, as proven in the context of the Firedrake project. A hierarchy of “software caches” is however needed in PyOP2 to minimize the overhead due to redundant actions (e.g., generating code each time the same parallel loop is encountered).
- Despite sharing relevant constructs (e.g., sets, maps), the PyOP2 do-

main specific language tends to be more compact and expressive than the OP2 counterpart. This is again a consequence of the run-time analysis.

- PyOP2 supports global sparse matrices, basic linear algebra operations and mixed types (e.g., mixed sets), which are essential features for integration with a finite element framework. OP2 has none of these.
- OP2 completely handles distributed-memory parallelism, including partitioning and distribution of data structures as well as mesh renumbering for increased data locality. PyOP2, as explained in Section 2.2.1.4, relies on an external software module, DMPlex, for these functionalities. DMPlex is much more versatile than OP2, and this plays a key role in performance optimization, as explained in Chapter 3.

2.2.3 Stencil Languages

A stencil defines how to access a set of values associated with a mesh element (e.g., vertex, cell) and its neighboring elements. In the literature, the word “stencil” is often used to refer to the special case in which the access rule is an affine function. This is the case of computational methods based on structured meshes, such as the finite difference method. However, since this thesis focuses on unstructured meshes, we generalize this notion. We characterize a stencil as follows:

Stencils for structured meshes Given an element i in the mesh, a stencil is a vector-valued function $f(i) = [f_1(i), f_2(i), \dots, f_n(i)]$ which retrieves the n elements that need to be updated when accessing i . A function f_j is affine and usually takes the form $f_j(i) = i * h + o$, with $h, o \in \mathbb{N}$.

Stencils for unstructured meshes Given an element i in the mesh and an affine access function g , a stencil is a vector-valued operator $f(i, g) = [f_1(i, g), f_2(i, g), \dots, f_n(i, g)]$ which retrieves the n elements that need to be updated when accessing i . A function f_j is non-affine and usually takes the form $f_j(i, g) = g(i) * h + o$, with $h, o \in \mathbb{N}$.

2.2.3.1 Stencil Languages for Unstructured Meshes

OP2 is an example of a language for implementing stencil-based computations on unstructured meshes. The maps in the OP2 language implement non-affine stencils.

Yet another example of language for unstructured mesh stencils is Liszt [DeVito et al., 2011]. Like OP2, Liszt supports multiple architectures, including distributed-memory execution via MPI and GPUs. The language is less flexible than OP2's, though. Meshes are constructed by composing the abstract data types of the language, namely vertices, edges, faces and cells, and fields can only be associated with these types. This is on one hand helpful, as the stencils can automatically be inferred (assuming that the mesh topology does not change over time), but on the other hand it makes integration with a finite element framework difficult, or simply unnatural. Consider the case³ in which quadratic or higher-order basis functions on triangles are used. The degrees of freedom are associated with both vertices and edges. In OP2, this is naturally expressible by defining a map between cells and degrees of freedom, whereas in Liszt one needs to manage two different fields (one for the degrees of freedom on the vertices and the other for those on the edges). A computation in Liszt is expressed through sequences of *for-comprehensions* over mesh elements. The for-comprehensions can be arbitrarily nested. One of the key prerequisites is that each field in a for-comprehension nest has a fixed state, one among read, write, or increment (for local reductions). This allows the compiler to automatically perform useful actions such as scheduling transformations (e.g., by rearranging iterations in a for-comprehensions nest) and placement of MPI calls. The Liszt compiler derives data dependency information automatically, while OP2 relies on access descriptors.

2.2.3.2 Stencil Languages for Structured Meshes

The field of domain specific languages for structured mesh computations has received a large number of contributions over the last decade.

SBLOCK [Brandvik and Pullan, 2010] is a Python framework for expressing computations using structured stencils. The run-time support

³The example was extracted from Rathgeber [2014]

automatically generates low-level code for multi-node many-core architectures. Mint is a framework based on pragma directives targeting GPUs that has been used to accelerate a 3D earthquake simulation [Unat et al., 2012]. Other stencil languages relying on auto-tuning systems for increasing the performance of the generated code were presented in Zhang and Mueller [2012], Datta et al. [2008], Christen et al. [2011].

An interesting approach is adopted in Pochoir [Tang et al., 2011], in which a compiler translates the high-level specification into cache-oblivious algorithms for multi-core CPUs. Interestingly, an attempt at integrating this system with a higher-level domain-specific language for finite difference methods failed due to constraints on the programming interface [Sun, 2016].

A stencil language explicitly aiming for generation of highly-efficient vector code was presented in Henretty et al. [2013].

In spite of a large research effort, it is however not clear whether and to what extent these languages have been adopted in production code.

2.3 Compilers and Libraries for Loop Optimization

In this section, we review state-of-the-art compilers and libraries for loop optimization. This will provide the necessary background for the contributions presented in Chapters 3 and 5.

2.3.1 Loop Reordering Transformations

The study of high level transformations for the optimization of loops in imperative languages dates back to the sixties. The initial focus was on techniques for improving data locality in loop nests; this was motivated by the observation that many programs spend a considerable fraction of time in executing these regions of code. A survey on the main results achieved between the sixties and the nineties was provided by Bacon et al. [1994]. Over the last twenty years, there has been a great deal of effort in trying to improve the effectiveness of loop transformations, as well as in developing tools for automating them. General-purpose compilers have become increasingly sophisticated (especially the *Intel* and *Cray* compilers), although they still often miss powerful optimization opportunities.

This is usually a consequence of complex or unstructured codes for which the analysis is too difficult or the lack of domain information. Polyhedral compilers, discussed in Section 2.3.3, are particularly effective in relatively simple affine loop nests, but there is no compelling evidence that analogous results could systematically be achieved in real-world applications.

A class of optimizations relevant for this thesis is the one based on the *reordering* of loop nest iterations. Well-known optimizations belonging to this class are:

Interchange This transformation consists of exchanging the position of two loops in a nest. Possible objectives are exposing as innermost loop a vectorizable dimension or increasing data locality.

Reversal When a loop is “reversed”, the order in which its iterations are executed is flipped. For instance, the reverse of a loop iterating from 0 to $n - 1$ with unitary increment is a loop from $n - 1$ to 0 with unitary decrement. This transformation can enable other transformations or, under certain circumstances, eliminate the need for some temporary variables.

Skewing Loop skewing, sometimes also called “time skewing” or “time tiling”, aims to improve data reuse and to expose parallelism in wave-front computations. In these computations, one or more arrays are updated at every loop iteration and the updates propagate like a wave over the subsequent iterations (e.g., $A[i][j] = f(A[i-1][j], A[i][j-1])$). We expand on loop skewing in Section 2.3.2.

Fission Sometimes also referred to as loop distribution, loop fission “splits” a loop into a sequence of loops. The new loops have the same iteration space as the original one, but include only a subset of statements. This may improve or even affect data locality in a loop accessing a significant number of datasets. Increase in loop overhead is a negative effect of the transformation.

Further, to this class of optimizations belong the two fundamental loop reordering transformations studied in Chapter 3 in the context of unstructured stencils:

Fusion A sequence of loops can be fused, or “merged”, to improve data locality and reduce loop overhead. In the simplest instance, all loops in a sequence have the same iteration space and, given S_1 a statement in a first loop and S_2 a statement in a subsequence loop, S_2 does not modify any data read by S_1 . In such a case, applying loop fusion is straightforward. In general, however, loops can have different bounds and the data dependencies in a set of statements may be non-trivial. In these cases, loop fusion becomes more challenging, or simply not feasible. The loop fusion problem has been tackled formally by Darte [2000].

Tiling Also known as *blocking*, loop tiling is probably one of the most studied and powerful transformations. Its main goal is improving data locality, although it is also sometimes used to extract parallelism. The basic idea is to “chunk” the iteration space of a loop nest into partitions of a given shape. This requires major changes to the loop nest structure, as shown in Listing 5. In this example, square-shaped tiles are executed with the objective of increasing data reuse along the j dimension. Depending on properties of the loop nest such as data dependency pattern and control flow, automating or even just implementing tiling may pose significant challenges. In particular, tiling a loop nest in presence of stencils is a non-trivial problem. Early work on this transformation was presented in Irigoin and Triolet [1988] and Ramanujam and Sadayappan [1992]. More recent studies have tackled automation and effectiveness of the tiling algorithms, such as Bondhugula et al. [2008], Acharya and Bondhugula [2015], Klöckner [2015]. The impact of the tile shape has been investigated by Grosser et al. [2014] and Krishnamoorthy et al. [2007b].

2.3.2 Composing Loop Tiling and Loop Fusion

Reordering transformations can be composed for improving their effectiveness. A case of particular interest for this thesis is the composition of loop fusion and loop tiling, in which a sequence of loops is fused by

⁴The example is partly extracted from www.netlib.org/utk/papers/autoblock/node2.html

LISTING 5: Illustration of loop tiling in a classic matrix-matrix multiplication kernel⁴. The matrices are square of size $N \times N$. If b is chosen small enough to fit some level of cache, data reuse can be achieved.

```

1 // Original implementation
2
3 for i = 1 to N, 1
4   for j = 1 to N, 1
5     for k = 1 to N, 1
6       C[i][j] += A[i][k]*B[k][j];
7
8
9 // Tiled implementation
10
11 for i0 = 1 to N, b
12   for j0 = 1 to N, b
13     for k0 = 1 to N, b
14       for i = i0 to min(i0+b-1, N)
15         for j = j0 to min(j0+b-1, N)
16           for k = k0 to min(k0+b-1, N)
17             C[i][j] += A[i][k]*B[k][j];

```

grouping multiple blocks of iterations into tiles. Such a transformation can turn data reuse across consecutive loops into data locality, thus optimizing memory bandwidth and memory latency. Composing loop fusion and loop tiling is complicated; automation is even more challenging, especially depending on the kind of stencils that need to be supported.

In the domain of computational methods for approximating the solution of PDEs, the composition of loop fusion and loop tiling is often referred to as *time tiling*. In these codes, a sequence of loops over the spatial dimensions is repeatedly executed within a time loop; time tiling fuses the spatial loops by building tiles crossing the time dimension. Time tiling has extensively been studied for structured stencil codes [Bondhugula et al., 2014, Holewinski et al., 2012, Zhou et al., 2012, Bondhugula et al., 2008]. It has instead received very limited attention in the context of unstructured stencil codes – where it is also known as *sparse tiling* [Strout et al., 2002] – because of the complexity inherent in performing data dependence analysis. Prior to this thesis, sparse tiling had only been applied “manually” to individual benchmarks, through “ad-hoc” strategies. In Chapter 3, the state-of-the-art is advanced by introducing:

- A technique for applying sparse tiling to *arbitrary* sequences of loops that are expressible with the *loop chain abstraction* [Krieger et al., 2013]. This contribution was a joint effort with the authors in Strout

et al. [2014].

- A system that automates this technique and enables execution on distributed-memory architectures.

With plain loop tiling (i.e., in the absence of loop fusion), a tile can be represented as a single block of iterations. This has been explained in the previous section and illustrated in Listing 5. Time and sparse tiling generalize this idea. The fused loops may either differ in iteration space or be characterized by non-trivial data dependencies. For constructing a legal scheduling, tiles need be assigned multiple blocks of iterations, one for each of the fused loops. To this purpose, there exist two different approaches:

Split tiling Tiles are constructed such that all data dependencies are satisfied and are executed according to a partial ordering. Many split tiling schemes have been studied for structured stencil codes. These schemes, which take the name of the tile shape they end up producing (such as *hexagonal* or *diamond* tiling), differ in the achieved trade-off between parallelism and data locality. The geometrical shape of a tile can be visualized by plotting the fused iteration space and by grouping iterations based on the tile they belong to.

Overlapped tiling Different tiles share subsets of iterations. A shared iteration is “owned” by only one tile and is executed redundantly by the set of overlapping tiles. These tiles store intermediate values into “ghost” regions of memory. This approach removes the need for a partial execution ordering, at the price of redundant computation.

Some of these approaches have been reviewed in Grosser et al. [2013]. In this thesis, we will employ a mixed split-overlapped sparse tiling scheme for unstructured stencil codes, suitable for execution on distributed-memory architectures.

2.3.3 Automation via Static Analysis

There are two alternatives for automating loop reordering transformations. Both of them rely on static analysis of source code:

Graph-based Representation General-purpose compilers analyze the source code and produce an intermediate representation (IR) based on a graph-like data structure (e.g., the static single assignment form, or SSA, in the LLVM compiler). Some kind of data dependence analysis asserts the legality of a transformation, while cost models are used to predict its impact on performance. Some compilers can expose the cost models directly to the user by textual reports. Users have some form of control over the optimization process: pragma directives can be used to choose explicitly how to optimize a loop nest (e.g., to set a specific unroll factor or to enforce vectorization), while compiler parameters allow tuning global optimization heuristics.

Polyhedral Model Several research compilers, and more recently also a fork of the LLVM compiler through a module called Polly [Grosser et al., 2012], can introduce reordering transformations based on geometric representations of loop nests. To model a loop nest as a *polyhedron*, two conditions must be satisfied: (i) loop bounds as well as array indices must be affine expressions in the enclosing loop indices and (ii) pointer aliasing must be known at compile-time. These conditions are often necessary in the case of graph-based IRs too, although in a more relaxed fashion (e.g., the Intel compiler can vectorize, to some extent, non-affine loop nests). Polyhedral compilers target parallelism and data locality by composing *affine scheduling functions*. A schedule defines the order in which the statement instances of a loop nest are executed; a scheduling function can be applied to change the original order. Once the polyhedron is available, different scheduling functions can be compared and applied.

If, on one hand, general-purpose compilers using graph-based IRs have now reached an impressive level of sophistication (our experience with the Cray and Intel autovectorization systems is remarkably positive), there is still quite a lot of debate on the effectiveness of polyhedral compilers. One of the main reasons is the lack of evidence: the performance evaluation of state-of-the-art polyhedral compilers is typically conducted on simplistic benchmarks that do not reflect the complexity of real-world applications. We will expand on this matter in Section 3.3.

The fact that we focus on unstructured stencil codes, which render the

loop nests non-affine, precludes the adoption of polyhedral compilers. Recently, there has been an effort in extending the polyhedral model to non-affine loops [Venkat et al., 2014], but it is far from clear whether this technology will ever be applicable in the real-world applications we are interested in.

2.3.4 Automation via Dynamic Analysis

If a stencil is unstructured, the memory access pattern is characterized by indirect accesses that can only be resolved at execution time. In such a case, loop reordering transformations can be enabled through inspector/executor strategies, as originally proposed by Salz et al. [1991]. Informally, an inspector is an additional piece of code that, at run-time, captures the data dependency pattern of an irregular loop nest into a suitable data structure. An executor is semantically equivalent to the original loop nest, but performs the iterations in a different order exploiting the information produced by the inspector. Examples of reordering transformations through inspector/executor schemes were provided by Strout et al. [2003].

To automate a reordering transformation in the presence of unstructured stencils, a compiler replaces loops with suitable inspector/executor schemes. Prior to this thesis, no compilers were capable of introducing complex transformations such as sparse tiling.

2.4 Domain-Specific Optimization

By restricting the attention to relatively narrow classes of programs, it is often possible to identify optimization opportunities that will be missed by general-purpose or polyhedral compilers. This is because, for instance, such optimizations rely on special mathematical properties of the problem being tackled. Most of the contributions in Chapters 3, 4 and 5 exploit this observation. In this section, we review some of the domain-specific optimization systems that inspired our work.

2.4.1 Tensor Contraction Engine

The Tensor Contraction Engine (TCE) is a successful project that turns the mathematical structure of expensive computations in the field of quantum chemistry into powerful optimizations [TCE contributors]. These codes need to execute long sequences of tensor contractions, or generalized matrix multiplications, which can easily result in teraflops of computation and terabytes of data for simultaneously storing huge dense matrices. The TCE provides a domain-specific language to express formulae in a mathematical style. The mathematical specification is transformed into low-level code while undergoing several optimization steps. Transformations aimed at reducing the operation count [Hartono et al., 2006, 2009] and finding the best trade-off between redundant computation and data locality [Lam et al., 2011], as well as low-level optimization [Lu et al., 2012] are applied in this framework. Many of these optimizations exploit the mathematical structure inherent in tensor contractions.

In Chapter 4 we use a similar approach for optimizing the operation count of finite element operators – we exploit the mathematical property that these operators are linear in test and trial functions to identify effective factorizations.

2.4.2 Halide

Ragan-Kelley et al. [2013] recently introduced Halide, a high level language for expressing image processing kernels. The run-time optimization system, which relies on auto-tuning to explore the transformation space, has been demonstrated to achieve a performance at least comparable to that of hand-written (and hand-optimized) codes, and in many cases to outperform them. Halide is a successful contribution to the landscape of domain-specific languages, as it is currently employed for development of production code by several companies⁵.

In Halide, an image processing pipeline is a sequence of interconnected stages. Each stage applies a numerical kernel – usually a structured stencil – to its input. Numerical kernels are pure functions applied over a 2D domain representing the image being processed. In realistic cases, an

⁵At least Google and Adobe have declared that some of their groups (more than 30 researchers and developers in total) are actively using Halide.

image processing pipeline can be quite complex and include even up to a hundred stages. What makes Halide powerful from the viewpoint of optimization is the fact that the schedules are decoupled from the numerical kernels. A schedule describes aspects like the iteration ordering and the trade-off between temporary values and redundant computation. These optimizations are fundamental in image processing pipelines and, as such, are treated as first-class citizens by Halide. Different schedules can be explored automatically or provided as user input.

2.4.3 Spiral

Spiral is a pioneering project on automated code generation starting from a high level specification of a mathematical problem [Püschel et al., 2005]. The domain of interest is digital signal processing (DSP). Spiral generates highly optimized DSP algorithms, such as the discrete Fourier transform, and autonomously tunes them for the underlying platform. To achieve that, the mathematical specification of a DSP algorithm is first transformed according to a set of rewrite rules. The resulting formulae are translated into an intermediate language, which enables a set of optimizations, including explicit vectorization and parallelization. Finally, low level code is produced, compiled, executed and timed. The last phase provides feedback to the system so that increasingly optimized implementations can be generated.

Spiral leverages the mathematical specification to apply powerful optimizations. The rewrite rules system itself is essential to simplify complex formulae. Another example is the loop fusion framework [Franchetti et al., 2005], which exploits mathematical properties to detect loop fusion opportunities that would be missed by lower level compilers.

2.4.4 Small-scale Linear Algebra

In several fields, such as graphics, media processing and scientific computing, many operations can be cast as small-scale linear algebra operations. By small-scale we mean that the size of some of the involved tensors can be as small as a few units, and only occasionally exceed a few hundreds elements. Despite the small size, it is important to optimize these operations because they may be applied iteratively (e.g., in a time-stepping

loop), thus accounting for a significant fraction of the overall execution time.

Libraries for linear algebra are tuned for large-scale problems and they become inefficient when tensors are small. Novel approaches, mostly centred on auto-tuning, have been developed over the last decade. In the domain of scientific computing, it is worth mentioning the technique employed by the finite element code *nek5000* [Fischer et al., 2008] to optimize small matrix multiplications [Shin et al., 2010]. A set of highly-optimized routines, each routine specialized for a particular size of the input problem, are generated and tuned for the underlying platform. At run-time, a dispatcher function picks one of such routines, based on the size of the input matrices. A higher level approach has recently been presented in Spampinato and Püschel [2014], in which the *LGen* language is used to write composite linear algebra operations. A set of rewrite rules and a transformation system deeply inspired by Spiral are used for optimization. Other famous libraries optimized for small-scale tensor operations are *LIBXSMM* [Heinecke et al., 2016] and *BLIS* [Van Zee and van de Geijn, 2015].

The field of small-scale linear algebra optimization systems is interesting because some techniques could be used for low-level optimization of finite element local assembly, a topic treated by this thesis in Chapter 5.

2.5 On the Terminology Adopted

Throughout the thesis we employ a standard terminology, very close to the one used in reference textbooks such as [Hennessy and Patterson, 2011]. We here review a set of relevant keywords. This will especially be useful when discussing the performance achieved by the proposed optimizations.

Compilers

General-purpose compiler With this term we generically refer to any open-source or commercial compilers capable of translating low level source code (e.g., Fortran, C, C++) into machine code. Examples are the GNU (*gcc*), Intel (*icc*), Cray and LLVM compilers. With “general-

purpose” we aim to distinguish the aforementioned compilers from all other higher level compilers, such as those based on the polyhedral model or those used for translating domain specific languages.

(Auto)vectorization Vectorization is a well-known paradigm that generalizes computation on scalars to computation on vectors – that is, arrays of contiguous elements. A single instruction, multiple data (SIMD) computation is one that employs vectorization to carry out a sequence of instructions. SIMD architectures, which are nowadays ubiquitous, emit vector code in two circumstances: (i) sections of a program are explicitly vectorized (e.g., through high level libraries, intrinsics instructions, or assembly code); (ii) a compiler transforms scalar code into vector code. The latter case is often referred to as autovectorization, since SIMD instructions are generated without user intervention. When possible and if demonstrated to be effective, autovectorization should be preferred over explicit vectorization for portability reasons. Autovectorization is typically applied to inner loops, although block vectorization [Larsen and Amarasinghe, 2000] is also supported by more advanced compilers (e.g., Intel’s).

Performance and Cost Models

(High) Memory pressure This is often used to emphasize the fact that one or more levels of the memory hierarchy (e.g., RAM, caches, registers) are stressed by a relatively large number of load/store instructions. A high memory pressure is often responsible for performance degradation.

Memory- and CPU-boundedness A section of code can be either CPU-bound or memory-bound. In the former case, the performance achieved is limited by the operation throughput of the CPU; in the latter case, the memory bandwidth or the memory latency are the limiting factors. The loop reordering transformations reviewed in Section 2.3 tackle memory-boundedness; for example, both tiling and fusion aim to maximize the cache hit ratio, thus reducing latency and memory pressure. Many domain-specific optimizations, as discussed in Section 2.4, target instead CPU-boundedness; for example, the Ten-

sor Contraction Engine and Spiral manipulate mathematical formulae to reduce the operation count of the resulting kernels.

Operational intensity and Roofline Model This parameter defines the ratio of total operations to total data movement (bytes) between the DRAM and the cache hierarchy for a given section of code. The operational intensity, which “*predicts the DRAM bandwidth needed by a kernel on a particular computer*”, is useful to derive *roofline plots* [Williams et al., 2009]. A roofline plot is particularly helpful to study the computational behaviour of a program, since it provides an insightful means to understand what the performance bottleneck is and, therefore, what kind of optimization is most useful.

Arithmetic intensity Sometimes, the term *arithmetic intensity* is used in place of *operational intensity*. The differences are that only the fraction of arithmetic operations emitted, instead of all operations, is considered and that the total data movement is to be interpreted as between the CPU and the last level of cache.

Miscellanea

Access function An access function specifies how the elements of an array are accessed. Usually, these are functions of one or more loop indices. Access functions can be constant, affine or non-affine, as already shown in Section 2.2.3.

Local and global reductions A reduction is a commutative and associative operation that is applied to a set of values to produce a scalar. For instance, the sum of a set of numbers is a reduction. In mesh-based computations, it is useful to distinguish between local and global reductions. A reduction is local if only applied to a (typically small) subset of mesh elements. A reduction is global if applied to an entire set of elements (e.g., a field associated with a set of degrees of freedom), thus introducing a global synchronization point in the computation.

Communication A communication indicates a generic form of interaction between two or more entities. The most obvious case is when two

processes on two different cores communicate explicitly via message passing; if the cores are on the same node the communication occurs via memory, whereas if they are on different nodes both the network and the memory are needed. However, the term can also be used in more general scenarios. We can say, for instance, that two tiles in a blocked iteration space communicate if their execution needs be synchronized. Intuitive terms like *communication-avoiding* or *communication-computation overlap* are often used to classify optimizations that aim to minimize communication.

Chapter 3

Automated Sparse Tiling for Irregular Computations

Many numerical methods for partial differential equations (PDEs) are structured as sequences of parallel loops. This exposes parallelism well, but does not convert data reuse between loops into data locality, since their working set is usually too big to fit in some level of cache. In Section 2.3.3, it was explained that loop fusion and loop tiling may be used to retain some of this potential data locality. This chapter introduces a mixed compiler/library system capable of applying these transformations to sequences of irregular loops, automatically. Challenges deriving from real-world applications are addressed. As reiterated throughout the chapter, parts of this work are the result of a joint collaboration with Strout et al. [2014].

3.1 Motivation

The focus of this chapter is improving data locality in unstructured mesh PDE solvers, such as those based on the finite volume or the finite element methods. Here, the loop-to-loop dependence structure is data-dependent due to indirect references such as `A[map[i]]` (see Sections 2.2.2 and 2.2.3). The `map` array stores connectivity information, for example from elements in the mesh to degrees of freedom. A similar pattern occurs in molecular dynamics simulations and graph processing, so both the theory and the tools that we will develop in this chapter are generalizable to these

domains.

Three motivating real-world applications for this work are Hydra, Volna and Seigen. Hydra [Reguly et al., 2016] is a computational fluid dynamics application used at Rolls Royce for the simulation of next-generation components of jet engines. Volna [Dutykh et al., 2011] is a computational fluid dynamics application for the modelling of tsunami waves. Seigen aims to solve the elastic wave equation using the discontinuous Galerkin finite element method for energy exploration purposes. All these applications are characterized by the presence of a time-stepping loop, in which several loops over the computational mesh (33 in Hydra, 10 in Volna, 25 in Seigen) are repeatedly executed. These loops are characterized by the aforementioned irregular loop-to-loop dependence structure. We will use Seigen, as well as other simpler benchmarks, for performance evaluation.

Because of the irregular memory access pattern, our approach to loop transformation is based on dynamic analysis, particularly on *inspector/executor schemes*. Among the possible dynamic loop optimizations, we target *sparse tiling*. We recall from Section 2.3.2 that sparse tiling aims to exploit data reuse across consecutive loops by composing two transformations, namely loop fusion and loop tiling. Given the presence of significant data reuse across consecutive loops, our hypothesis is that sparse tiling has potential in the class of unstructured mesh PDE solvers that we are targeting.

Summarizing, three main issues are tackled in this chapter:

- Previous approaches to sparse tiling were all based upon “ad-hoc” inspector/executor strategies; that is, developed “by hand”, per benchmark. We seek a general technique, applicable to arbitrary real-world computations on unstructured meshes.
- Automation is more than a desired feature because application specialists avoid complex optimizations harming source code comprehensibility. We therefore aim for a fully-automated framework, based upon domain-specific languages and a mixed compiler/library approach.
- A few studies have addressed the problem of fusing loops when these need be interleaved by routines for message passing. We are aware of none for the scenario in which the memory accesses pattern

is irregular. We fill this gap by introducing a sparse tiling scheme that performs redundant computation over partition boundaries to delay communication. The importance of this contribution stems from the fact that most scientific simulations require distributed-memory parallelism.

3.2 Context and Approach

Loop fusion and loop tiling have been widely studied in the literature. A considerable number of techniques for improving and automating these transformations have been proposed over the years. Their evaluation, however, has traditionally been limited to a small set of benchmarks (or “mini-applications”) and single-node performance. In particular, it has repeatedly been shown that simple stencil codes arising in finite difference methods [Zumbusch, 2013, Holewinski et al., 2012, Bondhugula et al., 2014], linear algebra routines [Buttari et al., 2008, 2009], and image processing kernels [Ragan-Kelley et al., 2013] can benefit from both loop fusion and loop tiling. This, unfortunately, does not shed light on the impact that these transformations could have in real-world applications, where the loop nests are often deeper, less structured, and characterized by irregular control flow. Since numerical methods for PDEs are often structured as sequences of complex, irregular loops (or “sweeps”) over the computational mesh, some obvious questions arise:

Applicability Can sparse tiling be adopted in real-life numerical methods for solving PDEs, and should performance improvements be expected?

Lack of evidence Why, despite decades of research, are non-trivial loop transformations rarely used in scientific simulations?

Challenges What are the theoretical and technical challenges that need be overcome to automate sparse tiling?

In this chapter, we tackle these problems in the following context:

Irregular codes Unstructured meshes are often used to discretize the computational domain, since they allow for an accurate representation

of complex geometries. Their connectivity is stored by means of adjacency lists (or equivalent data structure). This leads to indirect memory accesses within loop nests. Indirections break static analysis, thus making many compiler-based approaches to loop transformation (e.g., polyhedral optimization) ineffective. Runtime data dependence analysis enables dynamic loop optimization, although this results in additional overhead.

Realistic datasets Complex simulations usually operate on at least terabytes of data, hence execution on multi-node systems is required. Sparse tiling will have to coexist with distributed-memory parallelism.

Automation, but no legacy code Sparse tiling is an “extreme optimization”. An implementation in a low level language (e.g., C, Fortran) requires a great deal of effort, as a thoughtful restructuring of the application is necessary. In common with many other low level transformations, it also makes the source code impenetrable, affecting maintenance and extensibility. We therefore aim for a fully automated system based on domain-specific languages, which abstracts sparse tiling through a simple interface (i.e., a single construct to define a scope of fusible loops) and a tiny set of parameters for performance tuning (e.g., the tile size). We are not interested in supporting legacy code, where the key computational aspects (e.g., mesh iteration, distributed-memory parallelism) are usually hidden for software modularity, thus making automation almost impossible.

In this chapter, the problem of automatically applying sparse tiling to irregular codes based on shared- and/or distributed-memory parallelism is decomposed into two tasks:

1. establishing abstractions and devising algorithms to enable sparse tiling in arbitrary sequences of irregular loops (Sections 3.5-3.8);
2. integrating them with a framework that relies on domain-specific languages (Section 3.9).

Before addressing these two tasks, we elaborate on the theoretical and technical challenges that arise when applying loop fusion and loop tiling

to real-world applications (Section 3.3), and review the related work (Section 3.4).

3.3 Applying Loop Fusion and Loop Tiling is More Difficult than Commonly Assumed

We show in Listing 6 the “skeleton” of a typical PDE solver based on unstructured meshes. This will be useful throughout the analysis presented in this section.

We identify three classes of problems that are often neglected, or at least treated with scarce emphasis, in the relevant literature.

Fundamental questions We first consider the effectiveness of loop fusion and loop tiling in (un)structured mesh applications.

Computational boundedness Computational methods for PDEs are structured as sequences of loop nests, each loop nest characterized by its own operational intensity. Within the same application, some loop nests may be memory-bound, while others CPU-bound. This clearly depends on the numerical method itself, particularly on aspects such as the arithmetic complexity of the operators and the type of discretization employed (e.g., polynomial order of function spaces). Obviously, if most loop nests are CPU-bound, the benefits of sparse tiling on data locality will provide marginal gains. Before even thinking about aggressive optimizations, it is fundamental to determine the bottlenecks of an application. This boils down to answering two questions: (i) what fraction of the execution time is due to memory-bound loop nests; (ii) can CPU-boundedness be relieved by applying other optimizations (e.g., vectorization).

Loop tiling vs mesh renumbering Loop tiling and mesh renumbering are two different attempts to solving the same problem: improving the performance of mesh-based computations by increasing data locality. A mesh renumbering provides an effective way of iterating over a mesh by guaranteeing that consecutive iterations correspond to neighboring elements; if these

LISTING 6: The “bare” structure of a numerical method for solving a PDE. Three parallelizable sweeps over the mesh – over cells, nodes, and boundary nodes – are executed within a time-stepping loop. In the cells loop, the invocation of a kernel is shown. First, the (indirectly accessed) input data is “gathered” into suitable buffers. The data passed to the kernel is now contiguous in memory, which maximizes the likelihood of low level optimizations such as vectorization. Then, the kernel is executed. Finally, the computed values are “scattered” from the kernel’s output buffer to memory. Distributed-memory parallelism is achieved through MPI, in particular through the `MPI.Comm (...)` calls that separate different mesh sweeps. Additional calculations, for instance in `Calc (...)`, could also interleave the execution of consecutive loops.

```

1 // Time-stepping loop (T = total number of iterations)
2 for t = 1 to T {
3
4   // 1st sweep over the C cells of the mesh
5   for i in C {
6     buffer_0 = {0.0} // will store the kernel output
7     buffer_1 = gather_data ( A[f(map[i])], ... )
8     ...
9     kernel_1( buffer_0, buffer_1, ... );
10    scatter_data ( buffer_0, f(map[i]) )
11  }
12
13  Calc (...);
14  MPI_Comm (...);
15
16  // 2nd sweep over the N nodes of the mesh
17  for i in N {
18    ... // Similar to sweep 1
19  }
20
21  // Boundary conditions: sweep over the BV boundary nodes
22  for i in BV {
23    ... // Similar to sweep 1
24  }
25
26  Calc (...);
27  MPI_Comm (...);
28  ...
29 }

```

elements share some data values, data reuse is exploited. Just like loop tiling, a mesh renumbering can be considered a loop reordering transformation (see Section 2.3.1). Unfortunately, the relationship between them is unclear in the context of unstructured meshes. In this chapter, sparse tiling will be applied *on top of* meshes renumbered with the famous Reverse Cuthill McKee (RCM) algorithm.

Technical issues Recent works on fusion and tiling for structured mesh

applications have addressed automation (e.g., polyhedral compilers), composition of transformations (e.g., time tiling), techniques for minimizing communication (e.g., diamond tiling). However, the following aspects were rarely given the attention they actually deserve.

Unstructured meshes Although ad-hoc inspector-executor strategies for some proxy applications had previously been developed, general techniques for arbitrary computations on unstructured meshes have been missing until the work presented in this chapter¹. As already explained, the main problem with unstructured meshes is the presence of indirect memory accesses, which complicates the data dependence analysis needed for applying loop transformations.

Time tiling and distributed-memory parallelism We reiterate the fact that real-world computations require large-scale distributed-memory architectures. As Listing 6 shows, MPI calls usually separate consecutive mesh sweeps. This poses a big challenge to time tiling, because now all tiles close to the boundary of a mesh partition require special handling.

Time tiling and extra code The `Comp(...)` function in Listing 6 shows that additional computation may be performed between consecutive mesh sweeps. `Comp` could represent, for instance, check-pointing, I/O, or the resolution of a linear system through a function call to an external library. Moreover, conditional execution of loops (e.g., through `if-then-else`) may be present. The presence of additional code in between loops makes fusion extremely challenging.

Legacy code is usually impenetrable Loop transformation opportunities are often hidden in existing scientific codes. As explained in Strout [2013], common problems are: 1) potentially fusible or tiling loop nests are separated for code modularity; 2) handling of boundary conditions; 3) source code not amenable for data dependency analysis (e.g., extensive use of pointers, vir-

¹We reinforce once more that the generalized sparse tiling algorithm is the result of a joint collaboration amongst the authors of [Strout et al., 2014].

tual function calls).

Limitations inherent in the numerical method Two loops cannot be fused if they are separated by a global synchronization point. This is often a global reduction, either explicit (e.g., the first loop updates a global variable that is read by the second loop) or implicit (i.e., within an external function invoked between the two loops, as occurs in many iterative solvers for linear systems). By limiting the applicability of many loop optimizations, global synchronization points pose great challenges and research questions. If strong scaling is the primary goal and memory-boundedness is the key limiting factor, then interesting questions are: (i) can the numerical method be reformulated to relieve the constraints on low level optimization (which requires a joint effort between numerical analysts and performance specialists); (ii) can the tools be made more sophisticated to work around these problems; (iii) will the effort be rewarded by significant performance improvements.

All these issues will be addressed in the upcoming sections.

3.4 Related Work

Loop Chain

The data dependence analysis that we develop in this chapter is based on an abstraction called *loop chain*, which was originally presented in Krieger et al. [2013]. This abstraction is sufficiently general to capture data dependencies in programs structured as arbitrary sequences of loops. We will detail the loop chain abstraction in Section 3.5.

Inspector/Executor and Sparse Tiling

The loop chain abstraction provides sufficient information to create an inspector/executor scheme for an arbitrary unstructured mesh application. Inspector/executor strategies were first formalized by Salz et al. [1991]. They have been used to exploit data reuse and to expose shared-memory parallelism in several studies [Douglas et al., 2000, Strout et al., 2002, Demmel et al., 2008, Krieger and Strout, 2012].

Sparse tiling, which we reviewed in Section 2.3.4, is a technique based upon inspection/execution. The term was coined by Strout et al. [2002, 2004] in the context of the Gauss-Seidel algorithm and also used in Strout et al. [2003] in the Moldyn benchmark. However, the technique was initially proposed by Douglas et al. [2000] to parallelize computations over unstructured meshes, taking the name of *unstructured cache blocking*. In this work, the mesh was initially partitioned; the partitioning represented the tiling in the first sweep over the mesh. Tiles would then shrink by one layer of vertices for each iteration of the loop. This shrinking represented what parts of the mesh could be accessed in later iterations of the outer loop without communicating with the processes executing other tiles. The unstructured cache blocking technique also needed to execute a serial clean-up tile at the end of the computation. Adams and Demmel [1999] also developed an algorithm very similar to sparse tiling, to parallelize Gauss-Seidel computations. The main difference between Strout et al. [2002, 2004] and Douglas et al. [2000] was that in the former work the tiles fully covered the iteration space, so a sequential clean-up phase at the end could be avoided.

We reiterate the fact that all these approaches were either specific to individual benchmarks or not capable of scheduling across heterogeneous loops (e.g., one over cells and another over degrees of freedom). These limitations are addressed in this chapter.

Automated Code Generation and Optimization for Mesh-Based Computations

The automated code generation technique presented in Ravishankar et al. [2012] examines the data affinity among loops and performs partitioning with the goal of minimizing inter-process communication, while maintaining load balancing. This technique supports unstructured mesh applications (being based on an inspector/executor strategy) and targets distributed memory systems, although it does not exploit the loop chain abstraction and does not introduce any sort of loop reordering transformation.

Automated code generation techniques, such as those based on polyhedral compilers (reviewed in Section 2.3.3), have been applied to structured

mesh benchmarks or proxy applications. Notable examples are in Bondhugula et al. [2008], Grosser et al. [2012], Klöckner [2014]. There has been very little effort in providing evidence that these tools can be effective in real-world applications. Time-loop diamond tiling was applied in Bondhugula et al. [2014] to a proxy application, but experimentation was limited to shared-memory parallelism.

Overlapped Tiling

In structured codes, multiple layers of halo, or “ghost” elements, are often used to reduce communication [Basseti et al., 1998]. Overlapped tiling (see Section 2.3.2) exploits the very same idea: trading communication for redundant computation along the boundary [Zhou et al., 2012]. Several works tackle overlapped tiling within single regular loop nests (mostly stencil-based computations), for example Meng and Skadron [2009], Krishnamoorthy et al. [2007a], Chen et al. [2002]. Techniques known as “communication avoiding” [Demmel et al., 2008, Mohiyuddin et al., 2009] also fall in this category. To the best of our knowledge, overlapped tiling for unstructured mesh applications has only been studied analytically, by Giles et al. [2012]. Further, we are not aware of any prior techniques for automation.

3.5 The Loop Chain Abstraction for Generalized Inspector/Executor Schemes

In this section, we formalize the loop chain abstraction for unstructured mesh applications and discuss its relationship with inspector/executor schemes.

3.5.1 Relationship between Loop Chain and Inspector

The *loop chain* is an abstraction introduced in Krieger et al. [2013]. Informally, a loop chain is a sequence of loops with no global synchronization points, with attached some extra information to enable run-time data dependence analysis.

We reiterate that the presence of indirect memory accesses inhibits static loop optimization for data locality. The idea pursued in this chapter is to replace static with dynamic optimization, exploiting the information carried by a loop chain. Loop chains must somehow be added to or automatically derived (e.g., via a domain-specific language) from the input code. The inspector performs data dependence analysis using the information carried by the loop chain and produces a loop reordering, or sparse tiling schedule. This schedule is used by the executor, a piece of code that replaces the original sequence of loops.

Before diving into the description of the loop chain abstraction, it is worth observing that:

- The inspection phase introduces an overhead. In many scientific computations, the data dependence pattern is static – or, more informally, “the topology does not change over time”. This means that the inspection cost may be amortized over multiple iterations of the executor. If instead the mesh changes over time (e.g., in case of adaptive mesh refinement), a new inspection must be performed.
- To adopt sparse tiling in a code there are two options. One possibility is to provide a library and leave the application specialists with the burden of carrying out the implementation (re-implementation in case of legacy code). A more promising alternative consists of raising the level of abstraction: programs can be written in a domain-specific language; loop chain, inspector, and executor can then be automatically derived at the level of the intermediate representation. As we shall see in Section 3.9, the tools developed in this chapter enable both approaches.

These points will be further elaborated in later sections.

3.5.2 Definition of a Loop Chain

In Krieger et al. [2013], a loop chain is defined as follows:

- A loop chain \mathbb{L} consists of n loops, L_0, L_1, \dots, L_{n-1} . There are no global synchronization points in between the loops. Although there may be dependencies between successive loops in the chain, the execution order of a loop’s iterations does not influence the result.

- \mathbb{D} is a set of disjoint m data spaces, D_0, D_1, \dots, D_{m-1} . Each loop accesses (reads from, writes to) a subset of these data spaces. An access can be either direct (e.g., $A[i]$) or indirect (e.g., $A[\text{map}(i)]$).
- $R_{L_l \rightarrow D_d}(\vec{i})$ and $W_{L_l \rightarrow D_d}(\vec{i})$ are access relations for a loop L_l over a data space $D_d \in D$. They indicate which locations in the data space D_d an iteration $i \in L_l$ reads from and writes to, respectively. A loop chain must provide all access relations for all loops. For example, if L_l writes to the array A as $A[B(i)] = f(\dots)$, then the loop chain will have to provide an access relation $B_{L_l \rightarrow A}(\vec{i})$.

3.5.3 The Abstraction Revisited for Unstructured Mesh Applications

Motivated by the issues raised in Section 3.3 and inspired by the programming and execution models of OP2 (reviewed in Section 2.2.2), we revisit the loop chain abstraction. This new definition is more suitable for real-world unstructured mesh applications.

- A loop chain \mathbb{L} consists of n loops, L_0, L_1, \dots, L_{n-1} . There are no global synchronization points in between the loops. Although there may be dependencies between successive loops in the chain, the execution order of a loop's iterations does not influence the result.
- S is a set of disjoint m sets, S_0, S_1, \dots, S_{m-1} . Sets are used to represent iteration and data spaces. Possible sets are the cells in the mesh or the degrees of freedom associated with a function.

A set S is logically split into three contiguous regions: core (S^c), boundary (S^b), and non-exec (S^{ne}). Given a process P and a set S :

S^c : the iterations of S that exclusively belong to P .

S^b : the boundary region can be seen as the union of two sub-regions, owned (S^{owned}) and exec (S^{exec}). As shown in Figure 2.2, S^{owned} are iterations that belong to P which are redundantly executed by some other processes; S^{exec} are iterations from other processes which are redundantly executed by P . We will see that redundant computation preserves atomic execution – a prop-

erty that enables executing tiles without the need for synchronization.

S^{ne} : these are iterations of other processes that are communicated to P because they need be read to correctly compute S^b .

A set is uniquely identified by a name and the sizes of its three regions. For example, the notation $S = (\text{vertices}, C, B, N)$ defines the `vertices` set, which comprises C elements in the core region (iterations 0 to $C - 1$), B elements in the boundary region (iterations C to $C + B - 1$), and N elements in the non-exec region (iterations $C + B$ to $C + B + N - 1$).

- The *depth* is an integer indicating the extent of the boundary region of a set. This constant is the same for all sets.
- \mathbb{M} is a set of k maps, M_0, M_1, \dots, M_{k-1} . A map of arity a is a vector-valued function $M : S_i \rightarrow S_j^0 \times S_j^1 \times \dots \times S_j^{a-1}$ that connects each element of S_i to one or more elements in S_j . For example, if a triangular cell c is connected to three vertices v_0, v_1, v_2 , we have $M(c) = [v_0, v_1, v_2]$.
- A loop L_i over the iteration space S is associated with d descriptors, D_0, D_1, \dots, D_{d-1} . A descriptor D is a 2-tuple $D = \langle M, \text{mode} \rangle$. M is either a map from S to some other sets or the special placeholder \perp , which indicates that memory accesses are direct to some data associated with S itself. *mode* is one of $[r, w, i]$, meaning that a memory access is respectively of type read, write or increment.

With respect to the original definition, one crucial difference is the presence of sets in place of data spaces. In unstructured mesh applications, a loop tends to access multiple data spaces associated with the same set. The idea is to rely on sets, rather than data spaces, to perform data dependence analysis. This can significantly improve the inspection cost, because typically $|S| \ll |\mathbb{D}|$. Another crucial difference is the characterization of sets into the three regions core, boundary and non-exec. This separation is essential for enabling distributed-memory parallelism. The extent of the boundary regions is captured by the *depth* of the loop chain. Informally, the *depth* tells how many extra “strips” of elements are provided by the

neighboring processes. This allows some redundant computation along the partition boundary and also limits the depth of the loop chain (i.e., how many loops can be fused). The role of the parameter *depth* will be clear by the end of Section 3.8.

3.6 Loop Chain, Inspection and Execution Examples

LISTING 7: Section of a toy program that is used as a running example to illustrate the loop chain abstraction and show how the tiling algorithm works. Note that all parameters passed to the kernels are pointers.

```

1 for t = 0 to T {
2   // L0: loop over edges
3   for e = 0 to E {
4     x = X + e;
5     tmp_0 = tmp + edges2vertices[e + 0];
6     tmp_1 = tmp + edges2vertices[e + 1];
7     kernel1 (x, tmp_0, tmp_1);
8   }
9
10  // L1: loop over cells
11  for c = 0 to C {
12    res = R + c;
13    tmp_0 = tmp + cells2vertices[c + 0];
14    tmp_1 = tmp + cells2vertices[c + 1];
15    tmp_2 = tmp + cells2vertices[c + 2];
16    kernel2 (res, tmp_0, tmp_1, tmp_2);
17  }
18
19  // L2: loop over edges
20  for e = 0 to E {
21    tmp_0 = tmp + edges2vertices[e + 0];
22    tmp_1 = tmp + edges2vertices[e + 1];
23    kernel3 (tmp_0, tmp_1);
24  }
25 }

```

Using the example in Listing 7 – a plain C implementation of the OP2 program in Listing 4 – we describe the actions performed by a sparse tiling inspector. The inspector takes as input the loop chain illustrated in Listing 8. We show two variants, for shared-memory and distributed-memory parallelism. The value of the variable *mode* at line 19 in Listing 8 determines the variant to be executed.

LISTING 8: Building the loop chain for inspection.

```
1 nspector = init_inspector (...);
2
3 // Three sets, edges, cells, and vertices
4 E = set (inspector, "edges", core_edges, boundary_edges, nonexec_edges, ...);
5 C = set (inspector, "cells", core_cells, boundary_cells, nonexec_cells, ...);
6 V = set (inspector, "verts", core_vertices, boundary_vertices, nonexec_vertices, ...);
7
8 // Two maps, from edges to vertices and from cells to vertices
9 e2vMap = map (inspector, E, V, edges2vertices, ...);
10 c2vMap = map (inspector, C, V, cells2vertices, ...);
11
12 // The loop chain comprises three loops; each loop has some descriptors
13 // recall that r and i in a descriptor stand for ‘read’ and ‘increment’
14 loop (inspector, E, {⊥, r}, {e2vMap, i});
15 loop (inspector, C, {⊥, r}, {c2vMap, i});
16 loop (inspector, E, {e2vMap, i});
17
18 // Now can run the inspector
19 inspection = run_inspection (mode, inspector, tile.size, ...)
20 return inspection;
```

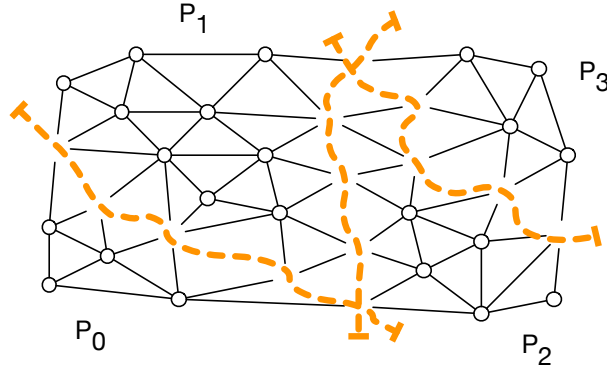


Figure 3.1: Partitioning of the seed loop. The vertices are illustrated to make the connectivity of the mesh clear, although they do not belong to any partition yet.

Overview

The inspector starts with partitioning the iteration space of a *seed loop*, for example L_0 . Partitions are used to initialize tiles: the iterations of L_0 falling in P_i – or, in other words, the edges in partition P_i – are assigned to the tile T_i . Figure 3.1 displays the situation after the initial partitioning of L_0 for a given input mesh. There are four partitions, two of which (P_0 and P_3) are not connected through any edge or cell. These four partitions correspond to four tiles, $[T_0, T_1, T_2, T_3]$, with $P_i = T_i$.

As detailed in the next two sections, the inspection proceeds by pop-



Figure 3.2: A snapshot of the mesh after tiling L_0 .

ulating T_i with iterations from L_1 and L_2 . The challenge of this task is guaranteeing that all data dependencies – read after write, write after read, write after write – are honored. The output of the inspector is eventually passed to the executor. The inspection carries sufficient information for computing sets of tiles in parallel. T_i is always executed by a single thread/process and the execution is atomic; that is, it does not require communication with other threads/processes. When executing T_i , first all iterations from L_0 are executed, then all iterations from L_1 and finally those from L_2 .

Inspection for Shared-Memory Parallelism

Similarly to OP2, to achieve shared-memory parallelism we use coloring. Two tiles that are given the same color can be executed in parallel by different threads. Two tiles can have the same color if they are not connected, because this ensures the absence of race conditions through indirect memory accesses during parallel execution. In the example we can use three colors: red (R), green (G), and blue (B). T_0 and T_3 are not connected, so they are assigned the same color. The colored tiles are shown in Figure 3.2. In the following, with the notation T_i^c we indicate that the i -th tile has color c .

To populate $[T_0^G, T_1^B, T_2^R, T_3^G]$ with iterations from L_1 and L_2 , we first have to establish a total ordering for the execution of partitions with different colors. Here, we assume the following order: green (G), blue (B), and red (R). This implies, for instance, that *all iterations* assigned to T_1^B must be executed *before all iterations* assigned to T_2^R . By “all iterations” we mean the iterations from L_0 (determined by the seed partitioning) as

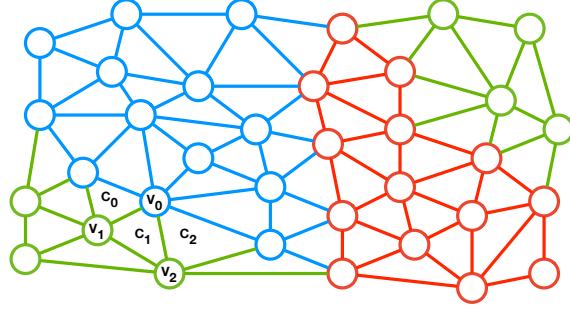


Figure 3.3: The vertices are written by L_0 , so a projection must be computed before tiling L_1 . Here, the projection is represented by the colored vertices.

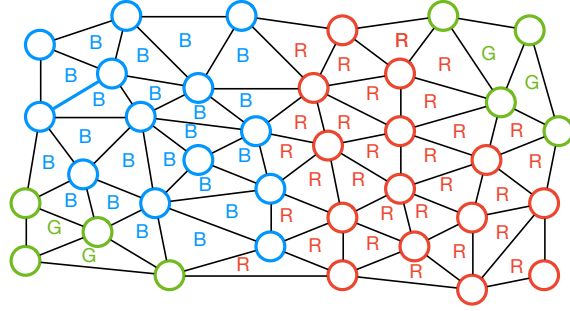


Figure 3.4: A snapshot of the mesh after tiling L_1 .

well as the iterations that will later be assigned from tiling L_1 and L_2 . We assign integer positive numbers to colors to reflect their ordering, where a smaller number means higher execution priority. We can assign, for example, 0 to green, 1 to blue, and 2 to red.

To schedule the iterations of L_1 to $[T_0^G, T_1^B, T_2^R, T_3^G]$, we need to compute a *projection* for any write or local reduction performed by L_0 . The projection required by L_0 is a function $\phi : V \rightarrow \mathbb{T}$ mapping the vertices in V – as indirectly incremented during the execution of L_0 , see Listing 7 – to a tile $T_i^c \in \mathbb{T}$. Consider the vertex v_0 in Figure 3.3. v_0 has 7 incident edges, 2 of which belong to T_0^G , while the remaining 5 to T_1^B . Since we established that $G \prec B$, v_0 can only be read after T_1^B has finished executing the iterations from L_0 (i.e., the 5 incident blue edges). We express this condition by setting $\phi(v_0) = T_1^B$. Observe that we can compute ϕ by iterating over V and, for each vertex, applying the maximum function (MAX) to the color of the adjacent edges.

We now use ϕ to schedule L_1 , a loop over cells, to the tiles. Con-



Figure 3.5: A snapshot of the mesh after tiling L_2 .

sider again v_0 and the adjacent cells $[c_0, c_1, c_2]$ in Figure 3.3. These three cells have in common the fact that they are adjacent to both green and blue vertices. For c_1 , and similarly for the other cells, we compute $\text{MAX}(\phi(v_0), \phi(v_1), \phi(v_2)) = \text{MAX}(B, G, G) = B = 1$. This establishes that c_1 must be assigned to T_1^B , because otherwise (c_1 assigned instead to T_0^G) a read to v_0 would occur before the last increment from T_1^B took place. Indeed, we recall that the execution order, for correctness, must be “all iterations from $[L_0, L_1, L_2]$ in the green tiles before all iterations from $[L_0, L_1, L_2]$ in the blue tiles”. The scheduling of L_1 to tiles is displayed in Figure 3.4.

To schedule L_2 to $[T_0^G, T_1^B, T_2^R, T_3^G]$ we employ a similar process. Vertices are again written by L_1 , so a new projection over V will be necessary. Figure 3.5 shows the output of this last phase.

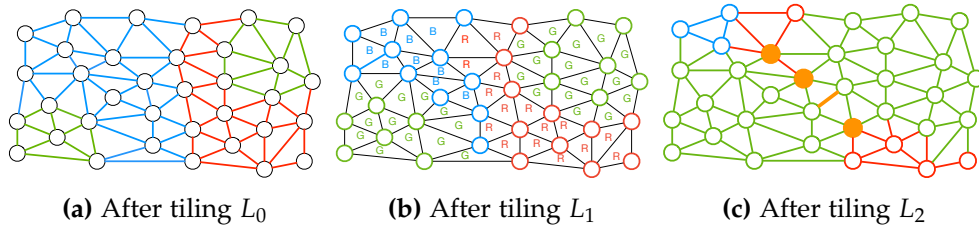


Figure 3.6: Tiling the program in Listing 7 for shared-memory parallelism can lead to conflicts. Here, the two green tiles eventually become adjacent, creating race conditions.

Conflicting Colors It is worth noting how T_2^R “consumed” the frontier elements of all other tiles every time a new loop was scheduled. Tiling a loop chain consisting of k loops has the effect of expanding the frontier of a

tile of at most k vertices. With this in mind, we re-inspect the loop chain of the running example, although this time employing a different execution order – blue (B), red (R), and green (G) – and a different seed partitioning. Figure 3.6 shows that, by applying the same procedure described in this section, T_0^G and T_3^G will eventually become adjacent. This violates the precondition that *tiles can be given the same color, and thus run in parallel, as long as they are not adjacent*. Race conditions during the execution of iterations belonging to L_2 are now possible. This problem will be solved in Section 3.8.1.

Inspection for Distributed-Memory Parallelism

In the case of distributed-memory parallelism, the mesh is partitioned and distributed to a set of processes. As shown in Listing 6, neighboring processes may exchange (MPI) messages before executing a loop L_j . A message includes all “dirty” dataset values required by L_j modified by any L_k , with $L_k \prec L_j$. In the running example, L_0 writes to vertices, so a subset of values associated with border vertices must be communicated prior to the execution of L_1 . To apply sparse tiling, the idea is to push all communications at the beginning of the loop chain: as we shall see, this increases the amount of data to be communicated, but also reduces the number of synchronizations (only 1 synchronization between each pair of neighboring processes per loop chain execution).

From Section 3.5.3 it is known that, in a loop chain, a set is logically split into three regions, *core*, *boundary*, and *non-exec*. The boundary tiles, which originate from the seed partitioning of the boundary region, will include all iterations that cannot be executed until the communications have terminated. The procedure described for shared-memory parallelism – now performed individually by each process on a partition of the input mesh – is modified as follows:

1. The core region of the seed loop L_0 is partitioned into tiles. Unless aiming for a mixed distributed/shared-memory scheme, there is no need to assign identical colors to unconnected tiles, as a process will execute its own tiles sequentially. Colors are assigned increasingly, with T_i given color i . As long as tiles with contiguous ID are also physically contiguous in the mesh, this assignment retains spatial

locality when “jumping” from executing T_i to T_{i+1} .

2. The same process is applied to the boundary region. Thus, a situation in which a tile includes iterations from both the core and the boundary regions is prevented by construction. Further, all tiles within the boundary region are assigned colors higher than those used for the core tiles. This constrains the execution order: no boundary tiles will be executed until all core tiles are computed.
3. We map the whole non-exec region of L_0 to a single special tile, T_{ne} . This tile has the highest color and will actually never be executed.

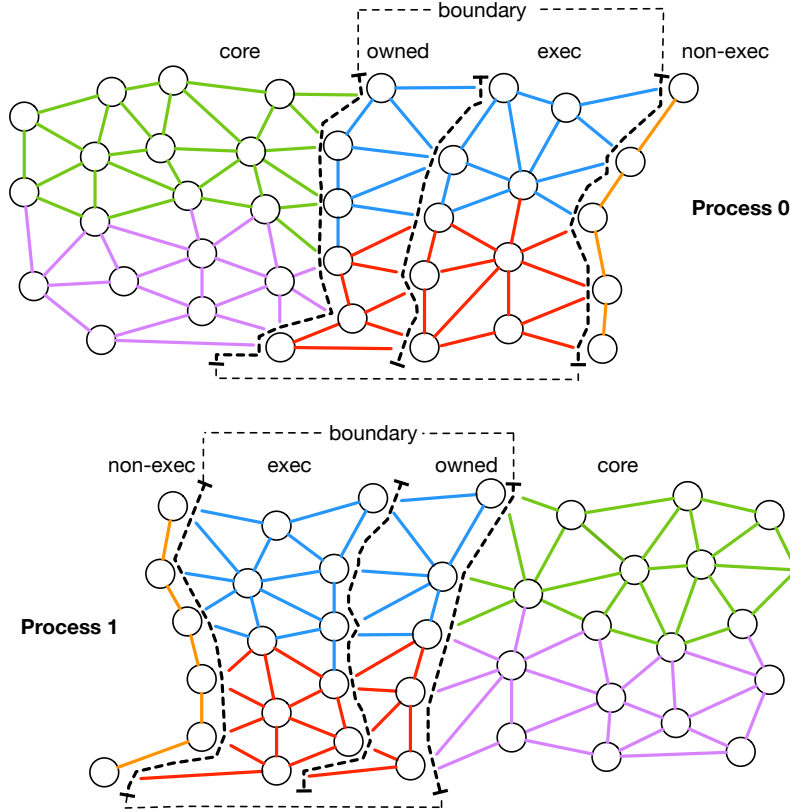


Figure 3.7: A snapshot of the two mesh partitions on Process 0 and Process 1 after inspecting the seed loop L_0 for distributed-memory parallelism. On each process, there are five tiles in total: two in the core region (green and violet), two in the boundary region (red and light blue), and T_{ne} . The boundary tiles can safely cross the owned and exec sub-regions (i.e., the private local iterations and the iterations to be redundantly computed, respectively). However, no tile can include iterations from both the core and the boundary regions.

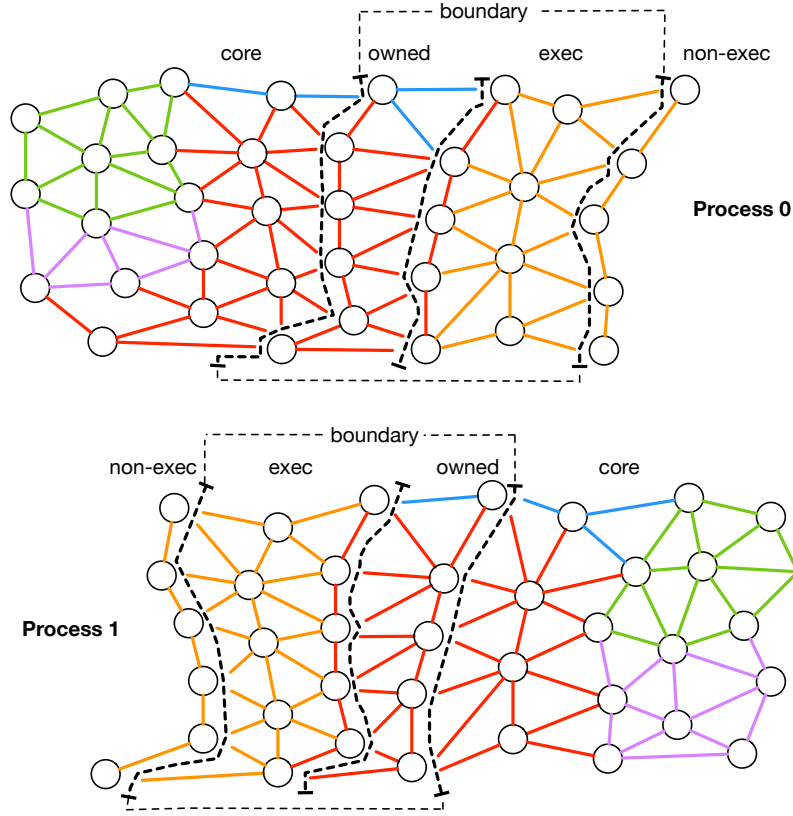


Figure 3.8: A snapshot of the two mesh partitions on Process 0 and Process 1 at the end of the inspection for distributed-memory parallelism. T_{ne} expands over the boundary region, which minimizes the amount of redundant computation to be performed. At the end of the execution phase, the orange edges will contain “dirty values”, but correctness is not affected as the exec region only includes off-process data. The boundary tiles expand over the core region: this is essential for correctness since none of the red and blue entities from $[L_0, L_1, L_2]$ can be executed until the MPI communications have terminated.

From this point on, the inspection proceeds as in the case of shared-memory parallelism. The application of the MAX function when scheduling L_1 and L_2 makes higher color tiles (i.e., those having lower priority) “expand over” lower color ones.

In Figure 3.7, a mesh is partitioned over two processes and a possible seed partitioning and tiling of L_0 illustrated. We observe that the two boundary tiles (the red and light blue ones) will expand over the core tiles as L_1 and L_2 are tiled, which eventually results in the scheduling illustrated in Figure 3.8. Roughly speaking, if a loop chain consists of n loops and, on each process, $n - 1$ extra layers of iterations are provided (the exec

regions in Figure 3.7), then all boundary tiles are correctly computed.

The schedule produced by the inspector is subsequently used by the executor. On each process, the executor starts with triggering the MPI communications required for the computation of boundary tiles. All core tiles are then computed, since no data from the boundary region is necessary. Hence, computation is overlapped with communication. As all core tiles are computed and the MPI communications terminated, the boundary tiles can finally be computed.

Efficiency considerations The underlying hypothesis is that the increase in data locality will outweigh the overhead induced by the redundant computation and by the bigger volume of data exchanged. This is motivated by several facts: (i) the loops being memory-bound; (ii) the core region being much larger than the boundary region; (iii) the amount of redundant computation being minimized through the special tile T_{ne} , which progressively expands over the boundary region, thus avoiding unnecessary calculations.

3.7 Data Dependency Analysis for Loop Chains

As with all loop optimizations that reschedule the iterations in a sequence of loops, any sparse tiling must satisfy the data dependencies. The loop chain abstraction, which we have described in Section 3.5, provides enough information to construct an inspector which analyzes all of the dependencies in a computation and builds a legal sparse tiling. We recall that one of the main assumptions in a loop chain is that each loop is fully parallel or, equivalently, that there are no loop carried dependencies.

The descriptors in the loop chain abstraction enable a general derivation of the storage-related dependencies between loops in a loop chain. The storage related dependencies between loops can be described as either flow (read after write), anti (write after read), or output (write after write) dependencies. In the following, assume that loop L_x , having iteration space S_x , always comes before loop L_y , having iteration space S_y , in the loop chain. Let us identify a descriptor of a loop L with $m_{S_i \rightarrow S_j}^{\text{mode}}$: this simply indicates that the loop L_i has iteration space S_i and uses a map

m to write/read/increment elements (respectively, $\text{mode} \in \{w, r, i\}$) in the space S_j .

The flow dependencies can then be enumerated by considering pairs of points (\vec{i} and \vec{j}) in the iteration spaces of the two loops L_x and L_y :

$$\{\vec{i} \rightarrow \vec{j} \mid \vec{i} \in S_x \wedge \vec{j} \in S_y \wedge m_{S_x \rightarrow S_z}^w(\vec{i}) \cap m_{S_y \rightarrow S_z}^r(\vec{j}) \neq \emptyset\}.$$

Anti and output dependencies are defined in a similar way. The anti dependencies for all pairs of loops L_x and L_y are:

$$\{\vec{i} \rightarrow \vec{j} \mid \vec{i} \in S_x \wedge \vec{j} \in S_y \wedge m_{S_x \rightarrow S_z}^r(\vec{i}) \cap m_{S_y \rightarrow S_z}^w(\vec{j}) \neq \emptyset\}.$$

While the output dependencies between loops L_x and L_y are:

$$\{\vec{i} \rightarrow \vec{j} \mid \vec{i} \in S_x \wedge \vec{j} \in S_y \wedge m_{S_x \rightarrow S_z}^w(\vec{i}) \cap m_{S_y \rightarrow S_z}^w(\vec{j}) \neq \emptyset\}.$$

In essence, there is a storage-related data dependence between two iterations from different loops (and therefore between the tiles they are placed in) when one of those iterations writes to a data element and the other iteration reads from or writes to the same data element.

There are local reductions, or “reduction dependencies” between two or more iterations of the same loop when those iterations “increment” the same location(s); that is, when they read, modify with a commutative and associative operator, and write to the same location(s). The reduction dependencies in L_x are:

$$\{\vec{i} \rightarrow \vec{j} \mid \vec{i} \in S_x \wedge \vec{j} \in S_x \wedge m_{S_x \rightarrow S_z}^i(\vec{i}) \cap m_{S_x \rightarrow S_z}^i(\vec{j}) \neq \emptyset\}.$$

The reduction dependencies between two iterations within the same loop indicates that those two iterations must be executed atomically with respect to each other.

As seen in the example in Section 3.6, our inspector algorithm handles data dependencies, including those between non-adjacent loops, by tracking *projections*. In the next section we explain how projections are constructed and used.

3.8 Formalization

3.8.1 The Generalized Sparse Tiling Inspector

The pseudo-code for the generalized sparse tiling inspector is shown in Algorithm 1. Given a loop chain and a “seed” tile size, the algorithm produces a schedule suitable for mixed distributed/shared-memory parallelism. In the following, we elaborate on the main steps of the algorithm. The notation used throughout the section is summarized in Table 3.1.

Symbol	Meaning
\mathbb{L}	The loop chain
L_j	The j -th loop in \mathbb{L}
S_j	The iteration space of L_j
S_j^c, S_j^b, S_j^{ne}	The core, boundary, and non-exec regions of S_j
S	A generic set in \mathbb{L}
D	A descriptor of a loop
r, w, i	Possible values for $D.mode$
\mathbb{T}	The set of all tiles
$\mathbb{T}[i]$	Accessing the i -th tile
ϕ_S	A projection $\phi_S : S \rightarrow \mathbb{T}$
Φ	The set of all available projections
σ_j	A tiling function $\sigma_j : S_j \rightarrow \mathbb{T}$ for L_j
ts	seed tile size

Table 3.1: Summary of the notation used throughout the section.

Choice of the seed loop The seed loop L_{seed} is used to initialize the tiles. Theoretically, any loop in the chain can be chosen as seed. Supporting distributed-memory parallelism, however, is cumbersome if $L_{seed} \neq L_0$. This is because more general schemes for partitioning and coloring would be needed to ensure that no iterations in any S_j^b are assigned to a core tile. A limitation of our inspector algorithm in the case of distributed-memory parallelism is that it must be $L_{seed} = L_0$.

In the special case in which there is no need to distinguish between core and boundary tiles (because a program is executed on a single shared-memory system), L_{seed} can be chosen arbitrarily. If we however pick L_{seed} in the middle of the loop chain ($L_0 \prec \dots \prec L_{seed} \prec \dots$), a mechanism for constructing tiles in the reverse direction (“backwards”), from L_{seed}

ALGORITHM 1: The inspection algorithm

Input: The loop chain $\mathbb{L} = [L_0, L_1, \dots, L_{n-1}]$, a tile size ts **Output:** A set of tiles \mathbb{T} , populated with iterations from \mathbb{L}

```
// Initialization
1 seed  $\leftarrow 0$ ;
2  $\Phi \leftarrow \emptyset$ ;
3  $C \leftarrow \perp$ ;

// Creation of tiles
4  $\sigma_{seed}, \mathbb{T} \leftarrow \text{partition}(S_{seed}, ts)$ ;
5 seed_map  $\leftarrow \text{find\_map}(S_{seed}, \mathbb{L})$ ;
6 conflicts  $\leftarrow \text{false}$ ;

// Schedule loops to tiles
7 do
8   color( $\mathbb{T}$ , seed_map);

9   for  $j = 1$  to  $n - 1$  do
10    project( $L_{j-1}, \sigma_{j-1}, \Phi, C$ );
11     $\sigma_j \leftarrow \text{tile}(L_j, \Phi)$ ;
12    assign( $\sigma_j, \mathbb{T}$ );
13  end for

14  if has_conflicts( $C$ ) then
15    conflicts  $\leftarrow \text{true}$ ;
16    add_fake_connection(seed_map,  $C$ );
17  end if
18 while conflicts;

// Inspection successful, create local maps and return
19 compute_local_maps( $\mathbb{T}$ );
20 return  $\mathbb{T}$ 
```

towards L_0 , is necessary. In Strout et al. [2014], we propose two “symmetric” algorithms to solve this problem, *forward tiling* and *backward tiling*, with the latter using the MIN function in place of MAX when computing projections. For ease of exposition, and since in the fundamental case of distributed-memory parallelism we are imposing $L_{seed} = L_0$, we here neglect this distinction².

²The algorithm implemented in the library presented in Section 3.9.1 supports backwards tiling for shared-memory parallelism.

Field	Possible values
<i>region</i>	core, boundary, non-exec
<i>iterations lists</i>	one list of iterations $[T_i]_j$ for each $L_j \in \mathbb{L}$
<i>local maps</i>	one list of local maps for each $L_j \in \mathbb{L}$; one local map for each map used in L_j
<i>color</i>	an integer representing the execution priority

Table 3.2: The tile data structure.

Tile initialization Let ts be the user-specified average tile size. The algorithm starts with partitioning S_{seed}^c into m subsets $\{P_0, P_1, \dots, P_{m-1}\}$ such that $|P_i| = ts$ (except possibly for P_{m-1}), $P_i \cap P_j = \emptyset$, and $\cup_{i=0}^{m-1} P_i = S_{seed}^c$. Among all possible legal partitionings, we choose the one that splits S_{seed}^c into blocks of ts contiguous iterations, with $P_0 = \{0, \dots, ts - 1\}$, $P_1 = \{ts, \dots, 2ts - 1\}$, and so on. We analogously partition S_{seed}^b into k subsets. We create $m + k + 1$ tiles, one for each of these partitions and one extra tile for S_{seed}^{ne} . We therefore have $\mathbb{T} = \{T_0^c, \dots, T_{m-1}^c, T_m^b, \dots, T_{m+k-1}^b, T_{m+k}^{ne}\}$.

A tile T_i has four fields, as summarized in Table 3.2.

- The *region* is used by the executor to schedule tiles in a given order. This field is set right after the partitioning of L_{seed} , as a tile (by construction) exclusively belongs to S_{seed}^c , S_{seed}^b , or S_{seed}^{ne} .
- The *iterations lists* contain the iterations in \mathbb{L} that T_i will have to execute. There is one *iterations list* $[T_i]_j$ for each $L_j \in \mathbb{L}$. At this stage of the inspection we have $[T_i]_{seed} = [T_i]_0 = P_i$, whereas still $[T_i]_j = \emptyset$ for $j = 1, \dots, n$.
- *Local maps* may be used for performance optimization by the executor in place of the global maps provided through the loop chain; this will be discussed in more detail in Section 3.11.
- The *color* gives a tile a scheduling priority. If shared-memory parallelism is requested, adjacent tiles are given different colors (the adjacency relation is determined through the maps available in \mathbb{L}). Otherwise, colors are assigned in increasing order (i.e., T_i is given color i). The boundary tiles are always given colors higher than that of core tiles; the non-exec tile has the highest color. The assignment of colors is carried by the function `color` in Listing 1.

Populating tiles by tracking data dependencies To schedule a loop to tiles we use projections. A projection is a function $\phi_S : S \rightarrow \mathbb{T}$. Initially, the projections set Φ is empty. Each time a loop is tiled, Φ may be added some new projections or old projections may be updated. Φ , and consequently the tiling functions for all loops in \mathbb{L} , are derived incrementally (within the loop at line 9 in Listing 1) starting from $\sigma_{seed} : S_{seed} \rightarrow \mathbb{T}$, the tiling function of L_{seed} . In the following, we discuss in detail how projections and tiling functions are constructed.

ALGORITHM 2: Projection of a tiled loop

Input: A loop L_j , a tiling function σ_j , the projections set Φ , the conflicts matrix C
Result: Update Φ and C

```

1  foreach D ∈ Lj.descriptors do
2      if D.map == ⊥ then
3          Φ = Φ ∪ σi;
4      else
5          inverse_map ← map_invert(D.map);
6          St, Sj, values, offset ← inverse_map;
7          φSt ← ⊥;
8          for e = 0 to St.size do
9              for k = offset[e] to offset[e + 1] do
10                 Tlast = T[values[k]];
11                 max_color ← MAX(φSt[e].color, Tlast.color);
12                 if max_color ≠ φSt[e].color then
13                     φSt[e] ← Tlast;
14                 end if
15             end for
16         end for
17         update(C, T, φSt);
18         Φ = Φ ∪ φSt;
19     end if
20 end foreach

```

Deriving a projection from a tiling function Algorithm 2 takes as input (the descriptors of) L_j and its tiling function $\sigma_j : S_j \rightarrow \mathbb{T}$ to update Φ . The algorithm also updates the conflicts matrix $C \in \mathbb{N}^{m \times m}$, which indicates whether two tiles having the same color will become adjacent once L_{j+1} is tiled.

A projection tells what tile a set element logically belongs to at a given point of the inspection. A new projection ϕ_S is needed if the elements of S

are written by a loop. Let us consider the non-trivial case in which writes or increments occur indirectly through a map $M : S_j \rightarrow S_t^0 \times S_t^1 \times \dots \times S_t^{a-1}$. To compute ϕ_{S_t} , we first determine the inverse map (an example is shown in Figure 3.9). Then, we iterate over all elements of S_t and, for each $e \in S_t$, we determine the last tile that writes to e , say T_{last} . This is accomplished by applying the MAX function over the color of the tiles accessing e . We finally simply set $\phi_{S_t}[e] = T_{last}$.

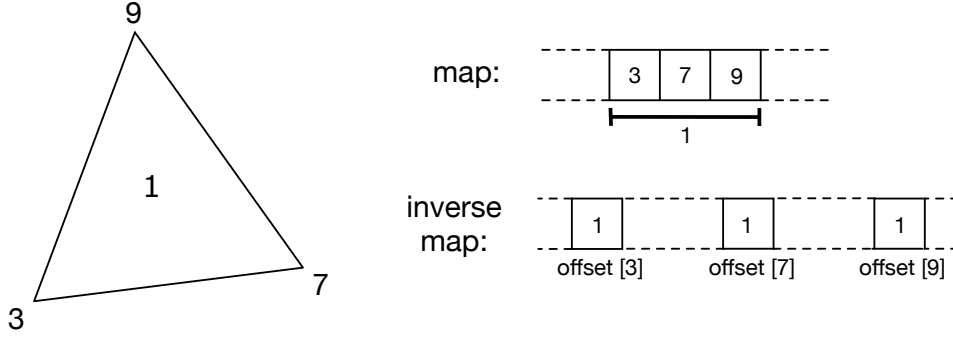


Figure 3.9: Representation of an inverse map. The original map shows that the triangular cell 1 is adjacent to three vertices, namely 3, 7, and 9. The inverse map associates vertices to cells. Since the mesh is unstructured, different vertices can be incident to a different number of cells. The array `offset` determines the distance between two consecutive vertices in the inverse map. For instance, all entries in the inverse map between `offset[3]` and `offset[4]` are cells incident to vertex 3 (in the illustrated case, the first of these is cell 1).

Deriving a tiling function from the available projections Using Φ , we compute σ_j as described in Algorithm 3. The algorithm is similar to the projection of a tiled loop, with the main difference being that now we use Φ to schedule iterations correctly. Finally, σ_j is inverted and the iterations are added to the corresponding iteration lists $[T_i]_j$, for all $T_i \in \mathbb{T}$.

Detection of conflicts If C indicates the presence of at least one conflict, say between T_{i_1} and T_{i_2} , we add a “fake connection” between these two tiles and loop back to the coloring stage. T_{i_1} and T_{i_2} are now connected, so they will be assigned different colors.

History of the algorithm A first algorithm for sparse tiling inspection was developed by the author of this thesis in conjunction with researchers

ALGORITHM 3: Building a tiling function

Input: A loop L_j , the projections set Φ **Output:** The tiling function σ_j

```
1  $\sigma_j \leftarrow \perp$ ;  
2 foreach  $D \in L_j.\text{descriptors}$  do  
3   if  $D.\text{map} == \perp$  then  
4      $\sigma_j \leftarrow \Phi[S_j]$ ;  
5   else  
6      $\text{arity} \leftarrow D.\text{map}.\text{arity}$ ;  
7      $\phi_S \leftarrow \Phi[D.\text{map}.S_j]$ ;  
8     for  $e = 0$  to  $S_j.\text{size}$  do  
9        $\sigma_j[e] \leftarrow T_\perp$  ;  
10      for  $k = 0$  to  $\text{arity}$  do  
11         $\text{adjacent\_tile} \leftarrow \phi_S[D.\text{map}.\text{values}[e * \text{arity} + k]]$ ;  
12         $\text{max\_color} \leftarrow \text{MAX}(\sigma_j[e].\text{color}, \text{adjacent\_tile}.\text{color})$ ;  
13        if  $\text{max\_color} \neq \sigma_j[e].\text{color}$  then  
14           $\sigma_j[e] \leftarrow \text{adjacent\_tile}$ ;  
15        end if  
16      end for  
17    end for  
18  end if  
19 end foreach  
20 return  $\sigma_j$ 
```

from multiple institutions, and was introduced in Strout et al. [2014]. In this section, a new, enhanced version of that algorithm has been presented. In essence, the major differences are: (i) support for distributed-memory parallelism; (ii) use of mesh coloring instead of a task graph for tile scheduling; (iii) speculative inspection with backtracking if a coloring conflict is detected; (iv) use of sets, instead of datasets, for data dependency analysis; (v) use of inverse maps for parallelization of the projection and tiling routines; (vi) computation of local maps. Most of these changes contributed to reduce the inspection cost.

3.8.2 The Generalized Sparse Tiling Executor

The sparse tiling executor is illustrated in Algorithm 4. It consists of four main phases: (i) exchange of halo regions amongst neighboring processes through non-blocking communications; (ii) execution of core tiles (in overlap with communication); (iii) wait for the termination of the communica-

ALGORITHM 4: The executor algorithm

Input: A set of tiles \mathbb{T} **Result:** Execute the loop chain

```
1  $\mathbb{T}^c, \mathbb{T}^b \leftarrow \text{group\_tiles\_by\_region}(\mathbb{T});$ 
2  $\text{start\_MPI\_comm}();$ 
3 foreach color do
4   | foreach  $T \in \mathbb{T}^c$  s.t.  $T.\text{color} == \text{color}$  do
5   |   |  $\text{execute\_tile}(T);$ 
6   | end foreach
7 end foreach
8  $\text{end\_MPI\_comm}();$ 
9 foreach color do
10  | foreach  $T \in \mathbb{T}^b$  s.t.  $T.\text{color} == \text{color}$  do
11  |   |  $\text{execute\_tile}(T);$ 
12  | end foreach
13 end foreach
```

tions; (iv) execution of boundary tiles.

As explained in Sections 3.6 and 3.8.1, a sufficiently deep halo region enables correct computation of the boundary tiles. Further, tiles are executed atomically, meaning that all iterations in a tile are computed without ever synchronizing with other processes. The depth of the boundary region, which affects the amount of off-process data to be redundantly computed, increases with the number n of loops to be fused. In the example in Figure 3.7, there are $n = 3$ loops, and three “strips” of extra vertices are necessary for correctly computing the fused loops without tile-to-tile synchronizations.

We recall from Section 3.5.3 that the *depth* of the loop chain indicates the extent of the boundary region. This parameter imposes a limit to the number of fusible loops. If \mathbb{L} includes more loops than the available boundary region – that is, if $n > \text{depth}$ – then \mathbb{L} will have to be split into shorter loop chains, to be fused individually. As we shall see (Section 3.9.3), in our inspector/executor implementation the *depth* is controlled by the Firedrake’s DMPlex module.

3.8.3 Computational Complexity of Inspection

Let N be the maximum size of a set in $\mathbb{L} = [L_0, L_1, \dots, L_{n-1}]$ and let M be the maximum number of sets accessed in a loop. If a is the maximum arity of a map, then $K = aN$ is the maximum cost for iterating over a map. K is also the worst-case cost for inverting a map. Let $p < 1$ be the probability that a conflict arises during inspection in the case of shared-memory parallelism; thus, the expected number of inspection rounds is $R = \frac{1}{1-p}$. Hence, the worst-case computational costs of the main inspection phases are as in Table 3.3.

Phase	Cost shared memory	Cost distributed memory
Partitioning	N	N
Coloring	RK	N
Projection	$R(nMNK^2)$	$nMNK^2$
Tiling	$R(nMNK)$	$nMNK$
Local maps	nM	nM

Table 3.3: Worst-case computational costs of the main inspection phases.

3.9 Implementation

The implementation of automated generalized sparse tiling is distributed over three software modules.

Firedrake The framework for the automated solution of PDEs through the finite element method (Section 2.2.1).

PyOP2 Firedrake produces numerical kernels to be applied over sets of mesh components. The parallel iteration over the mesh is handled by PyOP2 (Section 2.2.2).

SLOPE A library for writing generalized inspector/executor schemes, with primary focus on sparse tiling. PyOP2 uses SLOPE to apply sparse tiling to loop chains.

There are several reasons that motivate this structuring.

Simplicity of analysis The abstractions used in Firedrake and PyOP2 drastically simplify the analysis of input programs. For example, from

the parallel loop construct in PyOP2 (Section 2.2.2) we can derive the information that we need to construct a loop chain.

Flexibility Inspector/executor schemes can be expressed at three different layers of abstraction: in Firedrake programs, in PyOP2 programs, or directly in C. It is extremely intuitive and simple to use sparse tiling in a Firedrake program. Once the regions of code to be sparse tiled are identified, the inspector/executor schemes are automatically derived in the PyOP2 implementation. In the case of a pure PyOP2 program, the generation of inspector/executor schemes is instead only partly automated, since the separation of a set into the core, boundary and non-exec regions for distributed-memory parallelism is user’s responsibility. An inspector-executor scheme can also be written from scratch in a plain C program. In this case, the loop chain must be provided explicitly through direct calls to the SLOPE library.

Realistic simulations We aim to use generalized sparse tiling in real-world programs. The choice was then to use a framework, Firedrake, with a user base that could provide meaningful examples. The implementation effort is higher, but so is the potential scientific impact.

The interplay amongst Firedrake, PyOP2 and SLOPE is outlined in Figure 3.10 and discussed in more detail in the following sections.

3.9.1 SLOPE: a Library for Sparse Tiling Irregular Computations

SLOPE is an open source software that provides an interface to build loop chains and to express inspector/executor schemes for sparse tiling³.

The loop chain abstraction implemented by SLOPE has been formalized in Section 3.5.3. In essence, a loop chain comprises some sets (including the separation into core, boundary, and non-exec regions), maps between sets, and a sequence of loops. Each loop has one or more descriptors specifying what and how different sets are accessed. The example in Listing 8 illustrates the interface exposed by SLOPE.

³SLOPE is a contribution of this thesis and is available at <https://github.com/coneoproject/SLOPE>

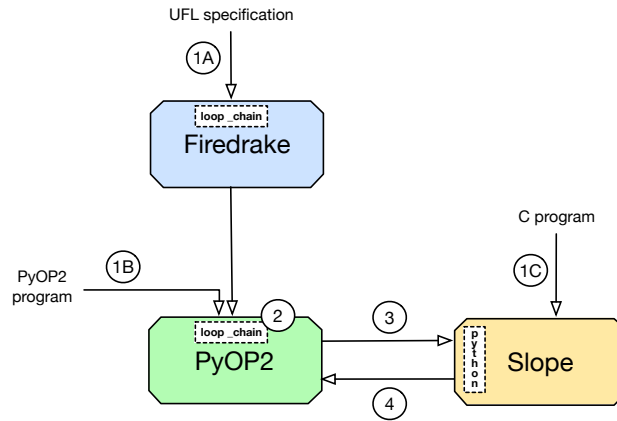


Figure 3.10: Sparse tiling in the Firedrake-PyOP2-SLOPE framework. There are three ways of sparse tiling a loop chain: decorating a Firedrake program (1A), decorating a sequence of loops in a PyOP2 program (1B), writing both the loop chain and the inspector/executor codes explicitly in C through calls to SLOPE (1C). Both (1A) and (1B) use the *loop_chain* interface (details in Section 3.9.2). The kernels generated within a *loop_chain* are pre-processed in PyOP2 (2) and forwarded to SLOPE through its python interface (3). SLOPE now has access to the loop chain, so it can generate an inspector/executor scheme and return it to PyOP2 (4). The inspector is compiled and executed. The result, a schedule (i.e., the output of Algorithm 1), is cached and used as input to the executor. Each time the same *loop_chain* is encountered in a Firedrake/PyOP2 program, the corresponding schedule is reused.

SLOPE implements the algorithms in Section 3.8.1. Further, it provides additional features to estimate the effectiveness and to verify the correctness of sparse tiling:

VTK file generator For each tiled loop, a file showing the mesh and the repartition into colored tiles is generated. The file is suitable for visualization in Paraview [Ayachit, 2015].

Inspection summary The inspector returns useful information concerning the sparse tiling process, including: the number and the average size of tiles, the total number of colors used (which can partly explain the performance of a shared-memory parallelization), time spent in the critical inspection phases.

In the case of shared-memory parallelism, the following sections of code are parallelized through OpenMP:

- The projection and tiling algorithms; in particular, the loop at line 8 of Algorithm 2 and the loop at line 8 of Algorithm 3).

- The execution of tiles having the same color; that is, the loops at lines 4 and 10 of Algorithm 4.

3.9.2 PyOP2: Lazy Evaluation and Interfaces

We focus on three relevant aspects of PyOP2: (i) the interface exposed to identify loop chains; (ii) the lazy evaluation mechanism that allows loop chains to be built; (iii) the interaction with SLOPE to build and execute inspector/executor schemes.

To apply sparse tiling to a sequence of loops, PyOP2 provides the *loop_chain* interface, as exemplified in Listing 5. This interface is exposed to the PyOP2 users, including Firedrake.

LISTING 5: The *loop_chain* interface in PyOP2. The name uniquely identifies a loop chain. Other parameters (most of them optional) are useful for performance evaluation (e.g., logging) and performance tuning. The *tile_size* specifies the initial average size for the seed partitions. The *fusion_scheme* allows to specify how to break a long sequence of loops into smaller loop chains, which makes it possible to experiment with a full set of sparse tiling strategies without having to modify the source code.

```
1 with loop_chain (name, tile_size, fusion_scheme, ...):
2     Any Python code here
```

PyOP2 exploits lazy evaluation of parallel loops to generate an inspector/executor scheme. The parallel loops encountered during the program execution – or, analogously, those generated through Firedrake – are pushed into a queue, instead of being executed immediately. The sequence of parallel loops in the queue is called the *trace*. If a dataset f needs to be read, for example because a user wants to inspect its values or a global linear algebra operation needs be performed, the trace is traversed – from the most recent parallel loop to the oldest one – and a new sub-trace produced. The sub-trace includes all parallel loops that must be executed to evaluate f correctly. The sub-trace can then be executed or further pre-processed.

All loops in a trace that were created within a *loop_chain* scope are sparse tiling candidates. In detail, the interaction between PyOP2 and SLOPE is as follows:

1. Listing 5 shows that a *loop_chain* defines a new scope. As this scope

is entered, a stamp s_1 of the trace is generated. This happens “behind the scenes”, because the *loop_chain* is a Python context manager, which can execute pre-specified routines prior and after the execution of the body. As the *loop_chain*’s scope is exited, a new stamp s_2 of the trace is computed. All parallel loops in the trace generated between s_1 and s_2 are placed into a sub-trace for pre-processing.

2. The pre-processing consists of two steps: (i) “simple” fusion – consecutive parallel loops iterating over the same iteration space that do not present indirect data dependencies are merged; (ii) generation of a loop chain representation for SLOPE.
3. In (ii), PyOP2 inspects the sequence of loops and translates all relevant data structures (sets, maps, loops) into a format suitable for the SLOPE’s Python interface. C code implementing an inspector for the loops in the *loop_chain* is returned by SLOPE. PyOP2 compiles and executes this code, which results in an *inspection* for the loop chain.
4. A “software cache” mapping *loop_chains* to *inspections* is used. This whole process needs therefore be executed only once for a given *loop_chain*.
5. The executor is built in an analogous way to the inspector.

3.9.3 Firedrake/DMPlex: the S-depth Mechanism for Extended Halo Regions

Firedrake uses DMPlex [Lange et al., 2015] to handle meshes. DMPlex is responsible for partitioning, distributing over multiple processes, and locally reordering a mesh. The MPI parallelization is therefore managed through Firedrake/DMPlex.

During the start-up phase, each MPI process receives a contiguous partition of the original mesh from DMPlex. The required PyOP2 sets, which can represent either topological components (e.g., cells, vertices) or function spaces, are created. As explained in Section 2.2.2, these sets distinguish between multiple regions: core, owned, exec, and non-exec. Firedrake initializes the four regions exploiting the information provided by DMPlex.

To support the loop chain abstraction, Firedrake must be able to allocate arbitrarily deep halo regions. Both Firedrake and DMPlex have been extended to support this feature⁴. A parameter called *S-depth* (the name has historical origins, see for instance Chronopoulos [1991]) regulates the extent of the halo regions. A value $S\text{-depth} = n$ indicates the presence of n strips of off-process data elements in each set. The default value is $S\text{-depth} = 1$, which enables computation-communication overlap when executing a single loop at the price of a small amount of redundant computation along partition boundaries. This is the default execution model in Firedrake.

3.10 Performance Evaluation - Benchmarks

The experimentation of generalized sparse tiling consisted of two phases:

1. Initially, the technique was tried in two benchmarks: a sparse Jacobi kernel and a proxy unstructured mesh application, originally developed as a demo for the OP2 framework. The objectives of this phase were (i) to explore the impact of generalized sparse tiling on performance, (ii) to characterize the circumstances where the approach is profitable, (iii) to identify the potential limitations of the technique in real applications, (iv) to prototype a compiler.
2. Then, a real application developed in Firedrake, Seigen (an elastic wave equation solver for seismological problems), was used for systematic performance evaluation. This is presented in Section 3.11. Thanks to its long sequence of loops, Seigen provided a whole suite of sparse tiling benchmark configurations.

In this section, we focus on phase 1. Both benchmarks are written in C. Sparse tiling was introduced manually using a preliminary version of SLOPE. A previous version of the inspector algorithms presented in this chapter, described in Strout et al. [2014], was used. As detailed next, one of the major drawbacks of this older inspector was its cost, which grew very rapidly with the number of loops in the chain and the number of

⁴The implementation was mostly carried out by Michael Lange.

Matrix name	Execution time reduction %	Speed-up
<i>ldoor</i>	40.34	12.11
<i>pwtk</i>	38.42	11.98
<i>thermal2</i>	25.78	11.08
<i>xenon2</i>	20.15	9.53
<i>audikw_1</i>	13.42	8.70
<i>nd24k</i>	-151.72	3.06

Table 3.4: Execution time reductions over the original implementation (in percentage) and speed-ups over the single-threaded tiled implementation for the sparse Jacobi solver with 15 threads.

distinct datasets accessed. Finally, only shared-memory parallelism via OpenMP was supported.

In all experiments presented in this section, the optimal tile size (i.e. the one leading to the best execution time) was determined empirically, for each combination of architecture and application.

3.10.1 Sparse Jacobi

The first benchmark was the sparse tiling of a Jacobi sparse matrix solver⁵. Given a sparse matrix A , and a vector \vec{f} , related by $A\vec{u} = \vec{f}$, each iteration of the sparse Jacobi method produces an approximation to the unknown vector \vec{u} . In our experiments, the Jacobi convergence iteration loop is unrolled by a factor of two and the resulting two loops are chained together (1000 iterations of the loop chain was executed). Using a ping-pong strategy, each loop reads from one copy of the \vec{u} vector and writes to the other copy. This experiment was run on an Intel Westmere (dual-socket 8-core Intel Xeon E7-4830 2.13 GHz, 24MB shared L3 cache per socket). The code was compiled using gcc-4.7.0 with options `-O3 -fopenmp`.

The Jacobi recurrence equation includes a sparse matrix vector multiplication and is representative of a broad class of sparse linear algebra applications. It is also an effective test-bed because different data dependency patterns can be examined simply by using different input matrices. In these experiments, a set of 6 input matrices, drawn from the University of Florida Sparse Matrix Collection [Davis and Hu, 2011], was used. The matrices were selected so that they would vary in overall data footprint,

⁵This section is partly extracted from Strout et al. [2014]; the experiments were conducted by Christopher D. Krieger, Catherine Olschanowsky, and Michelle Mills Strout

Architecture	Implementation	Execution time (s)	Speed-up
Westmere	<i>omp</i>	36.87	6.43
	<i>mpi</i>	31.0	7.66
	<i>tilde</i>	26.49	8.96
Sandy Bridge	<i>omp</i>	30.01	6.65
	<i>mpi</i>	24.42	8.17
	<i>tilde</i>	20.63	9.67

Table 3.5: Execution time (in seconds) and speed-ups over the slowest single-threaded implementation for the Airfoil benchmark. Respectively 16 and 24 threads/processes are used on the Sandy Bridge and Westmere machines.

from 45 MB to 892 MB, and in percentage of non-zeros, from very sparse at 0.0006% to much more dense at 0.5539% non-zeros.

Table 3.4 compares the performance of the tiled Jacobi solver to that of a simple blocked version. Both codes use OpenMP `parallel` for directives to achieve parallelism. The execution time reduction varied from 13% to 47% with the exception of the *nd24k* matrix, which showed as much as a 1.52x slowdown when sparse tiled. This matrix is highly connected, thus limiting the number of tiles that can be scheduled in parallel. The greater parallelism available under a blocked approach provides more benefit in this case than the performance improvements due to improved locality from full sparse tiling. Overall, speed-ups of between 8 and 12 times over the single-threaded tiled implementation were observed when using 15 threads; a clear outlier is again the *nd24k* matrix that did not scale past 3.2 times the single thread performance.

The values in Table 3.4 do not include the inspection time necessary to full sparse tile the loop chain. To break even when this cost is considered, the inspector time must be amortized over between 1000 and 3000 iterations of the executor, depending on the specific matrix being solved. We will further elaborate on this aspect in Section 3.10.3.

3.10.2 Airfoil

The second benchmark was Airfoil [Giles et al., 2005], a proxy finite volume application designed in the context of the OP2 project to represent the 3D viscous flow calculations typical of the Hydra CFD code [Reguly et al., 2016] at Rolls-Royce plc. It is a nonlinear 2D inviscid airfoil

code using an unstructured mesh, which solves the 2D Euler equations employing a scalar numerical dissipation. Airfoil has a predictor/corrector time-marching loop consisting of 2000 iterations, and iterates towards the steady state solution by using a control volume approach in each iteration [OP2 contributors, 2011]. At each time iteration, four parallel loops are executed. The first two loops, called *adt-calc* and *res-calc*, constitute the bulk of the computation. The *adt-calc* loop iterates over cells, reads from adjacent vertices and writes to a local dataset, whereas *res-calc* iterates over edges and exploits indirect mappings to vertices and cells for incrementing indirect datasets associated to cells. These loops share datasets associated with cells and vertices. The *res-calc* loop computes the flux over the interior edges. The third and fourth loops, called *bres-calc* and *update*, are less computationally expensive. The former computes the flux over the boundary edges, while the latter – a direct loop over cells – updates the current solution. Double-precision floating-point arithmetic is used.

Three implementations of Airfoil, *omp*, *mpi* and *tiled*, were compared on two shared-memory machines, an Intel Westmere (dual-socket 6-core Intel Xeon X5650 2.66 GHz, 12MB of shared L3 cache per socket) and an Intel Sandy Bridge (dual-socket 8-core Intel Xeon E5-2680 2.00Ghz, 20MB of shared L3 cache per socket). The code was compiled using the Intel *icc* 2013 compiler with optimizations enabled (*-O3*, *-xSSE4.2* on the Westmere and *-xAVX* on the Sandy Bridge).

The *omp* and *mpi* versions of Airfoil were implemented in OP2. The effectiveness of these parallelization schemes has been demonstrated in Giles et al. [2011]. The *tiled* implementation uses an early version of the SLOPE library (the differences with the inspector algorithms shown in Section 3.8.1 are discussed later) and is based on shared-memory parallelism via OpenMP. We manually unrolled the time loop by a factor of two to be able to tile over 6 loops in total.

Table 3.5 shows the runtime reduction achieved by sparse tiling the loop chain on the Westmere and Sandy Bridge architectures. The input unstructured mesh was composed of 1.5 million edges. It is worth noticing that both the *omp* and *tiled* versions suffer from the well-known NUMA effect as threads are always equally spread across the two sockets. Nevertheless, compared to *mpi*, the *tiled* version exhibits a peak runtime reduction

of 15% on the Westmere and of 16% on the Sandy Bridge.

Results shown for *tiled* do not include, however, the inspector overhead. By also including it, the aforementioned improvements over *mpi* reduce to roughly 10% on both platforms. In common with the sparse Jacobi solver, the slow-downs when including the inspection overhead are significant.

3.10.3 Outcome

Need for highly optimized inspection The inspection overhead can significantly affect sparse tiling. The situation may be even worse in real applications, as usually characterized by longer loop chains, or when the mesh changes over time. This experimental phase led to re-engineering the inspection scheme presented in Strout et al. [2014] into the version described in this chapter. To summarize, the critical differences are: (i) data dependency analysis abstracted to the level of sets, rather than datasets; (ii) optimistic coloring with backtracking in case of conflicts; (iii) parallelization of the projection and tiling routines through the use of inverse maps.

Need for automation The second lesson from this experimentation is that automation is indispensable. Writing the inspector as a sequence of calls to SLOPE is relatively simple, although tedious and error-prone. Integrating the executor is much more complicated, because this requires the rewriting of an entire sequence of loops. This is a severe limitation as it poses an implementation burden on potential users. These considerations led to the multilayer framework detailed in Section 3.9, which automatically generates inspector/executor schemes in Firedrake programs.

Need for distributed-memory support The Airfoil experiments highlighted that shared-memory parallelism over multi-socket architectures is drastically affected by the non-uniform memory access (NUMA) issue. The difference in execution time between the OP2 OpenMP and MPI versions is in this sense remarkable. As discussed in Regulý et al. [2016], the irregular nature of the computation makes it hard to find systematic solutions to the NUMA issue in the case of pure OpenMP parallelism. The sparse tiled implementation was also purely based on OpenMP, so it

suffered from the same problem. This led to the definition of a more general loop chain abstraction (Section 3.5.3) and to the introduction of more flexible inspector algorithms (Section 3.8.1), enabling distributed-memory execution. The MPI and the hybrid OpenMP/MPI execution models are naturally better options for unstructured mesh applications.

3.11 Performance Evaluation - Seigen: an Elastic Wave Equation Solver for Seismological Problems

In this section, sparse tiling is applied to a computation built on top of Firedrake, Seigen. The performance analysis presented in the following sections is an actual methodological contribution of the thesis. The objectives of this experimentation were to quantify and to motivate in detail the impact of the optimization in a complex, realistic simulation. For this, we executed a large set of experiments on multiple architectures, made use of profilers and analytical tools, and studied the correlation with key simulation parameters, such as the polynomial order and the mesh.

3.11.1 Computation

3.11.1.1 The Seismic Model

Seigen is a novel seismological modelling framework capable of solving the elastic wave equation on unstructured meshes. Exploiting the well-known velocity-stress formulation [Virieux, 1986], the seismic model is expressible as two first-order linear PDEs, which we refer to as velocity and stress. These governing equations are discretized in space through the discontinuous-Galerkin finite element method. The evolution over time is obtained by using a fourth-order explicit leapfrog scheme based on a truncated Taylor series expansion of the velocity and stress fields. The particular choice of spatial and temporal discretizations has been shown to be non-dissipative [Delcourte et al., 2009]. More details can be found in Jacobs et al. [2016]. Seigen is part of OPESCI, an ecosystem of software for elastic wave modeling [Gorman et al., 2015].

3.11.1.2 Choice of the Test Case

The Seigen framework has been implemented using Firedrake by Christian Jacobs⁶, along with a set of test cases. In this experimentation, we use the `explosive_source` test case. The test cases may differ in various aspects, such as the initial conditions of the system and the propagation of waves. However, they are all based upon the same seismological model; from a computational viewpoint, this means that, in a time step, the same sequence of loops is executed. Consequently, the performance analysis of `explosive_source` in Section 3.11.3 is generalizable to the other test cases. In fact, some of the conclusions will be generalizable to even completely different codes.

3.11.1.3 Implementation

In a time loop iteration, eight linear systems need be solved, four from velocity and four from stress. Each solve consists of three macro-steps (see also Section 2.1.4): assembling a global matrix A ; assembling a global vector b ; computing x in the system $Ax = b$. There are two global “mass” matrices, one for velocity and one for stress. Both matrices are

- Time invariant, so they are assembled before entering the time loop.
- Block-diagonal, as a consequence of the spatial discretization employed; a block belongs to an element in the mesh. The inverse of a block-diagonal matrix is again block-diagonal and is determined by computing the inverse of each block. The solution of the linear system $Ax = b$, expressible as $x = bA^{-1}$, can therefore be evaluated by looping over the mesh and computing a “small” matrix-vector product in each element, where the matrix is a block in A^{-1} .

Assembling the global vectors reduces to executing a set of loops over mesh entities, particularly over cells, interior facets, and exterior facets. Overall, twenty-five loops are executed in a time loop iteration. Thanks to the hierarchy of “software caches” employed by Firedrake, the translation from mathematical syntax into loops is only performed once.

⁶Formerly Imperial College London, now University of Southampton

3.11.1.4 Application of Sparse Tiling

Introducing sparse tiling into Seigen was relatively straightforward. Three steps were required: (i) embedding the time stepping loop in a *loop_chain* context (see Section 3.9.2), (ii) propagating the relevant user input for performance tuning, (iii) creating a set of *fusion schemes*. A fusion scheme establishes which sub-sequences of loops within a *loop_chain* will be fused and the respective seed tile sizes. If no fusion schemes were specified, all of the twenty-five loops would be fused using a default tile size. As we shall see, operating with a set of small loop chains and heterogeneous tile sizes is much more effective than fusing long sequences of loops. Hence, specifying multiple fusion schemes is likely to have a direct payoff in performance. As an example, one such scheme treats the loops arising in velocity and stress as two different loop chains.

3.11.1.5 Validation

Seigen has several mechanisms to validate the correctness of the seismological model and the test cases. The numerical results of all code versions (with and without tiling) were checked and compared. Paraview was also used to verify the simulation output.

3.11.1.6 Parametrization of the Computation

There are two parameters that we can vary in `explosive_source`: the polynomial order of the method and the input mesh.

Polynomial order q We will test the spectrum $q \in \{1, 2, 3, 4\}$. To test higher polynomial orders, changes to both the spatial and temporal discretizations would be necessary. For the spatial discretization, the most obvious choice would be tensor product function spaces. However, this functionality is still under development in Firedrake.

Mesh We use as input a two-dimensional rectangular domain of fixed size 300×150 tessellated with triangles. We will vary the mesh spacing h , which impacts the number of elements in the domain.

3.11.1.7 Computational Analysis of the Loops

We here discuss computational aspects of the twenty-five fusible loops. The following considerations derive from an analytical study of the data movement in the loop chain, extensive profiling through the Intel VTune Amplifier tool [Intel Corporation, 2016], and roofline models (available in Jacobs et al. [2016]).

Seigen should benefit from sparse tiling Not only does data reuse arise within single loops (e.g., by accessing vertex coordinates from adjacent cells), but also across consecutive loops, through indirect data dependencies. This makes Seigen a natural fit for sparse tiling.

Data reuse across solvers Eight “solver” loops perform matrix-vector multiplications in each mesh element. It is well established that linear algebra operations of this kind are memory-bound. Four of these loops arise from *velocity*, the others from *stress*. There is significant data reuse amongst the four *velocity* loops and amongst the four *stress* loops, since the same blocks in the global inverse matrices are accessed. We hypothesize performance gains if these loops were fused through sparse tiling.

Exterior facet loops have negligible cost Three loops implement the boundary conditions of the variational problems by iterating over the exterior mesh facets. The impact of these loops on the completion time is negligible, since their iteration space is order of magnitude smaller than that of cells and facets loops.

Data reuse across cells and facets loops Six loops iterate over the interior mesh facets to compute so called facet integrals. Facet integrals ensure the propagation of information between adjacent cells in discontinuous-Galerkin methods. The operational intensity of these loops is much lower than that of cell loops, and memory-boundedness is expected. Consecutive facet and cell integral loops share fields, which creates cross-loop data reuse opportunities. Again, sparse tiling might play an important role in transforming this data reuse into data locality.

Optimizing the operational intensity All computational kernels generated in Seigen are optimized through COFFEE (Chapters 4, 5, 6). In

essence: (i) the operation count is minimized by restructuring expressions and loop nests; (ii) auto-vectorization opportunities are created by using array padding and by enforcing data alignment.

3.11.2 Setup and Reproducibility

3.11.2.1 Fusion Schemes and Attempted Optimizations

The generality of the sparse tiling algorithms, the flexibility of the *loop_chain* interface, and the *S-depth* mechanism made it possible to experiment with a variety of fusion schemes without changes to the source code.

Five fusion schemes were devised, based on the following criteria: (i) amount of data reuse, (ii) amount of redundant computation over the boundary region, (iii) memory footprint (the larger, the smaller the tile size to fit in cache). The fusion schemes are summarized in Table 3.6 and illustrated in Figure 3.11. The full specification, along with the seed tile size for each sub loop chain, is available at Jacobs and Luporini [2016].

Fusion scheme	Number of sub loop chains	Criterion	<i>S-depth</i>
fs1	3	Fuse only a few cells and facets loops	2
fs2	8	Several short loop chains	2
fs3	6	fs2 and include all solver loops	2
fs4	3	More aggressive than fs3	3
fs5	2	Two loop chains: one for velocity and one for stress	4

Table 3.6: Summary of the fusion schemes adopted in Seigen. The *S-depth* column represents the number of off-process cell layers.

Furthermore, several optimizations, applicable to all fusion schemes, were tried:

Global and local maps Algorithm 1 computes so called local maps to avoid an extra level of indirection in the executor. We regard this as a *potential optimization*. Although no data reuse is available for the local maps (each fused loop has its own local maps), there might be benefits from improved hardware prefetching and memory latency. We will experiment with both global (i.e., original, as constructed by Firedrake and provided in the loop chain specification) and local (i.e., computed by SLOPE) maps.

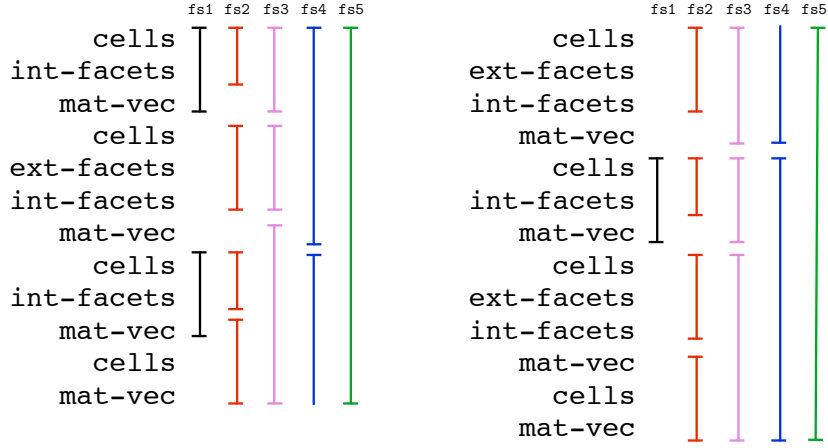


Figure 3.11: The sub loop chains in the five fusion schemes. *Cells*, *int-facets*, and *ext-facets* represent respectively the cell, interior facet, and exterior facet assembly loops, while *mat-vec* represents a solver.

Tile shape The seed loop partitioning and the mesh numbering determine the tile shape. The simplest way of creating tiles consists of “chunking” the seed iteration space every ts iterations, with ts being the initial tile size (see Section 3.8.1). The chunk partitioning inherits the original mesh numbering. In Firedrake, and therefore in Seigen, meshes are renumbered during initialization applying the reverse Cuthill–McKee (RCM) algorithm. Using chunk partitioning on top of an RCM-renumbered mesh has the effect of producing thin, rectangular tiles. This affects tile expansion, as a large proportion of elements lie on the tile border. There are potential solutions to this problem. The most promising would consist of using a Hilbert curve, rather than RCM, to renumber the mesh. This would lead to more regular polygonal tiles when applying chunk partitioning. Unfortunately, Hilbert curves are at the moment not supported in Firedrake. An alternative consists of partitioning the seed iteration space with a library like METIS [Karypis and Kumar, 2011] before applying RCM. As we shall see, this approach is not exempt from side effects.

Software prefetching In a loop, there are usually more than a single stream of memory accesses amenable to hardware prefetching (e.g., accesses to the indirection maps; direct accesses to data values; in-

direct accesses to data values if the mesh has a good numbering). Sparse tiling, unfortunately, impairs hardware prefetching for two reasons: (i) the virtual addresses streams are considerably shorter; (ii) tile expansion introduces irregularities in these streams. Software prefetching can be used together with hardware prefetching to minimize memory stalls. PyOP2 and SLOPE have been extended to emit intrinsics instructions for prefetching the iteration i 's maps and data values while executing iteration $i - 1$.

Extended boundary region The special non-exec tile T_{ne} (see Sections 3.6 and 3.8.1) reduces the amount of redundant computation in long loop chains by expanding over boundary tiles. There are two ways of creating T_{ne} : either an extra layer of data is added to the boundary region (e.g., see Figure 3.7) or during inspection, by searching for mesh boundaries. The current implementation only supports the first option. Manually deriving T_{ne} would be not only algorithmically complex, but also potentially very expensive.

3.11.2.2 Systems Configuration and Execution Modes

Extensive experimentation was performed on two Intel architectures, whose specification is reported in Table 3.7.

System	Erebus	CX1-Ivy
Node	1x4-core Intel I7-2600 3.4GHz	2x20-core Intel Xeon E5-2660 2.20GHz
DRAM	16 GB	64 GB
STREAM performance	18.5 GB/s (4.6 GB/s per core)	92.0 GB/s (4.6 GB/s per core)
Cache hierarchy	L1=32KB, L2=256KB, L3=8MB L3 is shared	L1=32KB, L2=256KB, L3=25MB L3 is shared per socket (50MB total)
Compilers	Intel icc 16.0.2	Intel icc 15.1
Compiler flags	-O3 -xHost -ip	-O3 -xHost -ip
MPI version	Open MPI 1.6.5	Intel MPI 5.1
MPI options	--bind-to-core	I.MPI.DEVICE ssm I.MPI.PIN yes I.MPI.PIN.MODE lib I.MPI.PIN.PROCESSOR.LIST map=bunch

Table 3.7: Systems specification.

Support for shared-memory parallelism is discontinued in Firedrake,

so only distributed-memory parallelism was tested. MPI processes were pinned to cores. The hyperthreading technology was not used. Erebus and CX1-Ivy were unstressed and exclusive access had been obtained when the runs were performed.

3.11.2.3 Meshes

The (average) number of degrees of freedom d assigned to a process mainly depends on the polynomial order q , the mesh spacing h and the number of cores n in a node. Meshes are chosen such that: (i) d fits in main memory; (ii) d exceeds the last level of cache; (iii) $\langle d, q, h \rangle$ ensure convergence of the simulation. A summary of the meshes used for experimentation is provided in Table 3.8.

System	h	d velocity				d stress			
		$q = 1$	$q = 2$	$q = 3$	$q = 4$	$q = 1$	$q = 2$	$q = 3$	$q = 4$
Erebus ($n = 4$)	1.0	138k	276k	460k	690k	276k	552k	920k	1379k
	1.2	96k	192k	320k	480k	192k	385k	641k	961k
CX1-Ivy ($n = 20$)	0.6	78k	157k	262k	393k	157k	314k	525k	787k
	0.8	44k	89k	149k	223k	89k	178k	298k	447k

Table 3.8: Summary of the meshes used for single-node experimentation in Seigen. d is the average number of degrees of freedom assigned to a process for a given variational form.

3.11.2.4 Timing Criteria

For each experiment, we collect three measurements.

Overall completion time (OT) Used to compute the maximum application speed-up when sparse tiling is applied.

Average compute time (ACT) Sparse tiling impacts the kernel execution time by increasing data locality. Communication is also influenced, especially in aggressive fusion schemes: the rounds of communication decrease, while the data volume exchanged may increase. ACT isolates the gain due to increased data locality from (i) the communication cost and (ii) any other action performed in Firedrake (executing

Python code) between the invocation of kernels. This value is averaged across the processes.

Average compute and communication time (ACCT) As opposed to ACT, the communication cost is also included in ACCT. By comparing ACCT and ACT, the communication overhead can be derived.

As we shall see, all of these metrics will be essential for a complete understanding of the sparse tiling performance. It is true that for much larger meshes ACT and ACCT should converge to OCT, but such an experimentation is not feasible as it would require weeks, possibly months, of compute time.

To collect OT, ACT and ACCT, the following configuration was adopted.

- All experiments were executed with “warm cache”; that is, with all kernels retrieved directly from the Firedrake’s software cache of compiled kernels, so code generation and compilation times are not counted.
- All of the non-tiled `explosive_source` tests were repeated three times. The sparse tiling search space is big (the product of all q , fusion schemes, tile sizes, meshes and a set of additional optimizations) and some tests can last longer than a hour, so for practical reasons the tiled `explosive_source` tests were repeated two times, instead of three. The minimum times are reported (negligible variance).
- The cost of global matrix assembly – an operation that takes place before entering the time loop – *is not* included in OT. Firedrake needs to be extended to assemble block-diagonal matrices directly into vectors (an entry in the vector would represent a matrix block). Currently, this is instead obtained in two steps: first, by assembling into a CSR matrix; then, by explicitly copying the diagonal into a vector (a Python operation). The assembly per se never takes more than 3 seconds, so it is reasonable to exclude this temporary overhead from our timing.
- The inspection cost due to sparse tiling *is* included in OT.

- Extra costs were minimized: no check-pointing, only two I/O sessions (at the beginning and at the end of the computation), and minimal logging.
- The time loop has a fixed duration T , while the time step depends on the mesh spacing h to satisfy the Courant–Friedrichs–Lewy necessary condition (i.e., CFL limit) for the numerical convergence. In essence, finer meshes require proportionately smaller time steps to ensure convergence. Furthermore, T cannot be reduced arbitrarily, which makes the performance exploration longer. A (prolonged) transitory period P is necessary so that the waves fully propagate across the domain. During P , the data movement is greatly reduced as most data values are unchanged. The effects of sparse tiling become evident only if T is sufficiently longer than P , so complete simulations had to be executed.

3.11.3 Results and Analysis

In this section, we report on hundreds of experiments aimed at quantifying the performance improvements obtainable in Seigen when sparse tiling is applied. Using the `explosive_source` test case, we explore a large set of parameters, which includes polynomial order, mesh, node architecture, fusion scheme, and many others. A generic instance of `explosive_source` optimized with sparse tiling will be referred to as a “tiled version”, otherwise the term “original version” will be used. The structure of this section is as follows:

1. We start with an overview of the maximum speed-ups obtained through sparse tiling. Some preliminary observations are made.
2. We delineate the structure of the search space exploration for determining the optimal sparse tiling version.
3. We motivate, in detail, through plots and the *loop chain analyzer* tool (introduced shortly), the performance of the various fusion schemes and optimizations attempted.
4. We provide further evidence from profiler reports.

5. We comment on the performance bottlenecks introduced by sparse tiling.

3.11.3.1 Summary of the Attained Speed-ups

The times that we report below derive from runs with 1 MPI process per physical core. The benefits from sparse tiling (if any) tend to be negligible in other types of runs (e.g., sequential runs). As elaborated in the following sections, this is a consequence of three factors: (i) the memory access latency is only marginally affected when a large proportion of bandwidth is available to the processes; (ii) hardware prefetching is impaired by the small iteration space of tiles; (iii) TLB misses are more frequent due to tile expansion.

Table 3.9 reports the completion times (OT) for the original and tiled versions of Seigen, on both Erebus and CX1-Ivy. For each node architecture, polynomial order q and mesh, the best tiled version time is reported; the search space exploration that led to this number will be detailed in the next section. The speed-up for OT achieved through sparse tiling is indicated as Ω^{OT} . Tables 3.10 and 3.11 show analogous information for ACT and ACCT.

Based on these tables, some preliminary observations can be made.

- Despite a similar amount of available bandwidth per core, an improved core architecture and a better cache hierarchy (see Table 3.7) the speed-ups on CX1-Ivy are generally not as high as on Erebus. Profiling through Intel VTune showed that the proportion of time spent on executing compute-bound loops is higher on CX1-Ivy than on Erebus, but further investigation is required to explain this behaviour. It would be interesting to carry out a similar performance exploration on a many-core architecture, like Intel’s Knights Landing, characterized by less powerful cores and a completely different memory system. Testing on multi-node systems is also high priority future work, as this will increase the pressure on the memory system due to inter-node communication.
- The performance improvements are generally greater than $1.10\times$, and often exceed $1.20\times$. In light of the limiting factors discussed in

the next sections, this is a promising result. While some of these limiting factors are inherent in Seigen and sparse tiling, others are simply due to shortcomings of the current implementation. We therefore envisage ample space for improvements. Ω^{ACT} and Ω^{ACCT} are, as expected, higher than Ω^{OT} . ACT, in particular, tells us that the benefits from the relieved memory pressure outweigh the redundant computation overhead.

- The performance improvements tend to increase with q . This is remarkable, but not surprising. The memory footprint of an iteration grows with q , hence all negative effects such as impaired hardware prefetching and TLB misses (properly documented in the next sections) caused by sparse tiling become less notable. This trend can be observed in all problem instances.

3.11.3.2 Structure of the Search Space Exploration

The best tiled version for a specific problem instance was determined empirically, trying all possible combinations out of a set of parameters. The

System	h	q	OT (s)	OT tiled (s)	Ω^{OT}
Erebus ($n = 4$)	1.0	1	687	596	1.15
		2	1453	1200	1.21
		3	3570	2847	1.25
		4	7057	5827	1.21
	1.2	1	419	365	1.15
		2	870	715	1.22
		3	1937	1549	1.25
		4	4110	3390	1.21
CX1-Ivy ($n = 20$)	0.6	1	859	813	1.06
		2	1712	1585	1.08
		3	3680	3378	1.09
		4	8051	6962	1.16
	0.8	1	396	390	1.02
		2	770	721	1.07
		3	1562	1457	1.07
		4	3263	2931	1.11

Table 3.9: Comparing the Seigen completion time OT on Erebus (number of processes $n = 4$) and CX1-Ivy ($n = 20$).

System	h	q	ACT (s)	ACT tiled (s)	Ω^{ACT}
Erebus ($n = 4$)	1.0	1	533	455	1.17
		2	1252	999	1.25
		3	3255	2549	1.28
		4	6585	5401	1.22
	1.2	1	313	267	1.17
		2	729	579	1.26
		3	1746	1360	1.28
		4	3837	3127	1.23
CX1-Ivy ($n = 20$)	0.6	1	484	448	1.08
		2	1149	1015	1.13
		3	2740	2471	1.11
		4	6354	5423	1.17
	0.8	1	191	175	1.09
		2	486	434	1.12
		3	1159	1068	1.09
		4	2654	2307	1.15

Table 3.10: Comparing the Seigen average compute time ACT on Erebus (number of processes $n = 4$) and CX1-Ivy ($n = 20$).

System	h	q	ACCT (s)	ACCT tiled (s)	Ω^{ACCT}
Erebus ($n = 4$)	1.0	1	581	503	1.16
		2	1334	1071	1.25
		3	3438	2712	1.27
		4	6881	5661	1.22
	1.2	1	340	293	1.16
		2	776	618	1.26
		3	1827	1437	1.27
		4	3987	3265	1.22
CX1-Ivy ($n = 20$)	0.6	1	638	586	1.09
		2	1468	1336	1.1
		3	3398	3087	1.1
		4	7745	6649	1.16
	0.8	1	230	247	0.93
		2	603	543	1.11
		3	1378	1278	1.08
		4	3061	2730	1.12

Table 3.11: Comparing the Seigen average compute and communication time ACCT on Erebus (number of processes $n = 4$) and CX1-Ivy ($n = 20$).

space of parameters was described in Section 3.11.2.1 and is summarized below.

Fusion scheme Five fusion schemes (fsX , $X \in \{1, 2, 3, 4, 5\}$) were studied (see Table 3.6).

Seed tile size For each fs and q , three or four tile sizes were tested. Four tile sizes were used with $q \in \{1, 2\}$. The tile sizes were chosen to maximize the likelihood of fitting in L2 or L3 cache. A less extensive experimentation with “more adverse” tile sizes showed that: (i) a very small value causes dramatic slow-downs (up to $8\times$ slower than the original versions); (ii) larger values cause proportionately greater increase in execution time.

Indirection maps Both local and global maps were tested.

Partitioning Two partitioning strategies were tested: `chunk` and `metis`.

Extended boundary region All experiments were repeated with and without the extended boundary region optimization discussed in Section 3.11.2.1.

Software prefetching and a small set of prefetch distances were also tested in a few instances of `explosive_source`, but no significant changes to the execution times were observed. It was decided, therefore, to exclude this parameter from the search space; this made it possible to execute the whole test suite in slightly less than five days.

An `explosive_source` instance is determined by three parameters:

Node architecture The two systems shown in Table 3.7 were used.

Polynomial order $q \in \{1, 2, 3, 4\}$.

Mesh The meshes shown in Table 3.8 were used (two meshes for each node architecture).

We experimented with $2 \times 4 \times 2 = 16$ `explosive_source` instances. For each of these instances, we tested the original Seigen version and a set of tiled versions. When $q \in \{1, 2\}$, a set of tiled versions consists of $5 \times 4 \times 2 \times 2 \times 2 = 160$ instances (otherwise, with $q \in \{3, 4\}$, the instances are

120). In total, we executed $8 \times (160 + 1) + 8 \times (120 + 1) = 2256$ versions of Seigen on single node.

Given the large number of problem instances, the results of the search space exploration are organized as follows. We show one plot for each of the sixteen `explosive_source` instances. A plot illustrates the search space exploration for given node architecture, h and q . The ACCT of the original version and a subset of tiled versions is reported on the y-axis. To make the plots readable, the impact of (i) local/global indirection maps, (ii) normal/extended boundary region, (iii) `chunk/metis` partitioning strategies are only discussed qualitatively. Fortunately, it is very straightforward to draw general conclusions about the effect of these optimizations. The raw execution times are available at Luporini [2016a].

3.11.3.3 Outcome of the Search Space Exploration

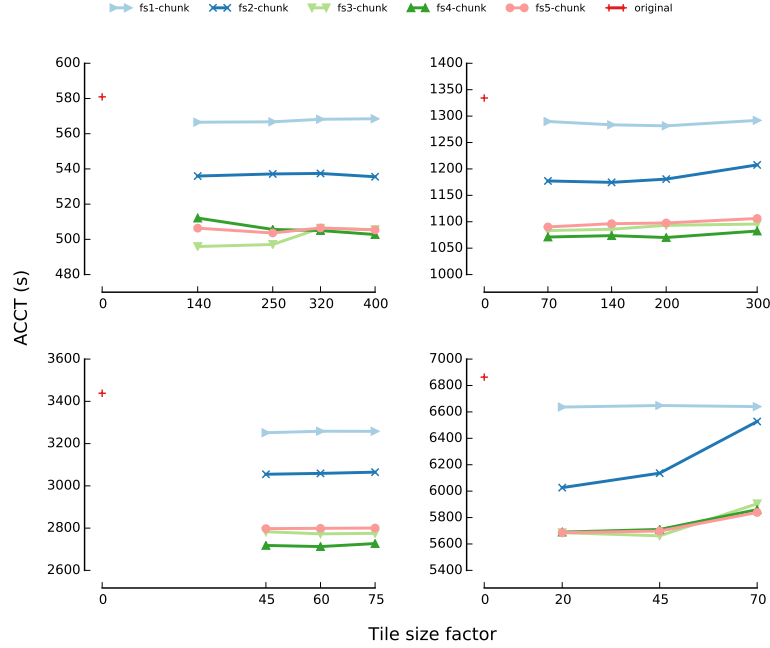
PyOP2 was enhanced with a *loop chain analyzer* (LCA) capable of estimating the best- and worst-case tile memory footprint, as well as the percentage of data reuse ideally achievable⁷. We use this tool, as well as Intel VTune, to explain the performance achieved.

Figure 3.12 and 3.14 illustrate the search space exploration on Erebus and CX1-Ivy, respectively. For reference, the ACCT of the original version is also reported (in red, null tile size). The general trend of the search space exploration is as follows.

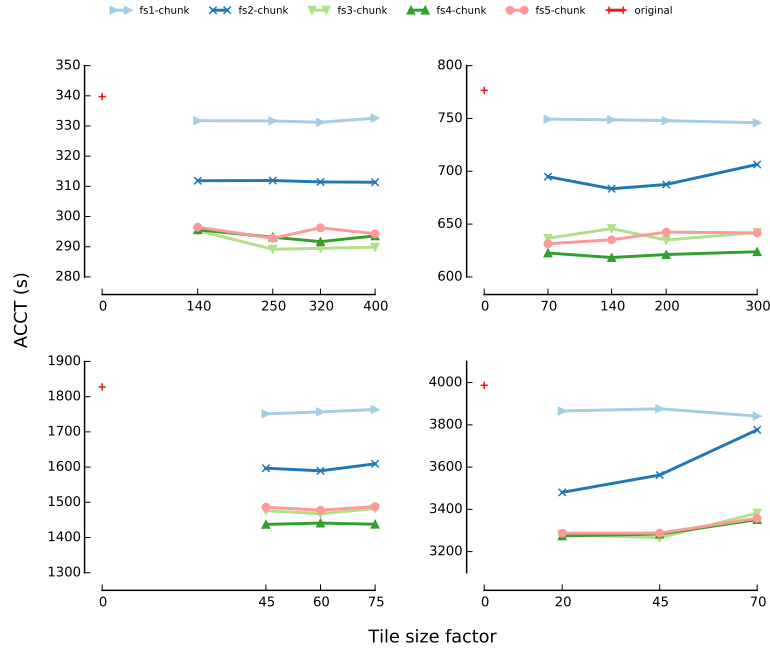
- `fs`, unsurprisingly, is the parameter having largest impact on the ACCT. By influencing the fraction of data reuse convertible into data locality, the amount of redundant computation and the data volume exchanged, fusion schemes play a fundamental role in sparse tiling. This makes automation much more than a desired feature: without any changes to the source code, multiple sparse tiling strategies could be studied and tuned. Automation is one of our major contributions, and this performance exploration justifies the implementation effort.
- There is a non-trivial relationship between ACCT, q and `fs`. The aggressive fusion schemes are more effective with high q – that is,

⁷It is part of our future plans to move this machinery into SLOPE, where the effects of tile expansion can be taken into account to provide better estimates.

Figure 3.12: Search space exploration on Erebus with $n = 4$ MPI processes. Two meshes ($h \in \{1.0, 1.2\}$) and four polynomial orders ($q \in \{1, 2, 3, 4\}$) are shown. Each plot shows the average compute and communication time (ACCT, y-axis) of five fusion schemes and the original version. The seed tile size of a loop chain in an fs, in terms of seed loop iterations, is the product of the “tile size factor” (x-axis) and a pre-established multiplier (an integer in the range $[1, 4]$; full list at Jacobs and Luporini [2016]). With tiling, global maps, chunk partitioning, and the extended boundary region optimization are used.

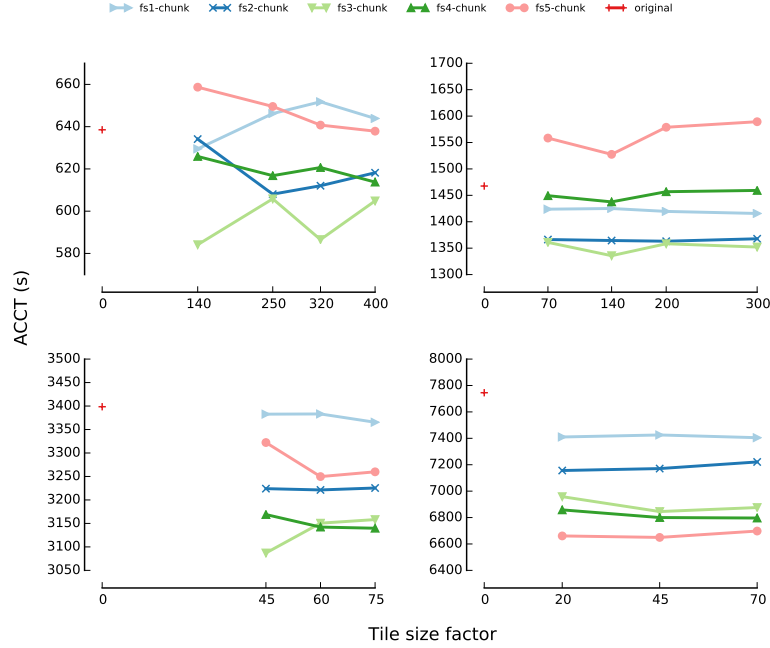


(a) $h = 1.0$.

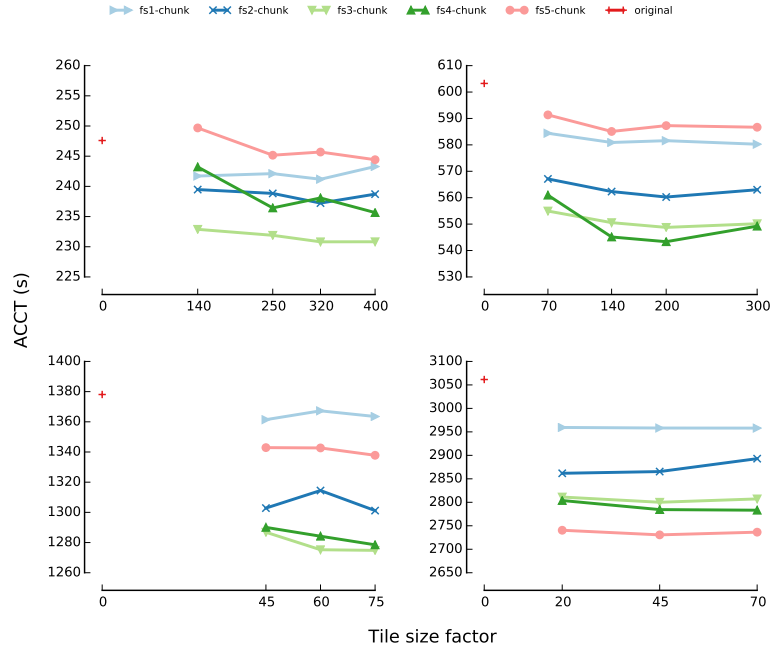


(b) $h = 1.2$.

Figure 3.14: Search space exploration on CX1-Ivy with $n = 20$ MPI processes. Two meshes ($h \in \{0.6, 0.8\}$) and four polynomial orders ($q \in \{1, 2, 3, 4\}$) are shown. Each plot shows the average compute and communication time (ACCT, y-axis) of five fusion schemes and the original version. The seed tile size of a loop chain in an fs, in terms of seed loop iterations, is the product of the “tile size factor” (x-axis) and a pre-established multiplier (an integer in the range $[1, 4]$; full list at Jacobs and Luporini [2016]). With tiling, global maps, chunk partitioning, and the extended boundary region optimization are used.



(a) $h = 0.6$.



(b) $h = 0.8$.

with larger memory footprints – while they tend to be less efficient, or even deleterious, when q is low. The extreme case is fs5, which fuses two long sequences of loops (twelve and thirteen loops each). In Figure 3.12 (Erebus), fs5 is never a winning choice, although the difference between fs3/fs4 and fs5 decreases as q grows. In Figure 3.15b (CX1-Ivy) this phenomenon is even more pronounced: while with $q = 2$ fs4 was almost $1.10\times$ faster than the best fs5, with $q = 3$ the difference was only $1.04\times$, and with $q = 4$ fs5 ended outperforming fs4 by roughly $1.02\times$. If this trend continued with $q > 4$, then the gain from sparse tiling could become increasingly larger.

- A non-aggressive scheme fuses only a few small subsets of loops. As discussed in later sections, these fusion schemes, despite affording larger tile sizes than the more aggressive ones (due to the smaller memory footprint), suffer from limited cross-loop data reuse. For fs1, LCA determines that the percentage of reusable data in the three fused loop chains decreases from 25% ($q = 1$) to 13% ($q = 4$). The drop is exacerbated by the fact that no reuse can be exploited for the maps. Not only are these ideal values, but also a significant number of loops are left outside of loop chains. The combination of these factors motivate the lack of substantial speed-ups. With fs2, a larger proportion of loops are fused and the amount of shared data increases. The peak ideal reuse in a loop chain reaches 54%, which translates into better ACCTs. A similar growth in data reuse can be appreciated in more aggressive fusion schemes, with a peak of 61% in one of the fs5's loop chains. Nevertheless, the performance of fs5 is usually worse than fs4. As we shall clarify in later sections, this is mainly due to the excessive memory footprint, which in turn leads to very small tiles. Speculatively, we tried running a sixth fusion scheme: a single loop chain including all of the 25 loops in a time iteration. In spite of an ideal data reuse of about 70%, the ACCT was always significantly higher than all other schemes.
- Figure 3.12 and 3.14 show the ACCT for a “good selection” of tile size candidates. Our approach was as follows. We took a very small set of problem instances and we tried a large range of seed tile sizes.

Very small tile sizes caused dramatic slow-downs, mostly because of ineffective hardware prefetching and TLB misses. Tile sizes larger than a fraction of L3 cache also led to increasingly higher ACCTs. If we consider $q = 4$ in Figure 3.12, we observe that the ACCT of fs2, fs3, and fs4 grows when the initial number of iterations in a tile is as big as 70. Here, LCA shows that the tile memory footprint is, in multiple loop chains, higher than 3MB, with a peak of 6MB in fs3. This exceeds the proportion of L3 cache that a process owns (on average), which explains the performance drop.

As explained, the tile size and the fusion scheme are the most important parameters of the search space exploration. Fortunately, general conclusions about the impact of the other optimizations can easily be drawn.

Indirection maps Using local maps provides marginal gains with fs1 and fs2; that is, only when there is none or very little reuse for the indirection maps. In all other cases, the original indirection maps, provided through the loop chain abstraction, lead to larger gains, despite the need for an extra level of indirection.

Partitioning The chunk partitioning, applied on top of the RCM-based mesh numbering, *always* outperforms the *metis* partitioning. The main reasons, as properly documented in Section 3.11.3.6, are the increase in TLB misses and a less effective hardware prefetching, caused by a more irregular tile expansion.

Extended boundary region Minimization of redundant computation through expansion of non-exec tiles, implemented by allocating an extra layer of data elements along the boundary region (see T_{ne} in Figure 3.7 and Section 3.11.2.1), *almost always* improves the ACCT. Further, when it does not, the performance difference tends to be negligible.

Summarizing, a very promising heuristic for a cost model might be: (i) never use local maps; (ii) always use chunk partitioning, ideally on top of a Hilbert curve (see also Section 3.11.3.6); (iii) always minimize redundant computation by means of a non-exec boundary region.

3.11.3.4 Testing the Hypothesis via Profilers

Our hypothesis was that speed-ups could be achieved as sparse tiling turns data reuse into data locality, thus diminishing the memory pressure and improving the memory latency. The combination of three different analyses provides compelling evidence that this was correct.

- The time spent in executing Python code is marginally affected by sparse tiling, irrespective of the number of loops fused. This was verified in several ways. First, we timed the experiments with just one tile covering the whole iteration space, for several types of loop chains, and then we compared to the case with no sparse tiling. On one hand, loop fusion reduces the number of “jumps” between Python and just-in-time compiled code proportionately to the loop chain length. On the other hand, the Python processing takes longer when sparse tiling is enabled, as a fused loop must be constructed from the original sequence generated by Firedrake. These appear to neutralize one another’s costs. Second, we profiled some test cases with Python’s cProfile, which gave us exact measurements of how much time is spent in each individual function. Illustrative graphs were produced from these profiles, and are available at [Luporini, 2016a]. Third, an indirect confirmation derives from the trend of ACT, which excludes the Python processing.
- Several VTune “general-exploration” and “advanced-hotspots” analyses confirmed that significant speed-ups derive from increased data locality. This was evident in all types of fusion schemes. For example, consider `fs5` and the `stress` loop chain. VTune shows that the execution times of the second and third solver loops are much smaller than that of the first loop. In addition, fewer L3 cache misses occur when loading the data values for the matrix-vector multiplication. Similar evidence arises from fusing cell and facet integral loops, although the gains are less pronounced.
- A VTune “bandwidth analysis” displays memory usage as a function of application time (in GB/s). By comparing the tiled and non-tiled versions, we observed that the former constantly consumes much less memory bandwidth (for both reads and writes). This

suggests that the processes are able to retrieve data from cache more often.

3.11.3.5 On the Inspection Overhead

As explained in Section 3.11.2.4, the inspection cost is included in OT. In this section, we quantify this overhead in a representative problem instance. In all other problem instances, the overhead was either significantly smaller or essentially identical (for reasons discussed below) to the one reported here.

We consider `explosive_source` on Erebus with $h = 1.0$, $q = 4$, and `fs5`. With this configuration, the time step was $t = 481 \cdot 10^{-6}$ (we recall from Section 3.11.2.4 that t is a function of h). Given the fixed simulation duration $T = 2.5$, in this test case 5198 time steps were performed. A time step took on average 1.15 seconds.

In each time step, twenty-five loops, fused as specified by `fs5`, are executed. We know that in `fs5` there are two sub loop chains, which respectively consist of thirteen and twelve loops. To inspect these two loop chains, 1.4 and 1.3 seconds were needed (average across the four MPI ranks, with negligible variance). Roughly 98% of the inspection time was due to the projection and tiling functions, while only 0.2% was spent on the tile initialization phase (see Section 3.8.1). These proportions are consistent across other fusion schemes and test cases.

After 200 time steps (less than 4% of the total) the inspection overhead was already close to 1%. Consequently, the inspection cost, in this test case, was eventually negligible. The inspection cost increases with the number of fused loops, which motivates the choice of `fs5` for this analysis.

3.11.3.6 Performance Limiting Factors

In this section, we discuss the computational and architectural factors that impaired sparse tiling in Seigen. The following considerations derive from a meticulous study of the data movement, the information provided by the loop chain analyzer previously introduced, and extensive profiling through VTune.

There are two types of performance limiting factors: (i) inherent in the application and its loop chains and (ii) due to flaws or deficiencies in the

sparse tiling implementation. We start with point (i).

S-depth As reiterated, a large boundary region enables fusing loops in presence of distributed-memory parallelism. The extent of this region grows proportionally with the number n of fused loops. Unfortunately, this has two undesirable effects. First, the redundant computation overhead tends to be non-negligible if some of the fused loops are compute-bound. Sometimes, the overhead could be even larger than the gain due to increased data locality. Second, the size of an *S-level* (a “strip” of boundary elements) grows with n , as outer levels include more elements than inner levels. This increases not only the amount of redundant computation, but also the volume of data to be communicated.

Limited data reuse across non-consecutive loops In Section 3.11.1, we have explained that Seigen appears to be an excellent sparse tiling candidate, with data reuse arising across consecutive loops and across velocity and stress solvers. Data reuse is however quite limited across non-consecutive, non-solver loops. Given a sequence of three loops $[L_x, L_y, L_z]$, the data reuse between L_x and L_y is usually greater than that between L_x and L_z .

Some solver loops are too far away in the loop chain We know that amongst the velocity solver loops, and analogously amongst the stress solver loops, there is substantial data reuse. Unfortunately, these loops are relatively far from each other in the loop chain. For example, the first and second velocity loops are separated by 8 loops. Turning data reuse into data locality is in this case cumbersome, since long loop chains suffer from the *S-depth* (discussed earlier) and the constrained tile size (discussed next) issues.

Constrained tile size The memory footprint of a tile grows quite rapidly with the number of fused loops. In particular, the matrices accessed in the velocity and stress solver loops have considerable size. The larger the memory footprint, the smaller the tile size which fits in cache. Allocating small tiles has multiple implications. First, the proportion of iterations lying on the border is often significant, which worsen tile expansion (see Section 3.6) thus affecting data locality.

Using small tiles also impairs hardware prefetching, since the virtual addresses streams are more irregular. Moreover, more tiles are needed to cover an iteration space. In the case of shared-memory parallelism, the larger the number of tiles, the higher the probability of detecting a coloring conflict, which results in higher inspection costs.

Limited data reuse in small loop chains With a large memory footprint, a fusion scheme with multiple, short loop chains (e.g., 2-3 loops each) could appear, at first glance, more promising: the data reuse in consecutive loops could be turned into data locality by using a small *S-depth* and relatively big tiles, hence mitigating most of the aforementioned issues. However, other problems arise. By limiting the extent of a loop chain, it may not be possible to fuse some of the velocity and stress solver loops. These loops are memory-bound, share a significant volume of data, and have a considerable impact on the execution time, so sparse tiling could provide substantial benefits. A second issue is inherent to the fact that data reuse is much smaller in short loop chains. Consider two loops L_x and L_y , respectively over cells and interior facets. For a given tile, during the execution of iterations from L_x , new fields and indirection maps are loaded from memory into cache. When executing iterations from L_y , new indirection maps need be fetched from memory (since L_y has a different iteration space than L_x , hence different maps). Locality on the shared data values is then exploitable, but it is evident that the ratio of data reuse over total data movement could, in some cases, really be small.

It is not unreasonable to expect some of these limiting factors to arise in other applications. Further issues are implementation-related (point (ii) above):

TLB misses A translation lookaside buffer (TLB) miss occurs whenever the CPU cannot retrieve the physical page corresponding to a virtual page. Since the TLB has a hierarchical structure, handling a TLB miss usually requires multiple accesses to memory. Hence, TLB misses are much more costly than cache misses. Sparse tiling

increases the TLB miss/hit ratio. This is evident (and more pronounced) when the tile size is small, in which case a TLB miss is likely to occur when jumping to executing a new loop. The problem is exacerbated by `metis` partitioning, which leads to irregular tile shapes. Here, tile expansion may eventually incorporate iterations living in completely different virtual pages. VTune experimentation with $q = 1$ and $q = 2$ versions of `explosive_source` showed that chunk- and `metis`-based sparse tiling suffer from an increase in TLB misses of roughly 16% and 35%, respectively. To mitigate this issue, larger virtual pages could be used. Linux’s Transparent Huge Pages, if enabled, automatically allocates memory in virtual pages of 2MB (instead of the default 4KB) as long as the base address is properly aligned. As future work, Firedrake could be extended by instantiating 2MB-aligned Numpy arrays; this is not straightforward as arbitrary alignment cannot be specified through the default Numpy interface.

Tile shape and expansion The chunk partitioning strategy, applied on top of the reverse Cuthill–McKee (RCM) algorithm used in Firedrake for mesh renumbering, leads to thin, rectangular tiles. As explained, this maximizes the fraction of iterations on the tile border, which in turn affects data reuse. The `metis` partitioning strategy did not help, for the reasons explained above. A possible solution to this issue would consist of using a Hilbert curve for mesh renumbering, and then chunk partitioning on top of it. This would minimize tile expansion while avoiding most of the negative low level implications (i.e., prefetching, TLB misses).

3.12 Conclusions and Future Work

Sparse tiling, and more generally time tiling, aims to turn the data reuse in a sequence of loops into data locality. In this chapter, three main problems have been addressed: the generalization of sparse tiling to arbitrary sequences of irregular loops through the loop chain abstraction, automation via DSLs, and effective support for shared- and distributed-memory parallelism. The major strength of this work lies in the fact that all algo-

rithmic and technological contributions derive from an in-depth study of a realistic applications. The performance issues we found through Seigen would never have been exposed by a set of simplistic benchmarks, as often used in the literature.

The thorough performance analysis of Seigen has shed much light on sparse tiling. However, the experimentation can still be extended in two ways:

Multi-node experiments The more aggressive fusion schemes, which make use of extended halo regions, may be affected or take advantage from network communication. Other issues or potentials inherent in sparse tiling could be exposed. Multi-node experiments have highest priority and are now in progress.

3D problems Since many real-world simulations are based on 3D problems, it would be natural to extend the performance evaluation of Seigen in this direction. At the moment of writing, however, Seigen still does not include 3D test cases.

Other applications Seigen was attractive for its long sequence of loops, which provides a complex, realistic scenario for testing sparse tiling. It would be particularly interesting to experiment with other explicit high-order discontinuous-Galerkin methods. Another class of appealing loop chains arises in matrix-free solvers.

In the longer term, our ambition is to work around the implementation-related performance limiting factors described in the previous section. We believe that using a Hilbert curve numbering may lead to a better tile shape, thus mitigating the performance penalties due to tile expansion, TLB misses and hardware prefetching.

Shared-memory parallelism was not as carefully tested as distributed-memory parallelism. First of all, we would like to replace the current OpenMP implementation in SLOPE with the MPI Shared Memory (SHM) model introduced in MPI-3. Not only does a unified programming model provide significant benefits in terms of maintainability and complexity, but the performance may also be greater as suggested by recent developments in the PETSc community. Secondly, some extra work would be

required for a fair comparison of this new hybrid MPI+MPI programming model with and without sparse tiling.

The experimentation was carried out on a number of “conventional” Intel Xeon architectures. Intel’s Knights Landing and IBM’s POWER8 have more bandwidth than a standard Xeon x86, but also a significantly larger number of cores and sockets. General-purpose many-core architectures might play a key role in next-generation high performance computing, so the same performance analysis in Section 3.11 should be repeated on these systems.

Finally, for a widespread adoption of sparse tiling, a cost model for automatic derivation of fusion schemes and tile sizes is still missing.

Chapter 4

Minimizing Operations in Finite Element Integration Loops

In this chapter, we present an algorithm for the optimization of a class of finite element local assembly kernels. This algorithm, which exploits fundamental mathematical properties of finite element operators, is proven to achieve a locally optimal operation count. In specified circumstances the optimum achieved is global. Extensive experimentation shows significant performance improvements over state-of-the-art finite element code generation systems in almost all cases. This validates the effectiveness of the algorithm presented here, and illustrates its limitations. The algorithm is implemented in COFFEE and is currently in use in the Firedrake framework. This chapter is an extended version of [Luporini et al., 2016a].

4.1 Motivation and Related Work

The need for rapid implementation of high performance, robust, and portable finite element methods has led to approaches based on automated code generation. This has been proven successful in the context of the FEniCS and Firedrake projects. We recall from Section 2.2.1 that, in these frameworks, the weak variational form of a problem is expressed in a high level mathematical syntax by means of the domain-specific language UFL. This mathematical specification is used by a domain-specific

compiler, known as a form compiler, to generate low-level C or C++ code for the integration over a single element of the computational mesh of the variational problem's left and right hand side operators. The code for assembly operators must be carefully optimized: as the complexity of a variational form increases, in terms of number of derivatives, pre-multiplying functions, or polynomial order of the chosen function spaces, the operation count increases, with the result that assembly often accounts for a significant fraction of the overall runtime. This aspect has previously been introduced in Section 2.1.5.

As demonstrated by the substantial body of research on the topic, automating the generation of such high performance implementations poses several challenges. This is a result of the complexity inherent in the mathematical expressions involved in the numerical integration, which varies from problem to problem, and the particular structure of the loop nests enclosing the integrals. General-purpose compilers, such as those by *GNU* and *Intel*, fail to exploit the structure inherent in the expressions, thus producing sub-optimal code (i.e., code which performs more floating-point operations, or “flops”, than necessary; we show this in Section 4.9). Research compilers, for instance those based on polyhedral analysis of loop nests, such as PLUTO [Bondhugula et al., 2008], focus on parallelization and optimization for cache locality, treating issues orthogonal to the question of minimising flops. The lack of suitable third-party tools has led to the development of a number of domain-specific code transformation (or synthesizer) systems. Ølgaard and Wells [2010] show how automated code generation can be leveraged to introduce optimizations that a user should not be expected to write “by hand”. Kirby and Logg [2006] and Russell and Kelly [2013] employ mathematical reformulations of finite element integration with the aim of minimizing the operation count. In Luporini et al. [2015] (and in Chapter 5, from which the article is extracted), the effects and the interplay of generalized code motion and a set of low level optimizations are analysed. It is also worth mentioning two new form compilers, UFLACS [Alnæs, 2016] and TSFC [Homolya and Mitchell, 2016], which particularly target the compilation time challenges of the more complex variational forms. The performance evaluation in Section 4.9 includes most of these systems.

However, in spite of such a considerable research effort, there is still no

answer to one fundamental question: can we automatically generate an implementation of a form which is optimal in the number of flops executed? In this chapter, we formulate an approach that solves this problem for a particular class of forms and provides very good approximations in all other cases. In particular, we will define “local optimality”, which relates operation count with inner loops. In summary, our contributions are as follows:

- We formalize the class of finite element integration loop nests and we build the space of legal transformations impacting their operation count.
- We provide an algorithm to select points in the transformation space. The algorithm uses a cost model to: (i) understand whether a transformation reduces or increases the operation count; (ii) choose between different (non-composable) transformations.
- We demonstrate that our approach systematically leads to a local optimum. We also explain under what conditions of the input problem global optimality is achieved.
- We integrate our approach with a compiler, COFFEE, which is in use in the Firedrake framework. The structure of COFFEE is discussed in Chapter 6.
- We experimentally evaluate using a broader suite of forms, discretizations, and code generation systems than has been used in prior research. This is essential to demonstrate that our optimality model holds in practice.

In addition, in order to place COFFEE on the same level as other code generation systems from the viewpoint of low level optimization, which is essential for a fair performance comparison:

- We introduce a transformation based on symbolic execution that allows irrelevant floating point operations to be skipped (for example those involving zero-valued quantities).

In Section 4.2 we introduce a set of definitions mapping mathematical properties to the level of loop nests. This step is an essential precursor

to the definition of the two algorithms – sharing elimination (Section 4.3) and pre-evaluation (Section 4.4) – through which we construct the space of legal transformations. The main transformation algorithm in Section 4.6 delivers the local optimality claim by using a cost model to coordinate the application of sharing elimination and pre-evaluation. We elaborate on the correctness of the methodology in Section 4.7. The numerical experiments are presented in Section 4.9. We conclude discussing the limitations of the algorithms presented and future work.

4.2 Loop Nests, Expressions and Optimality

In this section, we characterize global and local optimality for finite element integration. In order to make the chapter self-contained, we start by reviewing basic compiler terminology.

Definition 1 (Perfect and imperfect loop nests). A perfect loop nest is a loop whose body either 1) comprises only a sequence of non-loop statements or 2) is itself a perfect loop nest. If this condition does not hold, a loop nest is said to be imperfect.

Definition 2 (Independent basic block). An independent basic block is a sequence of statements such that no data dependencies exist between statements in the block.

We focus on perfect nests whose innermost loop body is an independent basic block. A straightforward property of this class is that hoisting invariant expressions from the innermost to any of the outer loops or the preheader (i.e., the block that precedes the entry point of the nest) is always safe, as long as any dependencies on loop indices are honored. We will make use of this property. The results of the next sections could also be generalized to larger classes of loop nests, in which basic block independence does not hold, although this would require refinements beyond the scope of this chapter.

We introduce some new concepts by mapping mathematical properties to the loop nest level. We start with the notion of a *linear symbol*. This will allow us to define a *linear loop* and, more generally, a (perfect) *multilinear loop nest*.

Definition 3 (Linear symbol). A symbol a in an expression e is linear if

1. a is an n -dimensional array, and
2. all occurrences of a in e are indexed through the same vector-valued access function $f = [f_0, \dots, f_{n-1}]$ (e.g., $a[f_0(\dots)][f_1(\dots)]$), and
3. all sub-expressions of e in which a appears are affine in a .

We discuss some simple examples (to relieve the notation, we set $a[i] \equiv a_i$). The symbol a is *not* linear in any of $a_i b + a_k$, $a_i b + a_{i+2}$, and $a_{ji} b + a_{ki}$, as condition 2 is violated. Condition 3 is violated for a in both b/a_i and $a_i b + a_i a_i$. a is instead linear in $a_i b + a_i$.

Definition 4 (Linear loop). Let L_i be a loop iterating over the space I through the iteration variable i . L_i is linear if in its body

1. i only appears as an array index, and
2. all symbols in which i appears are linear symbols.

Definition 5 (Multilinear loop nest). A multilinear loop nest of arity n is a perfect nest composed of n linear loops.

We will show that multilinear loop nests, which arise naturally when translating bilinear or linear forms into code, are important because they have a structure that we can take advantage of to reach a local optimum.

We now define two different classes of loops.

Definition 6 (Reduction loop). A loop L_i is said to be a reduction loop if in its body

1. i appears only as an array index, and
2. for each augmented assignment statement S (e.g., an increment), arrays indexed by i appear only on the right hand side of S .

Definition 7 (Order-free loop). A loop is said to be an order-free loop if its iterations can be executed in any arbitrary order.

Consider Equation 2.21 and the (abstract) loop nest implementing it illustrated in Figure 4.1. The imperfect nest $\Lambda = [L_e, L_i, L_j, L_k]$ comprises an order-free loop L_e (over elements in the mesh), a reduction loop L_i

```

for (e = 0; e < E; e++)
  ...
  for (i = 0; i < I; i++)
    ...
    for (j = 0; j < J; j++)
      for (k = 0; k < K; k++)
        
$$A_{ejk} += \sum_{w=1}^m \alpha_{eij}^w \beta_{etik}^w \sigma_{ei}^w$$


```

Figure 4.1: The loop nest implementing a generic bilinear form.

(performing numerical integration), and a multilinear loop nest $[L_j, L_k]$ (over test and trial functions). In the body of L_k , one or more statements evaluate the local tensor for the element e . Expressions (the right hand side of a statement) result from the translation of a form in high level matrix notation into code. In particular, m is the number of monomials (a form is a sum of monomials), α_{eij} and β_{etik} represents the product of a coefficient function (e.g., the inverse Jacobian matrix for the change of coordinates) with some linear symbols (e.g., test or trial functions), and σ_{ei} is a function of coefficients and geometry. We do not pose any restrictions on function spaces (e.g., scalar- or vector-valued), coefficient expressions (linear or non-linear), differential and vector operators, so σ_{ei} can be arbitrarily complex. We say that such an expression is in *normal form*, because the algebraic structure of a variational form is intact: products have not yet been expanded, distinct monomials can still be identified, and so on. This brings us to formalize the class of loop nests that we aim to optimize.

Definition 8 (Finite element integration loop nest). A finite element integration loop nest is a loop nest in which the following appear, in order: an imperfect order-free loop, an imperfect (perfect only in some special cases) reduction loop, and a multilinear loop nest whose body is an independent basic block in which expressions are in normal form. Test and trial functions (or derivatives thereof) are the linear symbols of the multilinear loop nest.

We then characterize optimality for a finite element integration loop nest as follows.

Definition 9 (Optimality of a loop nest). Let Λ be a loop nest, and let Γ be a transformation function $\Gamma : \Lambda \rightarrow \Lambda'$ such that Λ' is semantically

equivalent to Λ (possibly, $\Lambda' = \Lambda$). We say that $\Lambda' = \Gamma(\Lambda)$ is an optimal synthesis of Λ if the total number of operations (additions, products) performed to evaluate the result is minimal.

The concept of local optimality, which relies on the particular class of *flop-decreasing* transformations, is also introduced.

Definition 10 (Flop-decreasing transformation). A transformation which reduces the operation count is called flop-decreasing.

Definition 11 (Local optimality of a loop nest). Given Λ , Λ' and Γ as in Definition 9, we say that $\Lambda' = \Gamma(\Lambda)$ is a locally optimal synthesis of Λ if:

- the number of operations (additions, products) in the innermost loops performed to evaluate the result is minimal, and
- Γ is expressed as composition of flop-decreasing transformations.

The restriction to flop-decreasing transformations aims to exclude those apparent optimizations that, to achieve flop-optimal innermost loops, would rearrange the computation at the level of the outer loops causing, in fact, a global increase in operation count.

We also observe that Definitions 9 and 11 do not take into account memory requirements. If the execution of a loop nest were memory-bound – the ratio of operations to bytes transferred from memory to the CPU being too low – then optimizing the number of flops would be fruitless. Henceforth we assume we operate in a CPU-bound regime, evaluating arithmetic-intensive expressions. In the context of finite elements, this is often true for more complex multilinear forms and/or higher order elements.

Achieving optimality in polynomial time is not generally feasible, since the σ_{ei} sub-expressions can be arbitrarily unstructured. However, multilinearity results in a certain degree of regularity in α_{eij} and β_{eik} . In the following sections, we will elaborate on these observations and formulate an approach that achieves: (i) at least a local optimum in all cases; (ii) global optimality whenever the monomials are “sufficiently structured”. To this purpose, we will construct:

- the space of legal transformations impacting the operation count (Sections 4.3 – 4.5)

- an algorithm to explore and select points in the transformation space (Section 4.6)

4.3 Transformation Space: Sharing Elimination

We start by introducing the fundamental notion of sharing.

Definition 12 (Sharing). A statement within a loop nest Λ presents sharing if at least one of the following conditions hold:

Spatial sharing There are at least two identical sub-expressions, possibly just two symbols.

Temporal sharing There is at least one non-trivial sub-expression (e.g., an addition or a product) that is redundantly executed because it is independent of $\{L_{i_1}, L_{i_1}, \dots, L_{i_n}\} \subset \Lambda$.

To illustrate the definition, we show in Figure 4.2 how sharing evolves as factorization and code motion are applied to a trivial multilinear loop nest. In the original loop nest (Figure 4.2a), spatial sharing is induced by the symbol b_j . Factorization eliminates spatial sharing and creates temporal sharing (Figure 4.2b). Finally, generalized code motion [Luporini et al., 2015], which hoists sub-expressions that are redundantly executed by at least one loop in the nest¹, leads to optimality (Figure 4.2c).

<pre>for (j = 0; j < J; j++) for (i = 0; i < I; i++) a_{ji} += b_j * c_i + b_j * d_i</pre>	<pre>for (j = 0; j < J; j++) for (i = 0; i < I; i++) a_{ji} += b_j * (c_i + d_i)</pre>	<pre>for (i = 0; i < I; i++) t_i = c_i + d_i for (j = 0; j < J; j++) for (i = 0; i < I; i++) a_{ji} += b_j * t_i</pre>
(a) With spatial sharing	(b) With temporal sharing	(c) Optimal form

Figure 4.2: Reducing a simple multilinear loop nest to optimal form.

In this section, we study *sharing elimination*, a transformation that aims to reduce the operation count by removing sharing through the application of expansion, factorization, and generalized code motion. If the objective were reaching optimality and the expressions lacked structure, a transformation of this sort would require solving a large combinatorial

¹Traditional loop-invariant code motion, which is commonly applied by general-purpose compilers, only checks invariance with respect to the innermost loop.

problem – for instance to evaluate the impact of all possible factorizations. Our sharing elimination strategy, instead, exploits the structure inherent in finite element integration expressions to guarantee, after coordination with other transformations (an aspect which we discuss in the following sections), local optimality. Global optimality is achieved if stronger preconditions hold. Setting local optimality, rather than optimality, as primary goal is essential to produce simple and computationally efficient algorithms – two necessary conditions for integration with a compiler.

4.3.1 Identification and Exploitation of Structure

Finite element expressions can be seen as composition of operations between tensors. Often, the optimal implementation strategy for these operations is to be determined out of two alternatives. For instance, consider $J^{-T} \nabla v \cdot J^{-T} \nabla v$, with J^{-T} being the transposed inverse Jacobian matrix for the change of (two-dimensional) coordinates, and v a generic two-dimensional vector. The tensor operation will reduce to the scalar expression $(av_i^0 + bv_i^1)(av_i^0 + bv_i^1) + \dots$, in which v_i^0 and v_i^1 represent components of v that depend on L_i . To minimize the operation count for expressions of this kind, we have two options:

STRATEGY 1. Eliminating spatial and temporal sharing through generalized code motion. Spatial sharing is eliminated by capturing common sub-expressions; temporal sharing is eliminated by hoisting expressions out of some loops.

STRATEGY 2. Eliminating spatial sharing first – through product expansion and factorization – and temporal sharing afterwards, again through generalized code motion.

In the current example, depending on the size of L_i , applying Strategy 2 could reduce the operation count since the expression would be recast as $v_i^0 v_i^0 aa + v_i^0 v_i^1 (ab + ab) + v_i^1 v_i^1 cc + \dots$ and some hoistable sub-expressions would be exposed. On the other hand, Strategy 1 would have no effect as v only depends on a single loop, L_i . A second example showing the effect of Strategy 2 was provided in Figure 4.2. In general, choosing between the two strategies is challenging because multiple factors must be taken into account: the loop sizes, the increase in operations due to expansion, the

gain due to code motion, and the presence of common sub-expressions. Before addressing this problem (in Section 4.3.2), we need to understand under what conditions Strategy 2 is applicable. For this, we introduce a relevant class of expressions.

Definition 13 (Structured expression). We say that an expression is “structured in a loop nest Λ ” if and only if, for every symbol s_Λ depending on at least one loop in Λ , the spatial sharing induced by s_Λ may be eliminated by factorizing all occurrences of s_Λ in the expression.

Proposition 1. *An expression is structured in a loop nest Λ if Λ is multilinear.*

Proof. This follows directly from Definition 3 and Definition 5, which restrict the number of occurrences of s_Λ in a summand to at most 1. \square

If Λ were an arbitrary loop nest, a given symbol s_Λ could appear everywhere (e.g., n times in a summand and m times in another summand with $n \neq m$, as argument of a higher level function, in the denominator of a division), thus posing the challenge of finding the factorization that maximizes temporal sharing. If Λ is instead a finite element integration loop nest, it is guaranteed by Proposition 1 that any sub-expression including at least two instances of the same linear symbol can be handled using Strategy 2. As discussed in the next sections, this property will allow us to construct the space of flop-decreasing transformations by “composition” of Strategy 1 and Strategy 2.

Finally, we observe that the σ_{ei} sub-expressions can sometimes be considered “weakly structured”. This happens when a relaxed version of Definition 13 applies, in which the factorization of s_Λ only minimizes (rather than eliminates) spatial sharing (for instance, in the complex hyperelastic model analyzed in Section 4.9). Weak structure will be exploited by Algorithm 5 in the attempt to achieve optimality.

4.3.2 Global Analysis of the Expression

To evaluate the global impact of a transformation, we perform a so called *strategy selection analysis* on a *temporaries graph*, which models the input expression. As we shall see, this outperforms a simplistic approach in which sub-expressions are analyzed in “isolation”, because common sub-expressions are taken into account.

It is useful to start by introducing the notion of a *minimal common sub-expression*.

Definition 14 (Minimal common sub-expression). A sub-expression m within an expression e is said to be a minimal common sub-expression (MCS) if:

- m occurs at least twice in e , and
- any m' , a sub-expression obtained by removing an operation from m , has no common sub-expressions in e .

For example, in $ab + abc + abcd$ the sub-expression ab is an MCS, whereas abc is not, despite occurring twice.

A temporaries graph is a directed k -partite graph in which vertices are MCSs and edges represent read-after-write dependencies between MCSs (e.g., an edge from e_1 to e_2 indicates that e_1 is read in e_2). The k independent sets $\{T_i\}_{i=0}^{k-1}$ of vertices, or simply *levels*, are determined iteratively. Initially, Strategy 1 is applied to the input expression. This produces T_0 and modifies the input expression by replacing the MCSs in T_0 with appropriate temporaries. Then, Strategy 1 is applied to the modified expression; T_1 and the edges from T_0 to T_1 are in this way determined. This process is repeated k times, until no more MCSs can be extracted. An example of a temporaries graph is provided in Figure 4.3. It is worth observing that k can be quite large as the input is in normal form. This implies, for instance, that the operands of an inner product occurring multiple times in the variational form will be common sub-expressions in the translated scalar expression.

The *strategy selection analysis* uses a temporaries graph to determine whether applying Strategy 2 to some subsets of levels would lower the global operation count. If the MCSs in the graph are structured expressions, then this analysis can be accomplished in polynomial time (thanks to Proposition 1). Given two levels T_{i_1} and T_{i_2} such that $i_1 < i_2$, one can

1. Starting with $i = i_1$, calculate the total operation count for computing all sub-expressions in $\{T_j\}_{j=i}^{i_2}$. The operation count includes the loop sizes.
2. Inline the MCSs in T_i into $\{T_j\}_{j=i+1}^{i_2}$. The temporaries in T_i are thus discarded.



Figure 4.3: The temporary graph for an excerpt of code extracted from a hyperelastic model.

3. Apply Strategy 2 to all sub-expressions in $\{T_j\}_{j=i+1}^{i_2}$, factorizing any linear symbol/temporary.
4. Evaluate and store the new total operation count, which includes the loop sizes.
5. Increment i and repeat this process until $i = i_2$.

It is finally straightforward to determine for which range of levels (if any) the application of Strategy 2 improved the operation count. The cost and the effectiveness of the *strategy selection analysis* obviously depend on the number n of pairs $\langle i_1, i_2 \rangle$ that are evaluated (at most $k - 1$). Since during our experiments setting $n = k - 1$ never led to unacceptable code generation times², in the following we assume that the *strategy selection analysis* always considers all legal pairs $\langle i_1, i_2 \rangle$.

4.3.3 The Sharing Elimination Algorithm

Algorithm 5 describes sharing elimination gathering the considerations from the previous sections. It also introduces a model to minimize the operation count within the innermost loop once *strategy selection analysis* has been performed.

Algorithm 5 (Sharing elimination). The input of the algorithm is a tree representation a finite element integration loop nest.

²Even in the case of complex hyperelastic models, the code generation time never exceed a few seconds on a relatively old Sandy Bridge architecture.

1. Perform a depth-first visit of the loop tree to collect all MCSs. Apply Strategy 1 to these MCSs. This requires introducing some new temporaries. Repeat this process until there are no more MCSs.
2. Group the temporaries based on the linear loop they depend on. We have two disjoint sets in the case of bilinear forms and, trivially, a single set for linear forms. For each of these sets, build a *temporaries graph* and apply the *strategy selection analysis* discussed earlier.
3. Build the *sharing graph* $G = (S, E)$ for each expression in the body of the multilinear loop nest (these are the expressions transformed by the *strategy selection analysis*, which now include some temporaries). Each $s \in S$ represents a linear symbol or a temporary produced by the previous steps. An edge (s_i, s_j) indicates that a product $s_i s_j$ would appear if the sub-expressions including s_i and s_j were expanded.

Note: this and the following steps will only impact bilinear forms, since otherwise, due to linearity, $E = \emptyset$.

4. Partition S into n disjoint sets $\{S_1, \dots, S_n\}$, such that S_i includes all instances of a given symbol s in the expression. Transform G by merging $\{s_1, \dots, s_m\} \subset S_i$ into a unique vertex s (taking the union of the edges), provided that their factorization would not cause an increase in operation count.
5. Map G to an Integer Linear Programming (ILP) model for determining how to optimally apply Strategy 2. The solution is the set of linear symbols/temporaries that will be factorized. Let $|S| = n$; the ILP model then is as follows:

x_i : a vertex in S (1 if a symbol should be factorized, 0 otherwise)

y_{ij} : an edge in E (1 if s_i is factorized in the product $s_i s_j$, 0 otherwise)

n_i : the number of edges incident to x_i

$$\min \sum_{i=1}^n x_i, \text{ s.t. } \sum_{j|(i,j) \in E} y_{ij} \leq n_i x_i, \quad i = 1, \dots, n$$

$$y_{ij} + y_{ji} = 1, \quad (i, j) \in E$$

6. Perform a depth-first visit of the loop tree and, for each expression

independent of the multilinear loop nest, apply the most profitable between Strategy 1 and Strategy 2.

Note: this pass speculatively assumes that expressions are (weakly) structured in the reduction loop. If the assumption does not hold, the operation count will generally be sub-optimal because only a subset of factorizations and code motion opportunities may eventually be considered.

Although the primary goal of Algorithm 5 is operation count minimization within the multilinear loop nest, the enforcement of flop-decreasing transformations (steps (2) and (4)) and the re-scheduling of sub-expressions within outer loops (step (6)) also attempt to optimize the loop nest globally. We will further elaborate this aspect in Section 4.7.

4.3.4 Examples

In this section, we present a series of examples of increasing complexity.

4.3.4.1 Example 1

Consider again Figure 4.2a. There are no common sub-expressions, so the *strategy selection analysis* has no effect. The *sharing graph* is $G = (\{b_j, c_i, d_i\}, \{(b_j, c_i), (b_j, d_i)\})$. The ILP formulation leads to the code in Figure 4.2c.

4.3.4.2 Example 2

In Figure 4.4, Algorithm 5 is executed in a simple yet realistic scenario, which originates from the bilinear form of a Poisson equation in two dimensions. The temporaries graph, which consists of a single level, is used for performing *strategy selection analysis*. This leads to the synthesis in Figure 4.4b. The *sharing graph* is $G = (\{t_0, t_1, t_2, t_3\}, \{(t_0, t_2), (t_1, t_3)\})$, but since there are no factorization opportunities the ILP formulation has no effect.

4.3.4.3 Example 3

In this example, we focus on the ILP formulation. We consider a bilinear form extracted from a model of temperature-dependent multiphase flow

<pre> for (e = 0; e < E; e++) z0 = ... z1 = for (i = 0; i < I; i++) for (j = 0; j < J; j++) for (k = 0; k < K; k++) A_{ejk} += (((z0a_{ik} + z2b_{ik}) * (z0c_{ij} + z2d_{ij})) + ((z1a_{ik} + z3b_{ik}) * (z1c_{ij} + z3d_{ij}))) * W_i * det </pre> <p style="text-align: center;">(a) Normal form</p>	<pre> for (e = 0; e < E; e++) ... for (i = 0; i < I; i++) t_{det} = W_i * det for (k = 0; k < K; k++) t_{0k} = (z0a_{ik} + z2b_{ik}) t_{1k} = (z1a_{ik} + z3b_{ik}) for (j = 0; j < J; j++) t_{2j} = (z0c_{ij} + z2d_{ij}) * t_{det} t_{3j} = (z1c_{ij} + z3d_{ij}) * t_{det} for (j = 0; j < J; j++) for (k = 0; k < K; k++) A_{ejk} += t_{0k} * t_{2j} + t_{1k} * t_{3j} </pre> <p style="text-align: center;">(b) After sharing elimination</p>
---	---

Figure 4.4: Applying sharing elimination to the bilinear form arising from a Poisson equation in 2D. The operation counts are $E(f(z_0, z_1, \dots) + IJK \cdot 18)$ (left) and $E(f(z_0, z_1, \dots) + I(J \cdot 6 + K \cdot 9 + JK \cdot 4))$ (right), with $f(z_0, z_1, \dots)$ representing the operation count for evaluating z_0, z_1, \dots , and common sub-expressions being counted once. The synthesis in Figure 4.4b is globally optimal apart from the pathological case $I, J, K = 1$.

through porous media [Ølgaard and Wells, 2010], which we informally refer to as the “pressure equation”. Although the complete specification of the form is irrelevant for the purpose of this example, it is useful to know that (i) the problem is linear, (ii) there are in total six monomials, (iii) the gradient and the divergence of test and trial functions appear in some monomials (so several distinct linear symbols are present in the input expression).

Figure 4.5a shows the finite element integration loop nest at the end of step (2) in Algorithm 5; that is, once *strategy selection analysis* has been performed. The linear temporaries induce spatial sharing in the loop nest. It is not obvious to individuate the factorization that would result in a local optimum. One can derive the *sharing graph* directly from inspection of Figure 4.5a, obtaining $G = (\{t_{10_{ik}}, t_{10_{ij}}, t_{11_j}, t_{12_j}, t_{13_k}, t_{14_k}, t_{15_k}\}, \{(t_{10_{ik}}, t_{10_{ij}}), (t_{10_{ik}}, t_{11_j}), (t_{10_{ik}}, t_{12_j}), (t_{15_k}, t_{11_j}), (t_{15_k}, t_{12_j}), (t_{10_{ij}}, t_{14_k}), (t_{10_{ij}}, t_{13_k}), (t_{11_j}, t_{14_k}), (t_{11_j}, t_{13_k}), (t_{12_j}, t_{14_k}), (t_{12_j}, t_{13_k})\})$. The ILP formulation eventually retrieves three factorization candidates, as shown in Figure 4.5b.

4.3.4.4 Example 4

In the last example, we show how the *strategy selection analysis* impacts the operation count in a hyperelastic model. This is the same problem

```

for (e = 0; e < E; e++)
...
for (i = 0; i < I; i++)
...
for (j = 0; j < J; j++)
for (k = 0; k < K; k++)
    Ajk += (((t10ik * ((t10ij * t3) + (t4 * ((t11j * t2) + (t12j * t1)) * t6))) +
            (t8 * t9 * t15k * ((t11j * t2) + (t12j * t1)) * t0) +
            (t10ij * -1.0 * ((t14k * t2) + (t13k * t1)) * c4) +
            (t7 * ((t14k * t2) + (t13k * t1)) * ((t11j * t2) + (t12j * t1)) * c4) +
            (t5 * ((t14k * t11j) + (t13k * t12j)) * t0))) *
    Wi * det

```

(a) Before the ILP-driven factorization

```

for (e = 0; e < E; e++)
...
for (i = 0; i < I; i++)
    tdet = Wi * det
    t15 = t1 * t4 * t6
    t16 = (t0 * t5) + (t1 * t1 * t7 * c4)
    t17 = t2 * t0 * t8
    t18 = t2 * t4 * t6
    t19 = t1 * t0 * t8
    t20 = (t0 * t5) + (t2 * t2 * t7 * c4)

for (int k = 0; k < K; k++)
    t16k = (t10ik * t3) + (t13k * -1.0 * t1 * c4) + (t14k * -1.0 * t2 * c4)
    t17k = (t10ik * t15) + (t13k * t16) + (t14k * t2 * t1 * c5) + (t15k * t9 * t19)
    t18k = (t10ik * t18) + (t13k * t1 * t2 * c5) + (t14k * t20) + (t15k * t9 * t17)

for (j = 0; j < J; j++)
for (k = 0; k < K; k++)
    Ajk += (t10ij * t16k) + (t12j * t17k) + (t11j * t18k)

```

(b) After the ILP-driven factorization

Figure 4.5: Using the ILP model to factorize the expression arising from the pressure equation.

used for performance evaluation in Section 4.9. The code in Figure 4.6a is obtained by repeatedly applying Strategy 1 to the expression in normal form (step (1) in Algorithm 5). The temporaries graph, which consists of 6 levels, can easily be derived. For given values of I and K , the *strategy selection analysis* determines that applying Strategy 2 to the temporaries between levels T_0 and T_4 will improve the operation count. Strategy 1 is instead preferable for T_5 , which comprises the four temporaries t_{59_k} , t_{60_k} , t_{65_k} , t_{66_k} . The resulting synthesis is shown in Figure 4.6b. Intuitively, instead of executing N operations IK times (Figure 4.6a), now M operations are executed I times (Figure 4.6b). It is true that $M > N$, but the analysis

guarantees that I and K are such that the operation count has improved.

In this example, the application of Strategy 2 reduces the operation count by about $1.3\times$, on average (the actual value clearly depends on I and K). It is not rare, however, to encounter cases (e.g., more complex hyperelastic models) in which the reduction is even larger than $2\times$. We emphasize that here we are discussing the improvement from applying Strategy 2 “on top of” Strategy 1; the overall gain due to performing *strategy selection analysis* is usually much larger.

```

for (e = 0; e < E; e++)
...
for (i = 0; i < I; i++)
...
for (int k = 0; k < K; k++)
    t40 = ((t8 * t39k) + (t11 * t38k))
    t41 = ((t14 * t35k) + (t15 * t34k))
    t42 = (t41 * t13)
    t43 = ((t8 * t35k) + (t11 * t34k))
    t44 = (t43 * t16)
    t45 = ((t14 * t39k) + (t15 * t38k))
    t46 = (t45 * t20)
    t47 = (t40 * t21)
    t48 = (t0 * ((t42 + t44 + t46 + t47)/2))
    t49 = ((t48 + t48) * w1[0])
    t50 = (t43 * t13)
    t51 = (t40 * t20)
    t52 = ((t50 + t50 + t51 + t51)/2)
    t53 = (t41 * t16)
    t54 = (t45 * t21)
    t55 = ((t53 + t53 + t54 + t54)/2)
    t56 = (t24 * (t52 + t55) * t28)
    t57 = (t0 * t55)
    t58 = (t56 + ((t57 + t57) * w1[0]))
    t59k = (t40 * t37) + (t49 * t20) +
           (t45 * t33) + (t58 * t21)
    t60k = (t43 * t37) + (t49 * t13) +
           (t41 * t33) + (t58 * t16)
    t61 = (t0 * t52)
    t62 = (t56 + ((t61 + t61) * w1[0]))
    t63 = (t0 * ((t44 + t42 + t47 + t46)/2))
    t64 = ((t63 + t63) * w1[0])
    t65k = (t40 * t31) + (t62 * t20) +
           (t45 * t23) + (t64 * t21)
    t66k = (t43 * t31) + (t62 * t13) +
           (t41 * t23) + (t64 * t16)
for (j = 0; j < J; j++)
    for (k = 0; k < K; k++)
        ...

for (e = 0; e < E; e++)
...
for (i = 0; i < I; i++)
...
c0 = (0.5 * t0)
c1 = (c0 * ((t14 * t13) + (t8 * t16)))
c2 = (c0 * ((t14 * t20) + (t8 * t21)))
c3 = (c0 * ((t15 * t13) + (t11 * t16)))
c4 = (c0 * ((t15 * t20) + (t11 * t21)))
c5 = (c0 * ((t11 * t16) + (t15 * t13)))
c6 = (c0 * ((t8 * t16) + (t14 * t13)))
c7 = (c0 * ((t11 * t21) + (t15 * t20)))
c8 = (c0 * ((t8 * t21) + (t14 * t20)))
c9 = (w1[0] * 2)
c10 = (t24 * t28)
c11 = (c10 * ((t20 * t11) + (t21 * t15)))
c12 = (c10 * ((t13 * t11) + (t16 * t15)))
c13 = (c10 * ((t20 * t8) + (t21 * t14)))
...
c37 = ((t11 * t37) + (c3 * c36) + (t15 * t33) + (c24 * t16))
c38 = ((t8 * t37) + (c1 * c36) + (t14 * t33) + (c23 * t16))
c39 = ((c2 * c36) + (c25 * t16))
c40 = ((c4 * c36) + (c26 * t16))
c41 = (c9 * t21)
c42 = ((c29 * t20) + (c6 * c41))
c43 = ((c27 * t20) + (c5 * c41))
c44 = ((t8 * t31) + (c30 * t20) + (t14 * t23) + (c8 * c41))
c45 = ((t11 * t31) + (c28 * t20) + (t15 * t23) + (c7 * c41))
c46 = (c9 * t16)
c47 = ((t11 * t31) + (c27 * t13) + (t15 * t23) + (c5 * c46))
c48 = ((c28 * t13) + (c7 * c46))
c49 = ((t8 * t31) + (c29 * t13) + (t14 * t23) + (c6 * c46))
c50 = ((c30 * t13) + (c8 * c46))
for (int k = 0; k < K; k++)
    t59k = (t39k * c32) + (t38k * c33) + (t35k * c35) + (t34k * c34)
    t60k = (t35k * c38) + (t34k * c37) + (t39k * c39) + (t38k * c40)
    t65k = (t39k * c44) + (t38k * c45) + (t35k * c42) + (t34k * c43)
    t66k = (t35k * c49) + (t34k * c47) + (t39k * c50) + (t38k * c48)
for (j = 0; j < J; j++)
    for (k = 0; k < K; k++)
        ...

```

(a) Normal form

(b) After sharing elimination

Figure 4.6: Applying the *strategy selection analysis* to the bilinear form arising from a hyperelastic model in 2D.

4.4 Transformation Space: Pre-evaluation of Reductions

Sharing elimination uses three operators: expansion, factorization, and code motion. In this section, we discuss the role and legality of a fourth operator: reduction pre-evaluation. We will see that what makes this operator special is the fact that there exists a single point in the transformation space of a monomial (i.e., a specific factorization of test, trial, and coefficient functions) ensuring its correctness.

We start with an example. Consider again the loop nest and the expression in Figure 4.1. We pose the following question: are we able to identify sub-expressions for which the reduction induced by L_i can be pre-evaluated, thus obtaining a decrease in operation count proportional to the size of L_i , I ? The transformation we look for is exemplified in Figure 4.7 with a simple loop nest. The reader may verify that a similar transformation is applicable to the example in Figure 4.4a.

<pre> for (e = 0; e < E; e++) for (i = 0; i < I; i++) for (k = 0; k < K; k++) A_{ek} += d_e * b_{ik} * c_i + d_e * b_{ik} * d_i </pre> <p style="text-align: center;">(a) With reduction</p>	<pre> for (i = 0; i < I; i++) for (k = 0; k < K; k++) t_k += b_{ik} * (c_i + d_i) for (e = 0; e < E; e++) for (k = 0; k < K; k++) A_{ek} = d_e * t_k </pre> <p style="text-align: center;">(b) After pre-evaluation</p>
---	--

Figure 4.7: Exposing (through factorization) and pre-evaluating a reduction.

Pre-evaluation can be seen as the generalization of tensor contraction (reviewed in Section 2.1.5) to a wider class of sub-expressions. We know that multilinear forms can be seen as sums of monomials, each monomial being an integral over the equation domain of products (of derivatives) of functions from discrete spaces. A monomial can always be reduced to the product between a “reference” and a “geometry” tensor. In our model, a reference tensor is simply represented by one or more sub-expressions independent of L_e , exposed after particular transformations of the expression tree. This leads to the following algorithm.

Algorithm 6 (Pre-evaluation). Consider a finite element integration loop

nest $\Lambda = [L_e, L_i, L_j, L_k]$. We dissect the normal form input expression into distinct sub-expressions, each of them representing a monomial. Each sub-expression is then factorized so as to split constants from $[L_i, L_j, L_k]$ -dependent terms. This transformation is feasible³, as a consequence of the results in Kirby and Logg [2007]. These $[L_i, L_j, L_k]$ -dependent terms are hoisted outside of Λ and stored into temporaries. As part of this process, the reduction induced by L_i is computed by means of symbolic execution. Finally, L_i is removed from Λ .

The pre-evaluation of a monomial introduces some critical issues:

1. Depending on the complexity of a monomial, a certain number, t , of temporary variables is required if pre-evaluation is performed. Such temporary variables are actually n -dimensional arrays of size S , with n and S being, respectively, the arity and the extent (iteration space size) of the multilinear loop nest (e.g., $n = 2$ and $S = JK$ in the case of bilinear forms). For certain values of $\langle t, n, S \rangle$, pre-evaluation may dramatically increase the working set, which may be counter-productive for actual execution time.
2. The transformations exposing $[L_i, L_j, L_k]$ -dependent terms increase the arithmetic complexity of the expression (e.g., expansion tends to increase the operation count). This could outweigh the gain due to pre-evaluation.
3. A strategy for coordinating sharing elimination and pre-evaluation is needed. We observe that sharing elimination inhibits pre-evaluation, whereas pre-evaluation could expose further sharing elimination opportunities.

We expand on point (1) in the next section, while we address points (2) and (3) in Section 4.6.

³For reasons of space, we omit the detailed sequence of steps (e.g., expansion, factorization), which is however available at <https://github.com/coneoproject/COFFEE/blob/master/coffee/optimizer.py> in Luporini et al. [2016b].

4.5 Transformation Space: Memory Constraints

We have just observed that the code motion induced by monomial pre-evaluation may dramatically increase the working set size. Even more aggressive code motion strategies are theoretically conceivable. Imagine Λ is enclosed in a time stepping loop. One could think of exposing (through some transformations) and hoisting time-invariant sub-expressions for minimizing redundant computation at each time step. The working set size would then increase by a factor E , and since $E \gg I, J, K$, the gain in operation count would probably be outweighed, from a runtime viewpoint, by a much larger memory pressure.

Since, for certain forms and discretizations, hoisting may cause the working set to exceed the size of some level of local memory (e.g. the last level of private cache on a conventional CPU, the shared memory on a GPU), we introduce the following *memory constraints*.

CONSTRAINT 1. The size of a temporary due to code motion must not be proportional to the size of L_e .

CONSTRAINT 2. The total amount of memory occupied by the temporaries due to code motion must not exceed a certain threshold, T_H .

Constraint 1 is a policy decision that the compiler should not silently consume memory on global data objects. It has the effect of shrinking the transformation space. Constraint 2 has both theoretical and practical implications, which will be carefully analyzed in the next sections.

4.6 Selection and Composition of Transformations

In this section, we build a transformation algorithm that, given a memory bound, systematically reaches a local optimum for finite element integration loop nests.

4.6.1 The Main Transformation Algorithm

We address the two following issues:

1. *Coordination of pre-evaluation and sharing elimination.* Recall from Section 4.4 that pre-evaluation could either increase or decrease the op-

eration count in comparison with that achieved by sharing elimination.

2. *Optimizing over composite operations.* Consider a form comprising two monomials m_1 and m_2 . Assume that pre-evaluation is profitable for m_1 but not for m_2 , and that m_1 and m_2 share at least one term (for example some basis functions). If pre-evaluation were applied to m_1 , sharing between m_1 and m_2 would be lost. We then need a mechanism to understand which transformation – pre-evaluation or sharing elimination – results in the highest operation count reduction when considering the whole set of monomials (i.e., the expression as a whole).

Let $\theta : M \rightarrow \mathbb{Z}$ be a cost function that, given a monomial $m \in M$, returns the gain/loss achieved by pre-evaluation over sharing elimination. In particular, we define $\theta(m) = \theta^{pre}(m) - \theta^{se}(m)$, where θ^{se} and θ^{pre} represent the operation counts resulting from applying sharing elimination and pre-evaluation, respectively. Thus pre-evaluation is profitable for m if and only if $\theta(m) < 0$. We return to the issue of deriving θ^{se} and θ^{pre} in Section 4.6.2. Having defined θ , we can now describe the transformation algorithm (Algorithm 7).

Algorithm 7 (Transformation algorithm). The algorithm has three main phases: initialization (step 1); determination of the monomials preserving the memory constraints that should be pre-evaluated (steps 2-4); application of pre-evaluation and sharing elimination (step 5).

1. Perform a depth-first visit of the expression tree and determine the set of monomials M . Let S be the subset of monomials m such that $\theta(m) > 0$. The set of monomials that will *potentially* be pre-evaluated is $P = M \setminus S$.

Note: there are two fundamental reasons for not pre-evaluating $m_1 \in P$ straight away: 1) the potential presence of spatial sharing between m_1 and $m_2 \in S$, which impacts the search for the global optimum; 2) the risk of breaking Constraint 2.

2. Build the set B of all possible bipartitions of P . Let D be the dictionary that will store the operation counts of different alternatives.

3. Discard $b = (b_S, b_P) \in B$ if the memory required after applying pre-evaluation to the monomials in b_P exceeds T_H (see Constraint 2); otherwise, add $D[b] = \theta^{se}(S \cup b_S) + \theta^{pre}(b_P)$.

Note: \mathbb{B} is in practice very small, since even complex forms usually have only a few monomials. This pass can then be accomplished rapidly as long as the cost of calculating θ^{se} and θ^{pre} is negligible. We elaborate on this aspect in Section 4.6.2.

4. Take $\arg \min_b D[b]$.
5. Apply pre-evaluation to all monomials in b_P . Apply sharing elimination to all resulting expressions.

Note: because of the reuse of basis functions, pre-evaluation may produce some identical tables, which will be mapped to the same temporary variable. Sharing elimination is therefore transparently applied to all expressions, including those resulting from pre-evaluation.

The output of the transformation algorithm is provided in Figure 4.8, assuming as input the loop nest in Figure 4.1.

```
// Pre-evaluated tables
...
for (e = 0; e < E; e++)
  // Temporaries due to sharing elimination
  // (Sharing was a by-product of pre-evaluation)
  ...
  // Loop nest for pre-evaluated monomials
  for (j = 0; j < J; j++)
    for (k = 0; k < K; k++)
      Aejk += F'(...) + F''(...) + ...

  // Loop nest for monomials for which run-time
  // integration was determined to be faster
  for (i = 0; i < I; i++)
    // Temporaries due to sharing elimination
    ...
    for (j = 0; j < J; j++)
      for (k = 0; k < K; k++)
        Aejk += H(...)
```

Figure 4.8: The loop nest produced by the algorithm for an input as in Figure 4.1.

4.6.2 The Cost Function θ

We tie up the remaining loose end: the construction of the cost function θ .

We recall that $\theta(m) = \theta^{pre}(m) - \theta^{se}(m)$, with θ^{se} and θ^{pre} representing the operation counts after applying sharing elimination and pre-evaluation. Since θ is deployed in a working compiler, simplicity and efficiency are essential characteristics. In the following, we explain how to derive these two values.

The most trivial way of evaluating θ^{se} and θ^{pre} would consist of applying the actual transformations and simply count the number of operations. This would be tolerable for θ^{se} , as Algorithm 5 tends to have negligible cost. However, the overhead would be unacceptable if we applied pre-evaluation – in particular, symbolic execution – to all bipartitions analyzed by Algorithm 7. We therefore seek an analytic way of determining θ^{pre} .

The first step consists of estimating the *increase factor*, ι . This number captures the increase in arithmetic complexity due to the transformations exposing pre-evaluation opportunities. For context, consider the example in Figure 4.9. One can think of this as the (simplified) loop nest originating from the integration of the action of a mass matrix. The sub-expression $f_0 * B_{i0} + f_1 * B_{i1} + f_2 * B_{i2}$ represents the coefficient f over (tabulated) basis functions (array B). In order to apply pre-evaluation, the expression needs be transformed to separate f from all $[L_i, L_j, L_k]$ -dependent quantities (see Algorithm 6). By product expansion, we observe an increase in the number of $[L_j, L_k]$ -dependent terms of a factor $\iota = 3$.

```

for (i = 0; i < I; i++)
  for (j = 0; j < J; j++)
    for (k = 0; k < K; k++)
      Ajk += bij * bik * (f0 * Bi0 + f1 * Bi1 + f2 * Bi2)

```

Figure 4.9: Simplified loop nest for a pre-multiplied mass matrix.

In general, however, determining ι is not so straightforward since redundant tabulations may result from common sub-expressions. Consider the previous example. One may add one coefficient in the same function space as f , repeat the expansion, and observe that multiple sub-expressions (e.g., $b_{10} * b_{01} * \dots$ and $b_{01} * b_{10} * \dots$) will reduce to identical tables. To evaluate ι , we then use combinatorics. We calculate the k -combinations with repetitions of n elements, where: (i) k is the number of

(derivatives of) coefficients appearing in a product; (ii) n is the number of unique basis functions involved in the expansion. In the original example, we had $n = 3$ (for b_{i0} , b_{i1} , and b_{i2}) and $k = 1$, which confirms $\iota = 3$. In the modified example, there are two coefficients, so $k = 2$, which means $\iota = 6$.

If $\iota \geq I$ (the extent of the reduction loop), we already know that pre-evaluation will not be profitable. Intuitively, this means that we are introducing more operations than we are saving from pre-evaluating L_i . If $\iota < I$, we still need to find the number of terms ρ such that $\theta^{pre} = \rho \cdot \iota$. The mass matrix monomial in Figure 4.9 is characterized by the dot product of test and trial functions, so trivially $\rho = 1$. In the example in Figure 4.4, instead, we have $\rho = 3$ after a suitable factorization of basis functions. In general, therefore, ρ depends on both form and discretization. To determine this parameter, we look at the re-factorized expression (as established by Algorithm 6), and simply count the terms amenable to pre-evaluation.

4.7 Formalization

We demonstrate that the orchestration of sharing elimination and pre-evaluation performed by the transformation algorithm guarantees local optimality (Definition 11). The proof re-uses concepts and explanations provided throughout the chapter, as well as the terminology introduced in Section 4.3.3.

Proposition 2. *Consider a multilinear form comprising a set of monomials M , and let Λ be the corresponding finite element integration loop nest. Let Γ be the transformation algorithm. Let X be the set of monomials that, according to Γ , need to be pre-evaluated, and let $Y = M \setminus X$. Assume that the pre-evaluation of different monomials does not result in identical tables. Then, $\Lambda' = \Gamma(\Lambda)$ is a local optimum in the sense of Definition 11 and satisfies Constraint 2.*

Proof. We first observe that the cost function θ predicts the *exact* gain/loss in monomial pre-evaluation, so X and Y can actually be constructed.

Let c_Λ denote the operation count for Λ and let $\Lambda_I \subset \Lambda$ be the subset of innermost loops (all L_k loops in Figure 4.8). We need to show that there is no other synthesis Λ''_I satisfying Constraint 2 such that $c_{\Lambda''_I} < c_{\Lambda'_I}$ and

that Λ' is achieved through a sequence of flop-decreasing transformations. This holds if and only if

1. *The coordination of pre-evaluation with sharing elimination is optimal.*

This boils down to prove that

- a) *pre-evaluating any $m \in Y$ would result in $c_{\Lambda'_I} > c_{\Lambda'_I}$*
- b) *not pre-evaluating any $m \in X$ would result in $c_{\Lambda'_I} > c_{\Lambda'_I}$*

2. *Sharing elimination leads to (at least) a local optimum.*

We discuss these points separately

1. a) Let T_m represent the set of tables resulting from applying pre-evaluation to a monomial m . Consider two monomials $m_1, m_2 \in Y$ and the respective sets of pre-evaluated tables, T_{m_1} and T_{m_2} . If $T_{m_1} \cap T_{m_2} \neq \emptyset$, at least one table is assignable to the same temporary. Γ , therefore, may not be optimal, since θ only distinguishes monomials in “isolation”. We neglect this scenario (see assumptions) because of its purely pathological nature and its – with high probability – negligible impact on the operation count.
- b) Let $m_1 \in X$ and $m_2 \in Y$ be two monomials sharing some generic linear symbols. If m_1 were carelessly pre-evaluated, there may be a potential gain in sharing elimination that is lost, potentially leading to a non-optimum. This situation is prevented by construction, because Γ exhaustively searches all possible bipartitions in order to determine an optimum which satisfies Constraint 2⁴. Recall that since the number of monomials is in practice very small, this pass can rapidly be accomplished.
2. Consider Algorithm 5. Strategy 1 cannot increase the operation count as both code motion and common sub-expression elimination are flop-decreasing transformations. Strategy 2, instead, may increase the operation count due to product expansion. If Strategy 2

⁴Note that the problem can be seen as an instance of the well-known Knapsack problem

were carelessly applied, for instance as a step of a larger transformation, it would be possible to end up with an increased operational cost. This is avoided by construction (steps (2) and (4)). The *strategy selection analysis*, in particular, compares the operation counts of Strategy 2 and Strategy 1 (a flop-decreasing transformation) and the former is retained if and only if the new state shows an improved operation count. As all transformations that are applied to the input expressions in normal form are of flop-decreasing nature, local optima cannot be pruned from the search space.

The ILP model is derived from the *sharing graph* of the transformed expressions. This is used to drive Strategy 2 in the minimization of the operation count within the innermost loop (see Definition 11). At this point, proving the optimality of the innermost loop reduces to establishing the correctness of the model, which is relatively straightforward because of its simplicity. The model aims to minimize the operation count by selecting the most promising factorizations. The second set of constraints is to select all edges (i.e., all multiplications) exactly once. The first set of inequalities allows multiplications to be scheduled: once a vertex s is selected (i.e., once a symbol is decided to be factorized), all multiplications involving s can be grouped.

□

Throughout the chapter we have reiterated the claim that Algorithm 7 achieves a globally optimal flop count if stronger preconditions on the input variational form are satisfied. We state here these preconditions, in increasing order of complexity.

1. There is a single monomial and only a specific coefficient (e.g., the coordinates field). This is by far the simplest scenario, which requires no particular transformation at the level of the outer loops, so optimality naturally follows.
2. There is a single monomial, but multiple coefficients are present. Optimality is achieved if and only if all sub-expressions depending on coefficients are structured (see Section 4.3.1). This avoids ambiguity in factorization, which in turn guarantees that the output of step (7) in Algorithm 5 is optimal.

3. There are multiple monomials, but either at most one coefficient (e.g., the coordinates field) or multiple coefficients not inducing sharing across different monomials are present. This reduces, respectively, to cases (1) and (2) above.
4. There are multiple monomials, and coefficients are shared across monomials. Optimality is reached if and only if the coefficient-dependent sub-expressions produced by Algorithm 5 – that is, the by-product of factorizing test/trial functions from distinct monomials – preserve structure.

4.8 Code Generation

Sharing elimination and pre-evaluation, as well as the transformation algorithm, have been implemented in COFFEE, the compiler for finite element integration routines adopted in Firedrake. In this section, we briefly discuss the aspects of the compiler that are relevant for this chapter. A complete description of the compiler is provided in Chapter 6.

4.8.1 Expressing Transformations with COFFEE

COFFEE implements sharing elimination and pre-evaluation by composing building block transformation operators, which we refer to as *rewrite operators*. This has several advantages. The first is extensibility. New transformations, such as sum factorization in spectral methods, could be expressed by composing the existing operators, or with small effort building on what is already available. Second, generality: COFFEE can be seen as a lightweight, low level computer algebra system, not necessarily tied to finite element integration. Third, robustness: the same operators are exploited, and therefore tested, by different optimization pipelines. The rewrite operators, whose (Python) implementation is based on manipulation of abstract syntax trees (ASTs), comprise the COFFEE language. A non-exhaustive list of such operators includes expansion, factorization, re-association, and generalized code motion.

4.8.2 Independence from Form Compilers

COFFEE aims to be independent of the high level form compiler. It provides an interface to build generic ASTs and only expects expressions to be in normal form (or sufficiently close to it). For example, Firedrake has transitioned from a version of the FEniCS Form Compiler modified to produce ASTs rather than strings, to a newly written compiler (see also Section 2.2.1.2), while continuing to employ COFFEE. Thus, COFFEE decouples the mathematical manipulation of a form from code optimization; or, in other words, relieves form compiler developers of the task of fine scale loop optimization of generated code.

4.8.3 Handling Block-sparse Tables

For several reasons, basis function tables may be block-sparse (e.g., containing zero-valued columns). For example, the FEniCS Form Compiler implements vector-valued functions by adding (blocks of) zero-valued columns to the corresponding tabulations; this enormously simplifies code generation (particularly, the construction of loop nests), but also affects the performance of the generated code due to the execution of “useless” flops (e.g., operations like $a + 0$). In Ølgaard and Wells [2010], a technique to avoid iteration over zero-valued columns based on the use of indirection arrays (e.g. $A[B[i]]$, in which A is a tabulated basis function and B a map from loop iterations to non-zero columns in A) was proposed. This technique, however, produces non-contiguous memory loads and stores, which nullify the potential benefits of vectorization. COFFEE, instead, handles block-sparse basis function tables by restructuring loops in such a manner that low level optimization (especially vectorization) is only marginally affected. This is based on symbolic execution of the code, which enables a series of checks on array indices and loop bounds which determine the zero-valued blocks which can be skipped without affecting data alignment.

4.9 Performance Evaluation

4.9.1 Experimental Setup

Experiments were run on a single core of an Intel I7-2600 (Sandy Bridge) CPU, running at 3.4GHz, 32KB L1 cache (private), 256KB L2 cache (private) and 8MB L3 cache (shared). The Intel Turbo Boost and Intel Speed Step technologies were disabled. The Intel `icc` 15.2 compiler was used. The compilation flags used were `-O3`, `-xHost`. The compilation flag `xHost` tells the Intel compiler to generate efficient code for the underlying platform.

The Zenodo system was used to archive all packages used to perform the experiments: Firedrake [Mitchell et al., 2016], PETSc [Smith et al., 2016], `petsc4py` [Firedrake, 2016], FIAT [Rognes et al., 2016], UFL [Alnæs et al., 2016], FFC [Logg et al., 2016], PyOP2 [Rathgeber et al., 2016b] and COFFEE [Luporini et al., 2016b]. The experiments can be reproduced using a publicly available benchmark suite [Rathgeber et al., 2016a].

We analyze the execution time of four real-world bilinear forms of increasing complexity, which comprise the differential operators that are most common in finite element methods. In particular, we study the mass matrix (“Mass”) and the bilinear forms arising in a Helmholtz equation (“Helmholtz”), in an elastic model (“Elasticity”), and in a hyperelastic model (“Hyperelasticity”). The complete specification of these forms is made publicly available⁵.

We evaluate the speed-ups achieved by a wide variety of transformation systems over the “original” code produced by the FEniCS Form Compiler (i.e., no optimizations applied). We analyze the following transformation systems:

quad Optimized quadrature mode. Work presented in Ølgaard and Wells [2010], implemented in the FEniCS Form Compiler.

tens Tensor contraction mode. Work presented in Kirby and Logg [2006], implemented in the FEniCS Form Compiler.

auto Automatic choice between `tens` and `quad` driven by heuristic (de-

⁵https://github.com/firedrakeproject/firedrake-bench/blob/experiments/forms/firedrake_forms.py

tailed in Logg et al. [2012] and summarized in Section 2.1.5). Implemented in the FEniCS Form Compiler.

ufls UFLACS, a novel back-end for the FEniCS Form Compiler whose primary goals are improved code generation and execution times.

cfO1 Generalized loop-invariant code motion. Work presented in Luporini et al. [2015], implemented in COFFEE.

cfO2 Optimal loop nest synthesis with handling of block-sparse tables. Work presented in this chapter, implemented in COFFEE.

The values that we report are the average of three runs with “warm cache”; that is, with all kernels retrieved directly from the Firedrake’s cache, so code generation and compilation times are not counted. The timing includes however the cost of both local assembly and matrix insertion, with the latter minimized through the choice of a mesh (details below) small enough to fit the L3 cache of the CPU.

For a fair comparison, small patches were written to make `quad`, `tens`, and `ufls` compatible with Firedrake. By executing all simulations in Firedrake, we guarantee that both matrix insertion and mesh iteration have a fixed cost, independent of the transformation system employed. The patches adjust the data storage layout to what Firedrake expects (e.g., by generating an array of pointers instead of a pointer to pointers, by replacing flattened arrays with bi-dimensional ones).

For Constraint 2, discussed in Section 4.5, we set $T_H = \text{size}(\text{L2})$; that is, the size of the processor L2 cache (the last level of private cache). When the threshold had an impact on the transformation process, the experiments were repeated with $T_H = \text{size}(\text{L3})$. The results are documented later, individually for each problem.

Following the methodology adopted in Ølgaard and Wells [2010], we vary the following parameters:

- the polynomial degree of test, trial, and coefficient (or “pre-multiplying”) functions, $q \in \{1, 2, 3, 4\}$
- the number of coefficient functions $\text{nf} \in \{0, 1, 2, 3\}$

While constants of our study are

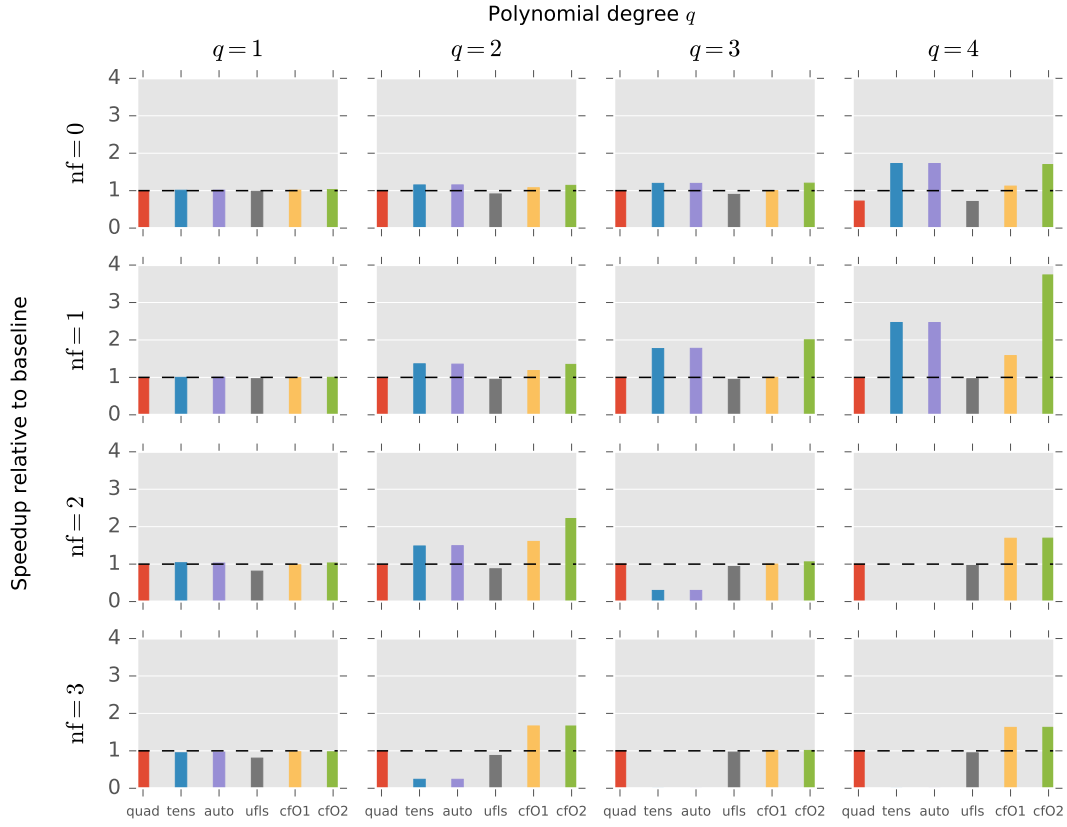


Figure 4.10: Performance evaluation for the *mass* matrix. The bars represent speed-up over the original (unoptimized) code produced by the FEniCS Form Compiler.

- the element family: Lagrange
- the mesh: tetrahedral with a total of 4374 elements
- exact numerical quadrature (we employ the same scheme used in Ølgaard and Wells [2010], based on the Gauss-Legendre-Jacobi rule)

4.9.2 Performance Results

We report the results of our experiments in Figures 4.10, 4.11, 4.12, and 4.13 as three-dimensional plots. The axes represent q , nf , and code transformation system. We show one subplot for each problem instance $\langle \text{form}, nf, q \rangle$, with the code transformation system varying within each subplot. The best variant for each problem instance is given by the tallest bar, which

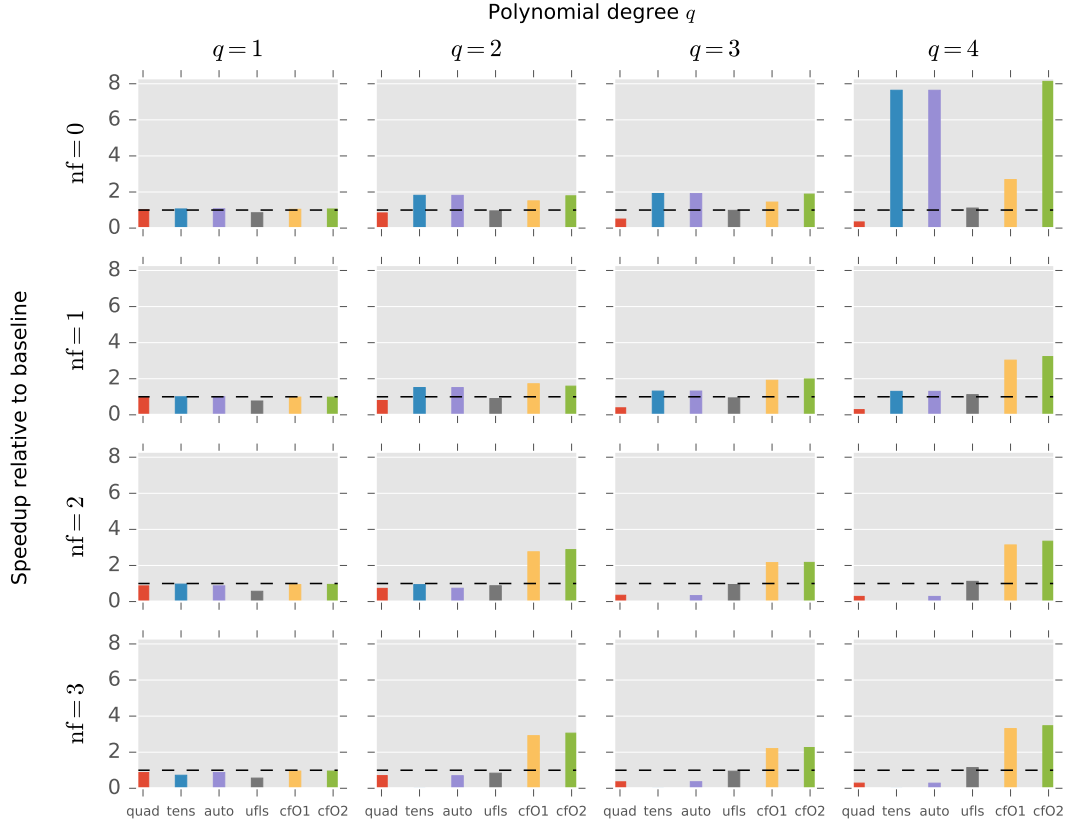


Figure 4.11: Performance evaluation for the bilinear form of a *Helmholtz* equation. The bars represent speed-up over the original (unoptimized) code produced by the FEniCS Form Compiler.

indicates the maximum speed-up over non-transformed code. We note that if a bar or a subplot are missing, then the form compiler failed to generate code because it either exceeded the system memory limit or was otherwise unable to handle the form.

The rest of the section is organized as follows: we first provide insights into the general outcome of the experimentation; we then comment on the impact of a fundamental low-level optimization, namely autovectorization; finally, we motivate, for each form, the performance results obtained.

High level view Our transformation strategy does not always guarantee minimum execution time. In particular, about 5% of the test cases (3

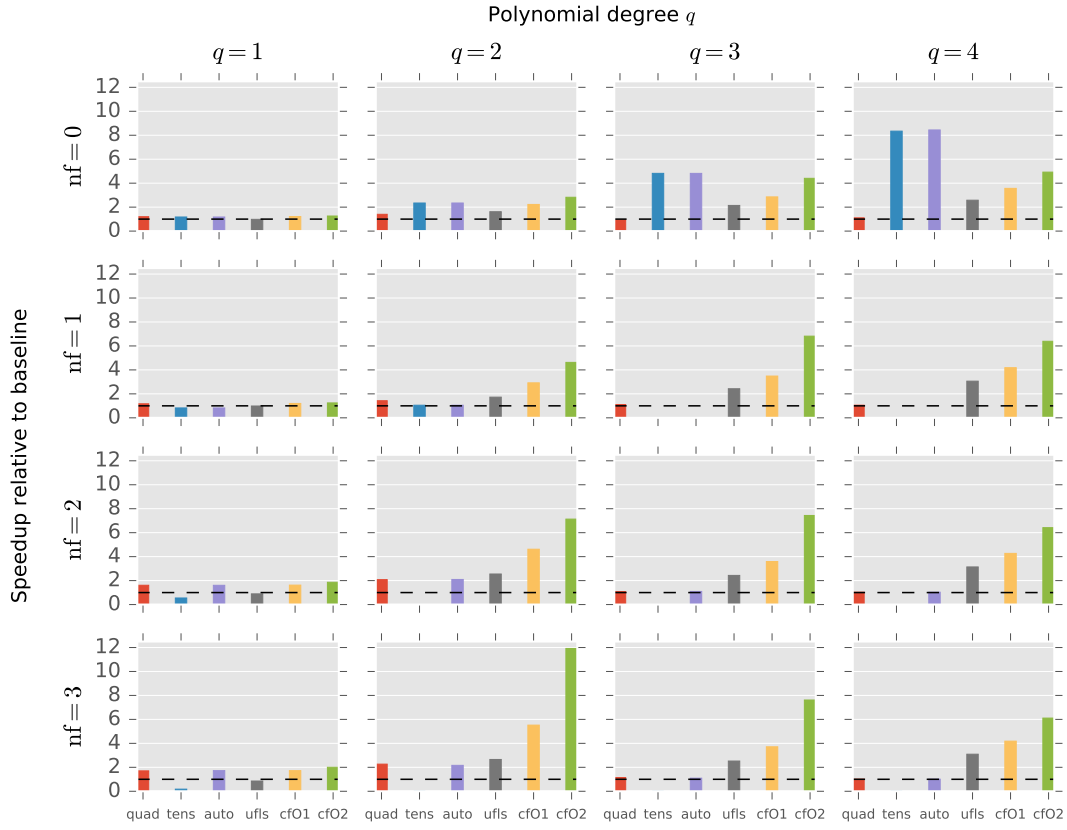


Figure 4.12: Performance evaluation for the bilinear form arising in an *elastic* model. The bars represent speed-up over the original (unoptimized) code produced by the FEniCS Form Compiler.

out of 56, without counting marginal differences) show that cf02 was not optimal in terms of runtime. The most significant of such test cases is the elastic model with $[q = 4, nf = 0]$. There are two reasons for this. First, low level optimization can have a significant impact on the actual performance. For example, the aggressive loop unrolling in tens eliminates operations on zeros and reduces the working set size by not storing entire temporaries; on the other hand, preserving the loop structure can maximize the chances of autovectorization. Second, the transformation strategy adopted when T_H is exceeded plays a key role, as we will later elaborate.

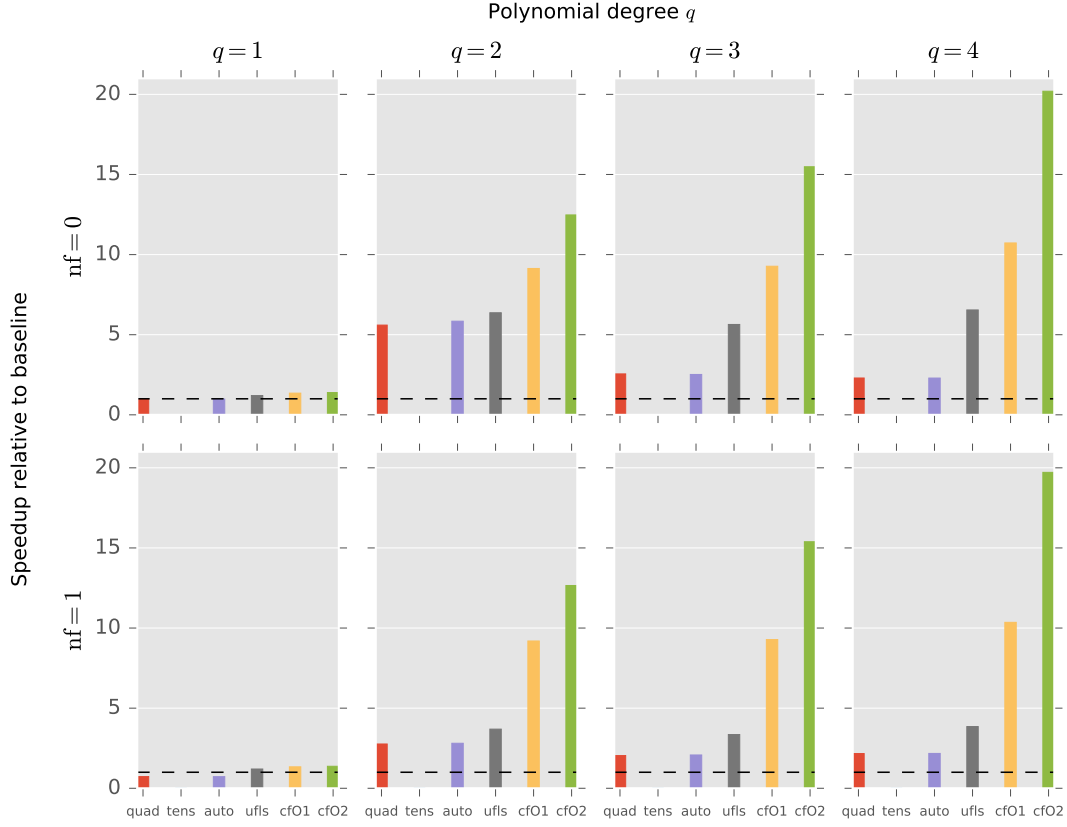


Figure 4.13: Performance evaluation for the bilinear form arising in a *hyperelastic* model. The bars represent speed-up over the original (unoptimized) code produced by the FEniCS Form Compiler.

Autovectorization We chose the mesh dimension and the function spaces such that the inner loop sizes would always be a multiple of the machine vector length. This ensured autovectorization in the majority of code variants⁶. The biggest exception is *quad*, due to the presence of indirection arrays in the generated code. In *tens*, loop nests are fully unrolled, so the standard loop vectorization is not feasible; the compiler reports suggest, however, that block vectorization [Larsen and Amarasinghe, 2000] is often triggered. In *ufls*, *cf01*, and *cf02* the iteration spaces have identical structure, with loop vectorization being regularly applied.

⁶We verified the vectorization of inner loops by looking at both compiler reports and assembly code.

Mass matrix We start with the simplest of the bilinear forms investigated, the mass matrix. Results are in Figure 4.10. We first notice that the lack of improvements when $q = 1$ is due to the fact that matrix insertion outweighs local assembly. For $q \geq 2$, cf02 generally shows the highest speed-ups. It is worth noting why auto does not always select the fastest implementation: auto always opts for tens, while for $nf \geq 2$ quad tends to be preferable. On the other hand, cf02 always makes the optimal decision about whether to apply pre-evaluation or not. Surprisingly, despite the simplicity of the form, the performance of the various code generation systems can differ significantly.

Helmholtz As in the case of Mass matrix, when $q = 1$ the matrix insertion phase is dominant. For $q \geq 2$, the general trend is that cf02 outperforms the competitors. In particular:

$nf = 0$ pre-evaluation makes cf02 notably faster than cf01, especially for high values of q ; auto correctly selects tens, which is comparable to cf02.

$nf = 1$ auto picks tens; the choice is however sub-optimal when $q = 3$ and $q = 4$. This can indirectly be inferred from the large gap between cf02 and tens/auto: cf02 applies sharing elimination, but it correctly avoids pre-evaluation because of the excessive expansion cost.

$nf = 2, 3$ auto reverts to quad, which would theoretically be the right choice (the flop count is much lower than in tens); however, the generated code suffers from the presence of indirection arrays, which break autovectorization and “traditional” code motion.

The slow-downs (or marginal improvements) seen in a small number of cases exhibited by ufls can be attributed to the presence of sharing in the generated code.

An interesting experiment we additionally performed was relaxing the memory threshold by setting $T_H = \text{size}(L3)$. We found that this makes cf02 generally slower for $nf \geq 2$, with a maximum slow-down of $2.16\times$ with $\langle nf = 2, q = 2 \rangle$. This effect could be worse when running in par-

allel, since the L3 cache is shared and different threads would end up competing for the same resource.

Elasticity The results for the elastic model are displayed in Figure 4.12. The main observation is that cf02 never triggers pre-evaluation, although in some occasions it should. To clarify this, consider the test case $\langle \text{nf} = 0, q = 2 \rangle$, in which tens/auto show a considerable speed-up over cf02. cf02 finds pre-evaluation profitable in terms of operation count, although it is eventually not applied to avoid exceeding T_H . However, running the same experiments with $T_H = \text{size}(\text{L3})$ resulted in a dramatic improvement, even higher than that obtained by tens. The reason is that, despite exceeding T_H by roughly 40%, the saving in operation count is so large ($5\times$ in this specific problem) that pre-evaluation would in practice be the winning choice. This suggests that our objective function should be improved to handle the cases in which there is a significant gap between potential cache misses and reduction in operation count.

We also note that:

- the differences between cf02 and cf01 are due to the perfect sharing elimination and the zero-valued blocks avoidance technique presented in Section 4.8.3.
- when $\text{nf} = 1$, auto prefers tens over quad, which leads to sub-optimal operation counts and execution times.
- ufls often results in better execution times than quad and tens. This is due to multiple factors, including avoidance of indirection arrays, preservation of loop structure, and a more effective code motion strategy.

Hyperelasticity In the experiments on the hyperelastic model, shown in Figure 4.13, cf02 exhibits the largest gains out of all problem instances considered in this section. This is a positive result, since it indicates that our transformation algorithm scales well with form complexity. The fact that all code transformation systems (apart from tens) show quite significant speed-ups suggests two points. First, the baseline is highly inefficient. With forms as complex as in the hyperelastic model, a trivial

translation of integration routines into code should always be avoided as even the best general-purpose compiler available (the Intel compiler on an Intel platform at maximum optimization level) fails to exploit the structure inherent in the expressions. Second, the strategy for removing spatial and temporal sharing has a tremendous impact. Sharing elimination as performed by `cf02` ensures a critical reduction in operation count, which becomes particularly pronounced for higher values of q .

4.10 Conclusions

We have developed a theory for the optimization of finite element integration loop nests. The chapter details the domain properties which are exploited by our approach (e.g., linearity) and how these translate to transformations at the level of loop nests. All of the algorithms shown in this chapter have been implemented in COFFEE, a publicly available compiler fully integrated with the Firedrake framework. The correctness of the transformation algorithm was discussed. The performance results achieved suggest the effectiveness of our methodology.

4.11 Limitations and Future Work

We have defined sharing elimination and pre-evaluation as high level transformations on top of a specific set of rewrite operators, such as code motion and factorization, and we have used them to construct the transformation space. There are three main limitations in this process. First, we do not have a systematic strategy to optimize sub-expressions which are independent of linear loops. Although we have a mechanism to determine how much computation should be hoisted to the level of the integration (reduction) loop, it is not clear how to effectively improve the heuristics used at step (6) in Algorithm 5. Second, lower operation counts may be found by exploiting domain-specific properties, such as redundancies in basis functions; this aspect is completely neglected in this chapter. Third, with Constraint 1 we have limited the applicability of code motion. This constraint was essential given the complexity of the problem tackled.

Another issue raised by the experimentation concerns selecting a proper threshold for Constraint 2. To solve this problem would require a more so-

phisticated cost model, which is an interesting question deserving further research.

We also identify two additional possible research directions: a complete classification of forms for which a global optimum is achieved; and a generalization of the methodology to other classes of loop nests, for instance those arising in spectral element methods.

Chapter 5

Cross-loop Optimization of Arithmetic Intensity for Finite Element Integration

In the previous chapter, a method to minimize the operation count of finite element integration loop nests, or “assembly kernels”, has been developed. Here, the focus is on the same class of kernels, but a complementary issue is tackled: the low level optimization of the resulting code.

This chapter is a revised version of Luporini et al. [2015], with extended examples and improved results.

5.1 Recapitulation and Objectives

We know that an assembly kernel is characterized by the presence of an affine, often non-perfect loop nest, in which individual loops are rather small: their trip count rarely exceeds 30, and may be as low as 3 for low order methods. In the innermost loop, a compute intensive expression evaluates an n -dimensional array, or element tensor, which represents the result of local assembly in an element of the discretized domain. More specifically: in bilinear forms, $n = 2$ and the output is referred to as the element matrix; in linear forms, $n = 1$ and the output is referred to as the element vector. With such a kernel structure, the objective of the low level optimization is maximizing register locality and SIMD vectorization.

We aim to maximize our impact on the platforms that are realistically used for finite element applications, so we target conventional CPU architectures rather than GPUs. The key limiting factor to the execution on GPUs is the stringent memory requirements. Only relatively small problems fit in a GPU memory, and support for distributed GPU execution in general purpose finite element frameworks is minimal. There has been some research on adapting local assembly to GPUs, although it differs from ours in several ways, including: (i) not relying on automated code generation from a domain-specific language, (ii) testing only very low order methods, (iii) not optimizing for cross-loop arithmetic intensity (the goal is rather effective multi-thread parallelization). In addition, our code transformations would drastically impact the GPU parallelization strategy, for example by increasing a thread's working set. For all these reasons, extending the research to GPU architectures is beyond the scope of this work. The related work on the subject is covered in Section 5.5, while intuitions about this research direction are provided in Section 5.6.

Achieving high performance on CPUs is non-trivial. The complexity of the mathematical expressions, which we know to be often characterized by a large number of operations on constants and small vectors, makes it hard to determine a single or specific sequence of transformations that is successfully applicable to all problems. Loop trip counts are typically small and can vary significantly, which further exacerbates the issue. Moreover, the memory access pattern can be either unit-stride ($A[i], A[i+1], A[i+2], \dots$) or multi-stride ($A[i], A[i+1], A[i+N], A[i+N+1], \dots$) – for example, as a consequence of skipping computation on zeros, see Section 4.8.3. We will show that general-purpose compilers, such as *GNU's* and *Intel's*, fail at maximizing the efficiency of the generated code because of such a particular structure. Polyhedral-model-based source-to-source compilers, for instance Bondhugula et al. [2008], can apply aggressive loop optimizations, such as tiling, but these are not particularly helpful in our context since they mostly focus on cache locality.

As in Chapter 4, we focus on optimizing the performance of assembly kernels produced through automated code generation, so we seek transformations that are generally applicable and effective. In particular, we introduce and study the following transformations:

Padding and data alignment SIMD vectorization is more effective when the CPU registers are packed (unpacked) by means of aligned load (store) instructions. Data alignment is achieved through array padding, a conceptually simple yet powerful transformation that can result in dramatic reductions in execution time.

Vector-register tiling Tiling at the level of vector registers exploits the peculiar memory access pattern induced by finite element operators (i.e., the linearity of the test and trial functions loops) to improve data locality.

Expression splitting Complex expressions are often characterized by high register pressure (i.e., the lack of available registers inducing the compiler to “spill” data from registers to cache). This transformation exploits the associativity property of the addition to distribute, or “split”, an expression into multiple sub-expressions to be computed in separate loop nests.

In addition, we analyze the effects of “more traditional” optimizations: loop unrolling, loop interchange, loop fusion and vector promotion. Some of these are not applied by general-purpose compilers, or are applied in a sub-optimal way; in such a case, they will be applied explicitly through our compiler, COFFEE.

To summarize, the contributions of this chapter are:

- The introduction of novel transformations that are demonstrated to improve the performance of assembly kernels. These transformations, implemented in COFFEE, aim to maximize register locality and SIMD vectorization.
- A study on the effectiveness of a set of well-known transformations as well as the introduction of extensions that, taking advantage of assembly kernel properties, maximize their impact.
- Extensive experimentation using a set of real-world forms commonly arising in finite element methods.
- A discussion concerning the generality of the transformations and their applicability to different domains.

5.2 Low-level Optimization

In this section, we describe three novel transformations that target register locality (expression splitting), SIMD vectorization (padding and data alignment), or both (vector-register tiling). Their ideation was directly inspired by the structure of assembly kernels. In particular, preliminary experimentation and profiling suggested that better performance could be achieved by optimizing resource usage within a CPU core. The implementation is carried out in COFFEE. Understanding the potential of these transformations in other computational domains requires a different kind of investigation, which we approach in Section 5.6.

5.2.1 Padding and Data Alignment

The absence of stencils makes it simple for a general-purpose compiler to auto-vectorize the computation of the element tensor¹. Nevertheless, vectorization is sub-optimal if data are not aligned to cache-line boundaries or if the innermost loop trip count is not a multiple of the vector length VL (especially when the loops are small as in assembly kernels).

Data alignment is enforced in two steps. First, all arrays (except the element tensor, for reasons discussed shortly) are allocated to addresses that are multiples of VL. This is achieved by adding special attributes to each declaration (e.g., `__attribute__((aligned(VL * 8)))`, with 8 being the size of a value in double precision). Second, their innermost dimension is padded by rounding the size to the nearest multiple of VL. For instance, assume the original size of a basis function array is 3×3 and $VL = 4$ (e.g. AVX processor, with 32-byte long vector registers and 8-byte double-precision floats); then, the padded version of the array will have size 3×4 . The compiler is explicitly informed about data alignment through suitable pragmas. For example, in the case of the Intel compiler, adding the annotation `#pragma vector aligned` to a loop declares that all of the memory accesses performed in its body will be aligned. This allows the compiler to generate aligned load and store instructions (e.g., `movapd`), which are dramatically faster than unaligned ones (e.g., `movupd`).

¹In practice, the GCC compiler does not auto-vectorize loops if these are too small; this indicates flaws in its cost model, since vectorization, in our hand-crafted experiments, was always found to be a winning choice.

As anticipated, the element tensor requires special attention. In our computational model, the element tensor is a kernel’s input parameter, so the aforementioned transformations cannot be applied. We therefore create a “shadow” copy of the element tensor, padded, aligned, and initialized to 0. The shadow element tensor replaces any occurrence of the original element tensor in the kernel. Right before returning to the caller, a loop nest will copy the relevant region of the shadow element tensor back into the input array.

This process often allows to safely round a loop trip count to the nearest multiple of VL, thus avoiding the introduction of a remainder (scalar) loop from the compiler (which would render vectorization less efficient). We distinguish two cases:

All memory accesses in the kernel are unit-stride It is trivial to verify whether the iterations introduced by rounding up the loop trip count will only write to the padded region of the element tensor. In such a case, the loop trip count can be rounded. Listing 6 illustrates the effect of padding and data alignment on top of generalized code motion in the weighted Laplace kernel which we introduced in Chapter 2, with loop trip counts properly rounded.

Offsets are used when accessing array values Verifying whether the transformation will alter the output is in this case less trivial. The intersection I between the set of extra iterations (in Listing 6, $\{4\}$) and the sets of *non* zero-valued columns in each array is computed. If $I \neq \emptyset$, the loop trip count cannot be rounded. In such a case, or if any offset is not a multiple of VL, the `#pragma vector aligned` also cannot be added.

5.2.2 Expression Splitting

In complex kernels, like Burgers in Listing 2, and on certain architectures, achieving effective register allocation can be challenging. If the number of variables independent of the innermost-loop dimension is close to or greater than the number of available CPU registers, poor register reuse is likely. This usually happens when the number of basis function arrays, temporaries introduced by either generalized code motion or pre-

LISTING 6: The assembly kernel for the weighted Laplace operator in Listing 1 after application of padding and data alignment on top of generalized code motion. An AVX architecture, which implies VL = 4, is assumed.

```

1 #define ALIGN __attribute__((aligned(32)))
2
3 void weighted_laplace(double A[3][3], double **coords, double w[3]) {
4     // K, det = Compute Jacobian (coords)
5
6     // Quadrature weights
7     static const double W[6] ALIGN = {0.5};
8
9     // Basis functions
10    static const double B[6][4] ALIGN = {{...}} ;
11    static const double C[6][3] ALIGN = {{...}} ;
12    static const double D[6][4] ALIGN = {{...}} ;
13
14    // Padded buffer
15    double PA[3][4] ALIGN = {{0.0}};
16
17    for (int i = 0; i < 6; i++) {
18        double f0 = 0.0;
19        for (int r = 0; r < 3; ++r) {
20            f0 += (w[r] * C[i][r]);
21        }
22        double T0[4] ALIGN;
23        double T1[4] ALIGN;
24        #pragma vector aligned
25        for (int j = 0; j < 4; j++) {
26            T0[j] = ((K[1]*B[i][j])+(K[3]*D[i][j]));
27            T1[j] = ((K[0]*B[i][j])+(K[2]*D[i][j]));
28        }
29        double T2[4] ALIGN;
30        double T3[4] ALIGN;
31        #pragma vector aligned
32        for (int k = 0; k < 4; k++) {
33            T2[k] = ((K[1]*B[i][k])+(K[3]*D[i][k]));
34            T3[k] = ((K[0]*B[i][k])+(K[2]*D[i][k]));
35        }
36        for (int j = 0; j < 3; j++) {
37            #pragma vector aligned
38            for (int k = 0; k < 4; k++) {
39                PA[j][k] += (T0[j]*T2[k] + T1[j]*T3[k])*det*W[i]*f0;
40            }
41        }
42    }
43 }
44 // Copy back the shadow tensor to the input array
45 for (int j = 0; j < 3; j++) {
46     for (int k = 0; k < 3; k++) {
47         A[j][k] = PA[j][k];
48     }
49 }

```

evaluation, and problem constants is large. For example, applying code motion to the Burgers example on a 3D mesh requires 24 temporaries for the ijk loop order. This can make hoisting of the invariant loads out of the k loop inefficient on architectures with a relatively low number of registers. One potential solution to this problem consists of suitably “splitting” the computation of the element tensor A into multiple sub-expressions. An example of this idea is given in Listing 7. The transformation can be regarded as a special case of classic loop fission, in which associativity of the addition is exploited to distribute the expression across multiple loops.

LISTING 7: The assembly kernel for the weighted Laplace operator in Listing 1 after application of expression splitting on top of generalized code motion. In this example, the split factor is 2.

```

1 void weighted_laplace(double A[3][3], double **coords, double w[3]) {
2   // Omitting redundant code
3   ...
4   for (int j = 0; j<3; j++) {
5     for (int k = 0; k<3; k++) {
6       A[j][k] += (T0[k]*T0[j])*det*W[i]*f0;
7     }
8   }
9   for (int j = 0; j<3; j++) {
10    for (int k = 0; k<3; k++) {
11      A[j][k] += (T1[k]*T1[j])*det*W[i]*f0;
12    }
13  }
14 }
15 ...

```

Splitting an expression has, however, several drawbacks. Firstly, it increases the number of accesses to A in proportion to the “split factor”, which is the number of sub-expressions produced. Also, depending on how splitting is done, it can lead to redundant computation. For example, the number of times the product $\text{det} * W3[i]$ is performed is proportional to the number of sub-expressions, as shown in the code snippet. Further, it increases loop overhead, for example through additional branch instructions. Finally, it might affect register locality: for instance, the same array could be accessed in different sub-expressions, requiring a proportional number of loads be performed; this is not the case of the running example, though. Nevertheless, the performance gain from improved register reuse can still be greater if suitable heuristics are used. Our approach consists of traversing the expression tree and recursively splitting it into

multiple sub-expressions as long as the number of variables independent of the innermost loop exceeds a certain threshold. The optimal threshold has to be determined explicitly for each problem; a good heuristic consists of counting how many distinct variables need be loaded at every loop iteration and comparing with the number of available registers.

5.2.3 Model-driven Vector-register Tiling

LISTING 8: The assembly kernel for the weighted Laplace operator in Listing 1 after application of vector-register tiling (on top of generalized code motion, padding, and data alignment). In this example, the unroll-and-jam factor is 1.

```

1 void weighted_laplace(double A[3][3], double **coords, double w[3]) {
2     // Omitting redundant code
3     ...
4     // Padded buffer (note: both rows and columns)
5     double PA[4][4] ALIGN = {{0.0}};
6
7     for (int i = 0; i<3; i++) {
8         // Omitting redundant code
9         // ...
10        for (int j = 0; j<4; j += 4)
11            for (int k = 0; k<4; k += 4) {
12                // Sequence of LOAD and SET intrinsics
13                // Compute PA[0][0], PA[1][1], PA[2][2], PA[3][3]
14                // One _mm256_permute_pd per k-loop LOAD
15                // Compute PA[0][1], PA[1][0], PA[2][3], PA[3][2]
16                // One _mm256_permute2f128_pd per k-loop LOAD
17                // ...
18            }
19        // Scalar remainder loop (not necessary in this example)
20    }
21    // Restore the storage layout
22    for (int j = 0; j<4; j += 4) {
23        for (int k = 0; k<4; k += 4) {
24            _mm256d r0 = _mm256_load_pd (&A[j+0][k]);
25            // LOAD PA[j+1][k], PA[j+2][k], PA[j+3][k]
26            r4 = _mm256_unpackhi_pd (r1, r0);
27            r5 = _mm256_unpacklo_pd (r0, r1);
28            r6 = _mm256_unpackhi_pd (r2, r3);
29            r7 = _mm256_unpacklo_pd (r3, r2);
30            r0 = _mm256_permute2f128_pd (r5, r7, 32);
31            r1 = _mm256_permute2f128_pd (r4, r6, 32);
32            r2 = _mm256_permute2f128_pd (r7, r5, 49);
33            r3 = _mm256_permute2f128_pd (r6, r4, 49);
34            _mm256_store_pd (&A[j+0][k], r0);
35            // STORE PA[j+1][k], PA[j+2][k], PA[j+3][k]
36        }
37    }
38 }
39 ...

```

One notable problem of assembly kernels concerns register allocation

and register locality. The critical situation occurs when the loop trip counts and the variables accessed are such that the vector-register pressure is high. Since the kernel's working set is expected to fit the L1 cache, it is particularly important to optimize register management. Standard optimizations, such as loop interchange, unroll, and unroll-and-jam, can be employed to deal with this problem. Tiling at the level of vector registers represents another opportunity. Based on the observation that the evaluation of an element matrix can be reduced to a summation of outer products along the j and k dimensions, a model-driven vector-register tiling strategy can be implemented. The computation of an element matrix is abstractly expressible as

$$A_{jk} = \sum_{\substack{x \in B' \subseteq B \\ y \in B'' \subseteq B}} x_j \cdot y_k \quad j, k = 0, \dots, 3$$

where B is the set of all basis functions or temporary variables accessed in the kernel, whereas B' and B'' are generic problem-dependent subsets. Regardless of the specific input problem, by abstracting from the presence of all variables independent of both j and k , the element matrix computation is always reducible to this form. Figure 5.1 illustrates how we can evaluate 16 entries ($j, k = 0, \dots, 3$) of the element matrix using just 2 vector registers, which represent a 4×4 tile, assuming $|B'| = |B''| = 1$. Values in a register are shuffled each time a product is performed. Standard compiler auto-vectorization for both GNU and Intel compilers, instead, executes 4 broadcast operations (i.e., “splat” of a value over all of the register locations) along the outer dimension to perform the calculation. In addition to incurring a larger number of cache accesses, it needs to keep between $f = 1$ and $f = 3$ extra registers to perform the same 16 evaluations when unroll-and-jam is used, with f being the unroll-and-jam factor.

The storage layout of PA, however, is incorrect after the application of this outer-product-based vectorization. It can be efficiently restored with a sequence of vector shuffles following the pattern highlighted in Figure 5.2, executed once outside of the ijk loop nest. The pseudo-code for the transformed weighted Laplace assembly kernel is shown in Listing 8.

	Initial configuration	After the first permutation	After the second permutation	After the third permutation																
x	<table><tr><td>0</td><td>1</td><td>2</td><td>3</td></tr></table>	0	1	2	3	<table><tr><td>0</td><td>1</td><td>2</td><td>3</td></tr></table>	0	1	2	3	<table><tr><td>0</td><td>1</td><td>2</td><td>3</td></tr></table>	0	1	2	3	<table><tr><td>0</td><td>1</td><td>2</td><td>3</td></tr></table>	0	1	2	3
0	1	2	3																	
0	1	2	3																	
0	1	2	3																	
0	1	2	3																	
	x	x	x	x																
y	<table><tr><td>0</td><td>1</td><td>2</td><td>3</td></tr></table>	0	1	2	3	<table><tr><td>1</td><td>0</td><td>3</td><td>2</td></tr></table>	1	0	3	2	<table><tr><td>2</td><td>3</td><td>0</td><td>1</td></tr></table>	2	3	0	1	<table><tr><td>3</td><td>2</td><td>1</td><td>0</td></tr></table>	3	2	1	0
0	1	2	3																	
1	0	3	2																	
2	3	0	1																	
3	2	1	0																	
	=	=	=	=																
A	<table><tr><td>0,0</td><td>1,1</td><td>2,2</td><td>3,3</td></tr></table>	0,0	1,1	2,2	3,3	<table><tr><td>0,1</td><td>1,0</td><td>2,3</td><td>3,2</td></tr></table>	0,1	1,0	2,3	3,2	<table><tr><td>0,2</td><td>1,3</td><td>2,0</td><td>3,1</td></tr></table>	0,2	1,3	2,0	3,1	<table><tr><td>0,3</td><td>1,2</td><td>2,1</td><td>3,0</td></tr></table>	0,3	1,2	2,1	3,0
0,0	1,1	2,2	3,3																	
0,1	1,0	2,3	3,2																	
0,2	1,3	2,0	3,1																	
0,3	1,2	2,1	3,0																	

Figure 5.1: The outer-product vectorization relies on permuting values directly within vector registers.

Initial configuration	After the first set of shuffles	After the second set of shuffles	Layout restored																																																																
<table border="1"> <tr><td>(0, 0)</td><td>(1, 1)</td><td>(2, 2)</td><td>(3, 3)</td></tr> <tr><td>(0, 1)</td><td>(1, 0)</td><td>(2, 3)</td><td>(3, 2)</td></tr> <tr><td>(0, 2)</td><td>(1, 3)</td><td>(2, 0)</td><td>(3, 1)</td></tr> <tr><td>(0, 3)</td><td>(1, 2)</td><td>(2, 1)</td><td>(3, 0)</td></tr> </table>	(0, 0)	(1, 1)	(2, 2)	(3, 3)	(0, 1)	(1, 0)	(2, 3)	(3, 2)	(0, 2)	(1, 3)	(2, 0)	(3, 1)	(0, 3)	(1, 2)	(2, 1)	(3, 0)	<table border="1"> <tr><td>(0, 0)</td><td>(1, 1)</td><td>(2, 2)</td><td>(3, 3)</td></tr> <tr><td>(0, 1)</td><td>(1, 0)</td><td>(2, 3)</td><td>(3, 2)</td></tr> <tr><td>(0, 2)</td><td>(1, 3)</td><td>(2, 0)</td><td>(3, 1)</td></tr> <tr><td>(0, 3)</td><td>(1, 2)</td><td>(2, 1)</td><td>(3, 0)</td></tr> </table>	(0, 0)	(1, 1)	(2, 2)	(3, 3)	(0, 1)	(1, 0)	(2, 3)	(3, 2)	(0, 2)	(1, 3)	(2, 0)	(3, 1)	(0, 3)	(1, 2)	(2, 1)	(3, 0)	<table border="1"> <tr><td>(0, 0)</td><td>(0, 1)</td><td>(2, 2)</td><td>(2, 3)</td></tr> <tr><td>(1, 0)</td><td>(1, 1)</td><td>(3, 2)</td><td>(3, 3)</td></tr> <tr><td>(0, 2)</td><td>(0, 3)</td><td>(2, 0)</td><td>(2, 1)</td></tr> <tr><td>(1, 2)</td><td>(1, 3)</td><td>(3, 0)</td><td>(3, 1)</td></tr> </table>	(0, 0)	(0, 1)	(2, 2)	(2, 3)	(1, 0)	(1, 1)	(3, 2)	(3, 3)	(0, 2)	(0, 3)	(2, 0)	(2, 1)	(1, 2)	(1, 3)	(3, 0)	(3, 1)	<table border="1"> <tr><td>(0, 0)</td><td>(0, 1)</td><td>(0, 2)</td><td>(0, 3)</td></tr> <tr><td>(1, 0)</td><td>(1, 1)</td><td>(1, 2)</td><td>(1, 3)</td></tr> <tr><td>(2, 0)</td><td>(2, 1)</td><td>(2, 2)</td><td>(2, 3)</td></tr> <tr><td>(3, 0)</td><td>(3, 1)</td><td>(3, 2)</td><td>(3, 3)</td></tr> </table>	(0, 0)	(0, 1)	(0, 2)	(0, 3)	(1, 0)	(1, 1)	(1, 2)	(1, 3)	(2, 0)	(2, 1)	(2, 2)	(2, 3)	(3, 0)	(3, 1)	(3, 2)	(3, 3)
(0, 0)	(1, 1)	(2, 2)	(3, 3)																																																																
(0, 1)	(1, 0)	(2, 3)	(3, 2)																																																																
(0, 2)	(1, 3)	(2, 0)	(3, 1)																																																																
(0, 3)	(1, 2)	(2, 1)	(3, 0)																																																																
(0, 0)	(1, 1)	(2, 2)	(3, 3)																																																																
(0, 1)	(1, 0)	(2, 3)	(3, 2)																																																																
(0, 2)	(1, 3)	(2, 0)	(3, 1)																																																																
(0, 3)	(1, 2)	(2, 1)	(3, 0)																																																																
(0, 0)	(0, 1)	(2, 2)	(2, 3)																																																																
(1, 0)	(1, 1)	(3, 2)	(3, 3)																																																																
(0, 2)	(0, 3)	(2, 0)	(2, 1)																																																																
(1, 2)	(1, 3)	(3, 0)	(3, 1)																																																																
(0, 0)	(0, 1)	(0, 2)	(0, 3)																																																																
(1, 0)	(1, 1)	(1, 2)	(1, 3)																																																																
(2, 0)	(2, 1)	(2, 2)	(2, 3)																																																																
(3, 0)	(3, 1)	(3, 2)	(3, 3)																																																																

Figure 5.2: Restoring the storage layout is the last step of the outer-product vectorization. The figure shows how 4×4 elements in the top-left block of the element matrix A can be moved to their correct positions. Each rotation, represented by a group of three same-colored arrows, is implemented by a single shuffle intrinsic.

Generalization In this section, we have considered assembly kernels arising from bilinear forms. The transformation can be generalized to linear forms provided that the loop over mesh elements is introduced in the computational model. The new dimension would induce an outer product with the test functions loop; hence, the element vector could be turned into a “multi-element” matrix, which would enable a similar vector-register tiling. This is however not implemented in COFFEE.

5.3 Experiments

The objective is to evaluate the impact of the code transformations presented in the previous sections in representative problems.

5.3.1 Setup

We use three bilinear forms, which we refer to as (i) *Helmholtz*, (ii) *Diffusion*, and (iii) *Burgers* (the names derive from the PDEs from which the bilinear forms were extracted). The three chosen forms lead to *real-life kernels* and

comprise the core differential operators in some of the most frequently encountered finite element problems in scientific computing. This is of crucial importance because distinct problems, possibly arising in completely different fields, may employ (subsets of) the same differential operators of our benchmarks, which implies similarities and redundant patterns in the generated code. Consequently, the proposed code transformations have a domain of applicability that goes far beyond that of the three analyzed equations.

The Helmholtz and Diffusion kernels are archetypal second order elliptic operators. They are complete and unsimplified examples of the operators used to model diffusion and viscosity in fluids, and for imposing pressure in incompressible fluids. As such, they are both extensively used in climate and ocean modeling. Very similar operators, for which the same optimizations are expected to be equally effective, apply to elasticity problems, which are at the base of computational structural mechanics. The Burgers kernel is a typical example of a first order hyperbolic conservation law, which occurs in real applications whenever a quantity is transported by a fluid (the momentum itself, in our case). While the two elliptic operators apply to scalar quantities, the chosen Burgers kernel applies to a vector-valued quantity; this impacts the generated code, as explained next. The operators we have selected are characteristic of both the second and first order operators that dominate fluids and solids simulations.

The benchmarks, including the UFL description, are available at [Luporini, 2014b]; for convenience, the studied bilinear operators are also summarized in Figures 5.3, 5.4, and 5.5. The benchmarks were executed over real unstructured meshes through Firedrake. The transformations are applied through COFFEE, which is used by Firedrake. The Diffusion code has already been shown in Listing 1. The Helmholtz equation uses the same differential operators as Diffusion. In the Helmholtz kernel code, the main differences with respect to Diffusion are the presence of additional arrays (the basis functions for the “mass term”) and constants for computing the element matrix. Burgers is a non-linear problem employing differential operators different from those of Helmholtz and relying on vector-valued quantities, which has a major impact on the generated assembly code (see Listing 2), where a larger number of ba-

$$\int_{\Omega} \nabla u \cdot \nabla v + uv \, dx \quad (5.1)$$

Figure 5.3: The Helmholtz bilinear form. The trial function u and the test function v belong to the space of continuous piecewise-defined polynomials of given degree (spanned by the usual Lagrange basis functions).

$$\int_{\Omega} \nabla u \cdot \nabla v \, dx \quad (5.2)$$

Figure 5.4: The Diffusion bilinear form. The trial function u and the test function v belong to the space of continuous piecewise-defined polynomials of given degree (spanned by the usual Lagrange basis functions).

$$\int_{\Omega} \frac{u^{n+1} - u^n}{dt} \cdot v + ((u^{n+1} \cdot \nabla)u^{n+1}) \cdot v + \nu \nabla u^{n+1} \cdot \nabla v \, dx \quad (5.3)$$

Figure 5.5: The Burgers operator. The solution u and the test function v belong to the space of vector-valued continuous piecewise-defined polynomials of given degree (spanned by the usual Lagrange basis functions). ν is a constant scalar viscosity. A backward Euler time discretization is used.

sis function arrays ($X1, X2, \dots$) and constants ($F0, F1, \dots, K0, K1, \dots$) are generated.

These problems were studied varying both the shape of mesh elements and the polynomial order q of the function spaces, whereas the element family, Lagrange, is fixed. As might be expected, the larger the element shape and q , the larger the iteration space. Triangles, tetrahedra, and prisms were tested as element shape. For instance, in the case of Helmholtz with $q = 1$, the size of the j and k loops for the three element shapes is, respectively, 3, 4, and 6. Moving to larger shapes has the effect of increasing the number of basis function arrays, since, intuitively, the behaviour of the equation has to be approximated also along a third axis. On the other hand, the polynomial order affects only the problem size (the three loops i, j , and k , and, as a consequence, the size of the X and Y arrays). A range of polynomial orders from $q = 1$ to $q = 4$ were tested; higher polynomial orders are excluded from the study because of current Firedrake limitations. In all these cases, the size of the element matrix rarely exceeds 30×30 , with a peak of 105×105 in Burgers with prisms and $q = 4$.

5.3.2 Test Environment

The experiments were run on a single core of an Intel architecture, a Sandy Bridge I7-2600 CPU running at 3.4 GHz, with 32KB of L1 cache and 256KB of L2 cache). The `icc 13.1` compiler was used. The compilation flags used were `-O2` and `-xAVX` for auto-vectorization (other optimization levels were tried, but they resulted in higher execution times).

The execution times are the average of three runs with “warm cache”; that is, with all kernels retrieved directly from the Firedrake’s cache, so code generation and compilation times are not counted. The timing includes the costs of both matrix insertion and mesh iteration.

5.3.3 Rationale of the Experimentation

We evaluate the impact of four transformations: generalized loop-invariant code motion (*licm*); padding and data alignment (*ap*); outer-product vectorization (*op-vect*); expression splitting (*split*). We also study *licm*, despite not considering it a real low level transformation (it is actually a rewrite operator, see Chapters 4 and 6), because measuring the impact of *ap*, *op-vect*, and *split* becomes realistic only when all additional loops and temporaries have been created.

Figure 5.6 shows the maximum speed-ups achieved by composing the four transformations over the original code generated by Firedrake via the FEniCS Form Compiler. The figure is a three-dimensional plot: each subplot is a specific $\langle \text{shape}, \text{form}, q \rangle$ problem instance, with q varying within each subplot. By referring to this figure, in the next sections we motivate the performance improvements obtained.

5.3.3.1 Impact of Generalized Loop-invariant Code Motion

In general, the speed-ups achieved by *licm* are notable, which is in line with what we have observed in Chapter 4. The main reasons are that in the original code, (i) sub-expressions invariant to outer loops are not automatically hoisted, while (ii) sub-expressions invariant to the innermost loop are hoisted, but their execution is not auto-vectorized. These observations derive from inspection of assembly code generated by the compiler.

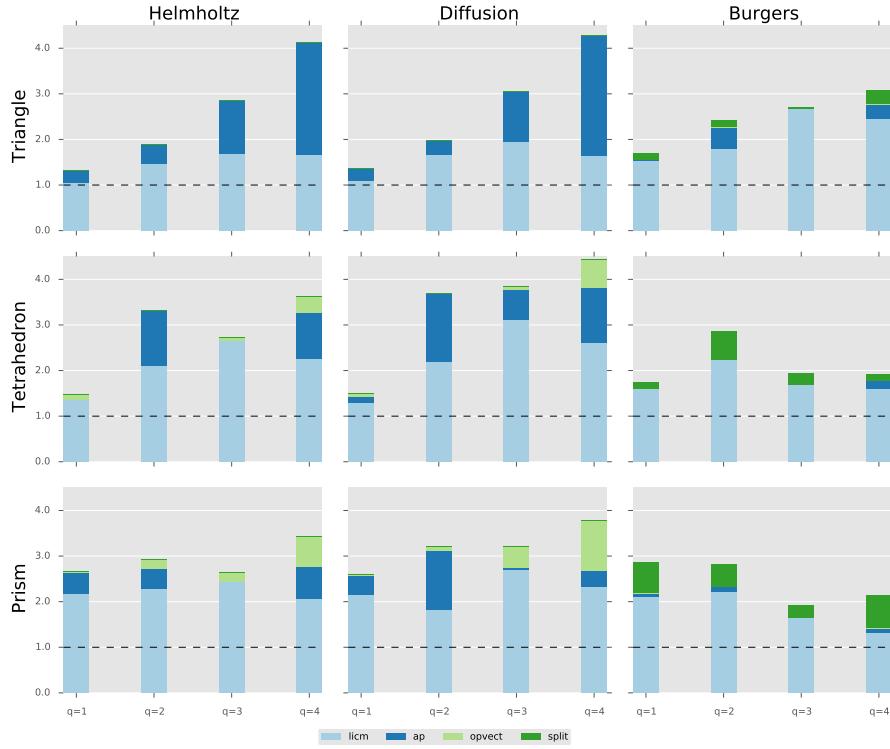


Figure 5.6: Maximum performance improvement on a Sandy Bridge due to generalized loop-invariant code motion, padding and data alignment, outer-product vectorization, and expression splitting over the original code produced by Fire-drake. The unroll and splitting factors – respectively for the outer-product vectorization and expression splitting – were determined empirically.

The gain tends to grow with the computational cost of the kernels: bigger loop nests (i.e., larger element shapes and polynomial orders) usually benefit from the reduction in redundant computation, even though extra memory for the temporary arrays is required. Some discrepancies to this trend are due to a less effective auto-vectorization. For instance, on the Sandy Bridge, the improvement at $q = 3$ is larger than that at $q = 4$ because, in the latter case, the size of the innermost loop is not a multiple of the vector length, and a remainder scalar loop is introduced at compile time. Since the loop nest is small, the cost of executing the extra scalar iterations can have a significant impact.

5.3.3.2 Impact of Padding and Data Alignment

Padding, which avoids the introduction of a remainder loop as described in Section 5.2.1, as well as data alignment, enhance the quality of auto-vectorization. Occasionally the impact of *ap* is marginal. These may be due to two reasons: (i) the non-padded element tensor size is already a multiple of the vector length; (ii) the number of aligned temporaries introduced by *licm* is so large to induce cache associativity conflicts (e.g. Burgers).

5.3.3.3 Impact of Vector-register Tiling

op-vect requires setting an unroll-and-jam factor. Here, we discuss the speed-ups obtained after a small set of feasible unroll-and-jam factors (between 1 and 4) were tried (i.e., the maximum speed-ups).

The rationale behind these results is that the effect of *op-vect* is significant in problems in which the assembly loop nest is relatively big. When the loops are short, since the number of arrays accessed at every loop iteration is rather small (between 4 and 8 temporaries, plus the element matrix itself), there is no need for vector-register tiling; extensive unrolling is sufficient to improve register re-use and, therefore, to maximize the performance. However, as the iteration space becomes larger, *op-vect* leads to improvements up to $1.4\times$ (Diffusion, prismatic mesh, $q = 4$ - increasing the overall speed up from $2.69\times$ to $3.87\times$).

Using the Intel Architecture Code Analyzer tool [Intel Corporation, 2012], we confirmed that speed ups are a consequence of increased register re-use. In Helmholtz $q = 4$, for example, the tool showed that when using *op-vect* the number of clock cycles to execute one iteration of the *j* loop decreases by roughly 17%, and that this is a result of the relieved pressure on both of the data (cache) ports available in the core.

The performance of individual kernels in terms of floating-point operations per second was also measured. The theoretical peak on a single core, with the Intel Turbo Boost technology activated, is 30.4 GFlop/s. In the case of Diffusion using a prismatic mesh and $q = 4$, we achieved a maximum of 21.9 GFlop/s with *op-vect* enabled, whereas 16.4 GFlop/s was obtained when only *licm* and *ap* were used. This result is in line with the expectations: analysis of assembly code showed that, in the *jk* loop

nest, which in this problem represents the bulk of the computation, 73% of instructions are actually floating-point operations.

Application of *op-vect* to the Burgers problem induces significant slow-downs due to the large number of temporary arrays that need be tiled, which exceeds the available logical registers on the underlying architecture. Expression splitting can be used in combination with *op-vect* to alleviate this issue; this is discussed in the next section.

5.3.3.4 Impact of Expression Splitting

Expression splitting relieves the register pressure when the element matrix evaluation needs to read from a large number of basis function arrays. As detailed in Section 5.2.2, the price to pay for this optimization is an increased number of accesses to the element matrix and, potentially, redundant computation.

For the Helmholtz and Diffusion kernels, in which only between 4 and 8 temporaries are read at every loop iteration, *split* tends to slow down the computation, because of the aforementioned drawbacks. Slow-downs up to $1.4\times$ were observed.

In the Burgers kernels, between 12 and 24 temporaries are accessed at every loop iteration, so *split* plays a key role since the number of available logical registers on the Sandy Bridge architecture is only 16. In almost all cases, a split factor of 1, meaning that the original expression was divided into two parts, ensured close-to-peak performance. The transformation negligibly affected register locality, so speed-ups up to $1.5\times$ were observed. For instance, when $q = 4$ and a prismatic mesh is employed, the overall performance improvement increases from $1.44\times$ to $2.11\times$.

The performance of the Burgers kernel on a prismatic mesh was 20.0 GFlop/s from $q = 1$ to $q = 3$, while it was 21.3 GFlop/s in the case of $q = 4$. These values are notably close to the peak performance of 30.4 GFlop/s. Disabling *split* makes the performance drop to 17.0 GFlop/s for $q = 1, 2$, 18.2 GFlop/s for $q = 3$, and 14.3 GFlop/s for $q = 4$. These values are in line with the speed-ups shown in Figure 5.6.

The *split* transformation was also tried in combination with *op-vect* (*split-op-vect*). Despite improvements up to $1.22\times$, *split-op-vect* never outperforms *split*. This is motivated by two factors: for small split factors, such

as 1 and 2, the data space to be tiled is still too big, and register spilling affects run-time; for higher ones, sub-expressions become so small that, as explained in Section 5.3.3.3, extensive unrolling already allows to achieve a certain degree of register re-use.

5.3.3.5 More Registers, Larger Vectors

To assess the impact of the transformations on architectures with different numbers of vector registers and SIMD lanes, we have repeated the same experiments on an Intel Xeon Phi (5110P, running at 1.05Ghz in native mode, 32KB L1 cache and 512KB L2 cache). The `icc 13.1` compiler was used. The compilation flag used for optimization was `-O3`.

In contrast to the Sandy Bridge, which only had 16 256-bit vector registers, the Xeon Phi has 32 512-bit vector registers. Since our transformations focus on register locality and SIMD vectorization, it is useful to study such a different platform.

The results of the experimentation are presented in Figure 5.7. Overall, the trend is similar to that observed on the Sandy Bridge, with a few exceptions. *licm* is occasionally inconsequential because the remainder loop overhead is more pronounced on the Xeon Phi, where the vector length is twice as long, which leads to proportionately larger fractions of scalar code. The pattern of *ap* and *op-vect*, instead, is much more similar to the one on the Sandy Bridge (higher speed-ups were often observed). The impact of *split* in Burgers is not as pronounced as on the Sandy Bridge, since register spilling is now limited by the presence of 32 logical vector units.

5.3.3.6 Summary of Results

We have analyzed the impact of three low level optimizations on top of *licm*. While *ap* is demonstrated to provide systematic improvements, the impact of *op-vect* and *split* is more difficult to predict. *op-vect* requires relatively large loop nests (the trip count of individual loops must be at least larger than 10) to be effective, as observed in Helmholtz and Diffusion. The largest gains in Burgers derive from using *split*, because of the high register pressure. Composing *op-vect* and *split* in Burgers rarely provided benefits, and most of these were significantly smaller than those achieved

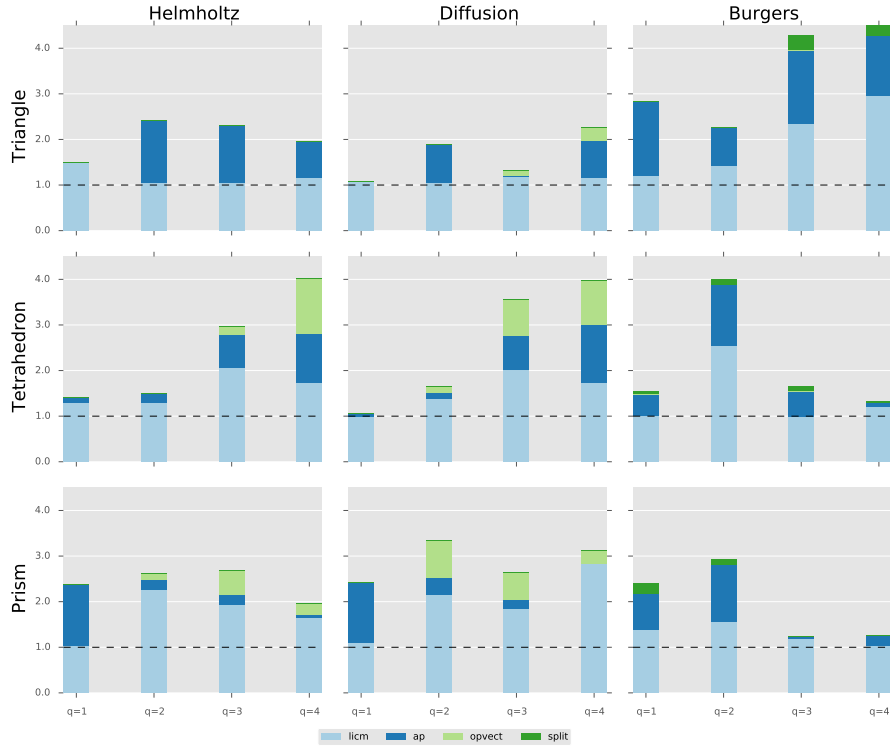


Figure 5.7: Maximum performance improvement on a Xeon Phi due to generalized loop-invariant code motion, padding and data alignment, outer-product vectorization, and expression splitting over the original code produced by Firedrake. The unroll and splitting factors – respectively for the outer-product vectorization and expression splitting – were determined empirically.

through *ap*. This was verified on both the Sandy Bridge and the Xeon Phi. It is unclear why on the Xeon Phi, in spite of a larger number of vector registers, the composite *split-op-vec* transformation did not result in significant performance improvements.

These results suggest that a cost model or an auto-tuning system to select the optimal composite transformation for a given problem would be of great help. We expand on this problem in Section 5.5.

5.4 Experience with Traditional Compiler Optimizations

In this section, we report on an experimentation with traditional optimizations: loop interchange, loop unroll, vector promotion and loop fusion.

The following sections also discuss the implementation and the use of these transformations in COFFEE.

5.4.1 Loop Interchange

All loops are interchangeable, provided that temporaries are introduced if the nest is not perfect. For the employed storage layout, the loop permutations ijk and ikj are likely to maximize the performance. Conceptually, this is motivated by the fact that if the i loop were in an inner position, then a significantly higher number of load instructions would be required at every iteration. We tested this hypothesis in manually crafted kernels. We found that the performance loss is greater than the gain due to the possibility of accumulating increments in a register, rather than memory, along the i loop. The choice between ijk and ikj depends on the number of load instructions that can be hoisted out of the innermost dimension. A good heuristic is to choose as outermost the loop along which the number of invariant loads is smaller so that more registers remain available to carry out the computation of the element tensor.

Our experience with the Intel and GNU compilers is contrasting: on one hand, the former applies this transformation following a reasonable cost model, while the latter is generally too conservative, even at highest optimization level. This behaviour was verified in different variational forms (by looking at assembly code and compiler reports), including the complex hyperelastic model analyzed in Chapter 4.

Loop interchange is implemented in COFFEE. However, it is not applied by any of the default optimization levels (see Section 6.2) due to the lack of a cost model capable of providing systematic performance improvements across a range of problems and general-purpose compilers.

5.4.2 Loop Unrolling

We first observe that manual full (or extensive) unrolling is unlikely to be effective for two reasons. Firstly, the ijk loop nest would need to be small enough such that the unrolled instructions do not exceed the instruction cache, which is rarely the case: it is true that in a local assembly kernel the minimum size of the ijk loop nest is $3 \times 3 \times 3$ (triangular mesh and polynomial order 1), but this increases rapidly with the polynomial

order of the method and the discretization employed (e.g. tetrahedral meshes imply larger loop nests than triangular ones), so sizes greater than $10 \times 10 \times 10$, for which extensive unrolling would already be harmful, are in practice very common. Secondly, manual unrolling is dangerous because it may compromise compiler auto-vectorization by either removing loops (most compilers search for vectorizable loops) or losing spatial locality within a vector register.

By comparison with implementations with manually-unrolled loops, we noticed that recent versions of compilers like GNU's and Intel's estimate close-to-optimal unroll factors when the loops are affine and their bounds are relatively small and known at compile-time, which is the case of our kernels. Our choice, therefore, is to relieve COFFEE from the duty of applying loop fusion and to leave the back-end compiler in charge of selecting unroll factors.

5.4.3 Vector promotion

Vector promotion is a transformation that “trades” a parallel dimension for space, thus creating SIMD vectorization opportunities for outer loops. In this section, we consider vector promotion for the sub-expressions that only depend on the integration loop (i.e., the *i* loop).

In Listing 9, the evaluation of the coefficient *w* on the basis functions in *C* is made vectorizable along the *i* loop by “promoting” the scalar *f* to an array of size 6. All sub-expressions hoisted at the level of the *i* loop (which result from applying the techniques described in Chapter 4) can be treated similarly. The cost of this transformation obviously depends on the amount of computation within the *i* loop: the larger the number of scalars to be turned into arrays, the bigger the resulting working set, which may lead to the same memory issues explained in Section 4.5. Loop tiling may be used to counteract this effect, but the implementation complexity would be significantly higher.

Neither the GNU nor the Intel compiler seems capable of applying this transformations, probably because of the non-trivial impact on the working set. In fact, it is challenging to propose a cost model that works well even just for the class of assembly kernels considered in this chapter. Vector promotion is implemented in COFFEE, but unused by any of the de-

LISTING 9: The assembly kernel for the weighted Laplace operator in Listing 1 after application of vector promotion on top of generalized code motion.

```

1 void weighted_laplace(double A[3][3], double **coords, double w[3]) {
2     // Omitting redundant code
3     ...
4     // Application of vector promotion    double f0[6] = {0.0};
5     for (int i = 0; i<6; i++) {
6         for (int r = 0; r < 3; ++r) {
7             f0[i] += (w[r] * C[i][r]);
8         }
9     }
10    for (int i = 0; i<6; i++) {
11        double T0[3];
12        double T1[3];
13        for (int j = 0; j<3; j++) {
14            T0[j] = ((K[1]*B[i][j])+(K[3]*D[i][j]));
15            T1[j] = ((K[0]*B[i][j])+(K[2]*D[i][j]));
16        }
17        double T2[3];
18        double T3[3];
19        for (int k = 0; k<3; k++) {
20            T2[k] = ((K[1]*B[i][k])+(K[3]*D[i][k]));
21            T3[k] = ((K[0]*B[i][k])+(K[2]*D[i][k]));
22        }
23        for (int j = 0; j<3; j++) {
24            for (int k = 0; k<3; k++) {
25                A[j][k] += (T0[j]*T2[k] + T1[j]*T3[k])*det*W[i]*f0[i]);
26            }
27        }
28    }
29 }

```

fault optimization pipelines (see also Section 6.2).

5.4.4 Loop Fusion

In assembly kernels arising from bilinear forms, test and trial functions may belong to the same function space. Further, the same subset of operators is sometimes applied to both sets of functions. In such a case, not only do the j and k loops have same trip count, but also sub-expressions that differ in just the j and k array indices appear. We refer to these as “almost common sub-expressions”. The clone loops created by generalized loop-invariant code motion can easily be fused (they have the same size and no data dependencies are present) and the redundant computation induced by the almost common sub-expressions be avoided. The result of this transformation can be observed by comparing Listing 10 to some of the previous code snippets, for instance Listing 6.

Although loop fusion is applicable by most general-purpose compil-

LISTING 10: The assembly kernel for the weighted Laplace operator in Listing 1 after application of loop fusion on top of generalized code motion.

```

1 void weighted_laplace(double A[3][3], double **coords, double w[3]) {
2     // Omitting redundant code
3     ...
4     for (int i = 0; i < 6; i++) {
5         double f0 = 0.0;
6         for (int r = 0; r < 3; ++r) {
7             f0 += (w[r] * C[i][r]);
8         }
9         double T0[3];
10        double T1[3];
11        // Fused loop with almost common sub-expressions detected
12        for (int r = 0; r < 3; r++) {
13            T0[r] = ((K[1]*B[i][r])+(K[3]*D[i][r]));
14            T1[r] = ((K[0]*B[i][r])+(K[2]*D[i][r]));
15        }
16        for (int j = 0; j < 3; j++) {
17            for (int k = 0; k < 3; k++) {
18                A[j][k] += (T0[j]*T0[k] + T1[j]*T1[k])*det*W[i]*f0;
19            }
20        }
21    }
22 }

```

ers, the detection of almost common sub-expression is not. There are several possible explanations for this, including: the transformation is of domain-specific nature; common sub-expression elimination occurs at an earlier stage in the optimization pipeline; common sub-expression elimination cannot distinguish different loop indices (i.e., it cannot detect almost common sub-expressions). We have therefore implemented this special version of loop fusion in COFFEE, with satisfactory results. In our experiments, this transformation results in relatively small performance improvements, ranging between 2% and 7%. The speed-ups, however, are systematic across different forms, discretizations and general-purpose compilers, so loop fusion is performed automatically in the optimization process. This is elaborated in Chapter 6.

5.5 Related Work

The code transformations presented in Section 5.2 are inspired by standard compiler optimizations and by the structure of the assembly kernels. Expression splitting is an abstract variant of loop fission based on properties of arithmetic operators. The outer-product vectorization is an imple-

mentation of tiling at the level of vector registers; tiling, or “loop blocking”, is commonly used to improve data locality (especially for caches). Padding has been used to achieve data alignment and to improve the effectiveness of vectorization; the idea of changing the storage layout by adding “ghost regions” is however widespread. A standard reference for the compilation techniques re-adapted in this work is Aho et al. [2007].

Our compiler-based optimization approach is made possible by the top-level DSL, which enables automated code generation. DSLs have been proven successful in auto-generating optimized code for other domains: Spiral [Püschel et al., 2005] for linear transforms in digital signal processing, [Spampinato and Püschel, 2014] for dense linear algebra, or Pochoir [Tang et al., 2011] and SDSL [Henretty et al., 2013] for image processing and finite difference stencils. Similarly, PyOP2 is used by Firedrake to express iteration over unstructured meshes in scientific codes. COFFEE improves automated code generation in Firedrake.

In Markall et al. [2010], the optimization of global assembly, rather than local assembly, has been treated for both CPUs and GPUs. Knepley and Terrel [2013] focus on improving the performance of assembly kernels on GPUs through efficient parallelization. In Krueel and Bana [2013], variants of the standard numerical integration algorithm have been specialized and evaluated for the PowerXCell processor. A standard reference for the optimization of both local and global assembly on GPUs is [Cecka et al., 2011]. All these studies, despite tackling low level optimization, lack an exhaustive study from the compiler viewpoint; in addition, none of them relies on automated code generation. The optimizations presented in Section 5.2 are also never mentioned.

COFFEE would benefit from a cost model or an auto-tuning system to select, for a given problem, the best combination of low level optimizations. This would relieve users from the burden of performance tuning. A cost model was introduced in Luporini et al. [2015], but in light of the achievements in Chapter 4, it now requires refinements to be effective. Many code generators, like those based on the Polyhedral model [Bondhugula et al., 2008] and those driven by domain-knowledge [Stock et al., 2011], make use of cost models. The alternative of using auto-tuning has been adopted by nek5000 [Shin et al., 2010] for small matrix-matrix multiplies, the ATLAS library [Whaley and Dongarra, 1998], FFTW [Frigo and

Johnson, 2005] for fast fourier transforms, Spiral [Püschel et al., 2005], and LGen [Spampinato and Püschel, 2014].

5.6 Applicability to Other Domains

We have demonstrated that our cross-loop optimizations for arithmetic intensity are effective in the context of automated code generation for finite element integration. In this section, we discuss their applicability in other computational domains and, more in general, their integrability within a general-purpose compiler.

There are neither conceptual nor technical reasons which prevent our transformations from being used in other (general-purpose, research, ...) compilers. It is challenging, however, to assess their potential in other computational domains. We here provide insights into this matter. The starting point of our work was the mathematical formulation of a finite element operator, expressible as:

$$\forall_{i,j} \quad A_{ij}^K = \sum_{q=1}^{n_1} \sum_{k=1}^{n_2} \alpha_{k,q}(a', b', c', \dots) \beta_{q,i,j}(a, b, c, d, \dots) \gamma_q(w_K, z_K) \quad (5.4)$$

The expression represents the numerical evaluation of an integral at n_1 points in the mesh element K computing the local element tensor A . Functions α , β and γ are problem-specific and can be intricately complex, involving for example the evaluation of derivatives. We can however abstract from the structure of α , β and γ to highlight a number of aspects

Optimizing mathematical expressions Expression manipulation (e.g. simplification, decomposition into sub-expressions) opens multiple semantically equivalent code generation opportunities, characterized by different trade-offs in parallelism, redundant computation, and data locality. The basic idea is to exploit properties of arithmetic operators, such as associativity and commutativity, to re-schedule the computation suitably for the underlying architecture. Loop-invariant code motion and expression splitting follow this principle, so they can be re-adapted or extended to any domains involving numerical evaluation of complex mathematical expressions (e.g. electronic structure calculations in physics and quantum chemistry

relying on tensor contractions, which we reviewed in Section 2.4.1). In this context, we highlight three points.

1. In (5.4), the summations correspond to reduction loops, whereas loops over indices i and j are fully parallel. In our computational model, a kernel is executed by a single thread, which is likely to be the best strategy for standard multi-core CPUs. On the other hand, we note that for certain architectures (for example GPUs) this could be prohibitive due to memory requirements. Intra-kernel parallelization is one possible solution: a domain-specific compiler could map mathematical quantifiers and operators to different parallelization schemes and generate distinct variants of multi-threaded kernel code. Based on our experience, we believe this approach is necessary for achieving performance portability.
2. The various sub-expressions in β only depend on (i.e. iterate along) a subset of the enclosing loops. In addition, some of these sub-expressions might reduce to the same values as iterating along certain iteration spaces. This code structure motivated the generalized loop-invariant code motion technique. The intuition is that whenever sub-expressions invariant with respect to different sets of affine loops can be identified, the question of whether, where and how to hoist them, while minimizing redundant computation, arises. Vector promotion also increases memory requirements due to the need for temporary arrays, so it is possible that for certain architectures the transformation could actually cause slow-downs (e.g. whenever the available per-core memory is small).
3. Associative arithmetic operators are the prerequisite for expression splitting. In essence, this transformation concerns resource-aware execution. In our context, expression splitting has been applied to improve register pressure. However, the underlying idea of re-scheduling (re-associating) operations to optimize for some generic parameters is far more general. It could be used, for example, as a starting point to perform kernel fission; that is, splitting a kernel into multiple parts, each part character-

ized by less stringent memory requirements (a variant of this idea for non-affine loops in unstructured mesh applications has been adopted in Bertolli et al. [2013]). In (5.4), for instance, not only can any of the functions α , β and γ be split (assuming they include associative operators), but α could be completely extracted and evaluated in a separate kernel. This would reduce the working set size of each of the kernel functions, an option which is particularly attractive for many-core architectures in which the available per-core memory is much smaller than that in traditional CPUs.

Code generation and applicability of the transformations All array sizes and loop bounds, for example n_1 and n_2 in (5.4), are known at code generation time. This means that “good” code can be generated. For example, loop bounds can be made explicit, arrays can be statically initialized, and pointer aliasing is easily avoidable. Further, all of these factors contribute to the applicability and the effectiveness of some of our code transformations. For instance, knowing loop bounds allows both generation of correct code when applying vector-register tiling and discovery of redundant computation opportunities. Padding and data alignment are special cases, since they could be performed at run-time if some values were not known at code generation time. Theoretically, they could also be automated by a general-purpose compiler through profile-guided optimization, provided that some sort of data-flow analysis is performed to ensure that the extra loop iterations over the padded region do not affect the numerical results.

Multi-loop vectorization Compiler auto-vectorization has become increasingly effective in a variety of codes. However, multi-loop vectorization involving the loading and storing of data along a subset of the loops characterizing the iteration space (rather than just along the innermost loop), is not supported by available general-purpose compilers. The outer-product vectorization technique presented in this chapter shows that two-loop vectorization can outperform standard auto-vectorization. In addition, we expect the performance gain to scale with the number of vectorized loops and the vector length (as

demonstrated in the Xeon Phi experiments). Although the automation of multi-loop vectorization in a general-purpose compiler is far from straightforward, especially if stencils are present, we believe that this could more easily be achieved in specific domains. The intuition is to map the memory access pattern onto vector registers, and then to exploit in-register shuffling to minimize the traffic between memory and processor. By demonstrating the effectiveness of multi-loop vectorization in a real scenario, our research represents an incentive towards a systematic study of this technique.

5.7 Conclusions

In this chapter, we have presented the study and systematic performance evaluation of a class of composable cross-loop optimizations for improving arithmetic intensity in finite element local assembly kernels. In the context of automated code generation for finite element local assembly, COFFEE is the first compiler capable of introducing low-level optimizations to simultaneously maximize register locality and SIMD vectorization. Assembly kernels have particular computational characteristics. Their iteration space is usually very small, with the size depending on aspects like the degree of accuracy one wants to reach (polynomial order of the method) and the mesh discretization employed. The data space, in terms of number of arrays and scalars required to evaluate the element tensor, grows proportionally with the complexity of the finite element problem. The various optimizations overcome limitations of current vendor and research compilers. The exploitation of domain knowledge allows some of them to be particularly effective, as demonstrated by our experiments on a state-of-the-art Intel platform. The generality and the applicability of the proposed code transformations to other domains has also been discussed.

Chapter 6

COFFEE: a Compiler for Fast Expression Evaluation

Sharing elimination and pre-evaluation, presented in Chapter 4, as well as the low level optimizations in Chapter 5, have been implemented in COFFEE¹, a high-level compiler integrated with Firedrake. In this chapter, the conception, architecture and interface of COFFEE are described. The codebase, which comprises more than 4000 lines of Python, is available at [Luporini, 2014a].

6.1 Overview

We recall from Section 2.2.1 that Firedrake users employ the Unified Form Language to express problems in a mathematical syntax. At run-time, the high-level specification is translated by a form compiler, the Two-Stage Form Compiler (TSFC) [Homolya and Mitchell, 2016], into one or more abstract syntax trees (ASTs) representing assembly kernels². ASTs are then passed to COFFEE for optimization. The output of COFFEE, C code, is eventually provided to PyOP2 [Markall et al., 2013], where just-in-time compilation and execution over the computational mesh take place. This structure of this tool-chain is outlined in Figure 6.1, along with an overview of the compilation pipeline in COFFEE.

¹COFFEE is the acronym for COmpiler For Fast Expression Evaluation.

²TSFC has recently replaced FFC, the FEniCS Form Compiler, which has been used for performance evaluation in the previous chapters.

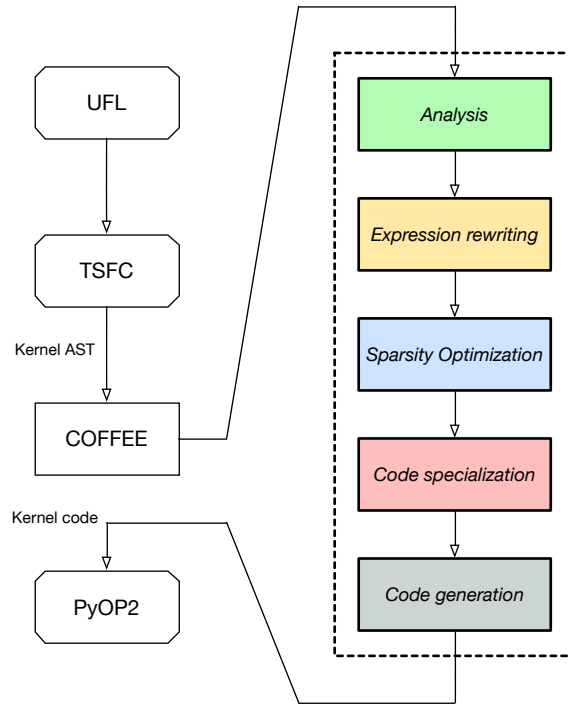


Figure 6.1: The COFFEE pipeline and its interaction with Firedrake.

6.2 The Compilation Pipeline

In common with general-purpose compilers, COFFEE provides multiple optimization levels: 00, 01, 02 and 03. Apart from 00, which essentially leaves the ASTs unchanged (useful for debugging), all optimization levels apply ordered sequences of transformations. In essence, the higher the optimization level, the more aggressive (and potentially slower) is the AST processing. In the following, when describing aspects of the optimization process common to 01, 02 and 03, we will use the generic notation 0x ($x \in \{1, 2, 3\}$).

The optimization level 0x can logically be split into three stages:

Expression rewriting Any transformations changing the structure of an expression. These are sharing elimination and pre-evaluation; or, more in general, any rewrite operators on top of which such higher level transformations are expressed (e.g., generalized code motion, factorization; full list provided in Section 6.4).

Sparsity Optimization The iteration spaces are restructured to skip useless

operations, such as those involving blocks of zeros in basis function tables. In particular, loops may be fissioned, their bounds changed, and offsets introduced for accessing non-zero array values. More details are presented in Section 4.8.3.

Code Specialization A combination of the low level transformations presented in Chapter 6 is applied.

These three stages are totally ordered. Indeed, it would be useless to apply any of the low level transformations until all loops and temporaries have been created.

The optimization process `0x` represents the core phase in COFFEE. Overall, the compilation pipeline consists of three phases:

Analysis During the analysis phase, an AST is visited and information are collected. In particular, candidates for expression rewriting are searched for. These are represented as special nodes in the AST, which we refer to as “expression nodes”. In plain C, we could think of an expression node as a statement preceded by a directive such as `#pragma coffee`. The purpose of the directive would be to trigger COFFEE’s `0x`, similarly to the way loops are parallelized through OpenMP. If no expression nodes are found, we jump directly to the last phase (i.e., code generation).

Optimization (0x or user-provided) In addition to `0x`, users can craft their own optimization pipelines by composing the individual transformations available in COFFEE. The compiler checks that the provided transformation sequence is legal. If the specified sequence of transformations is legal, the AST is processed. Specifically, for `0x`:

- 01** Expression rewriting reduces to generalized code motion, while only padding and data alignment as well as loop fusion are applied amongst the low level optimizations.
- 02** With respect to 01, there is only one, yet fundamental, change: expression rewriting now performs the whole sharing elimination procedure (i.e., Algorithm 5).
- 03** Algorithm 7, which coordinates sharing elimination and pre-evaluation, is executed. This is followed by sparsity optimization, loop fusion and padding and data alignment.

Code generation All optimizations have been applied, so a string representation of the transformed AST is produced and returned.

6.3 Plugging COFFEE into Firedrake

In this section, we explain how COFFEE interacts with the Firedrake ecosystem.

6.3.1 Abstract Syntax Trees

We start with highlighting peculiarities of the hierarchy of AST nodes.

Special nodes Some nodes have special semantics. A first example is the *expression node* described in the previous section. Furthermore, a whole sub-hierarchy of `LinAlg` nodes is available, with objects such as `Invert` and `Determinant` representing basic linear algebra operation. Code generation for these objects can be specialized based upon the underlying architecture and the size of the involved tensors. For instance, a manually-optimized loop nest may be preferred to a BLAS function when the tensors are small³. Yet another special type of node is `ArrayInit`, used for static initialization of arrays. An `ArrayInit` wraps an N -dimensional Numpy array [van der Walt et al., 2011] and provides a simple interface to obtain information useful for sparsity optimization, like the sparsity pattern of the array.

Symbols A `Symbol` represents a variable in the code. The *rank* of a `Symbol` captures the dimensionality of a variable, with a rank equal to N indicating that the variable is an N -dimensional array ($N = 0$ implies that the variable is a scalar). The rank is implemented as an N -tuple, each entry being either an integer or a string representing a loop dimension. The *offset* of a `Symbol` is again an N -tuple where each element is a 2-tuple. For each entry r in the rank, there is a corresponding entry $\langle scale, stride \rangle$ in the offset. Rank and offset are used as in Figure 6.2 to access specific memory locations. By clearly separating the rank and the offset of a `Symbol` –

³It is well-known that BLAS libraries are highly optimized for big tensors, while their performance tends to be sub-optimal with small tensors, which are very common in assembly kernels.

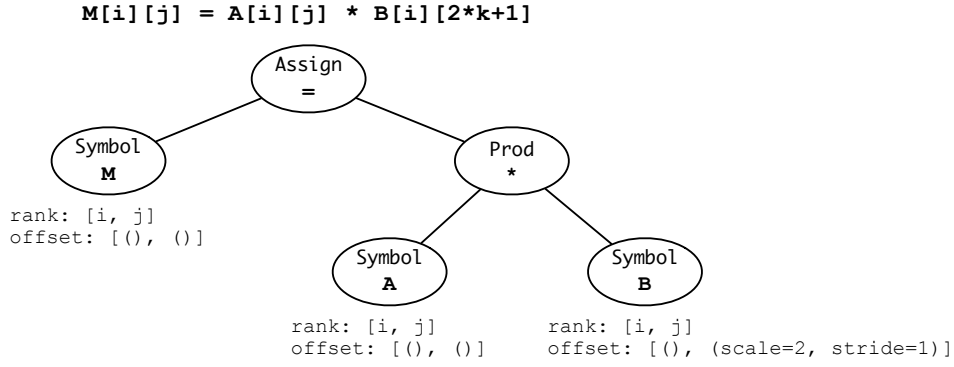


Figure 6.2: AST representation of a C assignment in COFFEE.

rather than storing a generic expression – the data dependency analysis required by the rewrite operators is greatly simplified. The underlying assumption is that all symbols’ access functions (Section 2.5) are affine in the loop indices. This is definitely the case for the class of kernels in which we are interested.

Building an AST Rather than using a parser, COFFEE exposes the whole hierarchy of nodes for explicitly building ASTs. This is because the compiler is meant to be used as an intermediate representation in a multilayer framework based on DSLs. To ease the construction of ASTs (especially nested loops), a set of utility functions is provided.

6.3.2 Integration with Form Compilers

COFFEE has been integrated with two form compilers: the FEniCS Form Compiler (FFC) and the Two-Stage Form Compiler (TSFC). These form compilers represent assembly kernels using their own internal language. The objective is to turn such a representation into an AST suitable for COFFEE.

FFC and COFFEE FFC was developed in the context of the FEniCS framework. In the early stages of this thesis, the FFC’s intermediate representation was modified to construct COFFEE ASTs, rather than C code. The following contributions were made:

- The mathematical expression evaluating the element tensor is represented in FFC as a tree data structure, or FFC AST. A limitation of an FFC AST was that its nodes – symbols or arithmetic operations – were not bound to loops. For instance, the FFC AST node corresponding to the symbol $A[i][j]$ could not separate the variable name A from the loop indices i and j . We have enriched FFC AST symbols with additional fields to capture this kind of information.
- Basis functions in an FFC AST are added a new field storing the dimensionality of the function space. This information is later used to enrich `ArrayInit` objects with a sparsity pattern. This enables sparsity optimization without requiring COFFEE to “sniff” array values.

The enriched FFC AST is intercepted prior to code generation and forwarded to a new module, where a COFFEE AST is constructed. In this module:

- the strings in the template originally used by FFC for code generation are now COFFEE AST objects.
- the FFC AST is visited and translated into a COFFEE AST by a suitable AST-to-AST converter routine.

TSFC and COFFEE TSFC was conceived to produce an input suitable for COFFEE. This is accomplished through an AST-to-AST converter, which translates the GEM representation (the internal language used by TSFC) of an assembly kernel into a COFFEE AST. The implementation was carried out by Myklós Homolya, the lead designer of TSFC.

6.4 Rewrite Operators

COFFEE implements sharing elimination and pre-evaluation by composing “building-block” operators, or “rewrite operators”. This has several advantages. Firstly, extensibility: novel transformations – for instance, sum-factorization in spectral methods – could be expressed using the existing operators, or with small effort building on what is already available. Secondly, generality: COFFEE can be seen as a lightweight, low

level computer algebra system, not necessarily tied to finite element integration. Thirdly, robustness: the same operators are exploited, and therefore stressed, by different optimization pipelines. The rewrite operators, whose implementation is based on manipulation of the kernel's AST, essentially compose the COFFEE language.

The most important rewrite operators in COFFEE are:

Generalized code motion A sub-expression that is invariant with respect to one or more loops can be hoisted at the level of an outer loop, thus reducing the operation count. This requires introducing a temporary (scalar, array) for each invariant sub-expression and, possibly, adding a “clone” loop to the nest (Several examples, e.g. Figure 4.1, have been provided throughout the thesis).

Expansion Exploiting distributivity, this transformation expands a product between two sub-expressions. Expansion has several effects: (i) exposing factorization opportunities (see Chapter 4); (ii) increasing the operation count; (iii) in some circumstances, relieving the register pressure by creating code motion opportunities.

Factorization The impact of factorizing, or collecting, identical symbols is twofold: (i) reducing the number of multiplications to be performed; (ii) more importantly, exposing code motion opportunities, as illustrated through sharing elimination and pre-evaluation.

Symbolic evaluation This operator evaluates sub-expressions that only involve statically initialized, read-only arrays (e.g., basis function tables). The result is stored into a new array, and the AST modified accordingly

All these operators are used by both sharing elimination and pre-evaluation (apart from symbolic evaluation, only employed by pre-evaluation).

The rewrite operators accept a number of options to enable users to steer the transformation process. With code motion, for example, one can specify what kind of sub-expressions should be hoisted (by indicating the invariant loops) or the maximum amount of memory that is spendable in temporaries. Factorization can be either “explicit” – in which case, a list of symbols to be collected or a loop dimension along which searching

for factorizable symbols are provided – or “heuristic” – with groups of recurring identical symbols being collected.

6.5 Features of the Implementation

This section focuses on the toolkit available in COFFEE for implementing and extending rewrite operators.

6.5.1 Tree Visitor Pattern

The need for a generic infrastructure for traversing ASTs has grown rapidly, together with the complexity of the compiler. In the early stages of COFFEE, any time a new transformation (e.g., a rewrite operator) or inspector (e.g., for dependence analysis) was required, one or more full AST traversals had to be implemented. The lack of a common interface for tree traversals also made the code less homogeneous and, as such, more difficult to understand. This led to the introduction of a tree visitor design pattern⁴, whose aim is to decouple the algorithms from the data structure on which they are applied.

As an example, consider an algorithm that needs to perform special actions when a `Symbol` or a `ForLoop` nodes are encountered (e.g., to collect loop dependence information). Then, a tree visitor will only need to implement three methods, namely `visit_Symbol` and `visit_ForLoop` – the actual handlers – as well as `visit_Node`, which will implement the “fallback” action for all other node types (e.g., a propagation of the visit).

Tree visitors exploit the hierarchy of AST nodes by always dispatching to the most specialized handler. For example, symbols are simultaneously of type `Symbol` and `Expression`, but if a `Symbol` is encountered and `visit_Symbol` is implemented, then `visit_Symbol` is executed, whereas `visit_Expression` (if any) is ignored.

Most of the algorithms in COFFEE exploit the tree visitor pattern.

⁴The tree visitor infrastructure was mainly developed by Lawrence Mitchell, and was inspired by that adopted in UFL, the language used to specify forms in Firedrake.

6.5.2 Flexible Code Motion

Code motion consists of hoisting a sub-expression out of one or more loops. We already know that this operator is used in different contexts: as a stand-alone transformation (optimization level 01), to implement sharing elimination, and to implement pre-evaluation.

When applying the operator, several pieces of information must be known:

- Which sub-expressions should be hoisted; for instance, should they be constant or invariant in at most one of the linear loops.
- Where sub-expressions should be hoisted; that is, how far in the loop nest (which affects the size of the temporaries).
- How much memory are we allowed to use in total for the temporaries.
- A list of previously hoisted sub-expressions, for applying common sub-expressions elimination.

COFFEE tracks all of the hoisted sub-expressions for quick retrieval. A dictionary mapping temporaries to metadata is employed. For a temporary t , the dictionary records:

- A reference to the hoisted expression e assigned to t .
- A reference to the loop in which e is lifted (if any).
- A reference to the declaration of t .
- Some extra fields.

This dictionary is updated after each invocation to the code motion operator and forms part of the “global state” that COFFEE maintains for each assembly kernel. Not only is the dictionary accessed by later calls to the code motion operator, but also by other operators, thus speeding-up the AST transformation process.

The code motion operator “silently” applies common sub-expressions elimination. A look-up to the dictionary tells whether a hoistable sub-expression e has already been assigned to a temporary t by a prior call to the operator; in such a case, e is replaced with t and no useless temporaries are introduced.

6.5.3 Tracking Data Dependency

Data dependency analysis is necessary to ensure the legality of transformations. For example:

- We may want to hoist a sub-expression e “as far as possible” in the loop nest, but after the last write to a variable read in e .
- When expanding a product, some terms may be aggregated with previously hoisted sub-expressions. This would avoid introducing extra temporaries and increasing the register pressure. For example, if we have $(a + b) * c$ and both a and b are temporaries created by code motion, we could expand the product and aggregate c with the sub-expressions stored by a and b . Obviously, this is legal as long as neither a nor b are accessed in other sub-expressions.
- To check whether fusing a sequence of loops is legal (see Section 5.4.4).
- To implement the *strategy selection analysis* in Section 4.3.2.

COFFEE uses a dependency graph to track data dependencies. The dependency graph has as many vertices as symbols in the code; a direct edge from A to B indicates that symbol B depends on (i.e., is going to read) symbol A . Since COFFEE relies on *static single assignment* – a property that ensures that variables are assigned exactly once – such a minimalistic data structure suffices for data dependence analysis.

6.5.4 Minimizing Temporaries

Both the code motion operator and loop fusion (Section 5.4.4) impact the number of temporaries in an assembly kernel. Once the AST has been transformed, a special routine attempts to remove the unnecessary temporaries. In addition to relieving the register pressure (this actually depends on how smart the underlying general-purpose compiler is), this has the effect of making the code more readable.

The main rule for removing a temporary t storing an expression e is that if t is accessed only in a single statement s , then e is inlined into s and t is removed. Secondly, if some of the transformations in the optimization pipeline reduced e to a symbol, then any appearance of t is also replaced by e .

6.6 On the Compilation Time

Firedrake and its various software components are implemented in Python, whereas the generated code is pure C. COFFEE has been written in Python for a natural integration with Firedrake. The process of transforming an AST usually takes fractions of seconds. For more complex forms, on a Sandy Bridge architecture, the AST processing takes not more than approximately 2 seconds. For extremely challenging forms, like those arising in the Holzapfel-Ogden hyperelasticity model, the code generation is carried out in 16 seconds; this is the only case, out of dozens, in which the processing time was higher than 3 seconds. We believe, however, that there is still ample space for optimizing the AST processing in COFFEE.

6.7 Overview of Applications Exploiting COFFEE

By default, Firedrake optimizes all local assembly kernels by using COFFEE at optimization level 02. This means that all applications written on top of Firedrake seamlessly exploit the technology described in this thesis. A non-comprehensive list of such applications is given below.

Thetis A framework for coastal and estuarine modelling [Thetis contributors, 2016]. Thetis has applications in the simulation of 3D baroclinic river dynamics. It exploits 3D layered meshes (so-called “extruded meshes”) and a large variety of finite element schemes. The lead developer, Tuomas Kärnä (Oregon Health and Science University) has observed that several simulations execute up to 30% faster when COFFEE is enabled (as by default).

Gusto A dynamical core package based upon compatible finite element methods [Gusto contributors, 2016], developed at Imperial College London by Coling Cotter, Jemma Shimplon, Hiroe Yamazaki, Andrew McRae and David Ham. The dynamical core is the part of an atmosphere model that actually solves the flow equations. Gusto is one of the key applications built on top of Firedrake.

Stability of jets and vortices Francis Poulin (University of Waterloo) is using Firedrake to study the stability characteristics of oceanic jets and

vortices (e.g., the Gulf Stream and Meddies). The focus is on understanding the structures produced and how the energy cascades across the different length scales.

Water waves and structures At University of Leeds, Firedrake is employed in a number of projects. Anna Kalogirou and Onno Bokhove are studying the generation of nonlinear rogue water waves and how these affect ships. Floriane Gidel and Onno Bokhove use Firedrake to solve the Benney-Luke equations to simulate freak waves (created, for example, when solitary waves encounter oblique walls). Tomasz Salwa, Onno Bokhove, Mark Kelmanson have developed a fluid-structure interaction model centered on water waves interacting with offshore wind turbines.

r-adaptivity on the sphere Andrew McRae, Chris Budd (University of Bath), Colin Cotter, Jemma Shimplon (Imperial College London) are working with Firedrake on moving-mesh methods for atmospheric problems on the Earth. By solving a Monge-Ampère-type equation on the sphere, the fundamental operation of adapting a mesh to a scalar monitor-function is carried out without impacting the mesh connectivity.

Most of these applications have played a key role in the development of COFFEE, either by providing interesting test cases or by simply exposing flaws in the transformation algorithms.

Chapter 7

Conclusions

In this final chapter, the achievements and the shortcomings of this thesis are reviewed. Future research directions, including an estimate of their potential scientific impact, are also discussed.

7.1 Summary

Novel techniques that improve the performance of numerical methods for solving partial differential equations have been introduced. Our work builds upon three cornerstones:

Solid motivations The performance optimization of a code must always start with an analysis of its bottlenecks and an assessment of its potentials. Furthermore, to avoid solving fictitious problems, real-world applications, kernels, and datasets must be used. This approach has systematically been adopted in this thesis.

Automation through high-level compilers Implementing and evaluating optimizations is challenging. Simplistic codes and benchmarks should be avoided for experimentation, since they often provide an incomplete picture of the computational domain. On the other hand, integrating optimizations with real codes is a long, tedious, error-prone task – notably, a task that users should not be expected to carry out on their own. Our solution to this issue is to insert compilers and libraries into frameworks based upon domain-specific languages. In

such environments, (i) domain specialists provide the real applications and (ii) performance optimization is automated “behind the scenes” – that is, without the need for user intervention.

Validation of the hypotheses The hypotheses behind any run-time improvements must always be validated. Optimizations, especially radical changes at the algorithmic level, may have unpredictable implications on the low-level performance. For instance, a transformation that reduces the operation count may impair the vectorizability of loops. All performance numbers reported in this thesis have been extensively analyzed through a variety of tools, including compiler reports and profilers.

In this thesis, we have investigated three main problems in the field of numerical methods on unstructured meshes.

Sparse tiling of irregular loops (Chapter 3) The biggest achievement of this chapter is an inspector/executor scheme for fusing arbitrary sequences of loops expressible by means of the loop chain abstraction. In fact, this technique is so general that any graph-based computation that adheres to the program model of the loop chain abstraction (or equivalent) is a potential optimization candidate. The first version of the generalized inspector/executor sparse tiling scheme was jointly devised with Strout et al. [2014]. The performance limitations of this inspector and an in-depth study of the typical requirements of real-world applications (e.g., execution on distributed-memory architectures) motivated the design and the implementation of a second generalized inspector/executor scheme, presented in Section 3.8.1. Automation was achieved through integration of SLOPE with the Firedrake/PyOP2 tool-chain. The extensive performance investigation of the seismological code in Section 3.11 clarifies the limitations and the potentials of sparse tiling. To the best of our knowledge, this is, to date, the first study that *simultaneously* attack (i) fusion/tiling of irregular loops, (ii) the optimization of real-world applications, (iii) automation.

Minimizing flops in finite element kernels (Chapter 4) Automated code generation for finite element assembly is especially interesting when the

kernels, as a consequence of the operators used in the problem specification, are characterized by the presence of complex mathematical expressions. Hand-writing these kernels requires a great deal of effort; even more complex is optimizing for the operation count. This thesis demonstrates that automated code generation and mathematical properties can be leveraged for reducing the operation count (in particular, for reaching a local optimum) in finite element assembly kernels. One of the main challenges tackled in this chapter is the coordination of different rewrite operators (e.g., common sub-expressions elimination, factorization, expansion), as subjected to a non-trivial interplay. Our algorithm shows significant performance improvements over state-of-the-art code generation systems for finite element assembly.

Low-level optimization of finite element kernels (Chapter 5) A second question arising when studying finite element kernels concerns the efficiency of the generated code. We have addressed this problem for conventional multi-core architectures. The peculiar structure of the assembly kernels (e.g., small loops, small working set distributed over a large number of variables/arrays) makes it difficult to find a specific sequence of transformations that maximizes the performance of all problems, on all architectures. We have investigated a number of novel and traditional compiler transformations, aimed at creating or improving SIMD vectorization and data locality. Amongst these, the most powerful is padding and data alignment, which exploits the memory access pattern of assembly kernels to increase the effectiveness of SIMD vectorization, at the price of a few additional scalar operations. This transformation has been demonstrated to provide systematic improvements in execution time across a range of problems. Although the idea behind the optimization is simple, the implementation conceals several challenges, including the handling of non unit-stride memory accesses.

The techniques produced in this thesis have been implemented in publicly available software. SLOPE is a C library to express inspector/executor schemes for sparse tiling. The work on finite element kernels is implemented in COFFEE. Both COFFEE and SLOPE are integrated with Firedrake.

7.2 Limitations

The limitations of this research have already been discussed in the previous chapters; here, we emphasize the most relevant.

Performance analysis and tuning of sparse tiling The system described in Chapter 3 automates sparse tiling in Firedrake programs through the *loop_chain* interface. This was a major step, as it made a very complex optimization easily accessible. What is still missing is a cost model, or a system, that facilitates or even automates the performance tuning. Most applications, such as Seigen (Section 3.11), are characterized by long sequences of heterogeneous loops. Multiple computational aspects need be considered: some loops may be memory-bound, while others compute-bound; the working set size may vary significantly amongst different subsets of loops; a loop may take much longer to execute than others; and so on. Altogether, these issues make it difficult to think of a system capable of autonomously identifying which particular loops in a loop chain should be fused. Auto-tuning could help, but the implementation would be non-trivial. Moreover, an auto-tuning system could require (i) a significant amount of time to retrieve a configuration and (ii) re-execution as some problem parameters change (e.g., the domain discretization). Experimenting with other programs and loops is however fundamental before addressing this problem.

Combination of low-level transformations in finite element kernels All optimizations presented in Chapter 5 can improve the performance of finite element kernels, but it is difficult to determine the optimal sequence of transformations for a given problem. While, on one hand, padding and data alignment shows consistent speed-ups across a variety of problems, it is much more challenging to understand how to compose the other transformations. The cost model suggested in Luporini et al. [2015] works well if the expression rewriting stage (Section 6.2) is limited to the sole generalized loop-invariant code motion. However, coordinating vector-register tiling and expression splitting, as well as the general-purpose transformations (especially vector-promotion; see Section 5.4 for the full list), becomes difficult if the potential of the whole expression rewriting engine is

exploited. This is a result of introducing more temporaries and complex sub-expressions in the outer loops, as well as creating more loops. Many low-level transformations are available in COFFEE, but none of them is automatically applied apart from padding/data-alignment and loop fusion. Users, therefore, have some responsibility for low-level performance tuning. Preliminary work on compiler auto-tuning is available at [Luporini, 2014a].

7.3 Future Research Directions

We recapitulate the open questions that arose from the three main chapters of the thesis and provide insights into possible research directions.

Extensive performance evaluation of sparse tiling The theory and the tools behind generalized sparse tiling are now mature. The next big step is extensive experimentation with computations arising in multiple domains; for instance, in addition to numerical methods on unstructured meshes (not necessarily finite element), molecular dynamics and graph processing. The potential of sparse tiling has not been fully discovered yet.

Sparse tiling in general-purpose or research compilers It is unclear whether sparse tiling could be automated in general-purpose or research (polyhedral-based) compilers. Although simple inspector/executor schemes are widespread (e.g., many compilers introduce alternative code paths for handling statically unknown loop bounds), the path towards supporting more advanced transformations is long and intricate. In fact, it is also unclear whether sparse tiling should be even considered a general-purpose transformation.

Sparse tiling and space-filling curves In Section 3.3, we have discussed the dichotomy between space-filling curves and loop tiling. Later, in Section 3.11, we have hypothesized that applying sparse tiling on top of a space-filling curve may significantly reduce the performance penalties that we are subjected to at the moment (e.g., load balancing, TLB misses). There is an on-going effort in the DMPlex community that will make space-filling curves available in Firedrake, so our hypotheses could be

verifiable relatively soon. We speculate that space-filling curves can have a great impact on the performance of sparse tiling.

Minimizing operations and sum-factorization in assembly kernels The strategy for minimizing the operation count developed in Chapter 4 targets a specific class of finite element integration loop nests. If the loop nest changes dramatically, a generalization of the strategy will be necessary. This may happen if the chosen function spaces have certain properties. For instance, in spectral element methods basis functions may be constructed from the tensor product of 1D basis functions. This enables the application of sum-factorization, a well-known technique for reducing the operation count (see for example Vos et al. [2010]). In essence, sum-factorization is the mathematical name for what we call generalized code motion in Chapter 4. The relationship between this optimization and our transformation model is yet to be investigated.

Minimizing operations and memory constraints in assembly kernels Two memory constraints have been introduced in Chapter 4. While Constraint 1 has been imposed to limit the transformation space, Constraint 2 has a direct impact on the main optimization algorithm. Both constraints leave some interesting questions unanswered. First, the heuristic for choosing the memory threshold is partly flawed: we have proved (Section 4.9) that a drastic reduction in operation count should overrule any constraints on the working set size. It is unclear how to effectively approximate the “cut-off” point, which is architecture- and problem-dependent. Second, Constraint 1 would be overly restrictive if the time dimension were included in the model of a finite element integration loop nest. Geometry-dependent sub-expressions would become generalized code motion candidates; this would make the transformation space even bigger. Supporting this kind of hoisting could dramatically improve the execution time of an application; for example, as explained in Section 3.11, Seigen would benefit from it. Further investigation in this direction is likely to be very rewarding.

Extensions to many-core architectures In this thesis, we have focused on the platforms that are typically used for unstructured mesh compu-

tations, that is, conventional CPU architectures. Two of the key limiting factors to the execution on many-core platforms (e.g., GPUs) are the stringent memory requirements of these computations and the lack of support from third-party libraries (e.g., PETSc). It would not be surprising if this scenario evolved over the next years. The upcoming generation of many-core architectures is in this sense promising, with traditional “accelerators” slowly becoming first-class platforms (e.g., nodes that can run a full-fledged operating system, larger memory systems, tighter coupling with the CPU through a shared address space), like the Intel’s Knights Landing. The COFFEE-related work is sufficiently mature for a generalization to non-standard platforms. Automated generation of efficient code for finite element kernels on GPUs has not been addressed.

Compiler auto-tuning for assembly kernels As explained in the previous section, low-level optimization of assembly kernels could greatly benefit from compiler auto-tuning. Auto-tuning techniques have been proven successful in a variety of frameworks based upon domain-specific languages, such as Spiral and Halide. This would require some new technology in COFFEE. Our hypothesis is that a minimalistic auto-tuning system, performing a brute-force search out of a few tens of promising code syntheses, could result in significant speed-ups. This consideration is the fruit of preliminary work on the subject, with experimentation limited to relatively simple problems.

Bibliography

- A. Acharya and U. Bondhugula. Pluto+: Near-complete modeling of affine transformations for parallelism and locality. In *ACM SIGPLAN Notices*, volume 50, pages 54–64. ACM, 2015.
- M. F. Adams and J. Demmel. Parallel multigrid solver algorithms and implementations for 3D unstructured finite element problem. In *Proceedings of SC99*, Portland, Oregon, November 1999.
- A. V. Aho, M. S. Lam, R. Sethi, and J. D. Ullman, editors. *Compilers: principles, techniques, and tools*. Pearson/Addison Wesley, Boston, MA, USA, second edition, 2007. ISBN 0-321-48681-1. URL <http://www.loc.gov/catdir/toc/ecip0618/2006024333.html>.
- M. S. Alnæs. Uflacs - ufl analyser and compiler system. <https://bitbucket.org/fenics-project/uflacs>, 2016.
- M. S. Alnæs, A. Logg, K. B. Ølgaard, M. E. Rognes, and G. N. Wells. Unified Form Language: a domain-specific language for weak formulations of partial differential equations. *ACM Trans Math Software*, 40(2):9:1–9:37, 2014. doi: 10.1145/2566630. URL <http://dx.doi.org/10.1145/2566630>.
- M. S. Alnæs, A. Logg, G. Wells, L. Mitchell, M. E. Rognes, M. Homolya, A. Bergersen, D. A. Ham, J. Ring, chrisrichardson, and K.-A. Mardal. ufl: The unified form language, Apr. 2016. URL <http://dx.doi.org/10.5281/zenodo.49282>.

- U. Ayachit. *The ParaView Guide (Full Color Version): A Parallel Visualization Application*. Kitware, Incorporated, paraview 4.3 edition, Jan. 2015. ISBN 1930934300. URL <http://www.amazon.com/exec/obidos/redirect?tag=citeulike07-20&path=ASIN/1930934300>.
- D. F. Bacon, S. L. Graham, and O. J. Sharp. Compiler transformations for high-performance computing. *ACM Comput. Surv.*, 26(4):345–420, Dec. 1994. ISSN 0360-0300. doi: 10.1145/197405.197406. URL <http://doi.acm.org/10.1145/197405.197406>.
- S. Balay, S. Abhyankar, M. F. Adams, J. Brown, P. Brune, K. Buschelman, L. Dalcin, V. Eijkhout, W. D. Gropp, D. Kaushik, M. G. Knepley, L. C. McInnes, K. Rupp, B. F. Smith, S. Zampini, and H. Zhang. PETSc Web page. <http://www.mcs.anl.gov/petsc>, 2015. URL <http://www.mcs.anl.gov/petsc>.
- F. Bassetti, K. Davis, and D. J. Quinlan. Optimizing transformations of stencil operations for parallel object-oriented scientific frameworks on cache-based architectures. In *Proceedings of the Second International Symposium on Computing in Object-Oriented Parallel Environments*, ISCOPE '98, pages 107–118, London, UK, UK, 1998. Springer-Verlag. ISBN 3-540-65387-2. URL <http://dl.acm.org/citation.cfm?id=646894.709707>.
- C. Bertolli, A. Betts, N. Lorient, G. Mudalige, D. Radford, D. Ham, M. Giles, and P. Kelly. Compiler optimizations for industrial unstructured mesh cfd applications on gpus. In H. Kasahara and K. Kimura, editors, *Languages and Compilers for Parallel Computing*, volume 7760 of *Lecture Notes in Computer Science*, pages 112–126. Springer Berlin Heidelberg, 2013. ISBN 978-3-642-37657-3. doi: 10.1007/978-3-642-37658-0_8.
- U. Bondhugula, A. Hartono, J. Ramanujam, and P. Sadayappan. A practical automatic polyhedral parallelizer and locality optimizer. In *Proceedings of the 2008 ACM SIGPLAN Conference on Programming Language Design and Implementation*, PLDI '08, pages 101–113, New York, NY, USA, 2008. ACM. ISBN 978-1-59593-860-2. doi: 10.1145/1375581.1375595. URL <http://doi.acm.org/10.1145/1375581.1375595>.
- U. Bondhugula, V. Bandishti, A. Cohen, G. Potron, and N. Vasilache. Tiling and optimizing time-iterated computations on periodic domains.

- In *Proceedings of the 23rd International Conference on Parallel Architectures and Compilation*, PACT '14, pages 39–50, New York, NY, USA, 2014. ACM. ISBN 978-1-4503-2809-8. doi: 10.1145/2628071.2628106. URL <http://doi.acm.org/10.1145/2628071.2628106>.
- T. Brandvik and G. Pullan. Sblock: A framework for efficient stencil-based pde solvers on multi-core platforms. In *Proceedings of the 2010 10th IEEE International Conference on Computer and Information Technology*, CIT '10, pages 1181–1188, Washington, DC, USA, 2010. IEEE Computer Society. ISBN 978-0-7695-4108-2. doi: 10.1109/CIT.2010.214. URL <http://dx.doi.org/10.1109/CIT.2010.214>.
- S. Brenner and R. Scott. *The Mathematical Theory of Finite Element Methods*. Texts in Applied Mathematics. Springer New York, 2007. ISBN 9780387759333. URL https://books.google.co.uk/books?id=ci4c_R0WKYYC.
- A. Buttari, J. Langou, J. Kurzak, and J. Dongarra. Parallel tiled qr factorization for multicore architectures. In *Proceedings of the 7th International Conference on Parallel Processing and Applied Mathematics*, PPAM'07, pages 639–648, Berlin, Heidelberg, 2008. Springer-Verlag. ISBN 3-540-68105-1, 978-3-540-68105-2. URL <http://dl.acm.org/citation.cfm?id=1786194.1786268>.
- A. Buttari, J. Langou, J. Kurzak, and J. Dongarra. A class of parallel tiled linear algebra algorithms for multicore architectures. *Parallel Comput.*, 35(1):38–53, Jan. 2009. ISSN 0167-8191. doi: 10.1016/j.parco.2008.10.002. URL <http://dx.doi.org/10.1016/j.parco.2008.10.002>.
- C. Cecka, A. J. Lew, and E. Darve. Assembly of finite element methods on graphics processors. *International Journal for Numerical Methods in Engineering*, 85(5):640–669, 2011. ISSN 1097-0207. doi: 10.1002/nme.2989. URL <http://dx.doi.org/10.1002/nme.2989>.
- L. Chen, Z.-Q. Zhang, and X.-B. Feng. Redundant computation partition on distributed-memory systems. In *Algorithms and Architectures for Parallel Processing, 2002. Proceedings. Fifth International Conference on*, pages 252–260, Oct 2002. doi: 10.1109/ICAPP.2002.1173583.

- M. Christen, O. Schenk, and H. Burkhart. PATUS: a code generation and autotuning framework for parallel iterative stencil computations on modern microarchitectures. In *Proceedings of the 2011 IEEE International Parallel & Distributed Processing Symposium*, IPDPS '11, pages 676–687, Washington, DC, USA, 2011. IEEE Computer Society. ISBN 978-0-7695-4385-7. doi: 10.1109/IPDPS.2011.70. URL <http://dx.doi.org/10.1109/IPDPS.2011.70>.
- A. T. Chronopoulos. s-step iterative methods for (non)symmetric (in)definite linear systems. *SIAM Journal on Numerical Analysis*, 28(6): 1776–1789, 1991. doi: 10.1137/0728088. URL <http://dx.doi.org/10.1137/0728088>.
- P. G. Ciarlet. Numerical analysis of the finite element method. Les Presses de l'Universite de Montreal, 1976.
- A. Darte. On the complexity of loop fusion. *Parallel Comput.*, 26(9):1175–1193, Aug. 2000. ISSN 0167-8191. doi: 10.1016/S0167-8191(00)00034-X. URL [http://dx.doi.org/10.1016/S0167-8191\(00\)00034-X](http://dx.doi.org/10.1016/S0167-8191(00)00034-X).
- K. Datta, M. Murphy, V. Volkov, S. Williams, J. Carter, L. Oliker, D. Patterson, J. Shalf, and K. Yelick. Stencil computation optimization and auto-tuning on state-of-the-art multicore architectures. In *Proceedings of the 2008 ACM/IEEE Conference on Supercomputing*, SC '08, pages 4:1–4:12, Piscataway, NJ, USA, 2008. IEEE Press. ISBN 978-1-4244-2835-9. URL <http://dl.acm.org/citation.cfm?id=1413370.1413375>.
- T. A. Davis and Y. Hu. The University of Florida sparse matrix collection. *ACM Transactions on Mathematical Software*, 38(1):1:1 – 1:25, 2011.
- S. Delcourte, L. Fezoui, and N. Glinsky-Olivier. A high-order Discontinuous Galerkin method for the seismic wave propagation. *ESAIM: Proceedings*, 27:70–89, 2009. doi: 10.1051/proc/2009020. URL <https://hal.archives-ouvertes.fr/hal-00868418>.
- J. Demmel, M. Hoemmen, M. Mohiyuddin, and K. Yelick. Avoiding communication in sparse matrix computations. In *Proceedings of International Parallel and Distributed Processing Symposium (IPDPS)*. IEEE Computer Society, 2008.

- Z. DeVito, N. Joubert, F. Palacios, S. Oakley, M. Medina, M. Barrientos, E. Elsen, F. Ham, A. Aiken, K. Duraisamy, E. Darve, J. Alonso, and P. Hanrahan. Liszt: a domain specific language for building portable mesh-based pde solvers. In *Proceedings of 2011 International Conference for High Performance Computing, Networking, Storage and Analysis, SC '11*, pages 9:1–9:12, New York, NY, USA, 2011. ACM. ISBN 978-1-4503-0771-0. doi: 10.1145/2063384.2063396. URL <http://doi.acm.org/10.1145/2063384.2063396>.
- C. C. Douglas, J. Hu, M. Kowarschik, U. Rüde, and C. Weiß. Cache Optimization for Structured and Unstructured Grid Multigrid. *Electronic Transaction on Numerical Analysis*, pages 21–40, February 2000.
- D. Dutykh, R. Poncet, and F. Dias. The VOLNA code for the numerical modeling of tsunami waves: Generation, propagation and inundation. *European Journal of Mechanics - B/Fluids*, 30(6):598 – 615, 2011. Special Issue: Nearshore Hydrodynamics.
- Firedrake. petsc4py: the Python interface to petsc, Apr. 2016. URL <http://dx.doi.org/10.5281/zenodo.49283>.
- P. F. Fischer, J. W. Lottes, and S. G. Kerkemeier. nek5000 Web page, 2008. <http://nek5000.mcs.anl.gov>.
- F. Franchetti, Y. Voronenko, and M. Püschel. Formal loop merging for signal transforms. In *Proceedings of the 2005 ACM SIGPLAN Conference on Programming Language Design and Implementation, PLDI '05*, pages 315–326, New York, NY, USA, 2005. ACM. ISBN 1-59593-056-6. doi: 10.1145/1065010.1065048. URL <http://doi.acm.org/10.1145/1065010.1065048>.
- M. Frigo and S. G. Johnson. The design and implementation of FFTW3. In *Proceedings of the IEEE*, pages 216–231, 2005.
- M. Giles, D. Ghate, and M. Duta. Using automatic differentiation for adjoint cfd code development. 2005.
- M. B. Giles, G. R. Mudalige, Z. Sharif, G. Markall, and P. H. Kelly. Performance analysis of the op2 framework on many-core architectures.

- SIGMETRICS Perform. Eval. Rev.*, 38(4):9–15, Mar. 2011. ISSN 0163-5999. doi: 10.1145/1964218.1964221. URL <http://doi.acm.org/10.1145/1964218.1964221>.
- M. B. Giles, G. R. Mudalige, C. Bertolli, P. H. J. Kelly, E. Laszlo, and I. Reguly. An analytical study of loop tiling for a large-scale unstructured mesh application. In *Proceedings of the 2012 SC Companion: High Performance Computing, Networking Storage and Analysis, SCC '12*, pages 477–482, Washington, DC, USA, 2012. IEEE Computer Society. ISBN 978-0-7695-4956-9. doi: 10.1109/SC.Companion.2012.68. URL <http://dx.doi.org/10.1109/SC.Companion.2012.68>.
- G. Gorman, M. de Aguiar, D. Ham, F. Herrmann, C. Jacobs, P. Kelly, M. Lange, C. Pain, M. Piggott, S. Sherwin, F. V. Zacarias, and M. Warner. OPESCI project web page. <http://www.opesci.org>, 2015.
- T. Grosser, A. Groesslinger, and C. Lengauer. Polly — performing polyhedral optimizations on a low-level intermediate representation. *Parallel Processing Letters*, 22(04):1250010, 2012. doi: 10.1142/S0129626412500107. URL <http://www.worldscientific.com/doi/abs/10.1142/S0129626412500107>.
- T. Grosser, S. Verdoolaege, A. Cohen, and P. Sadayappan. The promises of hybrid hexagonal/classical tiling for gpu. Research Report RR-8339, INRIA, July 2013. URL <https://hal.inria.fr/hal-00848691>.
- T. Grosser, A. Cohen, J. Holewinski, P. Sadayappan, and S. Verdoolaege. Hybrid hexagonal/classical tiling for gpus. In *Proceedings of Annual IEEE/ACM International Symposium on Code Generation and Optimization, CGO '14*, pages 66:66–66:75, New York, NY, USA, 2014. ACM. ISBN 978-1-4503-2670-4. doi: 10.1145/2544137.2544160. URL <http://doi.acm.org/10.1145/2544137.2544160>.
- Gusto contributors. The Gusto Project. <http://firedrakeproject.org/gusto/>, 2016.
- A. Hartono, Q. Lu, X. Gao, S. Krishnamoorthy, M. Nooijen, G. Baumgartner, D. E. Bernholdt, V. Choppella, R. M. Pitzer, J. Ramanujam, A. Rountev, and P. Sadayappan. Identifying cost-effective common

- subexpressions to reduce operation count in tensor contraction evaluations. In *Proceedings of the 6th International Conference on Computational Science - Volume Part I, ICCS'06*, pages 267–275, Berlin, Heidelberg, 2006. Springer-Verlag. ISBN 3-540-34379-2, 978-3-540-34379-0. doi: 10.1007/11758501_39. URL http://dx.doi.org/10.1007/11758501_39.
- A. Hartono, Q. Lu, T. Henretty, S. Krishnamoorthy, H. Zhang, G. Baumgartner, D. E. Bernholdt, M. Nooijen, R. Pitzer, J. Ramanujam, and P. Sadayappan. Performance optimization of tensor contraction expressions for many-body methods in quantum chemistry†. *The Journal of Physical Chemistry A*, 113(45):12715–12723, 2009. doi: 10.1021/jp9051215. URL <http://pubs.acs.org/doi/abs/10.1021/jp9051215>. PMID: 19888780.
- A. Heinecke, G. Henry, M. Hutchinson, and H. Pabst. LIBXSMM: accelerating small matrix multiplications by runtime code generation. In *Proceedings of the International Conference for High Performance Computing, Networking, Storage and Analysis, SC '16*, pages 84:1–84:11, Piscataway, NJ, USA, 2016. IEEE Press. ISBN 978-1-4673-8815-3. URL <http://dl.acm.org/citation.cfm?id=3014904.3015017>.
- J. L. Hennessy and D. A. Patterson. *Computer Architecture, Fifth Edition: A Quantitative Approach*. Morgan Kaufmann Publishers Inc., San Francisco, CA, USA, 5th edition, 2011. ISBN 012383872X, 9780123838728.
- T. Henretty, R. Veras, F. Franchetti, L.-N. Pouchet, J. Ramanujam, and P. Sadayappan. A stencil compiler for short-vector simd architectures. In *Proceedings of the 27th International ACM Conference on International Conference on Supercomputing, ICS '13*, pages 13–24, New York, NY, USA, 2013. ACM. ISBN 978-1-4503-2130-3. doi: 10.1145/2464996.2467268. URL <http://doi.acm.org/10.1145/2464996.2467268>.
- J. Holewinski, L.-N. Pouchet, and P. Sadayappan. High-performance code generation for stencil computations on gpu architectures. In *Proceedings of the 26th ACM International Conference on Supercomputing, ICS '12*, pages 311–320, New York, NY, USA, 2012. ACM. ISBN 978-1-4503-1316-2. doi: 10.1145/2304576.2304619. URL <http://doi.acm.org/10.1145/2304576.2304619>.

- M. Homolya and L. Mitchell. TSFC - two-stage form compiler. <https://github.com/firedrakeproject/tsfc>, 2016.
- Intel Corporation. *Intel architecture code analyzer (IACA)*, 2012. [Online]. Available: <http://software.intel.com/en-us/articles/intel-architecture-code-analyzer/>.
- Intel Corporation. Intel VTune Performance Analyzer. <https://software.intel.com/en-us/intel-vtune-amplifier-xe>, 2016.
- F. Irigoin and R. Triolet. Supernode partitioning. In *Proceedings of the 15th ACM SIGPLAN-SIGACT symposium on Principles of programming languages*, pages 319–329. ACM, 1988.
- C. T. Jacobs and F. Luporini. Seigen - an elastic wave equation solver for seismological problems. <http://https://bitbucket.org/ctjacobs/elastic-wave-equation/branch/assemble-into-dat-flatten>, 2016.
- C. T. Jacobs, M. Lange, F. Luporini, and G. J. Gorman. Application of code generation to high-order seismic modelling with the discontinuous Galerkin finite element method. 2016. In preparation.
- G. Karypis and V. Kumar. MeTis: Unstructured Graph Partitioning and Sparse Matrix Ordering System, Version 5.0. <http://www.cs.umn.edu/~metis>, 2011.
- R. C. Kirby and A. Logg. A compiler for variational forms. *ACM Trans. Math. Softw.*, 32(3):417–444, Sept. 2006. ISSN 0098-3500. doi: 10.1145/1163641.1163644. URL <http://doi.acm.org/10.1145/1163641.1163644>.
- R. C. Kirby and A. Logg. Efficient compilation of a class of variational forms. *ACM Trans. Math. Softw.*, 33(3), Aug. 2007. ISSN 0098-3500. doi: 10.1145/1268769.1268771. URL <http://doi.acm.org/10.1145/1268769.1268771>.
- A. Klöckner. Loo.py: Transformation-based code generation for gpus and cpus. In *Proceedings of ACM SIGPLAN International Workshop on Libraries, Languages, and Compilers for Array Programming, ARRAY’14*, pages 82:82–82:87, New York, NY, USA, 2014. ACM. ISBN 978-1-4503-2937-8. doi: 10.

1145/2627373.2627387. URL <http://doi.acm.org/10.1145/2627373.2627387>.

- A. Klöckner. Loo.py: From fortran to performance via transformation and substitution rules. In *Proceedings of the 2Nd ACM SIGPLAN International Workshop on Libraries, Languages, and Compilers for Array Programming, ARRAY 2015*, pages 1–6, New York, NY, USA, 2015. ACM. ISBN 978-1-4503-3584-3. doi: 10.1145/2774959.2774969. URL <http://doi.acm.org/10.1145/2774959.2774969>.
- M. G. Knepley and A. R. Terrel. Finite element integration on gpus. *ACM Trans. Math. Softw.*, 39(2):10:1–10:13, Feb. 2013. ISSN 0098-3500. doi: 10.1145/2427023.2427027. URL <http://doi.acm.org/10.1145/2427023.2427027>.
- C. D. Krieger and M. M. Strout. Executing optimized irregular applications using task graphs within existing parallel models. In *Proceedings of the Second Workshop on Irregular Applications: Architectures and Algorithms (IA³) held in conjunction with SC12*, November 11, 2012.
- C. D. Krieger, M. M. Strout, C. Olschanowsky, A. Stone, S. Guzik, X. Gao, C. Bertolli, P. Kelly, G. Mudalige, B. Van Straalen, and S. Williams. Loop chaining: A programming abstraction for balancing locality and parallelism. In *Proceedings of the 18th International Workshop on High-Level Parallel Programming Models and Supportive Environments (HIPS)*, Boston, Massachusetts, USA, May 2013.
- S. Krishnamoorthy, M. Baskaran, U. Bondhugula, J. Ramanujam, A. Rountev, and P. Sadayappan. Effective automatic parallelization of stencil computations. *SIGPLAN Not.*, 42(6):235–244, June 2007a. ISSN 0362-1340. doi: 10.1145/1273442.1250761. URL <http://doi.acm.org/10.1145/1273442.1250761>.
- S. Krishnamoorthy, M. Baskaran, and U. B. Ramanujam. Effective automatic parallelization of stencil computations. In *In ACM SIGPLAN PLDI 2007*, 2007b.
- F. Kruel and K. Bana. Vectorized opencl implementation of numerical integration for higher order finite elements. *Comput. Math. Appl.*, 66(10):

- 2030–2044, Dec. 2013. ISSN 0898-1221. doi: 10.1016/j.camwa.2013.08.026. URL <http://dx.doi.org/10.1016/j.camwa.2013.08.026>.
- C.-C. Lam, T. Rauber, G. Baumgartner, D. Cociorva, and P. Sadayappan. Memory-optimal evaluation of expression trees involving large objects. *Comput. Lang. Syst. Struct.*, 37(2):63–75, July 2011. ISSN 1477-8424. doi: 10.1016/j.cl.2010.09.003. URL <http://dx.doi.org/10.1016/j.cl.2010.09.003>.
- M. Lange, L. Mitchell, M. G. Knepley, and G. J. Gorman. Efficient mesh management in firedrake using petsc-dmplex. *CoRR*, abs/1506.07749, 2015. URL <http://arxiv.org/abs/1506.07749>.
- S. Larsen and S. Amarasinghe. Exploiting superword level parallelism with multimedia instruction sets. In *Proceedings of the ACM SIGPLAN 2000 Conference on Programming Language Design and Implementation, PLDI '00*, pages 145–156, New York, NY, USA, 2000. ACM. ISBN 1-58113-199-2. doi: 10.1145/349299.349320. URL <http://doi.acm.org/10.1145/349299.349320>.
- A. Logg, K.-A. Mardal, G. N. Wells, et al. *Automated Solution of Differential Equations by the Finite Element Method*. Springer, 2012. ISBN 978-3-642-23098-1. doi: 10.1007/978-3-642-23099-8.
- A. Logg, M. S. Alnæs, M. E. Rognes, G. Wells, J. Ring, L. Mitchell, J. Hake, M. Homolya, F. Rathgeber, F. Luporini, G. Markall, A. Bergersen, L. Li, D. A. Ham, K.-A. Mardal, J. Blechta, G.-T. Bercea, T. Airaksinen, N. Schlömer, H. P. Langtangen, C. J. Cotter, O. Skavhaug, T. Hirsch, J. B. Haga, and A. T. T. McRae. ffc: The fenics form compiler, Apr. 2016. URL <http://dx.doi.org/10.5281/zenodo.49276>.
- Q. Lu, X. Gao, S. Krishnamoorthy, G. Baumgartner, J. Ramanujam, and P. Sadayappan. Empirical performance model-driven data layout optimization and library call selection for tensor contraction expressions. *J. Parallel Distrib. Comput.*, 72(3):338–352, Mar. 2012. ISSN 0743-7315. doi: 10.1016/j.jpdc.2011.09.006. URL <http://dx.doi.org/10.1016/j.jpdc.2011.09.006>.
- F. Luporini. COFFEE code repository. <https://github.com/coneoproject/COFFEE>, 2014a.

- F. Luporini. Helmholtz, Advection-Diffusion, and Burgers UFL code. <https://github.com/firedrakeproject/firedrake/tree/pyop2-ir-perf-eval/tests/perf-eval>, 2014b.
- F. Luporini. Seigen - performance evaluation. <https://github.com/FabioLuporini/phd-thesis/tree/master/sparsesetiling>, 2016a.
- F. Luporini. SLOPE code repository. <https://github.com/coneoproject/SLOPE>, 2016b.
- F. Luporini, A. L. Varbanescu, F. Rathgeber, G.-T. Bercea, J. Ramanujam, D. A. Ham, and P. H. J. Kelly. Cross-loop optimization of arithmetic intensity for finite element local assembly. *ACM Trans. Archit. Code Optim.*, 11(4):57:1–57:25, Jan. 2015. ISSN 1544-3566. doi: 10.1145/2687415. URL <http://doi.acm.org/10.1145/2687415>.
- F. Luporini, D. A. Ham, and P. H. J. Kelly. An algorithm for the optimization of finite element integration loops. *Submitted to ACM Transactions on Mathematical Software (TOMS)*., 2016a.
- F. Luporini, L. Mitchell, M. Homolya, F. Rathgeber, D. A. Ham, M. Lange, G. Markall, and F. Russell. coffee: a compiler for fast expression evaluation, Apr. 2016b. URL <http://dx.doi.org/10.5281/zenodo.49279>.
- G. R. Markall, D. A. Ham, and P. H. Kelly. Towards generating optimised finite element solvers for GPUs from high-level specifications. *Procedia Computer Science*, 1(1):1815 – 1823, 2010. ISSN 1877-0509. doi: <http://dx.doi.org/10.1016/j.procs.2010.04.203>. URL <http://www.sciencedirect.com/science/article/pii/S1877050910002048>. ICCS 2010.
- G. R. Markall, F. Rathgeber, L. Mitchell, N. Lorient, C. Bertolli, D. A. Ham, and P. H. J. Kelly. Performance portable finite element assembly using PyOP2 and FEniCS. In *Proceedings of the International Supercomputing Conference (ISC) '13*, volume 7905 of *Lecture Notes in Computer Science*, June 2013. In press.
- J. Meng and K. Skadron. Performance modeling and automatic ghost zone optimization for iterative stencil loops on gpus. In *Proceedings of the 23rd International Conference on Supercomputing, ICS '09*, pages 256–265, New York, NY, USA, 2009. ACM. ISBN 978-1-60558-498-0. doi: 10.

1145/1542275.1542313. URL <http://doi.acm.org/10.1145/1542275.1542313>.

L. Mitchell, D. A. Ham, F. Rathgeber, M. Homolya, A. T. T. McRae, G.-T. Bercea, M. Lange, C. J. Cotter, C. T. Jacobs, F. Luporini, S. W. Funke, H. Büsing, T. Kärnä, A. Kalogirou, H. Rittich, E. H. Mueller, S. Kramer, G. Markall, P. E. Farrell, G. McBain, and A. N. Riseth. firedrake: an automated finite element system, Apr. 2016. URL <http://dx.doi.org/10.5281/zenodo.49284>.

M. Mohiyuddin, M. Hoemmen, J. Demmel, and K. Yelick. Minimizing communication in sparse matrix solvers. In *Proceedings of the Conference on High Performance Computing Networking, Storage and Analysis, SC '09*, pages 36:1–36:12. ACM, 2009. ISBN 978-1-60558-744-8. doi: <http://doi.acm.org/10.1145/1654059.1654096>.

K. B. Ølgaard and G. N. Wells. Optimizations for quadrature representations of finite element tensors through automated code generation. *ACM Trans. Math. Softw.*, 37(1):8:1–8:23, Jan. 2010. ISSN 0098-3500. doi: 10.1145/1644001.1644009. URL <http://doi.acm.org/10.1145/1644001.1644009>.

OP2 contributors. OP2 implementation of Airfoil. <https://github.com/OP2/OP2-Common/tree/master/apps/c/airfoil>, 2011.

M. Püschel, J. M. F. Moura, J. Johnson, D. Padua, M. Veloso, B. Singer, J. Xiong, F. Franchetti, A. Gacic, Y. Voronenko, K. Chen, R. W. Johnson, and N. Rizzolo. SPIRAL: code generation for DSP transforms. *Proceedings of the IEEE, special issue on "Program Generation, Optimization, and Adaptation"*, 93(2):232–275, 2005.

J. Ragan-Kelley, C. Barnes, A. Adams, S. Paris, F. Durand, and S. Amarasinghe. Halide: A language and compiler for optimizing parallelism, locality, and recomputation in image processing pipelines. In *Proceedings of the 34th ACM SIGPLAN Conference on Programming Language Design and Implementation, PLDI '13*, pages 519–530, New York, NY, USA, 2013. ACM. ISBN 978-1-4503-2014-6. doi: 10.1145/2491956.2462176. URL <http://doi.acm.org/10.1145/2491956.2462176>.

- J. Ramanujam and P. Sadayappan. Tiling multidimensional iteration spaces for multicomputers. *J. Parallel Distrib. Comput.*, 16(2):108–120, 1992. doi: 10.1016/0743-7315(92)90027-K. URL [http://dx.doi.org/10.1016/0743-7315\(92\)90027-K](http://dx.doi.org/10.1016/0743-7315(92)90027-K).
- F. Rathgeber. *Productive and efficient computational science through domain-specific abstractions*. PhD thesis, Imperial College London, 2014.
- F. Rathgeber, D. A. Ham, L. Mitchell, M. Lange, F. Luporini, A. T. T. McRae, G. Bercea, G. R. Markall, and P. H. J. Kelly. Firedrake: automating the finite element method by composing abstractions. *CoRR*, abs/1501.01809, 2015. URL <http://arxiv.org/abs/1501.01809>.
- F. Rathgeber, F. Luporini, and L. Mitchell. firedrake-bench: firedrake bench optimality paper release, Apr. 2016a. URL <http://dx.doi.org/10.5281/zenodo.49290>.
- F. Rathgeber, L. Mitchell, F. Luporini, G. Markall, D. A. Ham, G.-T. Bercea, M. Homolya, A. T. T. McRae, H. Dearman, C. T. Jacobs, gbts, S. W. Funke, K. Sato, and F. Russell. PyOP2: framework for performance-portable parallel computations on unstructured meshes, Apr. 2016b. URL <http://dx.doi.org/10.5281/zenodo.49281>.
- M. Ravishankar, J. Eisenlohr, L.-N. Pouchet, J. Ramanujam, A. Rountev, and P. Sadayappan. Code generation for parallel execution of a class of irregular loops on distributed memory systems. In *Proc. Intl. Conf. on High Perf. Comp., Net., Sto. & Anal.*, pages 72:1–72:11, 2012. ISBN 978-1-4673-0804-5.
- I. Z. Reguly, G. R. Mudalige, C. Bertolli, M. B. Giles, A. Betts, P. H. J. Kelly, and D. Radford. Acceleration of a full-scale industrial cfd application with op2. *IEEE Transactions on Parallel and Distributed Systems*, 27(5):1265–1278, May 2016. ISSN 1045-9219. doi: 10.1109/TPDS.2015.2453972.
- M. E. Rognes, A. Logg, D. A. Ham, M. Homolya, N. Schlömer, J. Blechta, A. T. T. McRae, A. Bergersen, C. J. Cotter, J. Ring, and L. Mitchell. fiat: the finite element automated tabulator, Apr. 2016. URL <http://dx.doi.org/10.5281/zenodo.49280>.

- D. Rossinelli, B. Hejazialhosseini, P. Hadjidoukas, C. Bekas, A. Curioni, A. Bertsch, S. Futral, S. J. Schmidt, N. A. Adams, and P. Koumoutsakos. 11 pflop/s simulations of cloud cavitation collapse. In *Proceedings of the International Conference on High Performance Computing, Networking, Storage and Analysis, SC '13*, pages 3:1–3:13, New York, NY, USA, 2013. ACM. ISBN 978-1-4503-2378-9. doi: 10.1145/2503210.2504565. URL <http://doi.acm.org/10.1145/2503210.2504565>.
- F. P. Russell and P. H. J. Kelly. Optimized code generation for finite element local assembly using symbolic manipulation. *ACM Transactions on Mathematical Software*, 39(4), 2013.
- J. H. Salz, R. Mirchandaney, and K. Crowley. Run-time parallelization and scheduling of loops. *IEEE Transactions on Computers*, 40(5):603–612, 1991.
- J. Shin, M. W. Hall, J. Chame, C. Chen, P. F. Fischer, and P. D. Hovland. Speeding up nek5000 with autotuning and specialization. In *Proceedings of the 24th ACM International Conference on Supercomputing, ICS '10*, pages 253–262, New York, NY, USA, 2010. ACM. ISBN 978-1-4503-0018-6. doi: 10.1145/1810085.1810120. URL <http://doi.acm.org/10.1145/1810085.1810120>.
- B. Smith, S. Balay, M. Knepley, J. Brown, L. C. McInnes, H. Zhang, P. Brune, sarich, stefanozampini, D. Karpeyev, L. Dalcin, tisaac, markadams, V. Minden, VictorEijkhout, vijaysm, K. Rupp, F. Kong, and SurtaiHan. PETSc: portable, extensible toolkit for scientific computation, Apr. 2016. URL <http://dx.doi.org/10.5281/zenodo.49285>.
- D. G. Spampinato and M. Püschel. A basic linear algebra compiler. In *International Symposium on Code Generation and Optimization (CGO)*, 2014.
- K. Stock, T. Henretty, I. Murugandi, P. Sadayappan, and R. Harrison. Model-driven simd code generation for a multi-resolution tensor kernel. In *Proceedings of the 2011 IEEE International Parallel & Distributed Processing Symposium, IPDPS '11*, pages 1058–1067, Washington, DC, USA, 2011. IEEE Computer Society. ISBN 978-0-7695-4385-7. doi: 10.1109/IPDPS.2011.101. URL <http://dx.doi.org/10.1109/IPDPS.2011.101>.
- M. Strout, F. Luporini, C. Krieger, C. Bertolli, G.-T. Bercea, C. Olschanowsky, J. Ramanujam, and P. Kelly. Generalizing run-time

- tiling with the loop chain abstraction. In *Parallel and Distributed Processing Symposium, 2014 IEEE 28th International*, pages 1136–1145, May 2014. doi: 10.1109/IPDPS.2014.118.
- M. M. Strout. Compilers for regular and irregular stencils: Some shared problems and solutions. In *Proceedings of Workshop on Optimizing Stencil Computations (WOSC)*, October 27, 2013.
- M. M. Strout, L. Carter, J. Ferrante, J. Freeman, and B. Kreaseck. Combining performance aspects of irregular Gauss-Seidel via sparse tiling. In *Proceedings of the 15th Workshop on Languages and Compilers for Parallel Computing (LCPC)*. Springer, July 2002.
- M. M. Strout, L. Carter, and J. Ferrante. Compile-time composition of runtime data and iteration reorderings. In *Proc. ACM SIGPLAN Conf. Prog. Lang. Des. & Impl. (PLDI)*, New York, NY, USA, June 2003. ACM.
- M. M. Strout, L. Carter, J. Ferrante, and B. Kreaseck. Sparse tiling for stationary iterative methods. *International Journal of High Performance Computing Applications*, 18(1):95–114, February 2004.
- T. Sun. Opesci-fd: automatic code generation package for finite difference models. 2016.
- Y. Tang, R. A. Chowdhury, B. C. Kuszmaul, C.-K. Luk, and C. E. Leiserson. The Pochoir stencil compiler. In *Proceedings of the Twenty-third Annual ACM Symposium on Parallelism in Algorithms and Architectures, SPAA '11*, pages 117–128, New York, NY, USA, 2011. ACM. ISBN 978-1-4503-0743-7. doi: 10.1145/1989493.1989508. URL <http://doi.acm.org/10.1145/1989493.1989508>.
- TCE contributors. The tensor contraction engine project. <http://www.csc.lsu.edu/~gb/TCE/>.
- Thetis contributors. The Thetis Project. <http://thetisproject.org>, 2016.
- D. Unat, J. Zhou, Y. Cui, S. B. Baden, and X. Cai. Accelerating a 3d finite-difference earthquake simulation with a c-to-cuda translator. *Computing in Science and Engg.*, 14(3):48–59, May 2012. ISSN 1521-9615. doi: 10.1109/MCSE.2012.44. URL <http://dx.doi.org/10.1109/MCSE.2012.44>.

- S. van der Walt, S. C. Colbert, and G. Varoquaux. The NumPy array: a structure for efficient numerical computation. *Computing in Science Engineering*, 13(2):22–30, March 2011. ISSN 1521-9615. doi: 10.1109/MCSE.2011.37.
- F. G. Van Zee and R. A. van de Geijn. BLIS: A framework for rapidly instantiating BLAS functionality. *ACM Transactions on Mathematical Software*, 41(3):14:1–14:33, June 2015. URL <http://doi.acm.org/10.1145/2764454>.
- A. Venkat, M. Shantharam, M. Hall, and M. M. Strout. Non-affine extensions to polyhedral code generation. In *Proceedings of Annual IEEE/ACM International Symposium on Code Generation and Optimization, CGO '14*, pages 185:185–185:194, New York, NY, USA, 2014. ACM. ISBN 978-1-4503-2670-4. doi: 10.1145/2544137.2544141. URL <http://doi.acm.org/10.1145/2544137.2544141>.
- J. Virieux. P-sv wave propagation in heterogeneous media; velocity-stress finite-difference method. *Geophysics*, 51(4):889–901, 1986. ISSN 0016-8033. doi: 10.1190/1.1442147. URL <http://geophysics.geoscienceworld.org/content/51/4/889>.
- P. E. J. Vos, S. J. Sherwin, and R. M. Kirby. From h to p efficiently: Implementing finite and spectral/hp element methods to achieve optimal performance for low- and high-order discretisations. *J. Comput. Phys.*, 229(13):5161–5181, July 2010. ISSN 0021-9991. doi: 10.1016/j.jcp.2010.03.031. URL <http://dx.doi.org/10.1016/j.jcp.2010.03.031>.
- R. C. Whaley and J. J. Dongarra. Automatically tuned linear algebra software. In *Proceedings of the 1998 ACM/IEEE Conference on Supercomputing, Supercomputing '98*, pages 1–27, Washington, DC, USA, 1998. IEEE Computer Society. ISBN 0-89791-984-X. URL <http://dl.acm.org/citation.cfm?id=509058.509096>.
- S. Williams, A. Waterman, and D. Patterson. Roofline: an insightful visual performance model for multicore architectures. *Commun. ACM*, 52(4): 65–76, Apr. 2009. ISSN 0001-0782. doi: 10.1145/1498765.1498785. URL <http://doi.acm.org/10.1145/1498765.1498785>.

- Y. Zhang and F. Mueller. Auto-generation and auto-tuning of 3d stencil codes on gpu clusters. In *Proceedings of the Tenth International Symposium on Code Generation and Optimization, CGO '12*, pages 155–164, New York, NY, USA, 2012. ACM. ISBN 978-1-4503-1206-6. doi: 10.1145/2259016.2259037. URL <http://doi.acm.org/10.1145/2259016.2259037>.
- X. Zhou, J.-P. Giacalone, M. J. Garzarán, R. H. Kuhn, Y. Ni, and D. Padua. Hierarchical overlapped tiling. In *Proceedings of the Tenth International Symposium on Code Generation and Optimization, CGO '12*, pages 207–218, New York, NY, USA, 2012. ACM. ISBN 978-1-4503-1206-6. doi: 10.1145/2259016.2259044. URL <http://doi.acm.org/10.1145/2259016.2259044>.
- G. Zumbusch. Vectorized higher order finite difference kernels. In *Proceedings of the 11th International Conference on Applied Parallel and Scientific Computing, PARA'12*, pages 343–357, Berlin, Heidelberg, 2013. Springer-Verlag. ISBN 978-3-642-36802-8. doi: 10.1007/978-3-642-36803-5_25. URL http://dx.doi.org/10.1007/978-3-642-36803-5_25.